

# Vacuum Technology and Applications

*David J. Hucknall*  
*BSc PhD CChem MRSC*

**B**UTTERWORTH  
**H**EINEMANN

Butterworth-Heinemann Ltd  
Linacre House, Jordan Hill, Oxford OX2 8DP



PART OF REED INTERNATIONAL BOOKS

OXFORD LONDON BOSTON  
MUNICH NEW DELHI SINGAPORE SYDNEY  
TOKYO TORONTO WELLINGTON

First published 1991

© Butterworth-Heinemann Ltd 1991

All rights reserved. No part of this publication may be reproduced in any material form (including photocopying or storing in any medium by electronic means and whether or not transiently or incidentally to some other use of this publication) without the written permission of the copyright holder except in accordance with the provisions of the Copyright, Designs and Patents Act 1988 or under the terms of a licence issued by the Copyright Licensing Agency Ltd, 90 Tottenham Court Road, London, England W1P 9HE. Applications for the copyright holder's written permission to reproduce any part of this publication should be addressed to the publishers.

**British Library Cataloguing in Publication Data**

Hucknall, David J.

Vacuum Technology and Applications.

I. Title

621.5

ISBN 0 7506 1145 6

**Library of Congress Cataloging-in-Publication Data**

Hucknall, D. J.

Vacuum Technology and Applications / David J. Hucknall.

p. cm.

Includes bibliographical references and index.

ISBN 0 7506 1145 6

1. Vacuum technology. I. Title.

TJ940.H83 1991

621.5'5—dc20

Printed and bound in Great Britain by  
Billings & Sons Ltd, Worcester

# Preface

---

It would be a daunting task to list the activities and the products to which vacuum technology makes a contribution. The range would extend from fundamental research in physics and chemistry to food packaging and from body scanners to jewellery. It would include essential sectors of advanced industrial activity such as information technology and the manufacture of complex metal alloys and ceramics.

Despite this immense range of applications, it is often apparent that knowledge of vacuum technology is quite limited, even in areas where its use is extensive. In my own experience, this is true both in academic and industrial establishments. Equipment, whether 'inherited' or built to the user's specifications will often have a fairly complex vacuum system. Too often this is regarded as a mere incidental, expected to work efficiently at the outset and continue to function for prolonged periods in the face of considerable abuse and negligible maintenance. Relatively important facts such as the function of the gas ballast valve on oil-sealed pumps or the working principles of a thermal conductivity gauge seem to be poorly understood by users and operators. Information has often been acquired by word of mouth from others only slightly more knowledgeable.

I have long admired books such as Van Atta's excellent *Vacuum Science and Engineering* and the immensely-detailed *Theory and Practice of Vacuum Technology* by Wutz, Adam and Walcher. The extent of the information and the rigour with which it is presented in both cannot be matched nor has it been my intention, in this book, to do so. My aim has been to present in a straight forward manner, a review of the most commonly encountered methods for the production, containment and measurement of sub-atmospheric pressures and to outline a number of very important applications.

I hope the material has been presented in a logical manner. For example, one has to have the theoretical means to assess the performance of a proposed or actual vacuum system. At the outset (Chapter 1), therefore, the relevant aspects are discussed in order to make this possible. In Chapters 2 and 3, the pumps used for the production of rough-medium and high-ultra-high vacua, respectively, are discussed. Both chapters deal with their principle, performance and applications. During the operation of vacuum systems, it is essential to measure total pressure; considerable information can also be obtained from residual gas analysis and partial pressure measurement. Devices for the measurement of both are described in Chapter 4. Leak detection is no longer confined to vacuum technology but is now used routinely as a method of non-destructive testing in a wide range of industries. Chapter 5 reviews all aspects of the subject, with particular emphasis on the use of He-specific mass spectrometer detectors in vacuum leak detection. Vacuum systems must, of course, be constructed from correctly-selected materials and assembled according to accepted procedures. Materials, components and fabrication are reviewed in Chapter 6. In Chapter 7, the

application of vacuum technology in critical areas of industrial activity such as thin-film technology, semiconductor manufacture, metallurgy and the chemical industry, is discussed. Chapter 8 is in the form of an Appendix that gathers together important material including units, conversion factors and some physical constants that cannot be conveniently included elsewhere. It also presents, briefly, the PNEUROOP procedures for establishing vacuum pump characteristics.

Finally, this book is not addressed to any particular group of users but to anyone in production, research and development whose work, either directly or indirectly, is concerned with vacuum technology.

# *Acknowledgments*

---

My most sincere thanks go to all who provided me with the drawings and photographs that appear in this book or who gave permission for them to be reproduced. I must, however, acknowledge specifically the cooperation of Hick, Hargreaves and Co Ltd (initially Mr I. Pemberton and then Mr K. Barber), Balzers AG (Mr N. S. Gaertner) and Arthur Pfeiffer Vakuumtechnik Wetzlar GmbH (Mr D. Fickler).

It goes without saying that this book would not have appeared without the assistance of my colleagues in Leybold Ltd and Leybold AG. In particular, I owe a considerable debt of gratitude to Dr K. G. Schneider, Managing Director of Leybold Ltd for his encouragement, comments and advice. (His help even extended as far as taking several of the Chapters on holiday.) It also gives me great pleasure to thank Mrs Renate McCarron for typing the manuscript with speed and accuracy.

Finally, I thank my wife Susan and my children, Rachel and Philip, for tolerating, weekend after weekend, the view of my back.

David J. Hucknall  
1991

# 1

## *Introduction*

---

### 1.1 General

Vacuum technology is indispensable to many branches of contemporary industry and research and will play an essential role in these activities in the future.

It is almost impossible to list all the areas in which vacuum technology is now used. From its initial association with research in physics, the range of applications has extended to important sectors of industrial activity, including metallurgy, mechanical, electrical and chemical engineering, making an incalculable contribution to process effectiveness and efficiency. The second half of the century has seen the emergence of many manufacturing processes relying on a vacuum environment, ranging from the production of strategic metals and alloys to meat packaging and freeze-drying coffee. Vacuum processes are used to produce special coated glass for buildings and cars and in the manufacture of optical devices, semiconductors and information-storage disks. The aerospace industry needs vast vacuum chambers for satellite testing whilst research in nuclear fusion and particle physics have increased the demands made on vacuum systems. Forecasts of the development of technology indicate that important activities will take place in the areas of advanced materials (ceramics, polymers, amorphous metals, composites), sensor technology, information technology (super LSI devices, 3D memory devices), computing, thin-film technology and medicine. Vacuum technology will make an essential contribution.

The object of vacuum technology is to reduce the number of gas particles in a system. At constant temperature, this always corresponds to a reduction in gas pressure. For example, a pressure decrease from atmospheric pressure to  $10^{-6}$  mbar corresponds to a billion-fold reduction in the number of particles in a system. Currently, it is possible to achieve  $10^{-13}$  mbar. A survey of a few of the activities performed under vacuum, classified according to the pressure region in which they take place, is given in Table 1.1.

A very basic vacuum system is shown in Figure 1.1. It consists of a vessel connected to a gas-transfer pump. The pump removes gas particles from the vessel. With gas-transfer pumps this usually involves compression of the gas to a pressure that is appropriate either for its exhaust to the atmosphere or transfer to a backing pump.

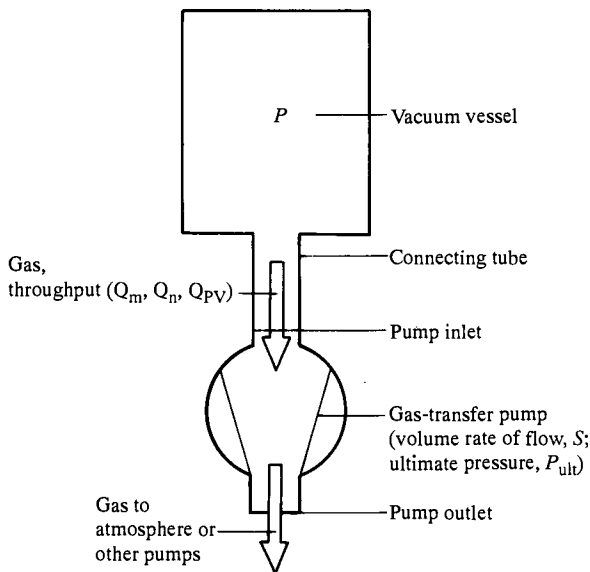
It is impossible to eliminate all sources of gas in a vacuum system. Even in the best-designed and -operated static systems, small leaks and slight outgassing occur and the resulting molecules have to be dealt with by the pumps.

Further, in many systems, significant quantities of gas and vapour have to be pumped either because they are evolved during the process or have been added deliberately to maintain reaction conditions (Figure 1.2).

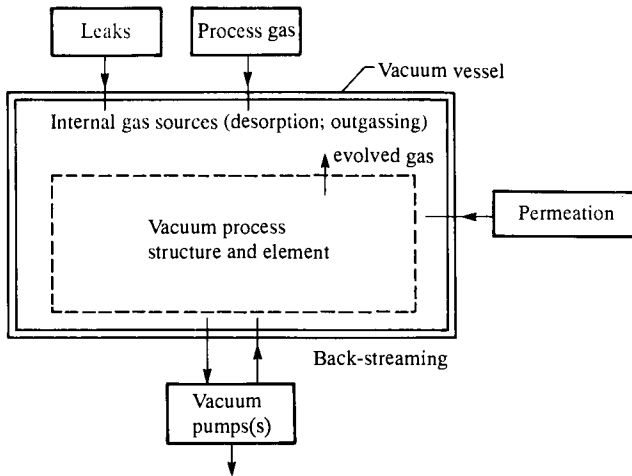
## 2 Vacuum Technology and Applications

**Table 1.1** Operating pressure range for various vacuum processes

Range	Application
Rough vacuum ( $10^3$ –1 mbar)	Drying, degassing, Food processing
Medium vacuum ( $1$ – $10^{-3}$ mbar)	Steel degassing, vacuum induction melting, freeze drying, vacuum distillation
High vacuum ( $10^{-3}$ – $10^{-7}$ mbar)	Coating: packaging material; architectural glass; magnetic, optical and other data storage media; electron beam and plasma processes
Ultra-high vacuum ( $<10^{-7}$ mbar)	Nuclear fusion, space simulation, surface science, molecular beam epitaxy



**Figure 1.1** Schematic diagram of a basic vacuum system using a gas-transfer pump



**Figure 1.2** Gas sources within a vacuum system ( $q_{in} < q_{out}$ , satisfactory behaviour;  $q_{out} < q_{in}$ , pressure cannot be maintained)

Obviously, in order to match the pumps with the process requirements, it is necessary to be able to quantify the amount of material entering the vacuum system and the ability of the pumps to deal with it.

In the present chapter, the essentials of gas behaviour at pressures below atmospheric pressure will be discussed. Particular attention will be paid to the flow of gases from vessels and through ducts, apertures, etc. The influence of this on characteristics of practical vacuum systems such as pump-down time will then be considered.

## 1.2 The gaseous state

### 1.2.1 The perfect gas

The state of a system containing a constant amount of material is determined by a small number of variables. Usually, these are pressure ( $P$ ), volume ( $V$ ) and temperature ( $T$ ). The volume of a substance is the space occupied by that substance. (For gases and vapours, the volume under consideration is the same as that of the containing vessel.) Pressure is defined as the force applied perpendicularly to a plane surface. The basic unit of pressure is equivalent to a force of one newton (1 N) applied to an area of  $1 \text{ m}^2$ . (The newton is the force necessary to move a mass of 1 kg so that it accelerates at a rate of  $1 \text{ m s}^{-1}$  per second ( $1 \text{ m s}^{-2}$ .) This unit is called the pascal ( $1 \text{ Pa} = 1 \text{ N m}^{-2}$ ). Other units of pressure are defined in the Appendix. If a constant mass of gas is taken and placed in a system where its temperature, volume and pressure can be measured, it will be seen that:



#### 4 Vacuum Technology and Applications

1. if  $V$  and  $T$  are fixed, we shall be unable to vary  $P$ ;
2. if  $P$  and  $T$  are chosen, the value of  $V$  is fixed.

This means that there is some equation (called an equation of state) that connects  $P$ ,  $V$  and  $T$ . Experiments by Boyle, Gay-Lussac and others showed that when the pressure is sufficiently low, all gases satisfy the relationship:

$$PV = nRT$$

where  $P$  is the pressure,  $V$  is the volume,  $T$  is the absolute temperature,  $R$  is a constant which is independent of the nature of the gas and  $n$  denotes the amount of substance of the gas (see Appendix). Boyle, for example, verified that, at constant temperature and for a fixed weight of gas, changes in the pressure when the volume is altered (or vice versa), could be predicted:

$$P_i V_i = P_f V_f \quad (i = \text{initial}, f = \text{final})$$

Gay-Lussac confirmed that, for a fixed amount of gas:

1. The volume of a gas increases with temperature at fixed  $P$ :

$$V_i/V_f = T_i/T_f$$

2. The pressure of a gas increases with temperature at fixed  $V$ :

$$P_i/P_f = T_i/T_f$$

A gas that obeys  $PV = nRT$  exactly is called *perfect* or *ideal*. At higher pressures, the equations of state for a gas are more complicated; some are empirical – designed to represent as closely as possible the measured values of  $P$ ,  $V$  and  $T$  – while others are theoretical.

##### 1.2.1.1 Gas mixtures

Bearing in mind the complexity of the gas mixtures that may be commonly encountered in vacuum technology (dry air, for example, contains twelve components (see Appendix, Table 8.3)), it is necessary to examine such multicomponent systems.

If we have an amount of substance ( $n_1$ ) of some gas (1) at a temperature ( $T$ ) in a container of volume  $V$ , then, according to Section 1.2.1, the pressure in the container would be given by:

$$p_1 = n_1 \left( \frac{RT}{V} \right)$$

Had another gas (2) been admitted to the empty container then, according to the amount of the substance of the gas, the pressure would have been:

$$p_2 = n_2 \left( \frac{RT}{V} \right)$$

Had the two (or more gases) been placed in the same container, the resultant pressure would have been given by Dalton's law of partial pressures. This states that the pressure exerted by a mixture of perfect gases is the sum of the pressures exerted by the individual gases occupying the same volume alone.

This is given by the expression:

$$P_{\text{TOTAL}} = p_1 + p_2 + p_3 + p_4 + \dots$$

where the gas mixture consists of gases 1,2,3,4, etc.

and:

$$P_{\text{TOTAL}} = (n_1 + n_2 + n_3 + \dots) RT/V$$

where the total amount,  $n = n_1 + n_2 + n_3 + \dots$

### Example 1

If 1 mol of  $\text{N}_2$  and 3 mol of Ar are admitted to an empty container ( $V = 10 \text{ l}$ ) at 298K, what is the total pressure?

Assuming perfect behaviour:

$$\begin{aligned} p_{\text{N}_2} &= n_{\text{N}_2} \left( \frac{RT}{V} \right) = 1 \times \frac{83.145 \text{ mbar l mol}^{-1} \text{ K}^{-1} \times 298\text{K}}{10 \text{ l}} \\ &= 2.478 \text{ bar} \end{aligned}$$

$$\begin{aligned} p_{\text{Ar}} &= n_{\text{Ar}} \left( \frac{RT}{V} \right) = \frac{3 \times 83.145 \text{ mbar l mol}^{-1} \text{ K}^{-1} \times 298\text{K}}{10 \text{ l}} \\ &= 7.433 \text{ bar} \end{aligned}$$

$$\therefore \underline{p_{\text{TOT}} = p_{\text{N}_2} + p_{\text{Ar}} = 9.911 \text{ bar}}$$

#### 1.2.1.2 Kinetic theory of gases

Based on experiment, it was found that, when the pressure is sufficiently low, all gases behave perfectly. In this state, the miniscule particles that make up the gas move freely and, apart from their collisions, do not interact whatsoever. The postulate that a gas consists of a huge number of discrete particles between which no forces are acting has led to a model of gas behaviour designated the *kinetic theory* of gases. The assumptions made on which to base the model are:

1. A gas consists of a huge number of particles of mass  $m$  in continual random motion.
2. The size of the particles is negligible when compared with the average distance they travel between collisions.
3. Collisions between particles are elastic (i.e. the total kinetic energy of the particles is maintained).

Because of the collisions, the gas particles constantly change their speed and direction of travel. The kinetic theory enables a number of significant

## 6 Vacuum Technology and Applications

values to be simply deduced. These include the collision frequency ( $z \text{ s}^{-1}$ ), the mean free path ( $\bar{l}$ ) (the average distance each particle travels between collisions). The calculation of these values is indicated below.

### (i) Velocity distribution

As a result of frequent collisions, gas particles will not have a constant velocity. The distribution function for the velocity components in a perfect gas according to the kinetic theory is given by the Maxwell–Boltzmann distribution.

The mean speed ( $\bar{c}$ ) is the average of the speed of the particles calculated using the Maxwell distribution:

$$\begin{aligned}\bar{c} &= (8 kT/\pi m)^{1/2} = (8RT/\pi M_r)^{1/2} \\ &= 145.51 (T/K)^{1/2} / (M_r)^{1/2} \text{ m s}^{-1}\end{aligned}$$

---

The most probable speed ( $c^*$ ) is the speed at which the distribution passes through a maximum:

$$c^* = (2 kT/m)^{1/2} = (2RT/M_r)^{1/2}$$

---

The root mean square speed (r.m.s.) ( $c$ ), also known as the effective velocity, is given by:

$$c = (3 kT/m)^{1/2} = (3RT/M_r)^{1/2}$$

---

### (ii) Collisions

The number of collisions per second made by a gas particle can be obtained from its speed. If it is assumed that two particles collide when they come within a certain distance ( $d$ ) of each other ( $d$  may be taken as the diameter of the particle) and that one particle moves at an average speed  $\bar{c}$  while the others are at rest, then the collision frequency (the number of hits/unit time) can be shown to be:

$$z = \bar{c}\sigma N/V$$

where  $\sigma = \pi d^2$  and there are  $N/V$  particles per unit volume. More realistically, instead of  $\bar{c}$ , the average relative speed of the colliding particles ( $\sqrt{2} \bar{c}$ ) should be used, giving:

$$z = \sqrt{2} \bar{c}\sigma N/V \text{ (the number of collisions made by a single particle)}$$

The total number of collisions ( $Z$ )/per unit volume/unit time:

$$Z = \frac{\sigma \bar{c} (N/V)^2}{\sqrt{2}} = \pi d^2 (4 kT/\pi m)^{1/2} (N/V)^2$$

---

*(iii) Mean free path*

The calculation of the collision frequency allows an expression for  $\bar{l}$  to be obtained. If a particle travels with a speed  $\bar{c}$  and collides with a frequency  $z$ , then  $\bar{l}$  is simply given by:

$$\begin{aligned}\bar{l} &= \bar{c}/z \\ &= kT/\sqrt{2} \sigma p\end{aligned}$$

In other words, the mean free path is proportional to pressure. Values for  $\bar{l}p$  are to be found in Table 8.4.

**1.2.2 Imperfections**

When deviations from the equation  $PV = nRT$  are observed, the gas under consideration is said to be behaving *imperfectly* or non-ideally.

Deviations are significant at high pressures and low temperatures and the reason for this lies in the interactions between the gas particles, leading eventually to their liquefaction or even solidification.

The relevance of deviations from ideality in vacuum technology lies in the effects of condensable vapours on the performance of mechanical pumps. A primary mechanical pump removes gas from a system at relatively low pressure and compresses it until a pressure greater than ambient (to about 1.3 bar) is reached.

For permanent gases, this presents no problem. Vapours, however, may condense during compression and seriously impair the efficiency of the pump.

Condensable materials that give cause for concern are those that have a partial pressure within the system being evacuated such that, during compression in the pump, the saturated vapour pressure of the material, at the working temperature of the pump, would be reached.

Under these conditions, material may enter the pump as a vapour but liquefy during compression. Further consideration is given to this topic in Section 2.2.2.2.

**1.3 Gas flow**

The flow of a fluid can be described by its flux (e.g. the gas flux). Such processes are extremely important in vacuum technology and in order to obtain a system that works efficiently, it is necessary to define both the nature of the flow and the flux rates.

Flow is generally controlled by pressure and friction (the effects of gravity will be ignored) although under some circumstances, frictional forces can also be ignored. In discussions of the nature of gas flow, the value of the Knudsen number ( $Kn$ ) is an important consideration. It is defined as the ratio of mean free path ( $\bar{l}$ ) to the width of the flow channel ( $d$ ):

$$Kn = \bar{l}/d$$

## 8 Vacuum Technology and Applications

Under conditions where  $\bar{l} \ll d$  ( $Kn \ll 1$ ), many collisions between particles occur and the gas can be regarded as a continuum (its molecular structure is not of consequence). Such conditions are fulfilled in the rough vacuum range. With continuum flow, the dynamic viscosity plays a significant role. Further, flow conditions can be defined by the value of Reynolds number ( $Re$ ):

$$Re = \frac{V\rho d}{\eta}$$

where  $V$  is the free steam velocity,  $\rho$  is the density of the fluid,  $d$  is the diameter of the fluid and  $\eta$  is the dynamic viscosity. For smooth tubes of circular cross-section, flow is laminar when  $Re < 2300$ . When  $Re$  exceeds 3000, flow becomes turbulent. Under the latter conditions, in vacuum systems, loosely held deposits on the walls of gas ducts may be swept up and transported towards the pumps.

In the high- and ultra-high vacuum regions,  $\bar{l}$  is greater than  $d$ . This corresponds to molecular flow conditions. They are characterized by:

$$Kn > 0.5$$

The transition region  $0.5 > Kn > 0.01$  is termed the Knudsen flow region and is difficult to treat theoretically.

### 1.3.1 Throughput

When a gas is flowing across a conducting element, the flux is defined as the ratio of the quantity of gas to the time. Corresponding to this we can define:

#### (a) Molar flow rate or molar throughput ( $Q_n$ )

$$Q_n = \Delta n / \Delta t; [Q_n] = \text{mol/time}; \text{mol s}^{-1}$$

where [ ] denotes 'units of . . .'  
and  $\Delta$  denotes a 'finite difference'

#### (b) Mass flow rate or mass throughput ( $Q_m$ )

$$Q_m = \Delta m / \Delta t; [Q_m] = \text{kg s}^{-1}$$

#### (c) Volume flow rate ( $Q_v$ )

$$Q_v = \Delta V / \Delta t; [Q_v] = \text{m}^3 \text{s}^{-1}$$

From the equation of state of an ideal gas ( $PV = nRT$ ), we can obtain relationships between these quantities. For example, under steady-state conditions ( $P$  and  $T$  constant),

$$P \cdot (\Delta V / \Delta t) = Q_n RT$$

where  $\Delta(PV) / \Delta t = Q_{PV}$  and is termed the  $PV$  throughput ( $[Q_{PV}] = \text{mbar l s}^{-1}; \text{Pa m}^3 \text{s}^{-1}$ ).

$$\text{or } Q_{PV} = Q_n RT$$

$$\text{and } Q_m = Q_n \cdot M$$

$$\text{and } Q_m = Q_{PV} \cdot \frac{M}{RT}$$

It should be noted that, in the definition of  $Q_{PV}$ , temperature is not specified. There are arguments that it is 'understood' that there is an implicit 'at T°C' in  $Q_{PV}$ . However, the use of  $PV$  throughput to describe gas flux results either in an ill-defined, implied temperature in the 'unit' or encourages its neglect (Ehrlich, 1986). The true gas flow rate is, therefore, given by the molar throughput, for example.

Leak rates are usually given in  $PV$  throughput since leakage at a certain rate ( $Q_{\text{leak}}$ ) will cause a pressure increase in a vacuum system isolated from the pumps:

$$Q_{\text{leak}} = V\Delta P/\Delta t \text{ (chamber volume constant)}$$

Ehrlich (1986) indicated that, certainly for calibrated leaks, the pressure and vacuum group of NIST (formerly the NBS) intended to use 'mol/s' as the unit of leakage.

Gas entering the inlet of a vacuum pump is measured in terms of the volume rate of flow ( $Q_V$ ). This is called the pumping speed ( $S$  or  $S^*$ ) of the pump:

$$\Delta V/\Delta t_{(\text{pump inlet})} = S^* = Q_{V, \text{ pump inlet}}; [S] = \text{m}^3 \text{ h}^{-1}; \text{ l s}^{-1}$$

The quantity of gas in  $PV$  units flowing in unit time across the inlet of a pump gives the throughput of the pump (also termed the pumping capacity) where:

$$(PV)_{\text{pump inlet}} = PS^* = Q_{PV, \text{ pump inlet}} \quad [ ] = \text{Pa m}^3 \text{ s}^{-1}, \text{ mbar l s}^{-1}$$

For many types of vacuum pump,  $S^*$  is independent of pressure over a large range of pressure (see the appropriate chapters). This means that  $Q_{PV, \text{ pump inlet}}$  will decrease with decreasing pressure. Procedures for measuring pump characteristics such as the volume rate of flow at the inlet have been documented by PNEUROOP (an association of manufacturers of compressors, vacuum pumps and pneumatic tools from 11 European countries). Details of the PNEUROOP procedures are given in Section 8.3.

### 1.3.2 Flow resistance/conductance

In practice, it is usually not possible to connect vacuum pumps directly to the system to be evacuated. The connecting pipework, valves etc. give rise to a pressure difference between the pump inlet and the vacuum chamber. The resistance to gas flow of the ducting is given by the ratio of the pressure difference across the gas-conducting path to the gas flux rate, i.e.  $\Delta P/Q$ . If the flow of electrical current according to Ohm's law is considered,  $U = IR$  or  $R = U/I$  where  $U$  is the potential difference and  $I$  is the magnitude of the current. Using this electrical analogy, if  $R$  is the resistance to gas flow, then  $\Delta P \equiv U$  and  $Q \equiv I$ . When the flow of electricity is considered, the reciprocal

of resistance is termed the conductance ( $L = I/U$ ). Similarly, the inverse of resistance to gas flow is termed flow conductance ( $C$ ) and is given by:

$$C = Q/\Delta P$$

Gas flow rate is often expressed in terms of  $PV$  throughput; this yields  $[C] = \text{m}^3 \text{s}^{-1}; \text{l s}^{-1}$ . As will be shown later,  $C$  may be calculated for relatively simple cases.

Electrical resistances may be connected in series or parallel:

$$\left. \begin{aligned} R_{\text{TOT}} &= R_1 + R_2 + R_3 + \dots \\ I/L_{\text{TOT}} &= I/L_1 + I/L_2 + I/L_3 + \dots \end{aligned} \right\} \text{series connection}$$

$$\left. \begin{aligned} I/R_{\text{TOT}} &= I/R_1 + I/R_2 + I/R_3 + \dots \\ L_{\text{TOT}} &= L_1 + L_2 + L_3 + \dots \end{aligned} \right\} \text{parallel connection}$$

In the case of fluid flow, equations for the total flow conductance (e.g.  $C_{\text{TOT}} = C_1 + C_2 + C_3 + \dots$ , for conductances in parallel) are only valid within certain limitations. This is because the flow of a fluid is not uniform over the length of the conductance. For components connected in parallel, the relevant equation will only be valid for tubes sufficiently far apart that they do not interfere with each other.

**1.3.2.1 Effective pumping speed**

Because of the resistance to gas flow in the connection between a vacuum chamber and its pumps, the effective speed of the pump at the chamber ( $S_{\text{eff}}$ ) is less than volume rate of flow of the pump at its inlet ( $S^*$ ). The relationship between  $S_{\text{eff}}$  and  $S^*$  is given by:

$$\frac{1}{S_{\text{eff}}} = \frac{1}{C} + \frac{1}{S^*}$$

It can be shown that  $S_{\text{eff}}/S^* = 0.9$  can only be achieved when the conductance exceeds  $S^*$  by a factor of 10. If the conductance is very much less than  $S^*$ ,  $S_{\text{eff}}$  is determined entirely by the conductance of the duct and not by the speed of the pump.

**1.3.3 Calculation of gas flow**

**1.3.3.1 Gas flow at pressures from  $10^3$  to 1 mbar**

(i) *Nozzles, apertures, orifices*

In such cases, in view of the short length of the flow channel, friction can be ignored.

If a gas flows from one side of an orifice, aperture or nozzle to the other, by maintaining a reduced pressure on the outlet side then:

$$Q_m = AP_0 \sqrt{\frac{2M}{RT_0}} \left(\frac{P_1}{P_0}\right)^{1/\gamma} \sqrt{\frac{\gamma}{\gamma-1} \left\{ 1 - \left(\frac{P_1}{P_0}\right)^{\frac{\gamma-1}{\gamma}} \right\}}$$

where  $P_0$  and  $P_1$  are the inlet and outlet pressures,  $T_0$  is the inlet temperature of the gas and  $A$  is the area of the orifice/aperture (or the minimum area of a nozzle) and  $\gamma$  is the ratio of specific heat capacities of the gas

$$(C_{p, \text{molar}}/C_{v, \text{molar}})$$

The above equation applies provided that  $P_1$  is greater than a critical pressure ( $P_{\text{crit}}$ ).

$Q_m$  increases as  $P_1$  decreases until a maximum value ( $Q_{m, \text{crit}}$ ) is reached. This occurs when  $P_1$  is equal to  $P_{\text{crit}}$ , given by

$$P_{\text{crit}}/P_0 = \left(\frac{2}{\gamma+1}\right)^{\frac{\gamma-1}{\gamma}}$$

$$Q_{m, \text{crit}} = AP_0 \left(\frac{2}{\gamma+1}\right)^{\frac{1}{\gamma-1}} \sqrt{\frac{2\gamma}{\gamma+1} \frac{M_r}{RT_0}}$$

$$Q_{PV, \text{crit}} = AP_0 \left(\frac{2}{\gamma+1}\right)^{\frac{1}{\gamma-1}} \sqrt{\frac{2\gamma}{\gamma+1} \frac{RT_0}{M_r}}$$

For air ( $\gamma = 1.4$ ), at 20°C,

$$\begin{aligned} Q_{PV, \text{crit}} &= 20AP_0 \text{ mbar l s}^{-1} \text{ (if } [A] = \text{cm}^2; [P_0] = \text{mbar)} \\ &= 15.7d^2P_0 \text{ mbar l s}^{-1} \text{ (if } [d] = \text{cm)} \end{aligned}$$

### (ii) Viscous flow in tubes

When gas flows through a long tube, the effects of internal friction (viscosity) cannot be neglected. Depending on the magnitude of Reynolds number (see earlier in this section), viscous flow can be laminar or turbulent. There is no precise boundary between the two flow regimes. Expressing Reynolds number in terms of  $PV$  throughput, for tubes of circular cross-section, laminar flow exists when:

$$\frac{Q_{PV}}{d} < 1.8 \times 10^3 \eta RT/M_r$$

where  $d$  is the tube diameter and  $\eta$  is the dynamic viscosity of the gas. If:

$$Q_{PV}/d > 3.2 \times 10^3 \eta RT/M_r$$

then the flow is turbulent.

For adiabatic, viscous flow through a tube of length ( $l$ ) and diameter ( $d$ ), where  $ld = 25\text{--}30$ , by making reasonable assumptions it can be shown that:

$$Q = \frac{1}{f} \cdot \frac{\pi^2 d^4 M_r}{16 (ld) RT_1} (P_1^2 - P_2^2)$$

where  $f$  is the flow resistance factor (friction coefficient) and  $P_1$  and  $P_2$  are the inlet and outlet pressures, respectively. For laminar flow in tubes, it can be shown that  $f = 64/Re$ . It can also be shown that:



12 Vacuum Technology and Applications

$$Re = \frac{4M_r}{\pi\eta RT_1} \left( \frac{Q_{PV}}{d} \right)$$

Substituting the values for  $f$  and  $Re$  in the above expression for  $Q_m$  and converting the latter into  $PV$  throughput, we obtain:

$$Q_{PV} = \frac{\pi d^4}{128\eta l} \left( \frac{P_1^2 - P_2^2}{2} \right)$$

For air at 20°C, this reduces to:

$$Q_{PV} = 135 \frac{d^4}{l} \left( \frac{P_1^2 - P_2^2}{2} \right) \text{ in mbar l s}^{-1}$$

where  $[l, d] = \text{cm}$ ,  $[P] = \text{mbar}$

By suitable rearrangement, such equations may be modified to yield expressions for the conductance:

$$C (\text{air, } 20^\circ\text{C}) = \frac{135d^4}{l} \frac{(P_1 + P_2)}{2} \text{ l s}^{-1}$$

For turbulent flow:

$$Q_{PV} = d \left\{ \frac{\pi^2 20}{16 \times 3.2} \frac{d^3 (P_1^2 - P_2^2)}{2l} \right\}^{4/7} \left( \frac{R}{M_r} \cdot T_1 \right)^{3/7} \left( \frac{4}{\pi\eta} \right)^{1/7}$$

For air at 20°C

$$Q_{PV} = 134d \left[ \frac{d^3 (P_1^2 - P_2^2)}{2l} \right]^{4/7} \text{ mbar l s}^{-1}$$

where  $[l, d] = \text{cm}$      $[P] = \text{mbar}$

For tubes with cross-sections other than circular, an important characteristic is the hydraulic radius ( $r_H$ ), defined as:

$$r_H = \frac{\text{Flow cross-sectional area}}{\text{Inner perimeter}}$$

For a duct of circular cross-section,  $r_H = d/4$ . This can be used in the expression for Reynolds number, yielding:

$$Re = 4r_H V \rho / \eta$$

For example, with a tube of rectangular cross-section (height  $a$ , width  $b$ ):

$$Re = 4 (ab/2(a+b)) V \rho / \eta$$

The mass flux ( $Q_m$ ) is given by:

$$Q_m = abV\rho = Q_{PV} \frac{M_r}{RT}$$

From the expression for  $Re$ , this yields, for laminar flow through a rectangular duct:

$$Q_{PV} = \frac{4a^3b^3}{65l\eta(a+b)^2} (P_1^2 - P_2^2)$$

$$[Q_{PV}] = \text{Pa m}^3 \text{ s}^{-1} \text{ if } [a,b,l,m] = \text{m}; [P] = \text{Pa}; [\eta] = \text{kg m}^{-1} \text{ s}^{-1}$$

For turbulent flow, an appropriate expression can be obtained.

### 1.3.3.2 Gas flow under conditions of high- and ultra-high vacua

Under these conditions, the mean free path ( $\bar{l}$ ) for gas particles is considerably larger than the smallest dimension ( $d$ ) of the flow channel. This is denoted as the region of molecular flow and is characterized by  $Kn$  ( $= \bar{l}/d$ )  $> 0.5$ . The implication of this is that gas particles will pass unhindered through an orifice and undergo wall-collisions *only* when passing through a tube. Although molecules would never collide if  $Kn$  was high enough, in some circumstances account must be taken of the fact that a few intermolecular collisions do occur and return particles in the direction from which they came. This can be done by the use of a factor representing the probability of particle transmission ( $\mathcal{P}$ ).

#### (i) Flow through an orifice

If it is assumed that a thin-walled orifice (area  $A = \pi d^2/4$  for a circular hole) separates a region at pressure  $P_1$  from one at lower pressure  $P_2$  then, under suitable conditions, it can be shown that:

$$Q_m = \frac{2A\mathcal{P}\Delta P}{\bar{c}} = Q_{PV} \frac{M_r}{RT}$$

$$\text{or } Q_{PV} = Q_m \frac{RT}{M_r} \text{ where } \Delta P = (P_1 - P_2)$$

Based on the assumption that  $\mathcal{P} = 1$  and inserting appropriate values:

$$Q_{PV} = \left( \frac{2\pi RT}{M_r} \right)^{1/2} \frac{d^2}{8} \Delta P$$

$$\text{or } C_{or} = \left( \frac{2\pi RT}{M_r} \right)^{1/2} \frac{d^2}{8} \left( \text{equivalent to } \frac{\bar{c}A}{4} \right)$$

where  $C_{or}$  is the conductance of an orifice.

If the orifice has a thickness which cannot be ignored (because particles will hit the wall), the above expressions are modified and give:

$$C_{or, \text{thick}} = \bar{c}A/4 \times \left( 1 - \frac{1}{4} \frac{l}{A} \right)$$

for an orifice of circumference  $s$ , area  $A$  and thickness  $l$ .

If the orifice is circular  $C_{\text{or, thick}} = \frac{\bar{c}A}{4} \times \left(1 - \frac{1}{2} \frac{l}{r}\right)$

(ii) *Flow through a long tube ( $l/d \geq 25$ )*

Under suitable conditions (random entrance to the tube by gas particles, diffuse reflectance after wall collisions, etc.), expressions can be obtained for the *PV* throughput and conductance. According to Knudsen, conductance, for example, was given by:

$$\begin{aligned} C_{\text{long tube}} &= C_{\text{Apert}} \times \mathcal{P}_{\text{long tube}} \\ &= \frac{A\bar{c}}{4} \times \frac{16A}{3ls} \end{aligned}$$

where  $A$  = area of tube,  $l$  and  $s$  are the length and circumference, respectively. For a tube of uniform, circular cross-section, this expression becomes:

$$C_{\text{long tube}} = \left(\frac{\pi RT}{18 M_r}\right)^{1/2} \frac{d^3}{l}$$

For long, rectangular ducts (width  $b$ , depth  $a$ ), the appropriate formula reduces to:

$$C = \frac{4}{3} \left(\frac{2RT}{\pi M_r}\right)^{1/2} \frac{a^2 b^2}{31(a+b)} \text{ when } a/b = 1$$

for values of  $a/b < 1$ , the expression must be multiplied by an appropriate factor.

(iii) *Conductance of a short tube*

The equations given above for a long tube have the problem that they predict an infinite conductance if shorter and shorter tubes are considered ( $l \rightarrow 0$ ). Obviously, the conductance should approach that of an orifice ( $C_{\text{or}}$ ). Dushman (1962) overcame the problem by considering a short tube as an aperture, the two sides of which are separated by the length of the tube:

$$\frac{1}{C_{\text{tube}}} = \frac{1}{C_L} + \frac{1}{C_{\text{or}}}$$

This yields:

$$C_{\text{tube}} = \left(1 + \frac{3ls}{16A}\right)^{-1} C_{\text{or}}$$

For a circular aperture, this gives:

$$C_{\text{tube}} = \left(1 + \frac{3l}{4d}\right)^{-1} C_{\text{or}}$$

$$= \left( \frac{2RT}{\pi M_r} \right)^{1/2} \frac{\pi d^3}{s(l+4/3d)}$$

$$= \left( \frac{\pi RT}{18M} \right)^{1/2} \frac{d^3}{l+4/3d}$$

### Example 2 (Use of simplified conductance formulae)

Estimate the effective speed ( $S_{\text{eff}}$ ) of a high-vacuum pump with  $S^* = 2000 \text{ l s}^{-1}$  connected to a vessel by a tube of circular cross-section having  $L = 90 \text{ cm}$  and  $D = 10 \text{ cm}$ . Assume flow is in the free-molecular regime.

For this situation,  $L/D = 9$ .

For a 'short' tube,

$$C = \frac{[\pi RT/18M]^{1/2} D^3}{(L + 4/3 D)} \text{ m}^3 \text{ s}^{-1}$$

For air at  $20^\circ\text{C}$ ,

$$C = [\pi \times 8.314 \text{ (JK}^{-1} \text{ mol}^{-1}) \times 293\text{K}/18 \times 28.95 \text{ g mol}^{-1}]^{1/2}$$

$$\times \frac{(0.1)^3}{(0.9+4/3 \times 0.1)}$$

Note:  $1 \text{ J} = \text{Nm}$ ;  $1 \text{ N} = 1 \text{ kg m s}^{-2} \Rightarrow 1 \text{ kg} = 1 \text{ N m}^{-1} \text{ s}^2$

$$\text{Hence } [\pi \times 8.314 \text{ (JK}^{-1} \text{ mol}^{-1}) \times 293\text{K}/18 \times 28.95 \text{ g mol}^{-1}]^{1/2}$$

$$= [\text{m}^2/\text{s}^2]^{1/2}$$

$$C = [121.19] \frac{\text{m}}{\text{s}} \times (9.68 \times 10^{-4}) \text{ m}^2$$

$$= 0.117 \text{ m}^3 \text{ s}^{-1}$$

$$= 117 \text{ l s}^{-1}$$

---


$$S_{\text{eff}} = S^*(C/S^* + C)$$

$$= 111 \text{ l s}^{-1}$$


---

#### (iv) Curved or bent tubes

In the case of curved tubes with a total axial length  $l$ , it appears that the transmission probability may be taken as that of an equivalent length of straight tube.

The formulae given above for conductance at low pressures are only approximately correct, even for simple cases. This is because the transmission probabilities described may be far too high for a particular arrangement and value of  $Kn$ . Clausing and others (see Van Atta, 1965; Carlson, 1979)

obtained correction factors which must be applied to the simple formulae. In the early 1960s, Davis and collaborators (see references, in Van Atta, 1965) used Monte Carlo methods in order to compute low-pressure conductances. The Monte Carlo calculations gave probabilities in excellent agreement with measured values for simple cases. The accuracy, however, depends on the number of gas molecules under consideration and a great deal of computational time may be required.

Recently, Wanetzky (1989) has presented correction factors for simple geometries in the form of graphs. They are claimed to be quite sufficient for general practical applications.

### 1.3.3.3 Gas flow at pressures from 1 to $10^{-3}$ mbar

In Section 1.3.3.1 (ii), the relationship:

$$Q_{PV} = \frac{\pi d^4}{128\eta l} P_{av} (P_1 - P_2)$$

was obtained for adiabatic, viscous flow. As the pressure is decreased, however, deviations from this expression occur. This is because at lower pressures, the gas adjacent to the tube wall has an appreciable velocity and is not stagnant as was assumed above. Van Atta (1965) referred to this as surface slip and the formula for  $Q_{PV}$  must be modified to take it into account:

$$Q_{PV} = \frac{\pi P_{av}}{L} (P_1 - P_2) \left( \frac{D^4}{128\eta} + \frac{D^3}{16\epsilon} \right)$$

In the modified formula,  $\epsilon$  is a coefficient determining the velocity of gas at the inner wall of the duct.

According to Van Atta, two processes can occur when gas particles interact with a surface:

1. Specular reflection – no ‘drag’ occurs and a uniform distribution of gas velocities across the tube results.
2. Absorption/re-emission occurs, giving a stagnant gas layer adjacent to the walls.

If  $f$  represents molecules interacting by mechanism (2), then a complex expression is obtained for  $Q_{PV}$ :

$$Q_{PV} = \left[ \frac{\pi}{128\eta} P_{av} d^4 + \frac{\pi}{16} \left( \frac{\pi RT}{2M_r} \right)^{1/2} \frac{2-f}{f} d^3 \right] \frac{P_1 - P_2}{l}$$

$$= (c_1 P_{av} d^4 + c_2 d^3) \frac{P_1 - P_2}{l}$$

When  $P_{av}$  is sufficiently high, the term  $c_2 d^3$  is less important than  $c_1 P_{av} d^4$  and the usual, viscous flow expression is obtained. When  $c_1 P_{av} d^4$  and  $c_2 d^3$  are of similar importance, the deviations noted above occur. Eventually,  $c_2 d^3$  dominates.

From the definition of conductance:

$$C = Q_{PV}/\Delta P$$

it can be shown that:

$$C = (c_1 P_{av} d^4 + c_2 d^{-3})/l$$

This means that, depending on the pressure, the conductance of a tube can change significantly.

Treatment of gas flow under conditions when both viscous and molecular flow are present is difficult. This is because  $\epsilon$  cannot be calculated from first principles. Knudsen approached the problem by carrying out appropriate experiments on gas flow (see Van Atta, 1965) for long tubes of constant circular cross-section. His equation can be written (see Wanetzky, 1989):

$$Q_{PV} = \frac{\pi d^4}{128\eta l} \frac{(P_1 - P_2)^2}{2} + \frac{d^3}{6l} \left( \frac{2\pi RT}{M_r} \right)^{1/2} \frac{1 + \left( \frac{M_r}{RT} \right)^{1/2} \frac{d}{\eta} (P_1 + P_2)/2}{1 + 1.24 \left( \frac{M_r}{RT} \right)^{1/2} \frac{d}{\eta} (P_1 + P_2)/2} (P_1 - P_2)$$

In order to give the correct results, the quantities in the above expression must have suitable units. For air at 20°C:

$$Q_{PV} = \left[ 135 \frac{d^4}{l} \bar{P} + 12.1 \frac{d^3}{l} \frac{(1 + 189 \bar{P}d)}{(1 + 235 \bar{P}d)} \right] (P_1 - P_2)$$

where  $[Q_{PV}] = \text{mbar l s}^{-1}$  when  $[d, l] = \text{cm}$  and  $[P] = \text{mbar}$

If a vacuum system is designed to work in this pressure region, calculation of throughput and conductances based on the above may be justified. With high-vacuum systems, however, this region is usually rapidly passed through in the chamber and pipework above the high-vacuum pump. In the fore-vacuum region, however, viscous flow conditions usually apply. With such systems, it may not be worth undertaking these calculations.

## 1.4 Vacuum system characteristics

The characteristics of vacuum pumps, such as pumping speed, ultimate pressure and so on, are dealt with in detail in Section 8.3. Characteristics such as ultimate pressure are also assigned to vacuum systems. For example, the ultimate operational pressure of the system is defined as the lowest pressure that can be obtained after evacuation for a given time. In practice, factors such as the type of vacuum pump and the presence of cold traps are important

but often of even greater influence on the attainable pressure are the gas sources within the system.

In a vacuum plant (see, for example, Figure 1.2), the pressure that may be achieved can be expressed according to the relationship:

$$P_{\text{system, t}} = \frac{Q_{\text{PV,degas}}(t) + Q_{\text{PV,vap}}(t) + Q_{\text{PV,leaks}}(t) + Q_{\text{PV,perm}}(t) + Q_{\text{PV,proc}}}{S_{\text{eff}}(t)} + P_{\text{ult,pump}}$$

where

$Q_{\text{PV,degas}}(t)$  represents the gas flux entering the plant due to desorption (from adsorbed gases) and outgassing (occluded gas)

$Q_{\text{PV,vap}}(t)$  represents the flux due to any volatile material in the system

$Q_{\text{PV,leak}}(t)$  and  $Q_{\text{PV,perm}}(t)$  take into account gas flux due to leaks and permeation

$Q_{\text{PV,process}}$  represents gas release due, for example, to heating or melting etc.

The importance of the individual terms will be discussed later, particularly in Chapter 6. Generally, however, it can be said that the higher the permissible starting pressure for a vacuum process and the lower the evolution of process gas, the more economical becomes the operation of the system. The process gas flux can sometimes be initially very high and may even determine the size of the pumping system selected for a process. It is recommended that to deal most effectively with the actual vacuum process, the sum of plant-related gas flux ( $Q_{\text{leak}}$ ,  $Q_{\text{degas}}$ , etc.) should be only 10% of  $Q_{\text{PV,process}}$ . Gas release has a considerable influence on the ease with which the operating pressure is achieved, particularly the time required to reach the working pressure. This aspect of system operation will now be discussed in detail.

### 1.4.1 Pump-down time

The basic equation for a vacuum system can be expressed as:

$$\begin{aligned} \frac{d(PV)}{dt} &= V \frac{dP}{dt} = Q_{\text{PV,in}} - Q_{\text{PV,out}} \\ &= Q_{\text{PV,in}} - PS_{\text{eff}} \end{aligned}$$

where  $V$  is the volume of the system and  $Q_{\text{PV,in}}$  takes into account all gas sources in the system, including leaks, outgassing, permeation, evaporation, process gases released, etc. For a clean, dry, leak-free vacuum system in which the process is not contributing gas, then:

$$\frac{-dP}{dt} = \frac{S_{\text{eff}}}{V} \cdot P$$

$$\text{or } \frac{S_{\text{eff}}}{V} \int dt = \int \frac{dP}{P}$$

$$\text{or } t = \frac{V}{S_{\text{eff}}} \ln \frac{P_0}{P}$$

where  $t$  is the pump-down time,  $P_0$  is the starting pressure and  $P$  is the required pressure. This equation gives the  $P$  versus time characteristic for the evacuation of the system under conditions where the pump is warm and  $S_{\text{eff}}$  is constant and  $P \gg P_{\text{ult,pump}}$ , where  $P_{\text{ult,pump}}$  is the ultimate pressure that can be achieved by the pump.

In the rough vacuum region, the application of this equation is fairly straightforward, as follows.

### Example 3

A chamber ( $V = 500$  l) is to be pumped down to 1 mbar from atmospheric pressure in 10 minutes using a single-stage oil-sealed rotary vane pump connected directly to the chamber. Assuming the speed of the pump to be constant over the pressure range and neglecting gas sources, what should the speed of the pump be?

$$\begin{aligned} S_{\text{eff}} &= \frac{V}{t} \ln \frac{P_0}{P} \\ &= 2.303 \times \frac{0.5 \text{ (m}^3\text{)}}{\frac{1}{6} \text{ (h)}} \ln \frac{10^3}{1} \\ &= 21 \text{ m}^3 \text{ h}^{-1} \end{aligned}$$

In practice, an additional allowance of 20% would be included and so a pump capable of attaining 1 mbar in 8 minutes would be used. Recalculation then gives  $S_{\text{eff}} = 25.9 \text{ m}^3 \text{ h}^{-1}$

Situations usually arise where the pumping speed is changing markedly with pressure because either more than one type of pump is in use and the pumps are not started simultaneously (see Example 4) or the ultimate pressure of the pump is not negligible in comparison to the pressure in the system.

Consider, first of all, Figure 8.4 (page 313). In the case where the pump is not operating with gas ballast, the pumping speed from atmospheric pressure down to approximately  $10^{-1}$  mbar is constant and independent of pressure ( $S^*_{\text{max}}$ ). At lower pressures,  $S^*$  decreases, due to the effects of back-streaming and internal leakage. This may be expressed as:



$$PS^*(P) = PS^*_{\max} - Q_{PV,in}$$

When  $Q_{PV,in} = PS^*_{\max}$ ,  $S^*(P) = 0$ . This point is reached when  $P$  is  $P_{ult}$  in  $PS^*_{\max}$ . We can now write:

$$PS^*(P) = PS^*_{\max} - P_{ult}S^*_{\max}$$

$$\text{or } S^*(P) = S^*_{\max} - \frac{P_{ult}}{P} S^*_{\max}$$

$$\text{or } S^*(P) = S^*_{\max} \left( 1 - \frac{P_{ult}}{P} \right)$$

If  $S_{eff}$  rather than  $S^*$  is used, then the corresponding expression becomes:

$$S_{eff}(P) = S_{eff,max} \left( 1 - \frac{P_{ult}}{P} \right)$$

Inserting this expression in the basic equation, it can be shown that:

$$P = P_0 \exp \left( - \frac{S_{eff,max}t}{V} \right) + \left( \frac{Q_{PV,in}}{S_{eff,max}} + P_{ult} \right) \left( 1 - \exp \left[ - \frac{S_{eff,max}t}{V} \right] \right)$$

This shows that the pressure in the system decreases exponentially and that after an appropriate interval,  $P_{ult,chamber}$  is obtained:

$$P_{ult,chamber} = P_{ult,pump} + \frac{Q_{PV,in}}{S_{eff}}$$

Obviously, for a clean, dry, leak-free system in which no process gases are produced or required:

$$PV_{in} = 0 \text{ and } P_{ult, chamber} = P_{ult, pump}$$

Finally, solving the equation for  $P$  in terms of  $t$ , the pump-down time required to reduce the pressure from  $P_0$  to  $P$ , yields:

$$t = \frac{V}{S_{eff,max}} \ln \frac{P_0 - P_{ult} - \left( \frac{Q_{PV,in}}{S_{eff,max}} \right)}{P - P_{ult} - \left( \frac{Q_{PV,in}}{S_{eff,max}} \right)}$$

#### Example 4

A clean, dry chamber ( $V = 20 \text{ m}^3 \text{ h}^{-1}$ ) has to be pumped down from atmospheric pressure (1013 mbar) to  $10^{-1}$  mbar by a directly connected pumping set ( $S_{eff} = S^*$ ) consisting of a single-stage, oil-sealed

rotary pump and a Roots pump which is started at 55 mbar. If the leak rate is  $10^{-1}$  mbar l s<sup>-1</sup>, calculate the pump-down time.

The characteristics of the pumping set (Figure 1.3) are as follows:

*Rotary pump*,  $S_{\max} = 250 \text{ m}^3 \text{ h}^{-1}$  ( $69 \text{ l s}^{-1}$ );  $P_{\text{ult}} < 2.5 \times 10^{-2}$  mbar

*Rotary + Roots pump (described as RUTA 1000/2)*

$S_{\max, \text{comb}} = 860 \text{ m}^3 \text{ h}^{-1}$  ( $239 \text{ l s}^{-1}$ );  $P_{\text{ult}} = 2.5 \times 10^{-3}$  mbar

The pumping-speed versus pressure curve on which calculation is based is shown in Figure 1.3. The procedure is as follows:

1. Evacuation to 55 mbar using the rotary pump only.
2. Evacuation from 55 to  $10^{-1}$  mbar using the combination.

(1) Pump-down time from 1013 to 55 mbar.

Rotary pump has a constant speed,  $S_{\max} = 69 \text{ l s}^{-1}$

$P_{\text{ult}}$  is ignored:

$$\begin{aligned} t_1 &= \frac{20000}{69} \ln \frac{1013 - \left(\frac{10^{-1}}{69}\right)}{55 - \left(\frac{10^{-1}}{69}\right)} \text{ s} \\ &= 289.9 \ln \frac{1013}{55} \text{ s} \\ &= 289.9 \times 2.91 \text{ s} \\ &= 14 \text{ min} \end{aligned}$$

(2) Pump-down time from 55 to  $10^{-1}$  mbar. The speed of the combination increases from  $700 \text{ m}^3 \text{ h}^{-1}$  at 55 mbar to  $860 \text{ m}^3 \text{ h}^{-1}$  at  $10^{-1}$  mbar. This is taken into account by using a constant, mean pumping speed of  $780 \text{ m}^3 \text{ h}^{-1}$  ( $216.7 \text{ l s}^{-1}$ ).

$$\begin{aligned} t_2 &= \frac{20000}{216.7} \ln \frac{55 - \left(\frac{10^{-1}}{216.7}\right)}{10^{-1} - (2.5 \times 10^{-3}) - \left(\frac{10^{-1}}{216.7}\right)} \\ &= 92.3 \ln \frac{55}{10^{-1} - (2.96 \times 10^{-3})} \\ &= 92.3 \times 6.3 \text{ s} \\ &= 9.75 \text{ min} \end{aligned}$$

Total pumping time,  $t = t_1 + t_2 = 23.75 \text{ min}$

Increasing by 20% allowance,  $t = 28.5 \text{ min}$

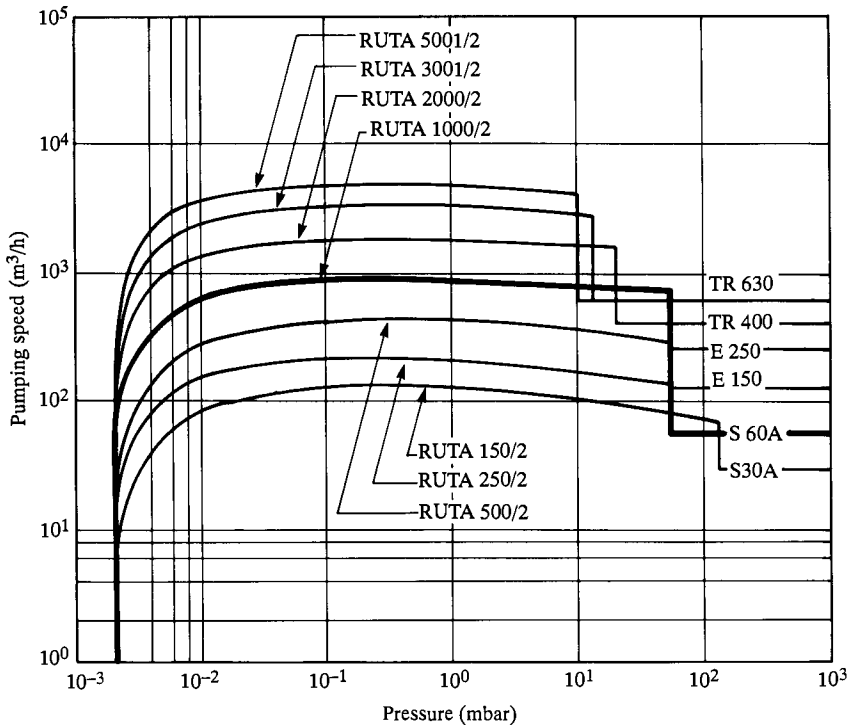


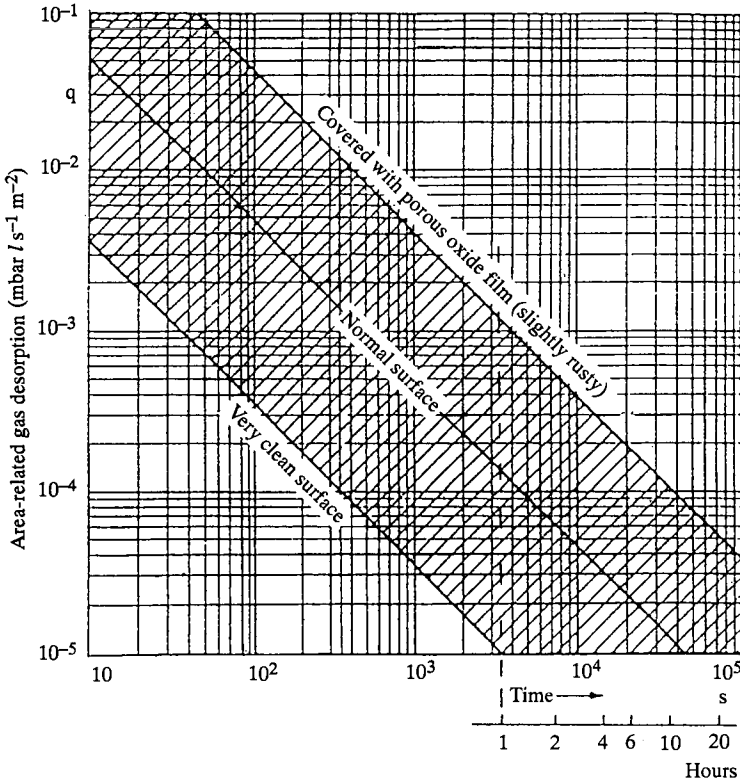
Figure 1.3 Pumping speed curves of two-stage RUTA pump systems

At pressures in the medium- and high-vacuum range, difficulties are encountered when attempting to calculate pump-down. This is because  $Q_{PV,in}$  (the gas load entering the system) may not be constant over the intervals concerned. The reason for this is that  $Q_{PV,in}$  consists of the following terms:

- Leaks:  $Q_{PV,leaks}$
- Degassing from the surfaces:  $Q_{PV,degas}$  where degassing = out-gassing + desorption
- Gas permeation through seals:  $Q_{PV,perm}$
- Gas released during the process:  $Q_{PV,process}$

Certainly,  $Q_{PV,degas}$  decreases with time (Figure 1.4).

In some circumstances, the degassing flux decreases slowly in comparison with the main gas flux pumped from the system and, in such cases,  $Q_{PV,in}$  is split into two terms –  $Q_{PV,in}$  (the constant load entering the system) and  $Q_{PV,degas}$  (which varies with time).



**Figure 1.4** Variation of area-related outgassing with pump-down time for various states of a surface

$Q_{PV,degas}$  is, itself, further subdivided for metals and non-metals but this will be considered in a later section. In practice, an acceptable estimate of the pump-down time can be made if three processes are considered:

1. Removal of gas from the volume of the system ( $t'_1$ ).
2. Removal of material outgassed from metal ( $t'_2$ ).
3. Removal of material outgassed from non-metals ( $t'_3$ ).

A pumping time for each is calculated as if it were the only process occurring and at a constant rate. The total pump-down time is the sum of all three:

$$t = t'_1 + t'_2 + t'_3$$

For example, if a chamber ( $\text{vol} = V$ ) is evacuated from  $P_0$  to  $P$ ,  $t'_1$  can be calculated from the expression:

$$t'_1 = \frac{V}{S_{\text{eff,max}}} \cdot \ln \frac{P_0}{P - P_{\text{ult, chamber}}}$$

$P_{\text{ult, chamber}}$  being obtained from

$$P_{\text{ult, chamber}} = P_{\text{ult, pump}} + \frac{Q'_{\text{PV, in}}}{S_{\text{eff, max}}}$$

$t'_2$  and  $t'_3$  are obtained from the appropriate 'degassing' constants:

$$t'_2 = \frac{A_M K_M}{S_{\text{eff, max}} (P - P_{\text{ult, chamber}})}$$

$K_M$  = area-related degassing constant for the metal

$A_M$  = surface area of the metal surface

$$t'_3 = \frac{A^2 K^2}{S_{\text{eff, max}}^2 (P - P_{\text{ult, chamber}})^2}$$

where  $A$  and  $K$  are appropriate for non-metals.

Degassing from a surface decreases with pumping time (Figure 1.4) and it has been found that a relatively simple formula can be used to describe measured degassing data. If log-log plots of the variation of degassing throughput with time are constructed, most material show (over a limited time) a linear relationship. A simple formula:

$$Q_{\text{PV, degas}} = \frac{a_1 A}{(t/1 \text{ h})^\alpha}$$

describes this behaviour, where  $a_1$  is the degassing rate per unit area after 1 h degassing and  $\alpha$  is a parameter that describes the decay of the outgassing throughput (it is the negative slope of  $\log Q$  versus  $\log t$  plots).  $a_1$  and  $\alpha$  depend not only on the material but also on its pre-treatment. For example, values for  $a_1$  and  $\alpha$  are  $5 \times 10^{-7}$  mbar l s<sup>-1</sup> and 1 for mild steel. For metals and ceramics, this formula is valid for  $t$  between a few seconds and up to 10 hours. For some plastics, the range of linearity is limited.

### Example 5

A metal chamber ( $V = 2 \text{ m}^3$ ;  $A_M = 4 \text{ m}^2$ ) has to be pumped down from 1013 mbar to  $10^{-2}$  mbar by a directly connected pumping set which is identical with that given in Example 4. Gas enters the system at a constant rate of  $5 \times 10^{-1}$  mbar l s<sup>-1</sup> and  $K_m$  has a value of 0.5 mbar l m<sup>-2</sup>.

(1) Pump-down time to 55 mbar:

$$\begin{aligned} t'_1 &= \frac{2000 \text{ l}}{69 \text{ l s}^{-1}} \ln \frac{1013 \text{ mbar}}{(55 - 10^{-2}) \text{ mbar}} \\ &= 29 \times 2.91 \text{ s} \\ &= 84.5 \text{ s} \end{aligned}$$

$$t'_2 = \frac{4 \text{ m}^2 \times 0.5 \text{ mbar l m}^{-2}}{69 \text{ l s}^{-1} \times 55 \text{ mbar}} = 5.2 \times 10^{-4} \text{ s}$$

(2) Pump-down time from 55 to  $10^{-2}$  mbar:

Over this pressure range, assume the speed of the pumping set is relatively constant =  $650 \text{ m}^3 \text{ h}^{-1}$  ( $180 \text{ l s}^{-1}$ ). [700 and  $600 \text{ m}^3 \text{ h}^{-1}$  at 55 and  $10^{-2}$  mbar]

$$t'_1 = \frac{2000}{180} \ln \frac{55 \text{ mbar}}{10^{-2} - (5.2 \times 10^{-3}) \text{ mbar}}$$

$$= \frac{2000}{180} \ln \frac{55}{4.8 \times 10^{-3}}$$

$$= 11.1 \times 9 \text{ s}$$

$$= 100 \text{ s}$$

$$t'_2 = \frac{4 \text{ m}^2 \times 0.5 \text{ mbar l s}^{-1}}{180 \times (4.8 \times 10^{-3})}$$

$$= 2.3 \text{ s}$$

The total pumping time is therefore 191 s (229 s with the appropriate factor).

Obviously, evacuation time is determined by the removal of gas from the volume. Under conditions of high vacuum, however, degassing from surfaces predominates – often to the point that it may be extremely difficult to achieve the required pressure in a given time. The quantity of gas and vapour released by the inner surfaces depends on the area of surface involved and on the amount of gas initially adsorbed. In high-vacuum systems, the pump-down time to a particular pressure is given by the equations already discussed. However, in the equation for  $t'_1$ , the speed of the backing pump should be inserted for  $S_{\text{eff,max}}$  and for pressure  $P$ , the pressure at which the high-vacuum pump is introduced, is substituted.

### Example 6

An empty stainless steel vessel ( $V = 40 \text{ l}$ ,  $A = 0.7 \text{ m}^2$ ) is to be evacuated to  $10^{-7}$  from 1000 mbar by means of a turbomolecular pump ( $S_{\text{eff}} = 200 \text{ l s}^{-1}$ ;  $P_{\text{ult}} = 10^{-10}$  mbar) backed by a two-stage rotary pump ( $S_{\text{eff}} = 5 \text{ l s}^{-1}$ ;  $P_{\text{ult}} < 10^{-3}$  mbar). The required backing pressure for the turbomolecular pump is  $10^{-1}$  mbar. Given that the 'degassing constant' is  $0.5 \text{ mbar l m}^{-2}$  and that the permeation rate is negligible, calculate the pump-down time:

$$t'_1 = \frac{40 \text{ l}}{5 \text{ l s}^{-1}} \ln \frac{1000 \text{ mbar}}{10^{-1}} \quad (P_{\text{ult,backing pump}} \text{ ignored})$$

$$t'_2 = \frac{0.7 \text{ m}^2 \times 0.5 \text{ mbar l m}^{-2}}{200 \text{ l s}^{-1} (10^{-7} - 10^{-10}) \text{ mbar}}$$

$$t'_1 = 1.3 \text{ min}$$

$$t'_2 = 1.75 \times 10^4 \text{ s}$$

$$= 292 \text{ min}$$

$$t = t'_1 + t'_2$$

$$= 293 \text{ min}$$

## References

- Carlson, R.W. (1979) *Vacuum Physics and Technology*, vol 14 of *Methods of Experimental Physics*, (Weissler, G.L. and Carlson, R.W. eds), Academic Press, London, p. 11
- Dushman, S. (1962) In *Scientific Foundations of Vacuum Technique*, 2nd edn, (Lafferty, J.M., ed.) Wiley: New York, p. 91
- Ehrlich, C.D. (1986) *Journal of Vacuum Science and Technology*, A4, 2384
- Van Atta, C.M. (1965) *Vacuum Science and Engineering*, McGraw-Hill, New York, p.23
- Wanetzky, E. (1989) In *Theory and Practice of Vacuum Technology*, (Wutz, M., Adam, H. and Walcher, W. eds) F. Vieweg and Son, Braunschweig/Wiesbaden, p.74

# 2

## *Vacuum pumps (rough–medium range)*

---

### **2.1 General introduction**

A large number of types of pump are available (Table 2.1) for use in vacuum plants in this pressure range and includes steam- and water-operated ejectors, liquid ring pumps, rotary vacuum pumps etc. Factors that influence the choice have been briefly outlined in Chapter 1 but include capacity, reliability and cost.

Vacuum pumps can be classified as either gas-transfer pumps or entrainment pumps, according to their overall pumping mechanism. Gas transfer pumps remove gas particles from the system, compress them in one or more stages and then exhaust the compressed gas either to atmosphere or to other pumps for further compression. Generally, pumps used in the rough–medium vacuum range operate by gas transfer.

Some gas transfer pumps, such as rotary pumps, operate by periodically increasing and decreasing the volume of the pump chamber. Others, such as Roots vacuum pumps, compress, but the volume of the chamber remains constant.

Although this chapter is concerned with pumps that are used in the range  $10^{+3}$  to  $10^{-3}$  mbar, it will be restricted to those used extensively in conventional vacuum technology (rotary pumps, Roots vacuum pumps, ejectors). It excludes a group that operate within the relevant range but produce only moderate vacua (a few hundred mbar). This group, which includes carbon vane pumps and single- and multi-stage side channel blowers, is useful in vacuum transport and mechanical handling but finds little application otherwise.

### **2.2 Rotary pumps**

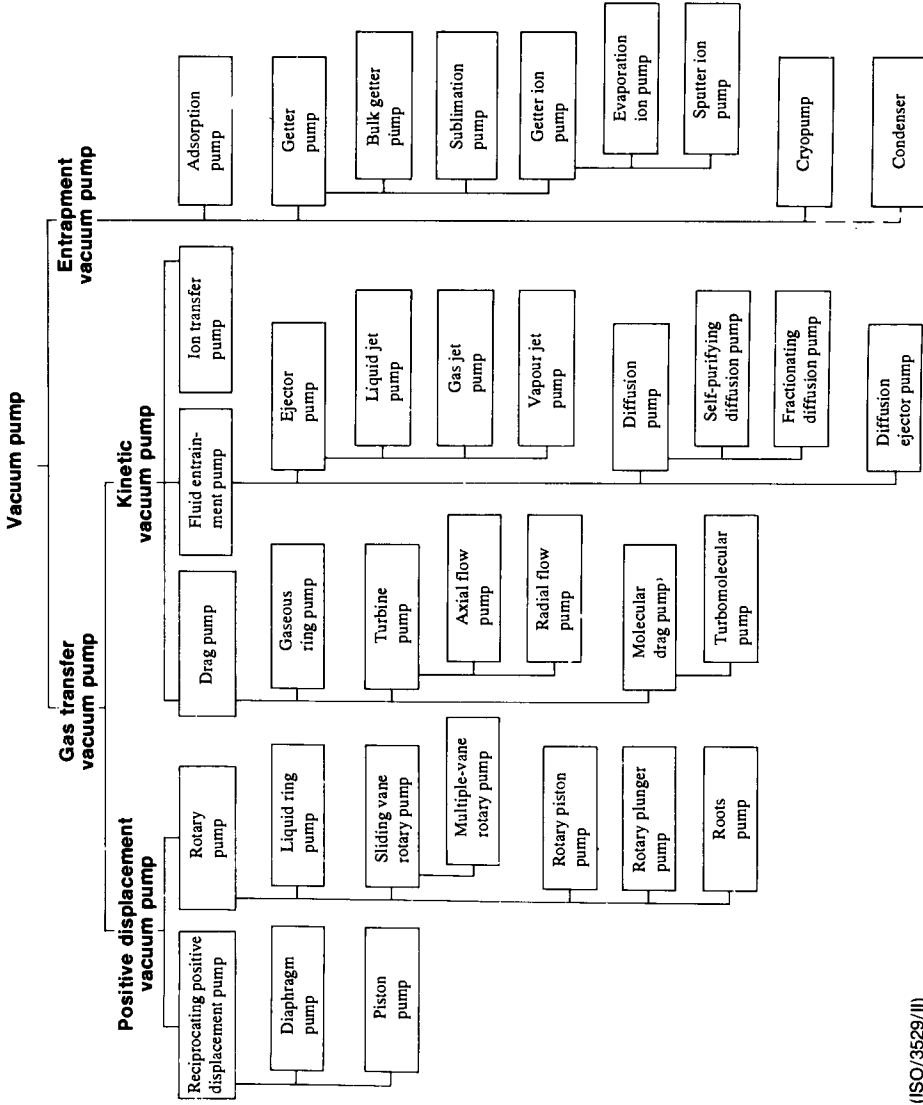
#### **2.2.1 Liquid ring pumps**

Liquid ring pumps are used extensively in processes where large amounts of gases and condensable vapours are to be handled. They are used particularly in the chemical, food, power and general process industries.

The pumps are simple and robust and consist of a vane wheel-type impeller mounted eccentrically within a cylindrical pump casing.

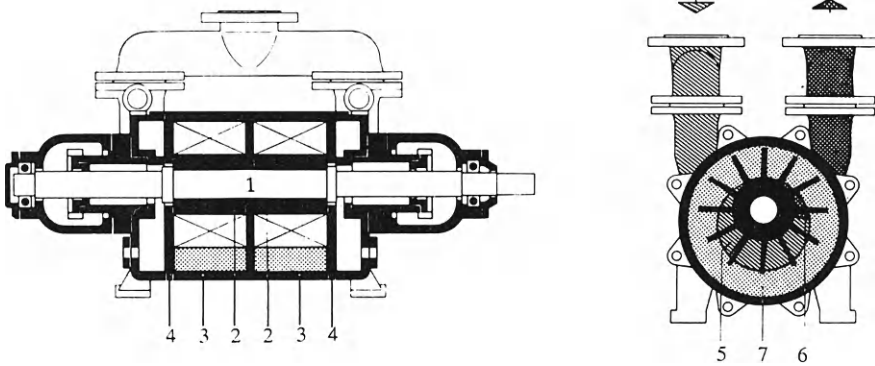
A service liquid (normally water) is continually supplied to the pump and as the impeller rotates the liquid is forced outwards to form a ring that rotates





(ISO/3529/II)

**Table 2.1** Pumps available in vacuum technology



**Figure 2.1** *Diagram showing the working principles of liquid ring pump. 1, shaft; 2, impeller; 3, casing; 4, guide plate; 5, suction port; 6, discharge port; 7, liquid ring. (Reproduced by kind permission of Hick Hargreaves and Co. Ltd.)*

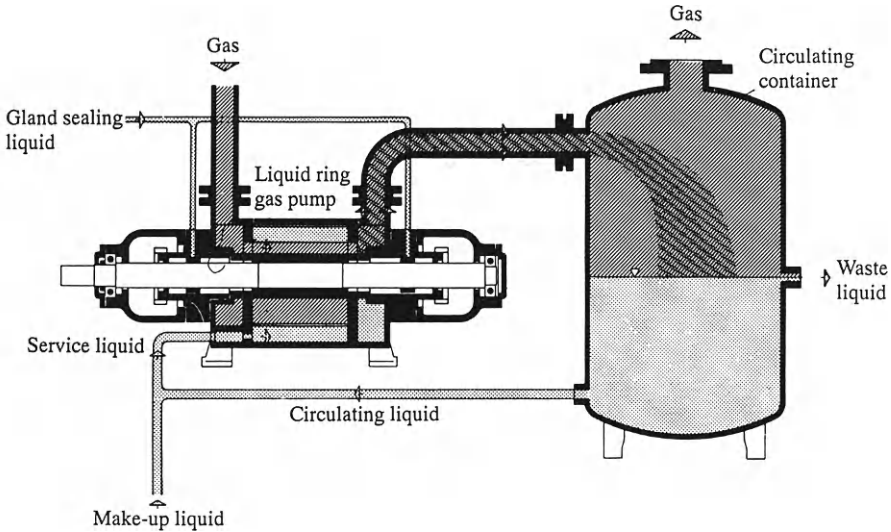
concentrically within the casing. The radially projecting vanes form a series of cells which, in the uppermost position, are completely filled with liquid. With rotation of the impeller, the liquid recedes and gas is drawn through a suction port. As rotation continues, liquid is forced into the cells, thereby compressing the gas that has entered. The gas is discharged through a discharge port, either to atmosphere (single-stage pump) or to a second stage for further compression (two-stage pump).

The service fluid has three functions. It:

1. Absorbs the energy supplied by the motor and transmits it to the gas being compressed.
2. Seals the individual cells.
3. Acts as a heat-transfer medium thus allowing the effective dissipation of the heat of gas compression.

It is normally supplied at a pressure equal to the discharge pressure of the pump. Water at 15°C is usually considered to be the sealant and, in assessments of pump performance, this is often assumed to be the reference situation. Other fluids may be used to suit certain process requirements but in most cases, the design and materials of construction of the pump can be adapted.

During the operation of the pump, warm service liquid is discharged continuously with the pumped gas (Figure 2.2). Downstream, the liquid can be separated from the gas in a separator. Fresh, cold liquid has to be added to maintain the amount and temperature of the fluid in the pump. In some modes of operation, no attempt is made to recover the service liquid. It is discharged to waste. Conservation of liquid can be achieved by partial recirculation (Figure 2.2) with the addition of sufficient cold make-up.



**Figure 2.2** Gas and liquid circulation in a liquid ring pump (Reproduced by kind permission of Hick Hargreaves and Co. Ltd.)

If complete recirculation is to be accomplished, then a heat exchanger has to be incorporated between the separator and the liquid ring pump.

The range of operation of the pump depends on the vapour pressure of the service liquid. With water at 15°C, a one-stage liquid ring pump will evacuate to about 200 mbar. A two-stage pump will operate down to about 30 mbar. Combination pumps (ejectors + liquid ring pumps; Roots pumps + ejectors + liquid ring pumps) will achieve significantly lower pressures.

A general pumping speed vs. inlet pressure curve for a liquid ring pump is shown in Figure 2.3. Although the 'theoretical' volume flow rate (given by the product of the effective pump volume and the rotational speed) is constant, the actual speed falls with decreasing inlet pressure. With liquid ring pumps, at suction pressures below certain limits (Figure 2.3), the onset of a phenomenon known as 'cavitation' may occur. This may cause severe damage to a pump in a relatively short time. Standard pumps are fitted with a manually operated inlet cock which allows atmospheric air to be admitted to the pump inlet, thereby limiting the inlet pressure and preventing cavitation.

The influence of service-fluid temperature on pump performance is shown clearly in Figure 2.4 in the case of water.

### 2.2.2 Rotary vane pumps

Oil-sealed rotary vane pumps are suitable for the direct production of rough (usually less than 80 mbar) and medium vacua. They are also used extensively to back Roots vacuum, turbomolecular and diffusion pumps. Single-stage and

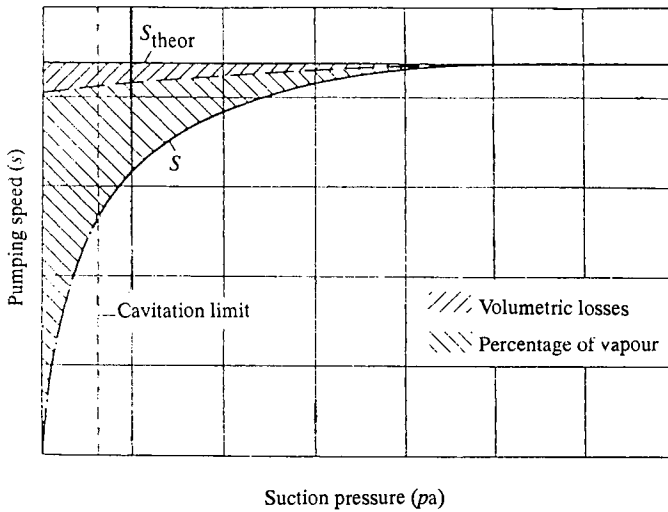


Figure 2.3 Pumping speed against pressure curve for a liquid ring pump

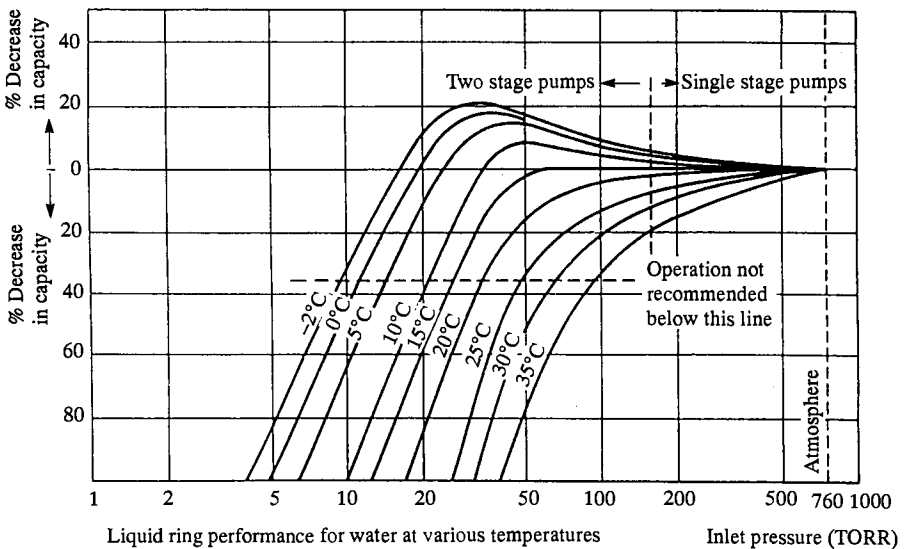


Figure 2.4 The effect of service-fluid temperature on pump performance

two-stage rotary vane pumps with speeds ranging from approximately 2 up to 200 m<sup>3</sup> h<sup>-1</sup> are available from most manufacturers although very large (several hundred m<sup>3</sup> h<sup>-1</sup>), single-stage pumps are also produced.

For general use, involving relatively clean and inert gases, it is not usual to protect the pump in any way. For highly demanding applications, however, in

which dirty, dusty gases, often containing condensable material, or highly corrosive or reactive compounds are used, complex protection devices must be incorporated in the pumping system. Such conditions are found in the semiconductor industry and frequently in metallurgical and chemical engineering applications. These will be discussed in much greater detail in Chapter 7.

Rotary vacuum pumps are essentially gas compressors. An oil-sealed mechanical pump isolates, with each revolution, a sample of gas which is then compressed and either passed on to a second stage for further compression or expelled via the exhaust valves. Oil sealing allows compression ratios (defined as  $p_{\text{outlet}}/p_{\text{inlet}}$ ) as high as  $10^{+5}$  or  $10^{+6}$  to be achieved.

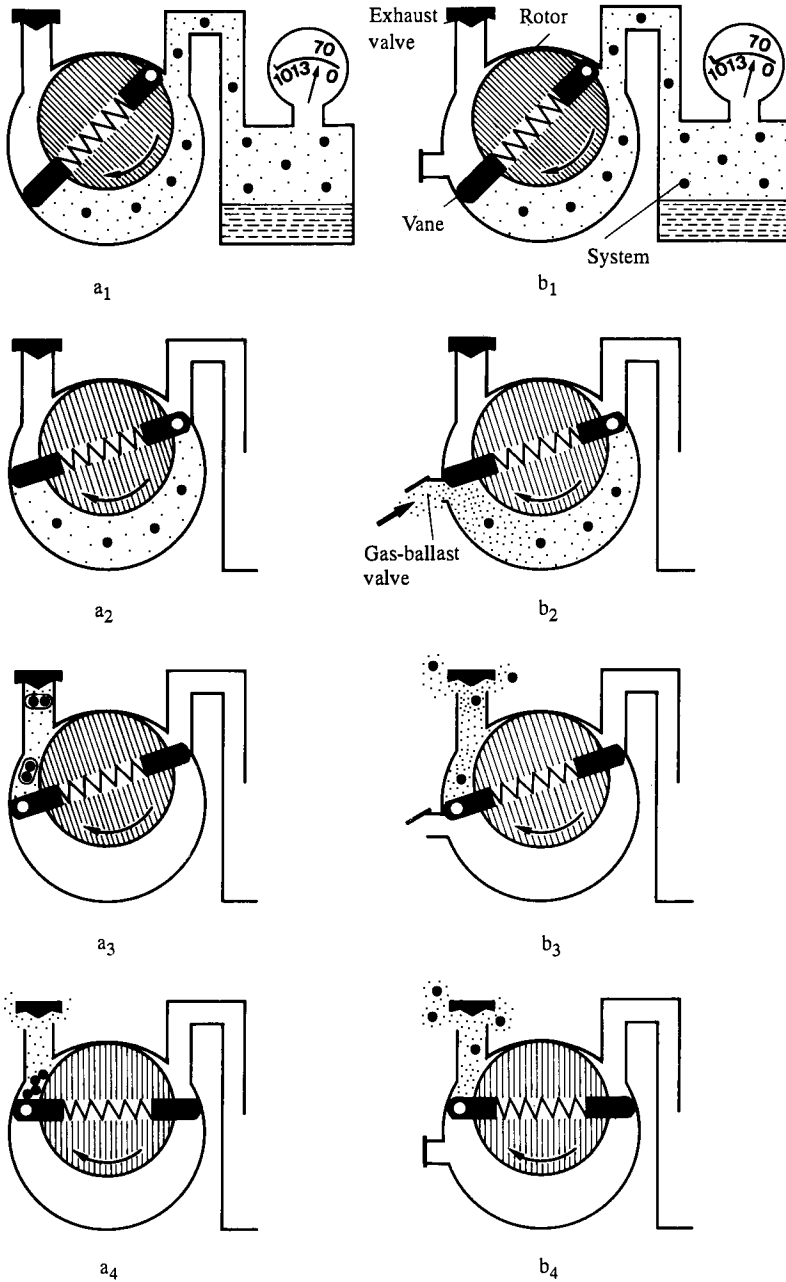
The pumping process is shown in Figure 2.5 (a<sub>1</sub>–a<sub>4</sub>) and (b<sub>1</sub>–b<sub>4</sub>). The details are as follows:

- (a<sub>1</sub>) The pump is connected to a system containing gas and vapour.
- (a<sub>2</sub>) Gas/vapour within the pump is isolated from the system and compression begins.
- (a<sub>3</sub>) Gas/vapour is compressed to a pressure just below that required to open the exhaust valve. During compression there is a danger that vapour may condense to form droplets of liquid.
- (a<sub>4</sub>) Compression has reached an extent (about 1.3 bar) where the exhaust valve opens and gas is expelled.
- (b<sub>1</sub>–b<sub>4</sub>) show the same process involving a pump fitted with a gas-ballast device. This sequence will be discussed later.

In Figure 2.5, gas from the system is compressed and expelled in one cycle. This is a single-stage pump. In a two-stage pump, instead of being expelled, compressed gas passes to a second stage for further compression. Lower working and ultimate pressures are produced by two-stage rotary pumps in comparison with the single-stage versions (Table 2.2).

Figures 2.6–2.8 show in much greater detail the construction of a modern two-stage rotary vane vacuum pump. Within the pump body, there is an eccentrically-mounted rotor driven by the motor. The rotor is fitted with radially sliding vanes which are in contact and therefore forced against the inner wall of the pump chamber. A film of oil provides the internal sealing. These form a working chamber which has a crescent-shaped cross-section. At the appropriate point of the cycle (Figure 2.5a<sub>1</sub>–a<sub>4</sub>), gas is drawn through the intake port by the increasing volume of the working space. Further rotation causes the inlet to be isolated from the pump chamber by the vanes. Thereafter, the volume of the working space begins to decrease and the gas is compressed. In one-stage pumps it is compressed to a pressure (about 1.3 bar) which will open the exhaust valves. In the two-stage pump, instead of being exhausted to the atmosphere, gas from the first stage is passed directly to the second stage where further compression takes place.

In the pump described, oil is taken from the reservoir and circulated within the structure using a gear pump. This ensures the efficient dissipation of the heat of compression of the gas through forced/natural convection at the

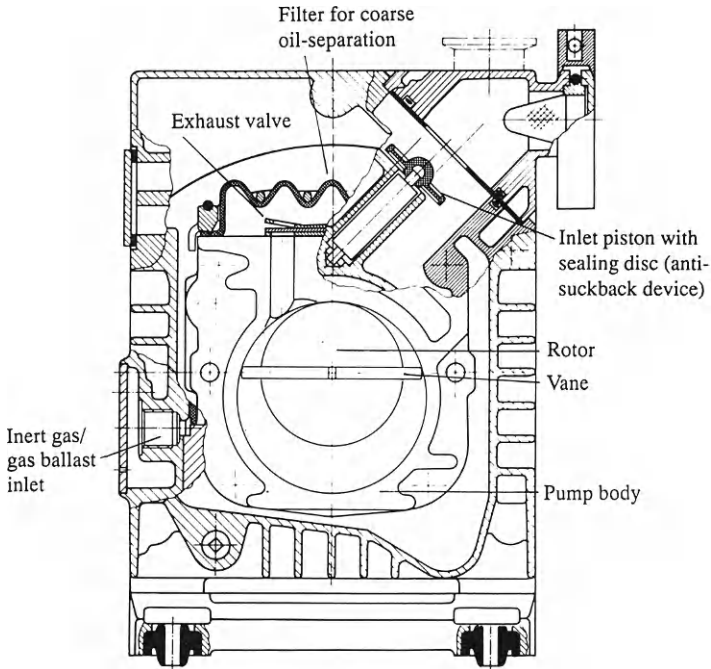


**Figure 2.5** Schematic diagram of the pumping process in a rotary vane pump, with gas ballast (*b<sub>1</sub>-b<sub>4</sub>*) and without gas ballast (*a<sub>1</sub>-a<sub>4</sub>*)

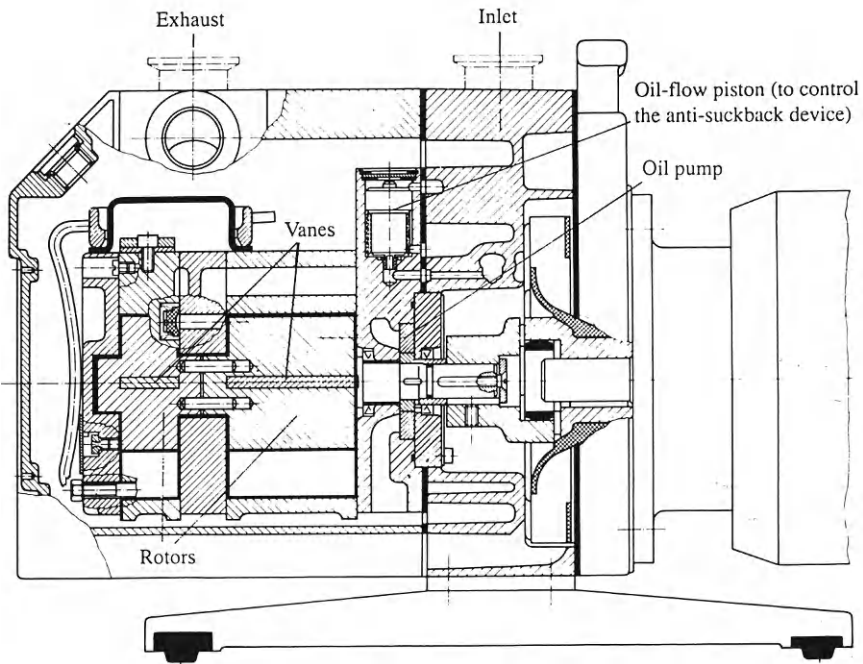
**Table 2.2** Comparison of the ultimate pressures produced by single- and two-stage rotary vane pumps

Type:	S4B	D4B	S8B	D8B	S16B	D16B	S25B	D25B
Ultimate partial pressure (without gas ballast) (mbar)	$< 4 \times 10^{-2}$	$< 1 \times 10^{-4}$	$< 4 \times 10^{-2}$	$< 1 \times 10^{-2}$	$< 2.5 \times 10^{-2}$	$< 1 \times 10^{-4}$	$< 2.5 \times 10^{-2}$	$< 1.10^{-4}$
Ultimate total press (with gas ballast) (mbar)	$< 10^0$	$< 5 \times 10^{-3}$	$< 10^0$	$< 5 \times 10^{-3}$	$< 6.5 \times 10^{-1}$	$< 5 \times 10^{-3}$	$< 6.5 \times 10^{-1}$	$< 5 \times 10^{-3}$

D = Two-stage; S = Single stage.

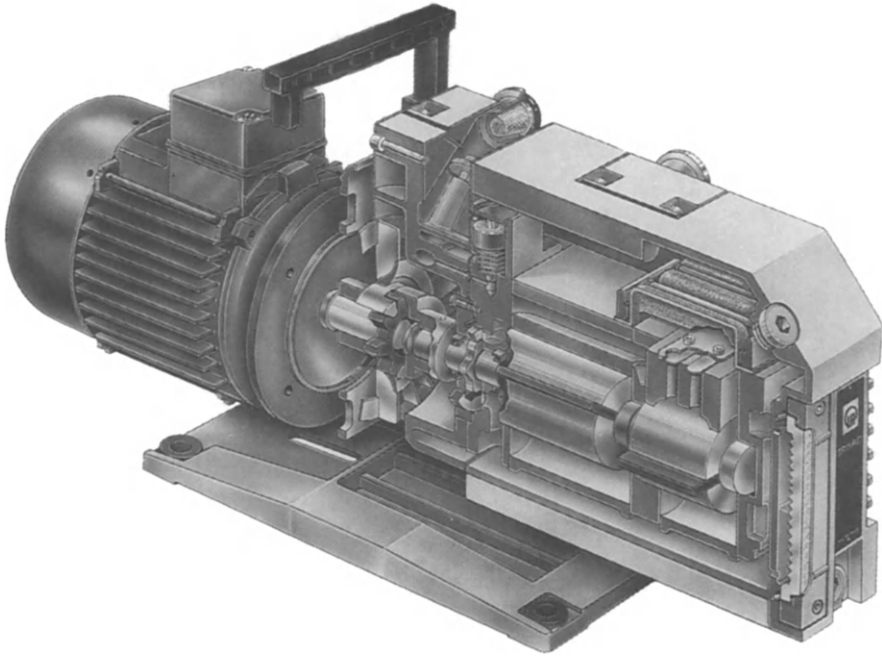


**Figure 2.6** Cross-section of a two-stage, oil-sealed rotary vane pump



**Figure 2.7** Cross-section of the side elevation of a two-stage rotary vane pump





**Figure 2.8** *Cut-away diagram showing a basic two-stage oil-sealed rotary vane pump (Leybold Trivac D25B)*

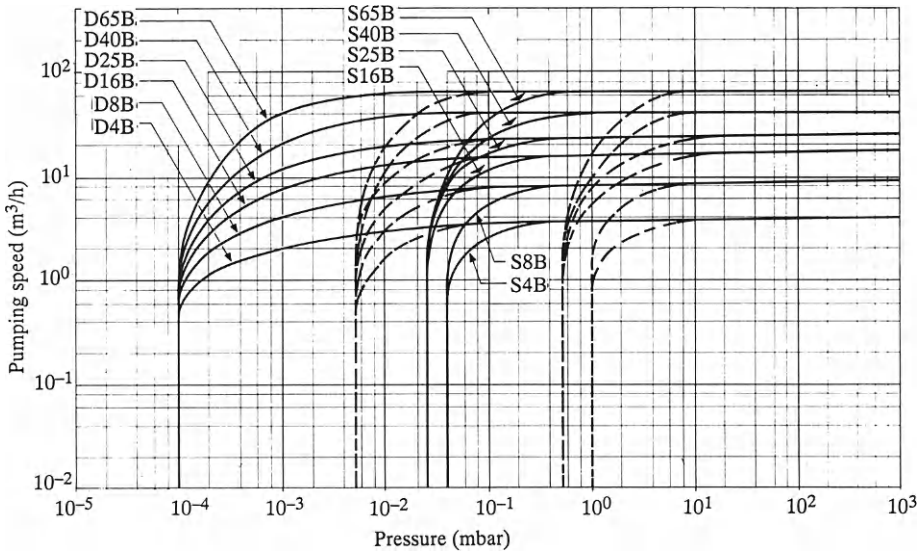
cooling fins. The gear pump can also be used in efficient oil filtration when necessary (see Chapter 7).

The pumping speed–pressure characteristics for a series of single- and two-stage rotary vane pumps are shown in Figure 2.9. From this it can be seen that the pumping speed remains constant from atmospheric pressure to close to the ultimate pressure. Thereafter, there is a very sharp fall in speed. The steepness of this decline indicates the efficiency of the pump. Obviously, a pump that works with full speed over a wide pressure range is superior to one that shows a gradual fall-off.

Figure 2.9 also shows clearly that lower working and ultimate pressures are produced by two-stage pumps in comparison to single-stage pumps. Further, with the gas-ballast valve in operation (see Section 2.2.2.2 Example 1 on the function of this device), the ultimate pressure increases by almost two orders of magnitude. This may be important in certain circumstances. For example, the possibility exists that a ballasted single-stage rotary pump may not achieve a sufficiently low pressure to satisfactorily back a diffusion pump.

#### **2.2.2.1 Function of the oil in oil-sealed vacuum pumps**

The fluid used in oil-sealed mechanical pumps (both rotary vane pumps and rotary piston pumps; see Section 2.2.3) has three functions:



**Figure 2.9** Pumping speed (volume flow rate) against pressure curves for single- and two-stage rotary vane pumps. The prefixes *S* and *D* refer to single- and two-stage pumps, respectively. The numbers refer to the pumping speed of the pump in units of  $\text{m}^3 \text{h}^{-1}$ . Thus *D16B* refers to a two-stage pump with  $S^* = 16 \text{ m}^3 \text{h}^{-1}$ . —, without gas ballast; ---, with gas ballast

1. Lubrication (of the bearings and sliding surfaces).
2. Sealing (the oil must form a seal between the vanes or the piston and the walls of the pump chamber).
3. Heat transfer (the heat of gas compression generated in the pump chamber must be dissipated throughout the pump structure).

An oil for use in rotary vacuum pumps must fulfil all these requirements. If it fails or if its function is impaired through chemical, thermal or mechanical interference, then pump performance will decline. These constraints mean that the characteristics of a pump fluid should include:

1. Suitably low vapour pressure.
2. Good thermal stability (to about  $100^\circ\text{C}$ ).
3. Good wetting ability.
4. Good resistance to a range of pumped gases.
5. Some solvent properties.

The sealants/oils that are used in rotary pumps are either *mineral oils* or *synthetic fluids*. Their suitability for this role is established from consideration of properties such as vapour pressure, viscosity (kinematic and dynamic), density, flash point, pour point, etc.

Mineral oils are suitably selected products of oil refineries. A mineral oil suitable for general use in vacuum pumps (for example, Para-B oil; Class ISO VG 100) tends to be composed predominantly of alkanes but small amounts of aromatics and hetero-cyclics are also present. It has good lubricating properties and will allow the attainment of low ultimate pressures. Its chemical resistance, however, is relatively poor, particularly for vigorous oxidants, and its solvent properties for polymers and strongly polar organic media is very low indeed. Typical applications of such fluids are the pumping of air and chemically inert gases, gases and vapours that have low reactivity towards aromatic compounds and/or those compounds with olefinic double bonds, and *some* water vapour. So-called white oil is standard vacuum pump fluid that has been distilled further and treated to remove aromatics, heterocyclics and olefinic material. Removal of these compounds means that white oil can be used for pumping gases and vapours such as halogens, hydrogen halides, Lewis acids ( $\text{AlCl}_3$ ,  $\text{BCl}_3$ , etc.) and halogenocarbons that react readily with multiple bonds.

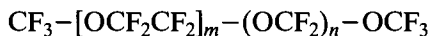
The term 'synthetic fluids' covers a diverse range of material including polyglycol-based oils, polychlorofluorocarbons and the so-called *inert* fluids such as perfluoropolyethers (PFPEs) and fluorosilicone oils. In certain chemical applications (see Chapter 7), for example those in which readily polymerizing compounds such as butadiene or styrene are to be pumped, very specialized sealants such as alkylsulphonic acid ester and dioctyl phthalate are also used. Experience has shown that, over a long period of time, they perform more satisfactorily than cheaper vacuum oils.

Of the so-called inert fluids, the perfluoropolyethers (trade names are FOMBLIN (Montedison), KRYTOX (Du Pont), AFLUNOX, TYRENO) and others are used in various applications. They will not react with many aggressive chemicals including fluorine, chlorine, other halogens and halogen hydrides, nitrogen and sulphur oxides and  $\text{UF}_6$ . They can also be used for pumping oxygen (they can withstand 52 and 6 MPa  $\text{O}_2(\text{g})$  at  $93^\circ\text{C}$  and  $175^\circ\text{C}$ , respectively). When used to pump Lewis acids (for example,  $\text{AlCl}_3$ ,  $\text{FeCl}_3$ ,  $\text{BCl}_3$ , etc.), PFPEs rapidly decompose, however. Conventional PFPEs contain the unit:



and it is the  $\text{O}-\text{CF}_2-$  bond that appears to be susceptible to attack by various chemical compounds.

The introduction of substituents to this basic structure as in:



PFPE - A



PFPE - B (Fomblin Y)

**Table 2.3** Reactivity of some vacuum fluids towards  $\text{AlCl}_3$  (measured by TGA)

Fluid	Onset $T$ ( $^{\circ}\text{C}$ )
Silicone	58
many $(-\text{OCF}_2)-\text{O}-$	72
some $(-\text{OCF}_2)-\text{O}-$	102
fluid containing $-(\text{CFCF}_2\text{O})_n-\text{CF}_2\text{CF}_3$ <div style="margin-left: 100px;"> <math>\begin{array}{c}   \\ \text{CF}_3 \end{array}</math> </div>	142

reduces reactivity by shielding this bond. This is shown in Table 2.3 in which the measured temperature for the onset of depolymerization by  $\text{AlCl}_3$  is given for various fluids.

Bachmann and Kuhn (1990), however, have obtained experimental results for aluminium etching which suggest that there is no real difference between a partially branched PFPE such as Fomblin Y and a significantly branched PFPE such as Krytox.

It should be noted, however, that PFPEs are 60–70 times more expensive than conventional mineral lubricants. Further, they react and form emulsions with mineral oils and scrupulous cleanliness should be observed when changing from one type of fluid to another.

Finally, it should be emphasized that, since the role of the oil is so critical to the performance of oil-sealed vacuum pumps, monitoring of its quality should be carried out regularly and the oil changed when necessary. A precise assessment can be made with, for example, mineral oils by measuring the properties shown in Table 2.4.

Various factors bring about changes in the physical and chemical properties of the lubricant. Premature ageing, for example, indicated by an increased viscosity and the appearance of C–O absorption bands in the infra-red spectrum, may be caused by the operation of the pump at too high a

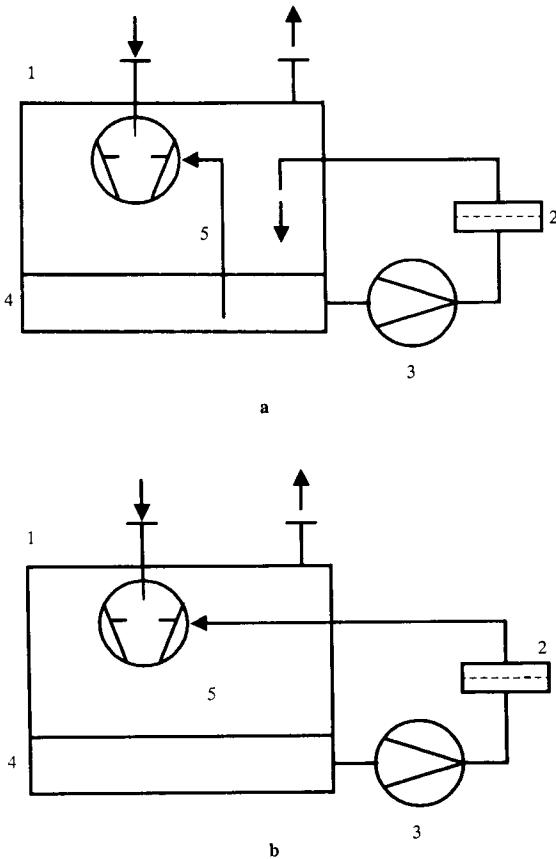
**Table 2.4** Assessment of mineral oil quality

Property measured	Method	Cause of change
Dynamic viscosity	Rotational viscometer	Accumulation of solids
Kinematic viscosity	Capillary viscometer	Ageing
TAN, TBN	Titration	Build-up of anions, cations
IR absorption	IR spectroscopy (400–4000 $\text{cm}^{-1}$ )	Impurities, ageing

IR = Infra-red; TAN = total acid number; TBN = total base number.

temperature. A decrease in viscosity is, with mineral oils, often symptomatic of the occurrence of condensation of oil-soluble vapour within the pump. This may be caused by a defective gas-ballast valve. Elaborate testing is not usually necessary. Routinely, it is usually sufficient to observe regularly the oil in the pump sight-glass in order to ensure that the level and the colour of the oils are correct and not altering rapidly because of decomposition or condensation.

Oil changes are obviously necessary at some stage and delay increases mechanical wear in the pump leading to a higher expenditure on maintenance. Where frequent changes would be necessary due to the nature of the pumped material (gases containing particulates and/or chemically-reactive substances), the situation can be improved significantly by the full- or partial-flow type filters (Figure 2.10). A by-pass filter returns filtered oil to a



**Figure 2.10** Schematic diagram of oil-filtration system for oil-sealed rotary pumps. (a) By-pass oil filter. 1, oil case; 2, oil filter; 3, oil circulation pump; 4, oil reservoir; 5, oil injection into the pump chamber. (b) Full-flow oil filter. 1, oil case; 2, oil filter; 3, oil circulation pump; 4, oil reservoir; 5, oil injection into the pump chamber

reservoir of untreated fluid. With a full-flow system, an oil pump within the vacuum pump forces fluid from the reservoir through the filter. Purified oil then returns, often in the vicinity of the bearings and shaft seals, thereby dislodging any undesirable material that may be accumulating. Oil filters may be of the physical or chemical type. The former act as mechanical filters and remove particulates down to  $7\mu\text{m}$ . Chemical filters consist of activated alumina and adsorb high molecular weight compounds. They also mechanically remove particles with sizes down to  $3\mu\text{m}$ .

### 2.2.2.2 Effects of condensable vapours on mechanical pump performance

A primary mechanical pump removes gas from a system at relatively low pressure and compresses it to approx. 1.3 bar. During compression, vapours that could be present may condense and seriously impair pumping efficiency. Materials of concern are those which have a partial pressure in the system such that, during compression, their saturated vapour pressures at the temperature of the pump would be achieved. Such substances may enter the pump in the vapour phase but would condense during compression.

Condensation affects pump performance in two ways:

1. Condensate leaving the exhaust valve contaminates the fluid in the pump reservoir. Contaminated oil eventually enters the pump and impairs efficiency.
2. Condensed material not leaving the exhaust re-evaporates during subsequent expansion, thereby reducing the pump capacity during the induction phase.

Water is ubiquitous and persistently causes problems in vacuum systems. Other materials, such as benzene, toluene, some organic acids, etc., which are encountered frequently in the chemical industry, will cause problems (see Sections 2.2.2.2.2 and 7.2).

To illustrate the circumstances under which condensation may arise, consider the following example.

#### Example 1

An attempt is made to evacuate a vessel containing an air ( $p = 1\text{ mbar}$ )/water ( $p = 1\text{ mbar}$ ) mixture using an oil-sealed rotary vane pump.

In the vessel, the total pressure of the mixture is 2 mbar. Non-condensable gases would be compressed to the exhaust pressure of the pump (about 1.3 bar) and, under these conditions, the compression ratio of the pump would be given by:

$$K = P_{\text{out}}/P_{\text{in}} = 1300/2 = 650$$

If the condensation of water vapour did *not* occur, then the mixture leaving the pump would consist of a mixture of air

( $p = 1 \times 650 = 650$  mbar) and water ( $p = 1 \times 650 = 650$  mbar). However, at the working temperature of the pump (about 70°C), the saturated vapour pressure of water is about 300 mbar. At this pressure and temperature, gas and liquid can coexist in equilibrium and an increase in pressure results in the formation of increasing amounts of liquid. Obviously, pumping will not occur and no gas will leave the exhaust valve.

Pump manufacturers are aware of the problems associated with pumping vapours and, in order to reduce the likelihood of condensation, they fit gas ballast valves to their pumps. The function of this device is shown in Figure 2.5 (b<sub>1</sub>–b<sub>4</sub>). From this it can be seen that immediately before the start of compression, the ‘gas ballast’ opens and admits gas to the pump chamber. The volume flow rate through the gas ballast is about  $0.1 S^*_{\text{pump}} \text{ m}^3 \text{ h}^{-1}$  and the ballast throughput is related to ambient pressure (about 1000 mbar). The additional gas causes the total pressure in the pump chamber to reach about 100 mbar *before* the start of compression:

$B \approx 0.1 S^* \text{ m}^3 \text{ h}^{-1}$ , where  $B$  is the volume flow rate of the ballast

$$Q_{\text{ballast}} = 0.1 S^* \times P_{\text{ambient}} \text{ mbar l s}^{-1}$$

$$= P_{\text{pump}} \times S^* \text{ mbar l s}^{-1}$$

∴ Pump  $\approx$  100 mbar

This lowers significantly the compression ratio of the pump thereby increasing considerably its ability to pump vapours. This is shown in Example 2.

### Example 2

Consider the circumstances in Example 1. With the gas ballast valve opened to admit ambient air, the following can be established (Table 2.5).

Table 2.5 Example 2

	$P_{\text{air}}$ (mbar)	$P_{\text{water}}$ (mbar)	$P_{\text{TOT}}$ (mbar)
Mixture in Example 1 prior to compression	1	1	2
Mixture prior to compression with gas ballast open	1+96	1+1.9*	99.9

\* Ambient air, at 20°C and 50% RH, contains approximately 1 V% water vapour

$$K \text{ (with ballast)} = \frac{1300}{100} = 13$$

On leaving the exhaust, therefore, the pumped gas has the composition:

$$P_{\text{air}} = 97 \times 13 = 1261 \text{ mbar}$$

$$P_{\text{water}} = 2.9 \times 13 = 37.7 \text{ mbar}$$

$P_{\text{water}}$  is obviously  $\ll 300$  mbar and no condensation will occur.

#### 2.2.2.2.1 Water vapour tolerance of a pump

The PNEUROP definition of water vapour tolerance ( $p_{\text{wo}}$ ) states that it corresponds to the maximum inlet pressure of water vapour that a ballasted pump can transport in continuous operation under normal conditions (20°C, 1013 mbar).

For an oil-sealed rotary pump,  $p_{\text{wo}}$  can be calculated from the expression:

$$p_{\text{wo}} = \frac{B}{S} \cdot \frac{p_{\text{outlet}} (p_s(T) - p_a)}{(p_{\text{outlet}} - p_s(T))}$$

where  $B$  and  $S$  have their usual meanings:

$p_{\text{outlet}}$  = the discharge pressure of the pump (about 1300 mbar)

$p_s(T)$  = saturated vapour pressure of the water vapour at the temperature measured at a specified point in the exhaust section of a steadily operating pump (usually the operating temperature)

$p_a$  = the partial pressure of water vapour in the air introduced as gas ballast.

$$p_a = 13 \text{ mbar for air at } 20^\circ\text{C with } 58\% \text{ RH}$$

According to this, if:

$$B = 0.15 S^*, p_{\text{outlet}} = 1333 \text{ mbar,}$$

$$T = 71^\circ\text{C } (p_s(71) = 325 \text{ mbar})$$

$$p_{\text{wo}} \approx 60 \text{ mbar}$$

Vapour tolerance changes with working conditions. This is shown in Table 2.6.

#### 2.2.2.2.2 Tolerance to other vapours

Although water vapour is the potentially condensable substance most likely to be encountered in general vacuum technology, other vapours may be pumped, particularly in chemical applications. Their effects may be assessed initially by means of Table 2.7.



**Table 2.6** *Effect of changing conditions on water vapour tolerance*

<i>Condition</i>	<i>Effect on water vapour tolerance</i>
Increase in ambient temperature	Increases
Increase in pump temperature	Increases
Increase in amount of permanent gas present in pumped material	Increases
Throttling $Q_{\text{gas}}$ ballast	Decreases
Increase in amount of vapour present in pumped material	Decreases

**Table 2.7** *Effects of vapours other than water on oil-sealed vacuum pumps*

	<i>Pumped substance insoluble in oil</i>	<i>Pumped substance soluble in oil</i>
$T_{\text{pump}} > T_{\text{b.p.}}$	No condensation	No condensation, limited dilution of oil
$T_{\text{pump}} < T_{\text{b.p.}}$	Condensation, emulsion formation	Condensation, unlimited dilution

$T_{\text{pump}}$  = working temperature of pump

$T_{\text{b.p.}}$  = boiling point of pumped substance at the discharge pressure of the pump

Vapour tolerances for substances other than water can be calculated using a more general form of the equation shown in section 2.2.2.2.1.

$$p_v = \frac{B}{S} \cdot \frac{p_{\text{outlet}}(p_{\text{sv}}(T) - p_{\text{v,B}})}{(p_{\text{outlet}} - p_{\text{sv}}(T))} + \frac{p_{\text{sv}}(T) \cdot p_{\text{perm}}}{(p_{\text{outlet}} - p_{\text{sv}}(T))}$$

where  $p_v$  = vapour tolerance

and  $B, S, p_{\text{outlet}}$  have been previously defined

$p_{\text{sv}}(T)$  = saturated vapour pressure of the substance at the operating temperature of the pump

$p_{\text{perm}}$  = the partial pressure of permanent gases at the pump inlet

$p_{\text{v,B}}$  = partial pressure of vapour in ballasting gas

If pure vapour is pumped ( $p_{\text{perm}} = 0$ ) and it is insoluble in oil, then a vapour tolerance  $p_{\text{vo}}$  is obtained which is comparable with  $p_{\text{wo}}$ .

In the calculation of  $p_{\text{v}}$ , there are additional factors that have to be considered. For example, if the pumped substance is soluble in oil, then  $p_{\text{sv}}(T)$  cannot be used in the calculation. What should be used is the partial pressure of the substance in oil at temperature  $T$ . This depends on concentration and its maximum permissible level depends on the design of the pump. If pump oil is used for bearing lubrication, then the allowable limits for dilution are dictated by the physical properties of the oil. If the bearings are separately lubricated, say with grease, the permissible dilution may be higher. Vapour tolerances for a modern gas-ballasted, single-stage rotary vane pump are given in Table 2.8.

**Table 2.8** Vapour tolerances for a rotary vane vacuum pump\*

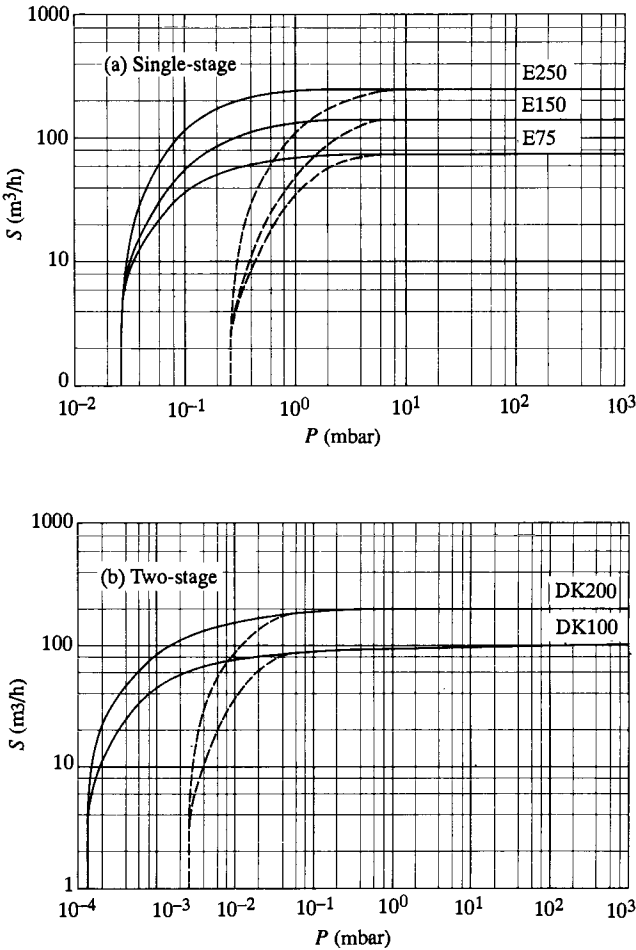
Substance	$P_{\text{vo}}$ (mbar)
Acetic acid	24
Acetone (propanone)	1013
Benzene	63
Ethanol	260
Methanol	1013
Toluene	19
Water	40

\* Leybold S25B, back pressure  $\approx 1013$  mbar; gas inlet temperature = 25°C; pump attained stable operating temperature

### 2.2.3 Rotary piston pumps

Rotary piston pumps (also known as rotary plunger pumps) are used widely in industrial applications to achieve pressures in the rough- and medium-vacuum range. For single-stage pumps, the ultimate partial pressure without gas ballast is approximately  $10^{-2}$  mbar; with gas ballast, the ultimate total pressure is  $10^{-1}$  mbar. Typical applications include vacuum impregnations, drying, extrusion and degassing. Two-stage pumps are used in similar applications. With and without gas ballast, their ultimate pressures are  $10^{-3}$  and  $10^{-4}$  mbar, respectively. Typical pumping speed against pressure curves are shown in Figures 2.11 and 2.12.

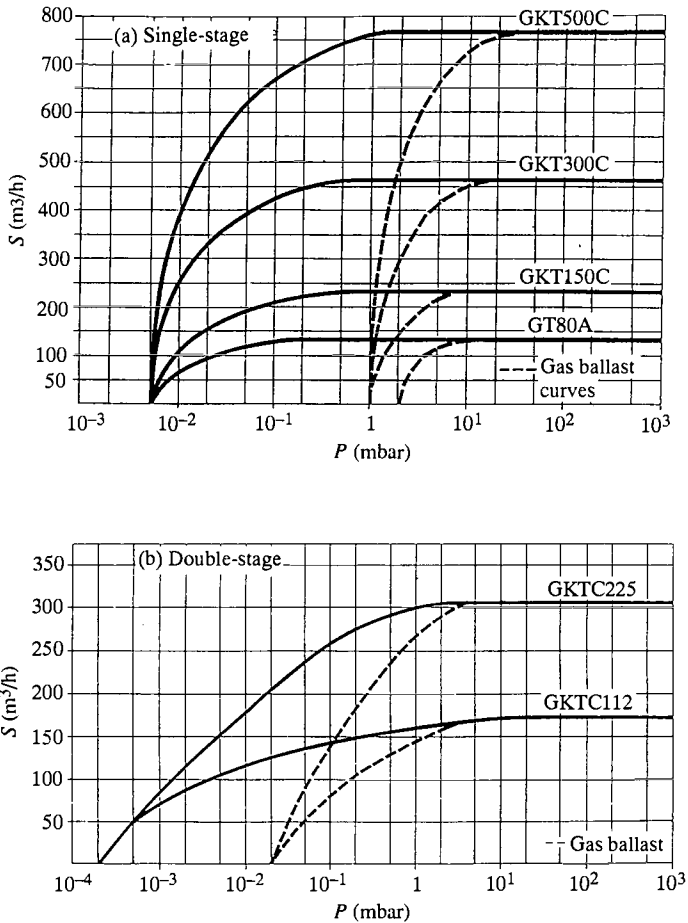
The pumping process in rotary piston pumps is shown in Figure 2.13. Within the pump chamber, a rotary piston with an integral, hollow slide valve, attached to an eccentric rotor, is turned and brings about periodic changes in the volume of the pump chamber. A film of oil between the piston and the chamber provides the sealing. The rotary piston divides the pump chamber into an expansion and a compression space, the volumes of which



**Figure 2.11** Pumping speed against pressure curves for Leybold rotary piston pumps

vary cyclically as the piston moves. As the volume of the expansion space increases, gas from the system being evacuated streams into the pump chamber via the ports in the slide valve. At the same time as gas is entering the expansion space, the volume of the compression space is decreasing, thereby compressing gas induced earlier until it has a pressure high enough to pass through the oil-sealed discharge valve. The slide valve moves freely within a lubricated hinge bar. During each revolution (360°), one working cycle (expansion/induction; compression/discharge) is completed.

A fuller description of the operational cycle of a rotary piston pump is given in Figure 2.14. Further, in this diagram, the function of the gas ballast is exactly as described in Section 2.2.2.2.



**Figure 2.12** Pumping speed against pressure curves for Kinney rotary piston pumps

In a rotary piston pump, clearances between the piston and housing are approximately 0.1 mm. Nearer the hinge box, they are 3–4 times larger. Because these clearances are greater than in vane pumps, piston pumps are much more tolerant of dusts. The supply of oil above the valves in the rotary piston pump has the same function as it does with rotary vane pumps (lubrication, sealing, heat dissipation), and fluids with precisely the same properties in both cases are used.

Powerful drive motors ensure that rotary piston pumps can start efficiently against vacuum at temperatures as low as  $12^\circ\text{C}$ . Under normal conditions, with unrestricted airflow, the operating temperature of a pump is  $50\text{--}70^\circ\text{C}$ . When a pump is operating under heavy load with gas ballast, the temperature is  $70\text{--}95^\circ\text{C}$ .

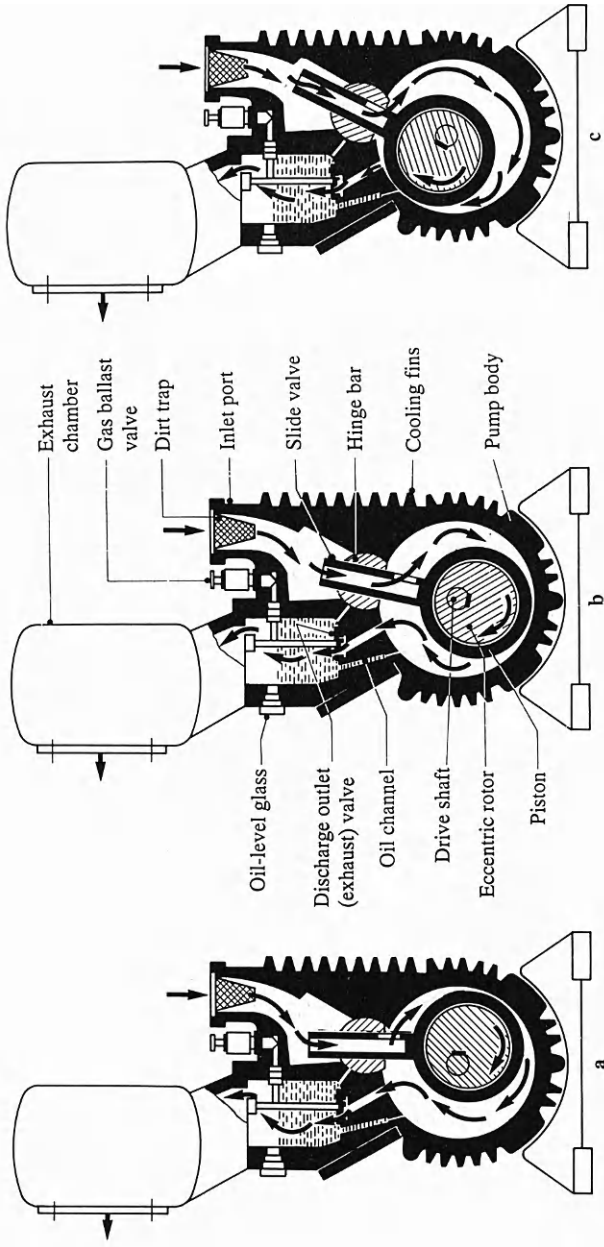
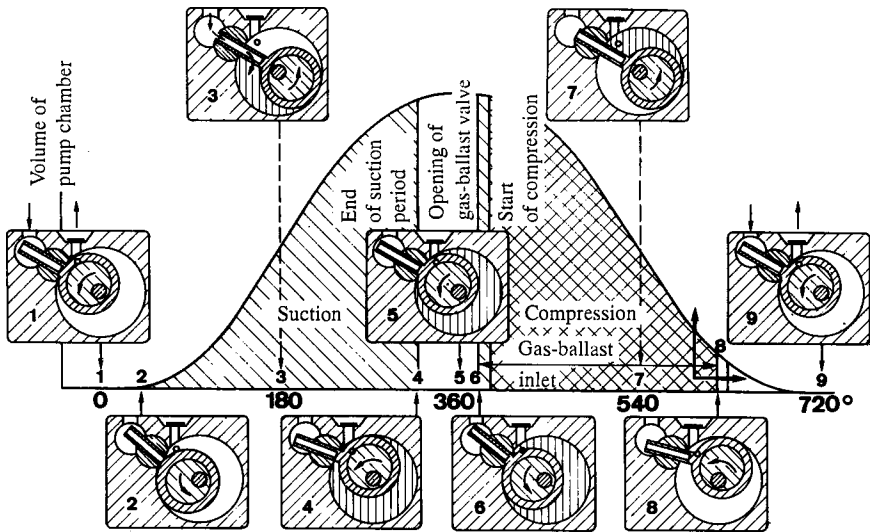


Figure 2.13 Sectional view of the working cycle of rotary piston pumps

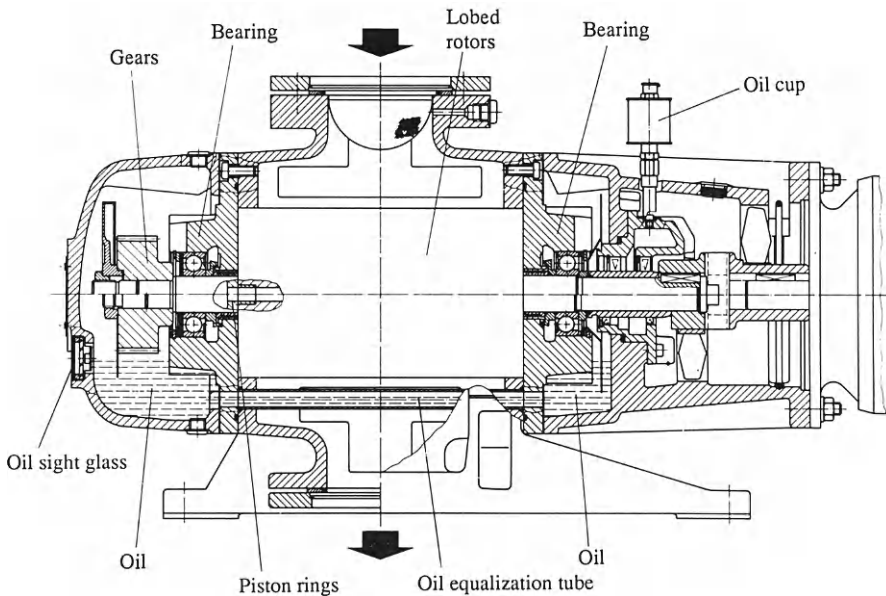


**Figure 2.14** Operation cycle of a rotary plunger pump. Position 1: Top dead point. Position 2: The slot in the suction channel of the slide valve is freed. Beginning of the suction period. Position 3: Bottom dead centre. The slot in the suction channel is totally free. The pumped-in gas (arrow) enters freely into the suction chamber (shown shaded). Position 4: The slot in the suction channel is closed again by the swivelling hinge bar. End of the suction period. Position 5: Top dead point; maximum space between the rotating piston and the stator. Position 6: Shortly before the beginning of the compression period the front surface of the rotating plunger frees the gas-ballast opening. Start of gas-ballast inlet. Position 7: The gas-ballast opening is totally free. Position 8: End of the gas-ballast inlet. Position 9: End of the pumping period

### 2.3 Roots vacuum pumps

Roots pumps are used extensively in vacuum technology. Used in combination with various types of backing pump (liquid ring pumps, oil-sealed rotary pumps), they allow lower pressures and higher pumping speeds in the rough-medium vacuum range to be obtained than can be achieved using primary pumps alone. The rotary vane pump has been found to be the most economical backing unit for a Roots vacuum pump under normal circumstances. When, however, the nature of the pumped material is such that it may adversely affect the fluid in the backing pump then liquid ring pumps are often used. In Section 2.2.1, for example, it was pointed out that, with water at 15°C as the service liquid, a two-stage liquid ring pump will operate down to about 30 mbar. Accordingly, such a pump in combination with a Roots vacuum pump can achieve about 1 mbar. A combination of a liquid ring pump with an air ejector allows lower pressures to be obtained initially (see Figure 2.32) and so a Roots pump plus air ejector plus liquid ring pump can reach a final pressure between 1 and  $10^{-1}$  mbar. Even lower pressures would demand a further Roots vacuum pump.

A longitudinal section of a Roots vacuum pump is shown in Figure 2.15. Within the pump chamber there are two lobed rotors having an approximately figure-of-eight cross-section. They contra-rotate at high speed (about 3500 r.p.m. at full speed). One rotor is driven by the motor while the other



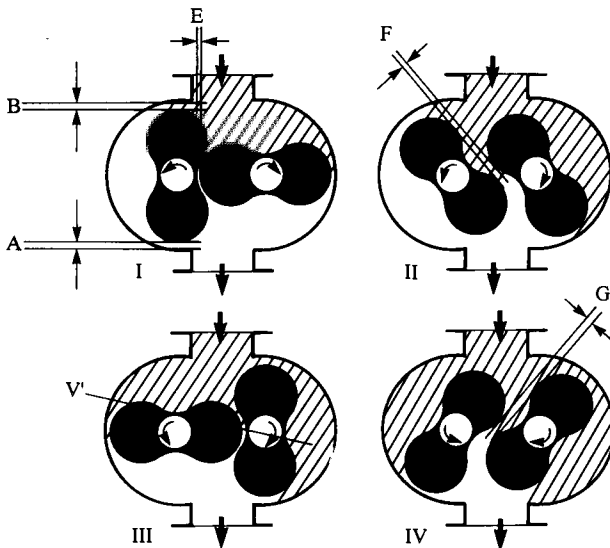
**Figure 2.15** *Longitudinal section of a Roots vacuum pump*

turns via synchromesh gears. The chamber of the pump contains no sealants and internal clearances are relatively large (Figure 2.16). They depend on the size of the pump, of course, and in a small unit ( $S^* 150 \text{ m}^3 \text{ h}^{-1}$ ),  $A = B$  and could be 0.1–0.15 mm and  $E = F = G$  and could be 0.15–0.25 mm. With a large pump, the actual weight of the rotors influences top and bottom clearances. For example, with a  $13000 \text{ m}^3 \text{ h}^{-1}$  pump,  $A = 0.3\text{--}0.4$ ,  $B = 0.85\text{--}0.9$ ,  $E = 0.9\text{--}1.0$ ,  $F = 0.85\text{--}0.95$  and  $G = 0.80\text{--}0.90$  (dimensions in mm).

The absence of sealants within the pump chamber of the Roots vacuum pump makes them attractive in processes where contamination by pump fluids could present problems. Further, since the internal clearances are relatively large, dry dusts may be tolerated.

There are lubricants in Roots vacuum pumps in both the drive- and gear-side compartments as Figure 2.15 shows but in conventional pumps, piston rings prevent penetration into the pumping chamber.

The principle of operation of the Roots vacuum pump is also shown in Figure 2.16. Considering the right-hand side of the pump, as the impellers move from positions I to II, the volume in the pump intake is increased. When the impellers assume the T-position shown in III, a volume of gas ( $V'$ ) is isolated. Further rotation to position IV allows the gas that had occupied  $V'$  to communicate with the pump outlet and it is compressed by gas at backing pressure entering the system. As the impellers rotate, compressed gas is ejected. These events also occur in the left-hand side of the pump at the appropriate moment in the impeller cycle.



**Figure 2.16** Clearances within the pumping chamber of a Roots vacuum pump



This means that the volume of gas displaced in a revolution is given by:

$$V_s = 4 \times V'$$

and  $S^*_{\text{theory}} = 4 \times n \times V'$

where  $n$  = the rotational speed of the impellers.

The throughput of a pump working under these conditions would be:

$$Q_{\text{theory}} = p_{\text{in}} S^*_{\text{theory}}$$

Since Roots vacuum pumps are not oil-sealed, there is internal leakage from the outlet to the inlet of the pump and the amount of gas effectively transported ( $Q_{\text{eff}}$ ) is given by the expression:

$$Q_{\text{eff}} = Q_{\text{theory}} - Q_{\text{int.leak}}$$

By analogy to the expression for  $Q_{\text{theory}}$ ,  $Q_{\text{int.leak}}$  may be given by:

$$Q_{\text{int.leak}} = p_{\text{out}} S_{\text{int.leak}}$$

where the term 'back pumping speed' has been given to  $S_{\text{int.leak}}$ ; (internal leakage = iL, hereafter).

$$S_{\text{iL}} = nV_{\text{iL}}$$

where  $V_{\text{iL}}$  is the volume of the back-streaming gas.

The efficiency of a Roots vacuum pump is defined as:

$$\eta = \frac{Q_{\text{eff}}}{Q_{\text{theory}}}$$

$$\begin{aligned} \eta &= 1 - \frac{Q_{\text{iL}}}{Q_{\text{theory}}} \\ &= 1 - \frac{p_{\text{out}} S_{\text{iL}}}{p_{\text{in}} S^*_{\text{theory}}} \\ &= 1 - K \frac{S_{\text{iL}}}{S^*_{\text{theory}}} \end{aligned}$$

where  $K = \frac{p_{\text{out}}}{p_{\text{in}}} = \text{compression ratio}$

The maximum compression exists at zero throughput and is defined as:

$$K_{\text{o,max}} = \left( \frac{S^*_{\text{theory}}}{S_{\text{iL}}} \right)_{\eta = 0}$$

and applies to air. It is usually measured according to the procedure given in PNEURO P Acceptance Specifications (Part I). This involves attachment of a measuring dome (as shown in Figure 8.1(a)) to the inlet side of the Roots pump. The outlet is connected to the backing pump via a T-piece fitted with a

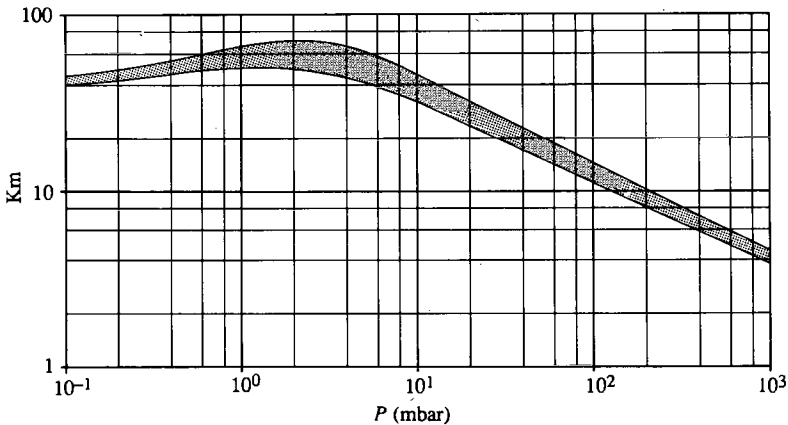
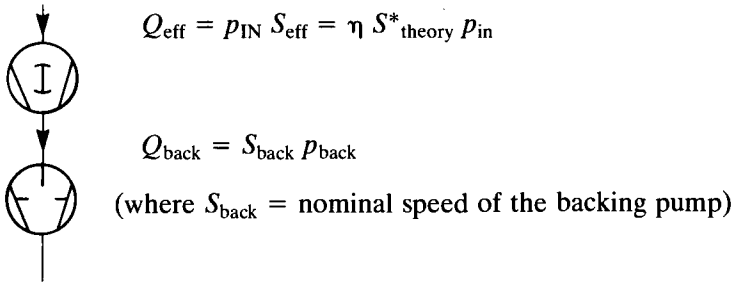
suitable, variable gas inlet valve and a pressure gauge. By varying the amount of gas admitted in the backing line, the pressures in the sealed dome and the backing line are measured with the pump running at normal rotational speed. Thus,  $K_{o,max}$  can be found.

Obviously,

$$\eta = 1 - \frac{K}{K_{o,max}}$$

The variation of  $K_{o,max}$  with outlet pressure is shown in Figure 2.17. The shape of this curve is worthy of comment. The compression ratio for a Roots vacuum pump is limited due to internal leakage and it is easy to explain the increase in  $K_{o,max}$  with decreasing backing pressure in these terms. This increase is not maintained, however, and a maximum value is attained at about 2 mbar. The decrease in  $K_{o,max}$  with decreasing pressure thereafter is a little more difficult to explain and it is believed that, at lower pressures, gas is adsorbed on the impellers when they face the discharge port of the pump and this is desorbed when they face the inlet.

Consider a backed Roots vacuum pump:



**Figure 2.17** Variation with forevacuum pressure of  $K_{o,max}$  for a Roots vacuum pump (reproduced by kind permission of Arthur Pfeiffer Vacuumtechnik Wetzlar GmbH)

Under steady conditions:

$$S_{\text{back}} p_{\text{back}} = \eta S^*_{\text{theory}} p_{\text{in}}$$

since

$$K = \frac{p_{\text{back}}}{p_{\text{in}}}$$

then

$$\begin{aligned} K &= \eta \frac{S^*_{\text{theory}}}{S_{\text{back}}} \\ &= \eta K_{\text{th}} \end{aligned}$$

where  $K_{\text{th}}$  is termed the *gradation*

From the expressions:

$$K = \eta K_{\text{th}}$$

and

$$\eta = 1 - \frac{K}{K_{\text{o,max}}}$$

it can be shown that

$$\eta = \frac{K_{\text{o,max}} - \eta K_{\text{th}}}{K_{\text{o,max}}}$$

or

$$\eta = \frac{K_{\text{o,max}}}{K_{\text{o,max}} + K_{\text{th}}}$$

This formula contains only characteristics of the combination Roots + backing pump. In order to obtain the pumping speed characteristics of a Roots + backing pump combination, the following data must be known:

(i)  $S^*$  theory

$$(= S^*_{\text{nominal}} - x \%(\text{motor losses}) = S^*_{\text{nominal}} - (2.5\% S^*_{\text{nominal}}) )$$

For example, with a Leybold RUVAC WA2000,

$$S^*_{\text{theory}} = 2050 - 2.5\% \approx 2000 \text{ m}^3 \text{ h}^{-1}$$

(ii) The experimentally determined values of  $K_{\text{o,max}}$  as a function of  $p_{\text{back}}$

(iii) The variation of  $S_{\text{back}}$  with  $p_{\text{back}}$

The calculation then proceeds as follows:

1. For each value of Roots pump backing pressure ( $p_{\text{back}}$ ),  $S_{\text{back}}$  can be obtained.
2.  $K_{\text{th}}$  can then be estimated knowing  $S_{\text{back}}$ .

3. Knowing  $K_{o,max}$  for the chosen value of  $p_{back}$ , the volumetric efficiency ( $\eta$ ) can be estimated.
4.  $p_{in}$  for the Roots vacuum pump can be calculated from:

$$p_{in} = p_{out} \frac{S_{back}}{S_{effective}}$$

5.  $p_{in}$  and  $S_{effective}$  yield the pumping speed characteristic of the combination.

### Example 3

Calculate  $S_{eff}$  and the intake pressure for a Roots/backing pump combination (Leybold RUVAC WA 1000 + E75 single-stage rotary piston pump) for backing pressures of 40 and 10 mbar.

*40 mbar*

At this pressure,  $S_{back}^* = 74 \text{ m}^3 \text{ h}^{-1}$  (from characteristic data)

$$S_{theor}^* = 1000 - 2.5\% = 975 \text{ m}^3 \text{ h}^{-1}$$

$$K_{th} = \frac{S_{theor}^*}{S_{back}^*} = \frac{975}{74} = 13.2$$

$$K_o \text{ (from published data)} = 16.5$$

$$\therefore \eta = \frac{K_o}{K_o + K_{th}} = 0.56$$

$$S_{eff} = \eta S_{theor}^* \\ = 542 \text{ m}^3 \text{ h}^{-1}$$

$$\text{and } p_{in} = p_{back} \times \frac{S_{back}^*}{S_{eff}} \\ = 5.5 \text{ mbar}$$

*10 mbar*

$$S_{back}^* = 74 \text{ m}^3 \text{ h}^{-1} \\ K_{th} = 13.2 \\ K_o = 27 \\ S_{eff} = 656 \text{ m}^3 \text{ h}^{-1}$$

$$p_{in} = 1.13 \text{ mbar}$$

Compression of a gas during the pumping process involves the performance of WORK on the gas.

Unless there is some means by which *heat* can flow easily to a *heat sink*, the temperature of the gas increases.

In oil-sealed mechanical pumps, one function of the oil is to transfer heat throughout the pump structure. With Roots vacuum pumps, the rotors are not in immediate contact with the pump housing and they tend to overheat if the *pressure* difference across the pump is too great.

The power required for pumping a gas, according to Noeller (1956) is:

$$W = n \times V_s (P_{out} - p_{in}) \text{ [kW]}$$

(Note 1 watt =  $10^3 \text{ Pa l s}^{-1}$ ; suitable adjustments must be made to the units)

This can be shown to be equal to:

$$S^*_{theory} p_{in} \left( \eta \frac{S^*_{theory}}{S^*_{back}} - 1 \right)$$

From this, there are obviously two ways of limiting the power requirements (i) limit  $p_{in}$  (ii) increase  $S^*_{back}$

In practice, there is a rule-of-thumb regarding the size of the backing pump that indicates that if the working pressure is 1 to  $10^{-2}$  mbar:

$$\frac{S_{Roots}}{S_{back}} \text{ can be } 10 : 1$$

If the working pressure is 1 to 100 mbar, the maximum pressure differential becomes an important factor:

$$\frac{S_{Roots}}{S_{back}} \text{ should be } 4\text{--}5 : 1$$

At low pressures (below 1 mbar), the power required by a Roots vacuum pump is determined mainly by frictional losses in the shaft-sealings, bearings, gears, etc. At higher pressures, however, the power required for pumping is significant.

### Example 4

(a) A Roots vacuum pump ( $S^*_{theory} = 2050 \text{ m}^3\text{h}^{-1}$ ) has to compress gas from 0.5 to 5 mbar. What power is required?

Use  $W = S^*_{theory} \Delta P$

$$S^*_{theory} = 2050 \text{ m}^3 \text{ h}^{-1} = \frac{2050 \times 10^3}{3600} \text{ l s}^{-1}$$

$$\Delta P = 4.5 \text{ mbar} = 450 \text{ Pa}$$

$$\therefore W = \frac{2050 \times 10^3}{3600} \times 450 \text{ Pa l s}^{-1}$$

$$\therefore W = 0.27 \text{ kW}$$

Now, in order to calculate the *total* power consumption, the mechanical losses have to be taken into account:

$$W_{\text{TOT}} = W_{\text{compression}} + \Sigma W_{\text{mech}}$$

The mechanical losses are proportional to  $S_{\text{th}}^*$  and so:

$$W_{\text{TOT}} = W_{\text{compression}} + \text{constant } S_{\text{th}}^*$$

where the constant depends on the type and construction of the pump.

It appears that a suitable expression might be:

$$W_{\text{TOT}} = S_{\text{th}}^* \Delta P + 20\% \text{ kW}$$

The value for  $W_{\text{TOT}}$  in Example 4(a), therefore, should be nearer 0.32 kW.

- (b) A Roots vacuum pump ( $S_{\text{th}}^* = 2150 \text{ m}^3 \text{ h}^{-1}$ ) has to compress air from 100 to 200 mbar. What power is required?

$$W_{\text{comp}} = S_{\text{th}}^* \Delta P$$

$$= \frac{2150 \text{ m}^3 \text{ h}^{-1} \times 10^3 \times 10^2 \times 10^2}{3600} \text{ Pa l s}^{-1}$$

$$= 5.97 \text{ kW}$$

and

$$W_{\text{TOT}} = 5.97 + \frac{5.97}{5} \text{ kW}$$

$$= 7.16 \text{ kW}$$

**Example 5**

A Roots vacuum pump (Leybold WA 2000;  $S_{th}^* = 2000 \text{ m}^3\text{h}^{-1} = 2050 - 2.5\%$  motor losses  $\text{m}^3 \text{h}^{-1}$ ) is backed with a pump having a speed of  $630 \text{ m}^3 \text{h}^{-1}$ . Calculate the power consumption with an inlet pressure of 13.3 mbar.

From the data given, the pressure in the backing line can be calculated:

$$Q_{th} = 2000 \times 13.30 = 630 \times P_{back}$$

$$P_{back} = 42 \text{ mbar}$$

The volumetric ( $\eta$ ) efficiency can also be calculated from the staging ratio ( $S_R$ ):

$$S_R = \frac{S_{th}^*}{S_{back}}$$

$$= \frac{2000}{630}$$

$$= 3.17$$

Note that  $S_R$  may alter as  $P_{back}$  decreases, particularly in the region  $\leq 10^{-1}$  mbar

$$\eta = \frac{Q_{actual}}{Q_{theoret}}$$

$$= 1 - \frac{P_{back} S_{iL}}{P_{in} S_{theor}}$$

$$= 1 - \frac{K_{working}}{K_{o,max}}$$

$K_{o,max}$  can be obtained from published data and at 42 mbar; its value is 18:

$$\text{Therefore, } \eta = 0.85$$

The power consumption for gas compression can now be estimated.

$$W = S_{th}^* p_{in} \frac{\eta S_{th}^*}{S_{back}} - 1$$

$$= \frac{556(1 \text{ s}^{-1}) \times 1330(\text{Pa})}{10^6} \left( \frac{0.85 \times 556}{175} - 1 \right) \text{ kW}$$

$$= 1.26 \text{ kW}$$

The total work expended will be approximately 1.5 kW. A portion of this is dissipated into the pump rotors that heat up and expand.

The temperature rise can be calculated from the expression:

$$\Delta T = T_{\text{inlet, gas}} \times \frac{\gamma - 1}{\gamma} \cdot \frac{p_{\text{back}}^{-1}}{p_{\text{inlet}}^{-1}} \cdot f(T)$$

where  $\gamma = C_p/C_v$ , the ratio of specific heats for the pumped gas (=1.4 for air)

$\eta$ ,  $p_{\text{back}}$  and  $p_{\text{inlet}}$  have their usual meanings

and  $f(T) = 1$  for  $10^2$ – $10^3$  mbar

= 0.5 for 50– $10^2$  mbar

= 0.2 for 1–50 mbar

Experience has shown that the maximum temperature for gas discharge should be  $150^\circ\text{C}$  (this would cause the temperature of the shaft seals to rise to  $80^\circ\text{C}$ ), and  $T_{\text{inlet}} + \Delta T \leq 150^\circ\text{C}$ . Indeed, it may be necessary to chill the inlet gas to prevent this value being exceeded.

To limit the power requirements and to prevent excessive temperature rise, various methods of control are used:

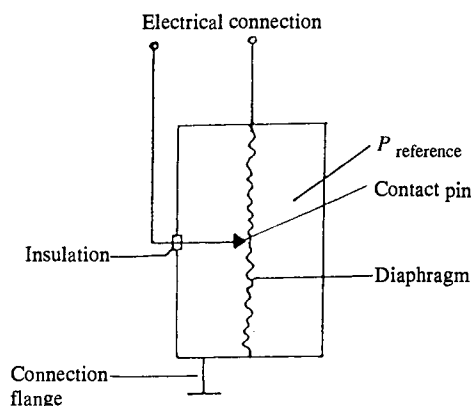
1. Start the booster at low pressures (10–100 mbar) using a pressure switch.
2. Reduce the staging ratio (theoretical booster displacement/actual backing pump speed) by use of a larger backing pump (1:1 may be considered).

### 2.3.1 Pressure-sensitive switch (Figure 2.18)

Roots vacuum pumps can be fitted with a simple control device in the form of a switch that operates at a pre-set pressure. The switch consists of a chamber divided into two compartments by a metal diaphragm. One side of the diaphragm is connected to the inlet of the Roots pump while the other contains gas at a pre-set pressure. A Roots + backing pump system so equipped will pump down initially using only the backing pump. This is because the electrical circuit for the Roots vacuum pump is not complete until the contact pin and diaphragm in the switch are in contact and this depends on the pressure difference across the diaphragm. When the critical pressure has been reached (pre-set according to requirements), deflection of the diaphragm will touch the pin and complete the circuit. The pressure can be set according to a useful rule-of-thumb expression:

$$p_{\text{start}} = \frac{\Delta p_{\text{max}}}{K_{\text{th}} - 1}$$





**Figure 2.18** *Schematic diagram showing the operation of a pressure-sensitive switch*

where  $\Delta p_{\max}$  is the maximum acceptable differential pressure across the Roots pump according to the manufacturer's specifications. For example, with a series of Leybold Roots vacuum pumps, WA 150, WA 250 and WA 2000,  $\Delta p_{\max} = 130, 80$  and  $50$  mbar, respectively.  $K_{\text{th}}$  has its usual meaning and is given by  $S_{\text{th}}^*/S_{\text{back}}$ .

In practice, there are cases in which  $\Delta p_{\max}$  may vary significantly from the manufacturers' published data due partly to the nature of the material being pumped. For example, complex organic molecules have values of  $\gamma$  that are significantly smaller than that of air and this leads to higher values of  $\Delta p_{\max}$  being tolerated.

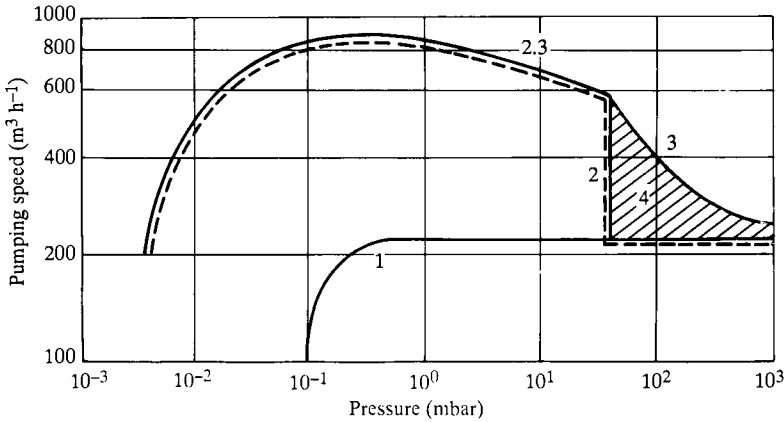
### 2.3.2 By-pass line and pressure relief valve

A Roots pump fitted with a pressure-sensitive switch can be started only after the attainment of a pre-set pressure. Until this has been reached, the backing pumps evacuate the system through the Roots pump. This reduces significantly the effective pumping speed at the chamber. The pumping speed pressure characteristics of such a system are shown in Figure 2.19 (broken curve).

A modification that allows the Roots pump to be started at atmospheric pressure at the same time as the backing pump is shown in Figures 2.20 and 2.21. It consists of a by-pass line and pressure-relief valve that protects the pumps by opening when an excessive pressure exists across the Roots vacuum pump. In Figure 2.19, the curves marked 3 and 2,3 represent the characteristics of a system fitted with a by-pass valve.

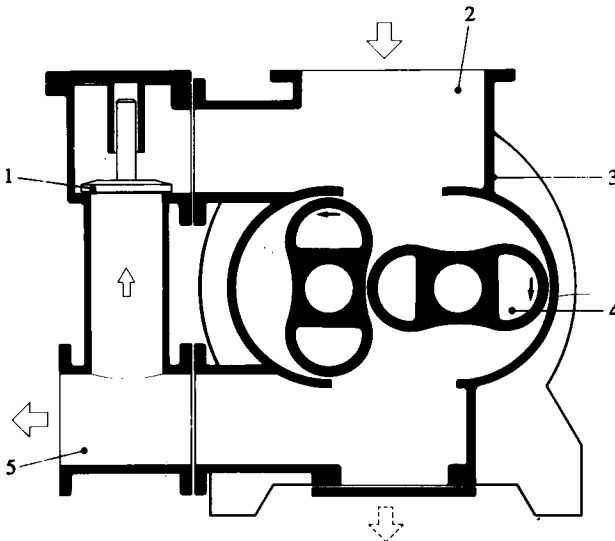
This arrangement is widely used when systems containing Roots pumps operate at high intake pressures. The pressure-relief valve is adjusted so that it opens when  $(p_{\text{out}} - p_{\text{in}})$  exceeds a certain value.

Backflow through the by-pass from outlet to inlet limits the  $\Delta P$  during the early part of pump-down. The by-pass valve closes automatically after the backing pump has brought the pressure difference to a safe level.

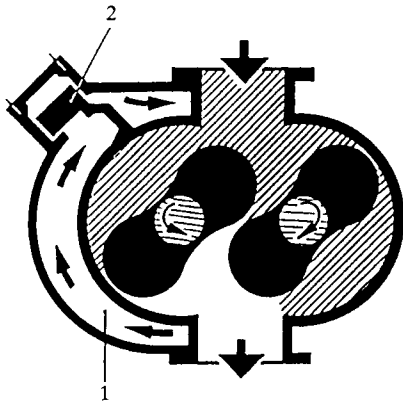


**Figure 2.19** Pumping speed against pressure characteristics for a backing pump and Roots vacuum pump systems.

Curve 1, Speed curve for an oil-sealed backing pump ( $S^* = 250 \text{ m}^3 \text{ h}^{-1}$ ).  
 Curve 2, Speed curve for a conventional Roots vacuum pump ( $S^* = 930 \text{ m}^3 \text{ h}^{-1}$  with  $S^* = 250 \text{ m}^3 \text{ h}^{-1}$ ; starting pressure = 40 mbar). Curve 3, Speed curve for a Roots vacuum pump with integrated by-pass line/valve (maximum pumping speed as in curve 2). Area 4, Gain in speed when using a Roots pump that can be switched on at the same time as the backing pump. Note that the system with the Roots pump gives a high volume flow rate while that of a backing pump is declining.



**Figure 2.20** Roots vacuum pump with by-pass (reproduced by kind permission of Arthur Pfeiffer Vakuumtechnik Wetzlar GmbH) 1, pressure relief valve; 2, inlet; 3, pump housing; 4, rotor; 5, outlet

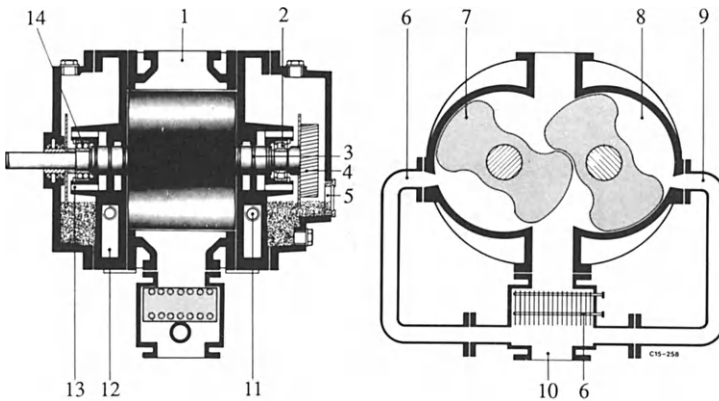


**Figure 2.21** Roots vacuum pump with integrated by-pass line. 1, by-pass line; 2, by-pass valve. In practice the pressure-relief valve and the by-pass line are integrated into the casting for the pump housing

### 2.3.3 Use of a discharge-gas cooler

A further device for extending the acceptable pressure range for continuous operation is the installation of a gas cooler at the outlet port of the Roots vacuum pump.

This is shown in Figure 2.22. The gas cooler is a water-cooled heat exchanger and a small amount of chilled gas is fed back into the pump. This cools the pump in the immediate vicinity of the rotors thereby overcoming the problem of overheating.



**Figure 2.22** Roots vacuum with discharge-gas cooler (reproduced by kind permission of Arthur Pfeiffer Vakuumentchnik Wetzlar GmbH) – 1, inlet; 2, bearing (moveable); 3, labyrinth seal; 4, synchromesh gear; 5, oil sight glass; 6, cooling gas inlet; 7, rotor; 8, pump chamber; 9, gas cooler; 10, pressure connection; 11, sealing gas connection; 12, heating chamber; 13, oil return pipe; 14, bearing (fixed)

### 2.3.4 Control of the speed of the Roots pump

This can be achieved using:

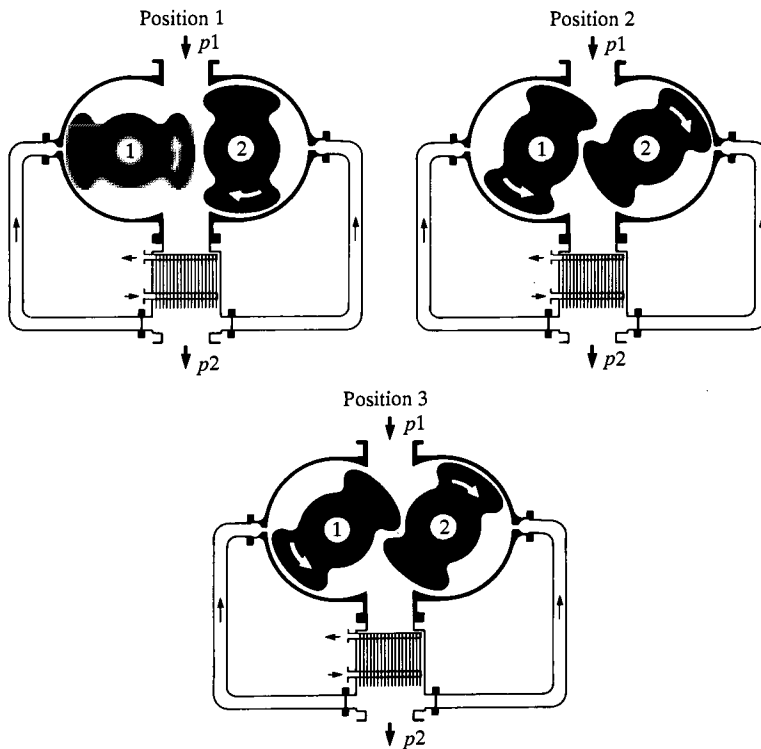
1. Magnetic coupling.
2. Variable frequency motor controller (Heinen and Schwartz, 1986).
3. Fluid coupling – a constant torque transmission mode is normally used.

These systems can be set to run the booster at a speed that is dependent on the load. The pump runs slowly when started at atmospheric pressure and reaches full speed only at low pressures.

Further details of the operation of a gas-cooled pump are shown in the series of diagrams in Figure 2.23.

Considering the left-hand side of the pump:

1. *In position 1* gas flows into the pump but the cold-gas inlet is closed during this phase.
2. *In position 2* the pump intake port is isolated and pumped gas is mixed with cold gas that cools the rotor.



**Figure 2.23** Principle of operation of a Roots vacuum pump with discharge-gas cooler

3. *In position 3* exhausted gas passes through the heat exchanger. Part of the cooled gas is then used to chill the pump.

Because of the resonant gas column in the discharge outlet, silencers are necessary.

## 2.4 Dry vacuum pumps

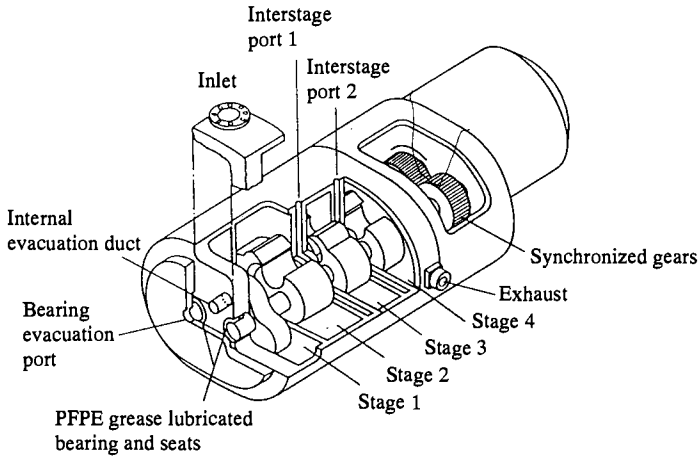
Oil-sealed pumps are sources of potential problems in vacuum systems. Misused or inadequately trapped, they can cause significant contamination. Used on systems containing corrosive gases and/or abrasive particles, the pump fluid is highly susceptible to attack or change unless carefully selected and protected by efficient filters. The cost of maintenance of a PFPE-sealed pump, fitted with complex oil filtration and monitoring systems, is high. Further, since chemically unreactive fluids can dissolve large amounts of hazardous gas, considerable care must be exercised (and significant cost expended) in the handling and disposal of used filters and oil. Partly for this reason and partly because of increasing demands for 'clean' vacua, so-called dry vacuum pumps have been developed in which the gas-handling chamber is free of sealants. Growth in the use of dry pumps has been phenomenal. Hablanian (1991) reported that there were no oil-free primary pumps in use in Japan in 1984 but some 2000 were in use by mid-1989.

Dry pumps, based on various concepts, have evolved over a period of years (Hablanian, 1988). Some, such as the molecular drag pumps, are based on long-established principles, whilst others, such as Vulliez's scroll pump (1974), are based on more recent concepts.

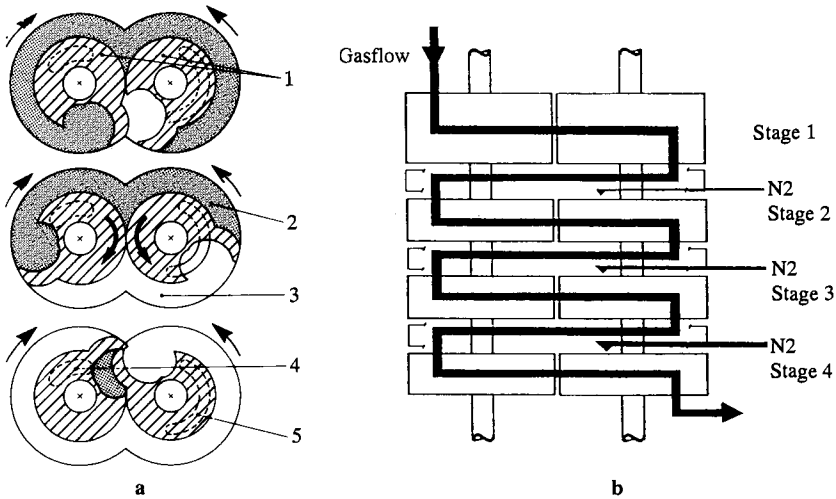
It has already been pointed out that one function of the fluid in oil-sealed pumps is to act as the sealant between the high- and low-pressure sides of the pump. Extremely high compression ratios can be attained in this way; for example, a one-stage, oil-sealed rotary vane pump can easily achieve a compression ratio of  $10^{+4}$ . In the absence of sealants, single-stage compression ratios are much more restricted. With the Roots vacuum pump, Figure 2.17 shows that, over a range of forevacuum pressures, the  $K_{o,max}$  values are significantly below  $10^2$  and may be as low as 10.

### 2.4.1 Roots and claw-type pumps

To achieve acceptably-low inlet pressures whilst compressing against atmospheric pressure, multi-stage dry pumps are available commercially which are based on either Roots-type rotors (Bürger *et al.*, 1990) or claw impellers (see, for example, Berges and Goetz, 1988). A third type has both Roots and claw stages (Wycliff, 1987). A schematic diagram of a Roots/claw-type four-stage pump is shown in Figure 2.24. A schematic diagram of a pump working on the Northey principle (claw-type) is shown in Figure 2.25. The characteristics of some commercially available dry pumps are shown in Table 2.9. All three versions show remarkably similar characteristics.



**Figure 2.24** Diagram showing the components of a four-stage Roots claw-type dry pump (reproduced by kind permission of Edwards High Vacuum International)  
 Stage 1 = Roots; Stages 2, 3, 4 = claw-type rotors



**Figure 2.25** Schematic diagram of pumping principle of a multi-stage, Northey-type claw pump. (a) 1, rotors; 2, compression space; 3, suction space; 4, exhaust slot; 5, suction slot; (b) Stages 1–4 are of the same 'hook and claw' design. An interstage inert gas purge prevents the accumulation of particulates and reactive gaseous material

**Table 2.9** Some examples of dry vacuum pump

Characteristic	LH	Edwards	Ebara	Kashiyama	Unozawa
Pumping speed range ( $\text{m}^3/\text{h}^{-1}$ )	25-500	30-500	58-920	42-1000	66-400
Ultimate pressure (mbar)	$6 \times 10^{-2}$ to $1 \times 10^{-3}$	$3 \times 10^{-2}$ to $4 \times 10^{-4}$	$2 \times 10^{-1}$ to $1 \times 10^{-3}$	$9 \times 10^{-1}$ to $6 \times 10^{-4}$	$8 \times 10^{-2}$ to $4 \times 10^{-4}$
Pumping principle: Basis	Claws (4-stages)	Roots (1x) + claws (3x)	3-lobe-Roots (5x)	Screw (2 rotors)	3-lobe Roots (5x)
System	Claws + Roots	Roots/claws + Roots	Roots (3x) + Roots (3x)	Screw + Roots	Roots (5x) + Roots
Delivery	Vertical	Horizontal	Vertical	Vertical	Vertical

As in conventional Roots pumps, the rotor shafts and timing gears are oil lubricated but rotary shaft seals isolate these areas from the pump chamber. A purge gas such as  $N_2$  may be admitted to the separate stages in order to improve gas flow through the pump. Since they operate at relatively high rotational speeds (about 3000 rpm), water-cooling is necessary to dissipate the heat generated in the bearings, at shaft seals and by gas compression. Details of the claw-only pumps have been given by Berges and Goetz (1988); the Roots-claw-type pump has been described on various occasions (see, for example, Laurenson and Turrell, 1988; Zakrzewski *et al.*, 1988; and Wong *et al.*, 1988).

Experience with dry pumps in demanding applications such as aluminium etching (Bachmann and Kuhn, 1990) indicate that they are reliable and their maintenance costs are low. Possible disadvantages are, however, the cost of water for cooling and the increased consumption (by a factor of 3 compared with a purged vane pump) of nitrogen.

#### 2.4.2 Piston pumps

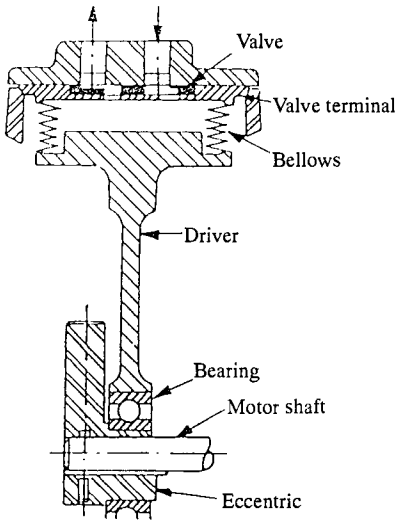
An entirely different approach to dry pumping involves a four-stage reciprocating piston device (Hablanian, 1988; Bez and Guarnaccia, 1990). In the design described by Hablanian, four equal-sized pistons ( $d \sim 10$  cm) operate in a reciprocating manner at approximately 1200 rpm. Each piston/cylinder has a dual valve system and the sliding surfaces are coated with a hard-wearing polymer with a low coefficient of friction. The characteristics of such pumps are similar to single-stage oil-sealed mechanical pumps, and it was reported (Hablanian, 1988) that ultimate pressures of approximately  $10^{-2}$  mbar could be achieved with continuous operation at about 30 mbar. Pumps of this type appear to be available with a very restricted range of pumping speeds.

A design of pump which has found a restricted application in vacuum technology is the metal bellows pump. In such pumps, a flexible bellows (made of stainless steel, for example) is attached to a driver assembly containing a sealed, permanently lubricated bearing (Figure 2.26). An eccentric provides motion for the displacement of the bellows. In a typical pump, the valves are also made of stainless steel with Teflon gaskets and Viton O-rings. Metal bellows pumps have been used to back hydrocarbon-free pumping systems used for cryopump regeneration and a tritium-handling facility (Coffin, 1982).

#### 2.4.3 Molecular drag pump

The precursor of the turbomolecular pump has often been regarded as the Gaede molecular drag pump (Gaede, 1913). The action of this pump is based on directing the motion of gas particles by means of a fast-moving wall facing a fixed wall. The pumping speed is determined by the geometry of the intervening channel and the speed of the moving wall. For a simple drag pump, a zero-flow compression ratio of about  $10^7$  for air is predicted theoretically. Some designs for molecular drag pumps were briefly reviewed





**Figure 2.26** A schematic diagram of a metal bellows pump (reproduced by kind permission of the Parker Hannifin Corporation)

by Van Atta (1965). Friberg (1958) subsequently improved the efficiency of these devices. Later work, including the development of a hybrid TMP-drag pump, was discussed by Maurice (1974) who claimed a zero-flow compression ratio of  $10^8$ .

The molecular drag pump continues to attract attention and Duval *et al.* (1988) have reviewed the characteristics of the drum-type pump. This device consists of a cylindrical rotor (fitted at the top with a bladed impeller) turning at high speed (tens of thousands of rpm) around a coaxial stator consisting of a helically grooved stator. According to theory, the compression ratio of such a pump is a complex function of pump geometry ( $\gamma$ ), drum length ( $l$ ) and velocity ( $V$ ), pressure ( $P$ ), pumping speed ( $S$ ), gas density ( $\rho$ ) and channel geometry:

$$k = e^{\gamma l} + \frac{SP}{\rho} f \left\{ \gamma, l, \text{channel geometry}, V \right\}$$

This formula is complex and a simplified version is:

$$K_0 = e^{\gamma l}$$

where  $K_0$  is the zero-flow compression ratio.

The pumping speed is proportional to the rotational speed of the drum, the cross-sectional area of the stator-rotor channel and the angle of the helical channel on the stator.

The characteristics of the molecular drag pump are interesting in that it has a high compression ratio in the viscous flow range and can operate with full

pumping speed at  $10^{-1}$  to  $10^{-2}$  mbar. A typical commercially available drag pump has a relatively small ( $100 \text{ l s}^{-1}$ ) pumping speed and an ultimate vacuum limited to about  $10^{-7}$  mbar, mainly because of pump outgassing. It will tolerate an inlet pressure in continuous operation of about 10 mbar and an exhaust pressure up to 50 mbar.

Molecular drag pumps have very low pumping speeds at the higher end of their working range. They may, however, be combined with diaphragm or other types of dry pump to give an arrangement that can work between  $10^{-5}$  mbar and atmospheric pressure. An interesting pump combination that can achieve  $10^{-9}$  mbar involves a turbomolecular pump backed by the drag/dry backing pump combination.

#### 2.4.4 Scroll pump

An extremely interesting dry ‘booster’ pump is the metal bellows pump invented by Vulliez (1974). The pump has been used to handle radioactive material such as tritium (Coffin, 1982) but, possibly because of cost and its very restricted speed ( $S_{\text{max}} \sim 5 \text{ l s}^{-1}$ ), the applications have been limited. In the scroll pump, a moving plate with spiral channels is made to oscillate within a stationary plate also with spiral channels. Clearances of about  $10 \mu\text{m}$  are maintained between the spirals. The relative motion of the fixed and moving spirals first traps and then continuously compresses gas until it leaves the device through a valve. A motor-driven crank generates orbital motion at a vertex of an equilateral triangular plate which contains the moving spiral. The moving spiral is connected to the pump body by gas-tight bellows.

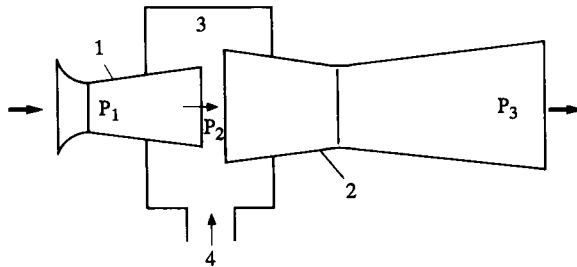
The pump gives a high compression ratio (about  $10^4$ ) at blank-off and, under similar conditions, Coffin reported that the pump achieved  $5 \times 10^{-3}$  mbar with an outlet pressure of 70 mbar. At lower outlet pressures (20 mbar),  $10^{-3}$  was obtained.

## 2.5 Fluid entrainment pumps

### 2.5.1 Introduction

Fluid entrainment pumps represent an extremely useful group of gas transfer pumps. In these ‘kinetic vacuum pumps’ a stream of so-called ‘motive’ fluid, which may be a liquid, vapour or non-condensable gas, is supplied to a nozzle and expands pseudo-isentropically with a resulting very large increase in velocity. If the motive fluid and the gas to be pumped (the ‘suction’ fluid) are mixed, the suction gas particles are entrained and carried towards the pump outlet. If such a device operates under conditions of viscous or intermediate flow, it is called an ejector pump. Under molecular flow conditions, it is a diffusion pump.

### 2.5.2 Ejector pumps



**Figure 2.27** Schematic diagram of an ejector pump. 1, nozzle (Laval nozzle); 2, diffuser (Venturi nozzle); 3, mixing region; 4, connection to vessel

Ejector pumps, such as steam or air ejectors, often in combination with liquid ring pumps, are used extensively for refinery, chemical and other processes in which large quantities of condensable and non-condensable gases are handled.

In an ejector, a steady flow of gas or vapour (inlet conditions  $P_1$ ,  $h_1$  and  $C_1$  where  $P$ ,  $h$  and  $C$  are the pressure, specific enthalpy and velocity, respectively) flows through a nozzle and is accelerated by a pressure drop. For an ideal, frictionless nozzle in which a perfect gas expands adiabatically and reversibly, application of the steady-flow energy equation (see, for example, Eastop and McConkey, 1986) shows that at a section (area  $A$ ) downstream from the inlet, the velocity is:

$$C = \{2(h_1 - h)\}^{1/2}$$

(In most practical applications, the velocity at the inlet is negligible compared with that at the exit.)

The area per unit mass flow,

$$\begin{aligned} \frac{A}{\dot{m}} &= \frac{v}{C} \quad \text{where } v \text{ is the specific volume of the fluid} \\ &= \frac{v}{\{2(h_1 - h)\}^{1/2}} \end{aligned}$$

Since  $h = C_p T$  for a perfect gas:

$$\frac{A}{\dot{m}} = \frac{v}{\{2 C_p (T_1 - T)\}^{1/2}} \quad \text{where } C_p \text{ is the specific heat of the fluid at a constant pressure.}$$

As  $Pv = RT$  and  $(T/T_1) = (P/P_1)^{(\gamma-1)/\gamma}$

$$\frac{A}{\dot{m}} = \frac{RT}{P \left\{ 2C_p T_1 \left( 1 - \frac{T}{T_1} \right) \right\}^{1/2}}$$

if the pressure ratio  $P/P_1 = x$ , then:

$$\frac{A}{\dot{m}} = \frac{RT_1 x^{(\gamma-1)/\gamma}}{P_1 x \{2C_p T_1 (1-x)^{(\gamma-1)/\gamma}\}} = \frac{\text{const.}}{\{(x^{2/\gamma} - x^{(\gamma+1)/\gamma})\}^{1/2}}$$

For a convergent-only nozzle, fluid will attain the speed of sound at the exit when the pressure difference across it is large enough. This is defined as the critical pressure ratio ( $P_{\text{crit}}/P_1$ ) and, for a perfect gas, this is

$$\frac{P_{\text{crit}}}{P_1} = \left( \frac{2}{\gamma+1} \right)^{\frac{\gamma}{\gamma-1}}$$

For a perfect, diatomic gas ( $N_2$ ,  $O_2$ , air),  $\gamma = 1.4$  and this ratio is 0.528.

In a convergent-divergent (Laval nozzle), the section of minimum area is termed the throat. The fluid velocity at the throat of a nozzle operating at its design pressure ratio is the velocity of sound under these conditions. The flow up to the throat is sub-sonic and, after the throat, it is supersonic. Sonic flow requires a diverging duct to accelerate it.

When the gas stream enters the diffuser a process of isentropic compression occurs. Motive fluid and entrained gas is compressed from  $P_2$  to  $P_3$  (see Figure 2.27). During supersonic compression, the reduction in gas volume takes place faster than the velocity decrease. This necessitates a decreasing area. At sonic velocity, these rates are equal and no further reduction is necessary. Beyond this point, a divergent section is required. The maximum exhaust pressure attainable is that for which the flow velocity of the jet is converted completely to random velocity. The design of the diffuser and the inlet conditions must be such that this requirement is fulfilled otherwise the jet will be unable to sustain the pressure differential and will break down.

### 2.5.2.1 Steam ejectors

Large quantities of steam can be generated in the chemical, metallurgical and other industries. If sub-atmospheric pressures are also required (e.g. for distillation in the chemical industry; for degassing in the steel industry), then the use of steam ejectors is extremely convenient. A formula such as that derived earlier for the critical pressure ratio in a nozzle, applies to perfect gases only but, if the expansion of steam in nozzle follows the law  $Pv^k = \text{constant}$  ( $k$  is the approximate isentropic index for steam;  $k = 1.3$  and 1.135 for initially superheated and dry, saturated steam, respectively), then it can be shown that:

$$\frac{P_{\text{crit}}}{P_1} = \left( \frac{2}{k+1} \right)^{\frac{k}{k-1}} = 0.546 \text{ (superheated steam)}$$

and

$$\frac{A}{m} = \frac{v}{\{2(h_1 - h)\}^{1/2}}$$

where the properties of steam can be obtained from tables or an enthalpy-entropy chart.

The compression ratio of steam ejectors is in the range 10 to 20 for inlet pressures below 1 mbar, decreasing to 3 or less in stages that discharge against atmospheric pressure.

For a fixed supply pressure, the consumption of the driving steam increases in proportion to the compression ratio (Mangnall, 1989).

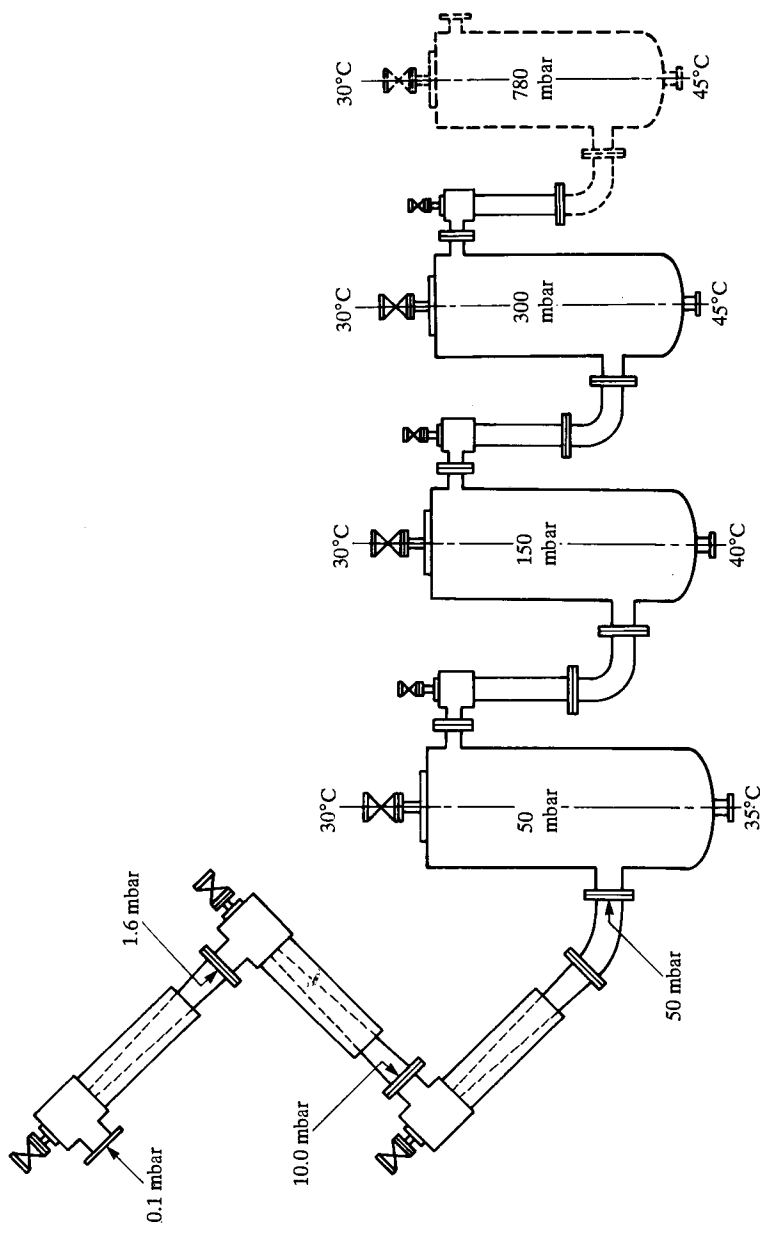
This fact imposes a limit on the use of a single-stage ejector. For example, a steam ejector removing gas at, say, 170 mbar and discharging against atmospheric pressure, has a compression ratio of 6. This can quite easily be dealt with by a single-stage unit. With a suction pressure of 30 mbar, however, the corresponding compression ratio would be in excess of 30. This is beyond the economic range of a single-stage ejector and a multiple stage ejector would have to be used. In Table 2.10, the suction (inlet) pressure as a function of the number of stages is given for steam ejector pumps.

With multi-stage pumps, condensers are placed, if possible, between the stages in order to remove both the motive steam and any condensables which could interfere with subsequent stages. A six-stage ejector system is shown in Figure 2.28. From the diagram, it can be seen that the first stage compresses the pumped fluid to 1.6 mbar. The second stage delivers this to a third ejector at 10 mbar, and so on. There is no condenser between ejectors 1, 2 and 3 since the motive steam cannot be condensed with normal cooling water.

Condensers may be of the spray or jet type or they may be surface condensers. In some chemical applications, the use of surface condensers is precluded because of solidification on the tubes of relatively involatile

**Table 2.10** *Typical values for the suction pressure as a function of the number of stages (\* represents the initial steam pressure) (Noeller, 1989)*

No. of stages	Suction pressure (mbar)	
	> 7 bar*	< 6 bar*
1	100	300
2	30	100
3	4	30
4	0.2	4
5	0.05	0.2
6	0.005	0.05
7	0.001	0.005



**Figure 2.28** Schematic diagram of a six-stage steam ejector pump set with direct contact condensers (Reproduced by kind permission of Hick Hargreaves and Co. Ltd.)

material carried over from the process. When the condensate is either too unpleasant or too valuable to be discharged with the coolant, surface condensers must be used.

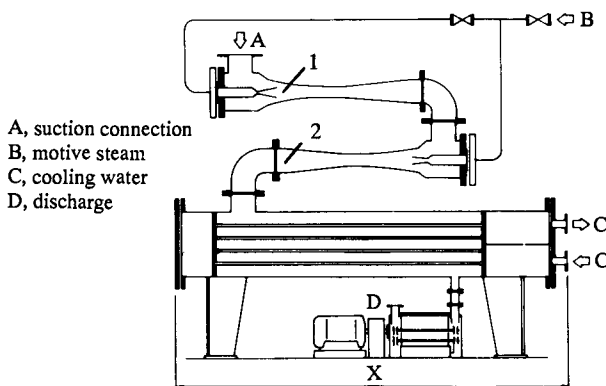
As interstage condensers operate at reduced pressure, it is necessary to provide a suitable method for the removal of condensate. If the condensers can be mounted high enough, the simplest system involves barometric drain legs of at least 10.5 m in height passing to a hotwell. Low-level condensers are usually supplied with centrifugal extraction pumps. A suitable vacuum reservoir can be used with batch processes.

When barometric height is not available, steam ejector/water-ring pump combinations may be used. An installation is shown in Figure 2.29. Ejector stages 1 and 2 convey the pumped material and the steam to a water-cooled surface condenser. This is a shell-and-tube heat exchanger with two tube passes and one shell pass. Condensate and non-condensables, including water vapour at a pressure corresponding to its saturated vapour pressure at the condenser temperature are then transferred to the water ring pump. A large multi-stage steam ejector/water ring pump, used for ladle degassing is shown in Figure 2.30. The set consists of four ejectors combined with two condensers and a water ring pump. Suction capacity of 300 kg air/h at 0.7 mbar demands 14 t/h steam at 186°C and 10 bar pressure. The condenser cooling-water consumption is 530 m<sup>3</sup>/h with water inlet and exit temperatures of 28°C and 40°C, respectively.

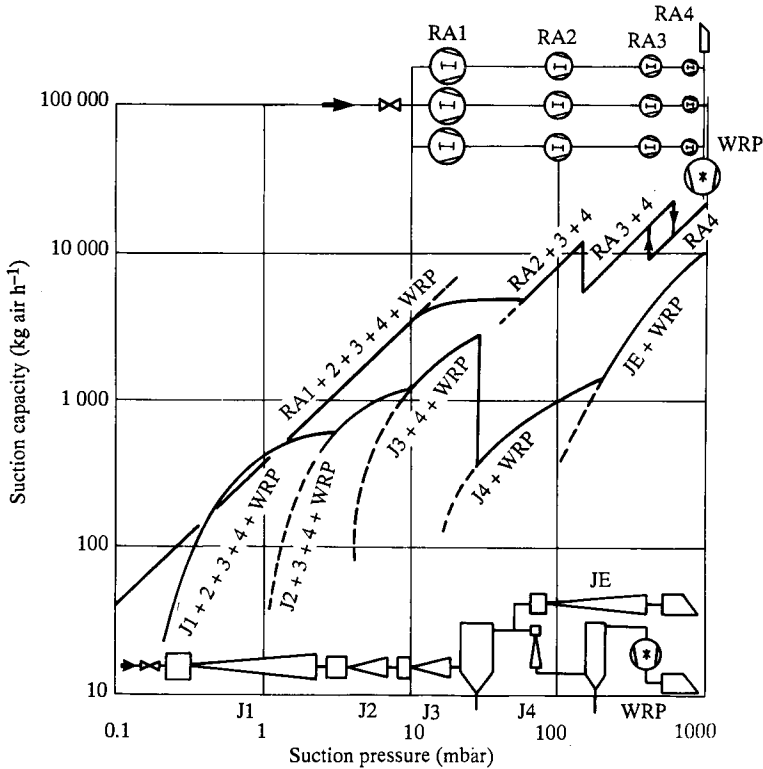
#### 2.5.2.2 *Oil vapour ejectors*

Oil vapour ejector pumps are suitable for pumping quantities of gas and vapour in the pressure range 1 to 10<sup>-3</sup> mbar.

They are used in processes where large quantities of gas and water vapour are evolved which may contain significant amounts of dust or other difficult materials. Typical applications are in plastic coating (for packaging) and some



**Figure 2.29** *Two-stage steam ejector/water ring pump combination (reproduced by kind permission of Hick Hargreaves and Co. Ltd.)*



**Figure 2.30** Suction characteristics for a large steam ejector set ( $300 \text{ kg h}^{-1}$  at  $0.7 \text{ mbar}$ ) and a mechanical pump set ( $300\,000 \text{ m}^3 \text{ h}^{-1}$  at  $0.1\text{--}10 \text{ mbar}$ ) used in steel degassing ( $100\text{--}200 \text{ t}$ )

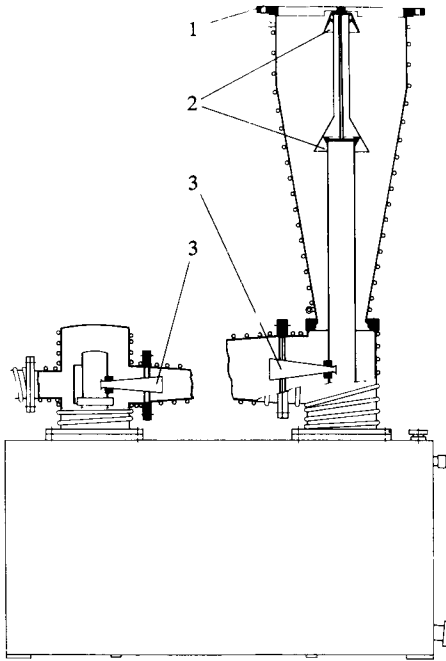
metallurgical and chemical processes. Figure 2.31 shows a typical oil vapour booster pump. The two vertical jets operate as they do in diffusion pumps (see Chapter 3) while the horizontal ejector stages work as indicated earlier.

The top jet nozzle of oil vapour booster pumps are usually surrounded by water-cooled baffles/guard rings in order to control backstreaming of vapour from the pump to the system.

Oil-ejector and booster pumps are available with a large range of pumping speeds from a few hundred to several thousand  $\text{l s}^{-1}$ . The higher density of the vapour stream in the nozzle means that only the outer layers of the vapour stream are permeated with gas. Further, due to the construction of the nozzles, the surface through which diffusion takes place is much smaller than that of diffusion pumps and the specific pumping speed is therefore much smaller.

Due to the high mass flow of gas that may be encountered, the vapour jets may be deflected and to ensure that vapour reaches the wall it is necessary to





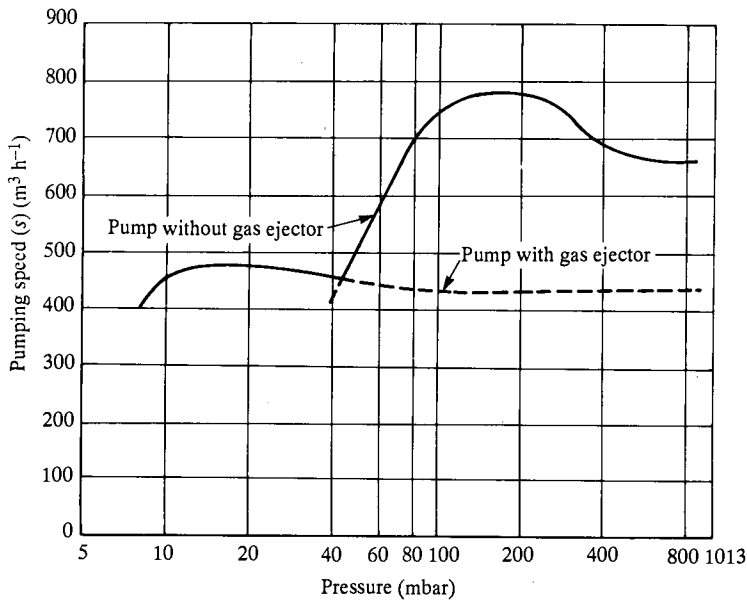
**Figure 2.31** *Schematic diagram of an oil booster pump (with diffusion and ejector stages). 1, high-vacuum connection; 2, diffusion stages; 3, ejector stages*

have a tapering pump body. Oil vapour ejector pumps currently in production (see, for example, Figure 2.31) have one or more diffusion and several ejector stages. The diffusion stages give high pumping speeds at pressures between  $10^{-4}$  and  $10^{-3}$  mbar while the ejector stages give high gas throughputs at high pressure and high critical backing pressure (a few mbar). It should be noted, however, that continuous working at maximum throughput will lead to oil-loss into the backing line.

### 2.5.2.3 *Air ejectors*

In certain circumstances, either where there is no steam or the cost of steam makes multi-stage ejectors or steam ejector/liquid ring pump combinations uneconomical, atmospheric air ejectors may be used. For example, an air ejector can be added directly to the inlet of a liquid ring pump (LRP). This allows lower pressures to be achieved than is possible with a liquid ring pump alone. For example, the pumping speed versus pressure characteristics for such a combination are shown in Figure 2.32.

To use fully the speed of the LRP during evacuation, the air ejector supply is fitted with a valve that opens only when the cross-over point is reached.



**Figure 2.32** Pumping speed versus pressure curves for a liquid ring pump with and without a gas ejector

## References

- Bachmann, P. and Kuhn, M. (1990) *Vacuum*, **41**, 1825  
 Berges, H.-P. and Goetz, D.G. (1988) *Vacuum*, **38**, 761  
 Bez, E. and Guarnaccia, D.G. (1990) *Vacuum*, **41**, 1819  
 Bürger, H.-D., Rossmann, E., Crinquette, J.-M. and Taberlet, M. (1990) *Vacuum*, **41**, 1822  
 Coffin, D.O. (1982) *Journal of Vacuum Science and Technology*, **20**, 1126  
 Duval, P., Raynaud, A. and Saulgeot, C. (1988) *Journal of Vacuum Science and Technology*, **A6**, 1187  
 Eastop, T.D. and McConkey, A. (1986) *Applied Thermodynamics*, 4th edn., Longman Scientific, Harlow, p.321  
 Friberg, J. (1958) *Fr. Pat.*, B. F. No 1,166,292  
 Gaede, W. (1913) *Annales Physik*, **41**, 337  
 Hablanian, M.H. (1988) *Journal of Vacuum Science and Technology*, **A6**, 1177  
 Hablanian, M.H. (1990) *Vacuum*, **41**, 1814  
 Heinen, R. and Schwartz, W. (1986) *Vakuum-Technik*, **8**, 231  
 Laurenson, L. and Turrell, D. (1988) *Vacuum*, **38**, 665  
 Mangnall, K. (1989) *Vacuum/Pressure Producing Machines and Associated Equipment*, Hick, Hargreaves and Co. Ltd., Bolton

- Maurice, L. (1974) Proceedings of the 6th International Vacuum Congress. *Japanese Journal of Applied Physics*, Suppl. 2, Pt. 1
- Noeller, H.G. (1956) In *1956 Vacuum Symposium Transactions*, Pergamon, London p. 57
- Noeller, H.G. (1989) In *Theory and Practice of Vacuum Technology*, (Wutz, M., Adam, H. and Walcher, W. eds) F. Vieweg and Son, Braunschweig/Wiesbaden, p. 197
- Van Atta, C.M. (1965) *Vacuum Science and Engineering*, McGraw-Hill, New York, p. 211
- Vulliez, P. (1974) U.S. Patent 3,802,809
- Wong, W., Laurenson, L., Livesey, R.G. and Troup, A.P. (1988) *Journal of Vacuum Science and Technology*, **A6**, 1183
- Wycliff, H. (1987) *Journal of Vacuum Science and Technology*, **A5**, 2608
- Zakrzewski, E., May, P. L. and Emslie, B.S. (1988) *Vacuum*, **38**, 757

# 3

## *Vacuum pumps (high–ultra-high range)*

---

### 3.1 General introduction

Up to the 1950s, there was little demand for vacuum systems working at pressures below  $10^{-6}$  mbar and diffusion pumps were considered adequate for most purposes. Subsequently, however, research and developments in areas such as atomic and nuclear physics, nuclear fusion, space technology, surface science, etc. led to demands for better vacua both qualitatively (defined by total pressure measurement) and quantitatively (defined by residual gas analysis). This in turn led to a surge of development work in the late 1950s and 1960s on the attainment and measurement of vacua (Van Atta, 1965; Weston, 1985).

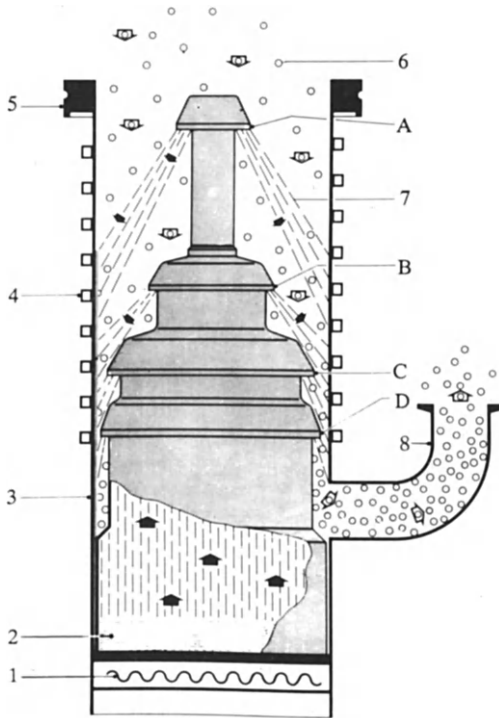
This chapter will review the types of pumps that are available in order to achieve vacua in the range from  $10^{-3}$  mbar to the lowest attainable levels. These pumps are divided into two types – there are those (gas-transfer pumps) in which pumped particles are compressed before removal by a backing pump and those (entrapment pumps) in which gas particles that have entered from the system are trapped either chemically or physically within the pump. Diffusion and turbomolecular pumps belong to the former category while sorption pumps and cryopumps are examples of the latter.

### 3.2 Gas transfer pumps

#### 3.2.1 Diffusion pumps

Some theoretical aspects of fluid entrainment pumps were discussed in Chapter 2, where it was pointed out that a diffusion pump is an entrainment pump working under conditions of molecular flow. A typical diffusion pump is shown in Figure 3.1.

In the pump, the working fluid is heated and when the operating pressure is achieved, vapour rises inside the jet assembly. The vapour accelerates as it passes through the jets in the form of a stream that is directed downwards and radially across the space between the jet assemblies and the inner pump wall. Some gas particles, moving with normal thermal velocities, approach the vapour jet, penetrate the surface and are carried downwards to the interspace between jets. Eventually, the gas is compressed to a pressure at which it can be removed by a backing pump at the discharge port. The working region of a diffusion pump is mainly below  $10^{-3}$  and the compression ratios that can be



**Figure 3.1** *Cross-sectional view of a conventional diffusion pump. 1, heater; 2, boiler; 3, pump body; 4, cooling coil; 5, high-vacuum flange connection; 6, gas particles; 7, vapour jet; 8, backing vacuum connection port; A–D, nozzles*

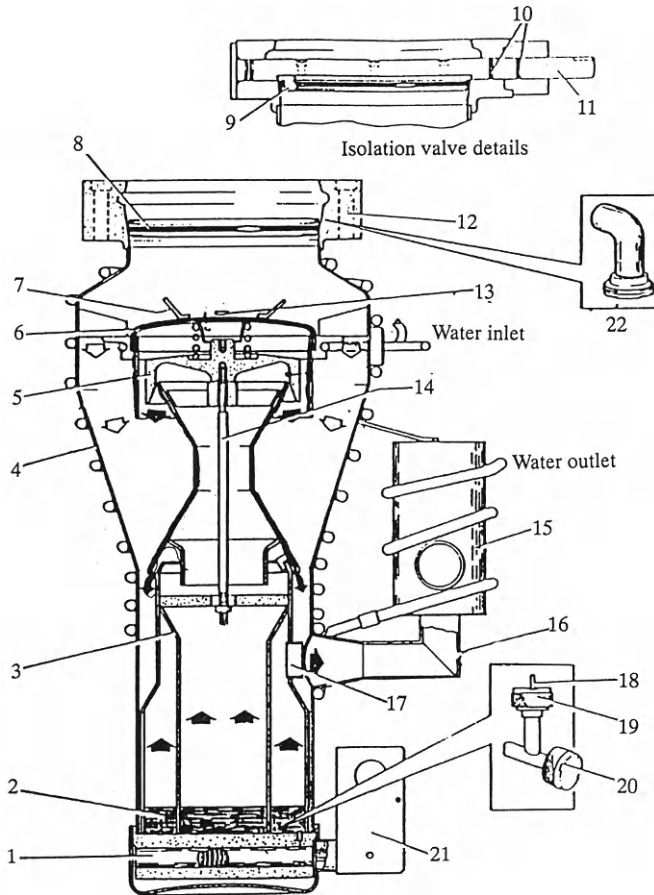
achieved are quite high. For example, with an inlet pressure of  $10^{-8}$  mbar and a backing pressure of  $10^{-1}$  mbar, the pumped gas is compressed by a factor of  $10^{+7}$  for a gas such as  $N_2$ . The specified pumping speed is essentially constant over the whole working range of the pump.

A great deal of effort has gone into the study of diffusion pump design and performance (Van Atta, 1965) but a detailed understanding of the mechanism of jet formation, gas entrainment and pumping has not been achieved. Theoretical derivations of the compression ratio under conditions of zero flow have, however, given an expression of the form  $e^{\beta n_v L \sigma}$  where  $n_v$  is the average value of the number density of the vapour and  $\sigma$  depends on the nature of the gas. Van Atta commented that the first stage of modern diffusion pumps, particularly with organic pumping fluids, is significantly undersupplied with vapour. So marginal is  $n_v$  for the first-stage jet that, although the compression ratio is adequate for air, the corresponding value for He and  $H_2$  is poor. This problem arises through efforts to obtain a high pumping speed for air whilst avoiding excessive back-streaming.

There have been few innovations in the design of diffusion pumps. A relatively recent advance was the pump that incorporates in one container a cooled baffle and valve (see Power *et al.*, 1974a,b) (Figure 3.2). This will be described subsequently.

### 3.2.1.1 Diffusion pump fluids

Fluids that are used in diffusion pumps should have certain properties (Laurenson, 1987) including a low vapour pressure, resistance to thermal



**Figure 3.2** Cross-sectional view of a diffusion pump with an integrated cooled baffle and valve (reproduced by kind permission of Edwards High Vacuum International) 1, Cartridge heater; 2, boiler fluid; 3, vapour tube assembly; 4, pump body; 5, first stage jet assembly; 6, baffle cap; 7, extractor grips; 8, isolation valve; 9, valve plate; 10, 'O' rings; 11, valve spindle; 12, inlet flange; 13, retaining strap; 14, tie rod; 15, condenser; 16, backing tube; 17, ejector jet tube; 18, dipstick; 19, fluid filler connection; 20, drain connection; 21, terminal box; 22, roughing connection

decomposition/oxidation, general chemical resistance, etc. The saturated vapour pressure of the pump fluid or of its decomposition products is a very important factor that affects the ultimate achievable pressure.

The choice of fluid greatly influences the performance of the pump and depends on the application. Mercury used to be used extensively as a diffusion pump fluid but for various reasons it is now rarely employed. Extensively applied, however, are the following:

1. Hydrocarbon-based fluids.
2. Synthetic oils.

The former are produced by the molecular distillation of suitable mineral oils. Several are available from manufacturers and well-known types are Apiezon A, B and C and Diffelen (light, normal and ultra). Repeated exposure to oxygen-containing gas will degrade these fluids, as will heating for long periods. A fluid, based on 'alkylnaphthalene' has been developed by Edwards High Vacuum. It is claimed to have a 'fair' resistance to oxidation and a good chemical resistance to acids, alkalis and halogens.

Synthetic materials include silicone-oils (typically the Dow Corning fluids DC 702, 704 and 705), polyphenyl ethers (trade names: Santovac 5 (Monsanto), Convalex 10 (CVC Inc.), Ultralen) and perfluoropolyethers (Fomblin, Krytox). Polyphenyl ether has a vapour pressure of less than  $10^{-9}$  mbar at 20°C. It has excellent thermal stability and good chemical resistance. Typical applications are for clean HV and UHV systems.

Although PFPE fluids may have desirable chemical and physical properties, diffusion pumps charged with these fluids may have their speeds reduced significantly. Further, Laurensen (1987) reported that, with small pumps, pumping became erratic and the ultimate vacuum was an order of magnitude higher than expected. PFPEs have very low specific heats and heats of vaporization and it was found (Laurensen, 1987) that reducing the heater power by 25% restored performance.

Depending on the type of fluid used, the ultimate pressure of silicon diffusion pump fluids is in the range  $10^{-6}$  to  $10^{-9}$  mbar at 20°C. They have excellent thermal stability and chemical resistance. When, however, decomposition does occur, the products are electrically insulating. This leads to an alteration in the space-charge characteristics of ion sources, quadrupoles, etc.

### **3.2.1.2 Back-streaming**

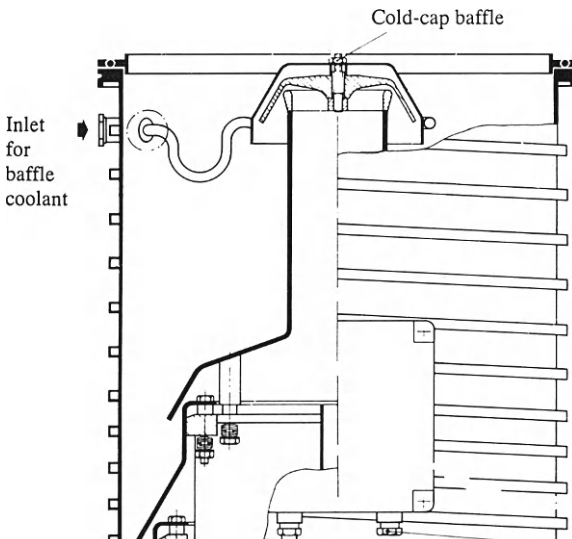
In actuality, the vapour stream emerging cannot be regarded as well-defined and travelling in a downwards direction radially across the pump. Through random scattering or directional scattering from a coherent vapour jet, some molecules of working fluid migrate in the direction of the vacuum chamber. This results in the back-streaming of the fluid and is a major source of contamination in diffusion-pumped systems. A further effect involves back-migration whereby fluid that has condensed in the region of the orifice re-evaporates.

In order to minimize back-streaming, suitable traps and baffles are inserted between the first-stage jet and the system being pumped. Power and Crawley

(1954) devised a water-cooled guard-ring extending below the lip of the upper jet to intercept and condense the randomly-directed vapour molecules originating in the boundary layer adjacent to the nozzle surface. The use of a water-cooled cap placed over the first-stage jet with a skirt projecting far enough down to intercept the boundary layer (and thereby reduce back-streaming) was described by Vekshinsky *et al.* (1959). A typical cold-cap baffle fitted to the top jet is shown in Figure 3.3. With a standard, water-cooled cap, backstreaming can be reduced by a factor of between 50 and 100% with a relatively small reduction in the pump speed (about 10%).

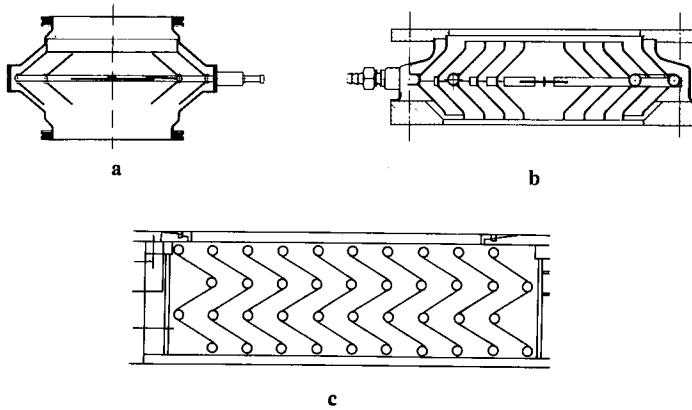
A particularly efficient baffle for the reduction of back-streaming incorporates metal chevrons inserted between the pump and the system. Several designs are shown in Figure 3.4. Back-streaming oil particles have a high probability of being intercepted. Unfortunately, the more effective the baffle in the reduction of back-streaming, the more it will reduce the effective speed of the pump. For example, there is a 3-fold reduction in pumping speed across the baffle shown in Figure 3.4(c). By appropriate cooling (water, liquid N<sub>2</sub> or a suitable refrigerant), almost completely oil-free vacua can be obtained.

Although a suitably baffled diffusion pump using fluids with low vapour pressure and low back-streaming may allow pressures within the UHV range to be achieved, the use of liquid-nitrogen-cooled traps may be necessary to prevent significant interference from any back-streaming and back-migration that does take place. Such traps must have both a high efficiency for condensation and a high conductance. A typical trap is shown in Figure 3.5.

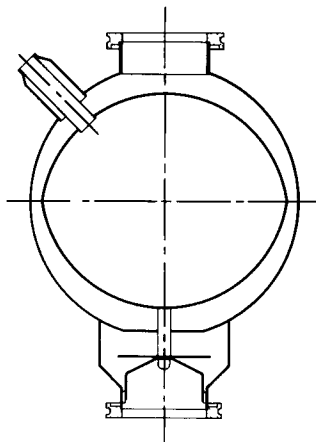


**Figure 3.3** Cross-section of part of the jet assembly of a large diffusion pump (Leybold DI 30 000)





**Figure 3.4** Examples of chevron baffles. (a) Section through shell baffle (Leybold), (b) Section through Astrotorus baffle (Leybold), (c) Chevron baffle (Philips)



**Figure 3.5** Section through a spherical cold trap

With liquid-nitrogen cooled traps, automatic refilling units are recommended since this ensures long-term temperature stability, and hence efficiency, and a lower consumption of coolant.

Dubois (1988) recommended that, for optimum performance, the seal between the diffusion pump and the liquid  $N_2$ -cooled trap should be metal and of the knife-edge type. Finally, it should be remembered that cold-cap baffles should always be used in conjunction with low-temperature traps otherwise pump performance may be impaired through condensation of fluid on the cold surfaces.

### 3.2.1.3 Critical backing pressure

The fore-vacuum pressure has a considerable influence on the vapour jet in fluid entrainment pumps. This has been discussed by Florescu (1960). If the fore-pressure is sufficiently low, the vapour jet can bridge the aperture between the jet assembly and the wall of the pump. The vapour jet has a vertical thickness of a few mm at the wall.

With increasing fore-pressure, the vapour jet terminates in a shock front. Above the shock front, molecules have net velocity directed downwards; below the front, the molecules are randomly directed. It eventually retreats to a position where the vapour stream can no longer reach the walls and effective pumping ceases. This is called the critical backing pressure. The value of the critical backing pressure depends on several factors that were listed by Van Atta (1965). For multi-stage diffusion pumps, the value is approximately  $5 \times 10^{-1}$  mbar. The performance of the backing pump must be such that it will deal with the highest throughput presented by the diffusion pump without allowing the fore-line pressure to approach the critical value.

Diffusion-pump technology is mature and very few advances have been made since the 1970s (Power *et al.*, 1974a,b). Pumps that are suitable for UHV are constructed with stainless steel bodies and nickel-plated copper or steel jets. The innovation of Power *et al.* was to incorporate a cooled baffle and a valve into the pump (see Figure 3.2). The purpose of such a design modification was partly to eliminate a number of seals (and hence the risk of leakage) and partly to reduce the size and weight of the pump. As shown in Figure 3.2, the pump consists of a three-stage jet assembly with a top stage that is large compared with that of a conventional diffusion pump. The diameter of the body of the pump is increased in the region of the top jet to accommodate both it and the baffle and guard assembly.

Diffusion pumps continue to play an important role in high- and ultra-high vacuum technology. It has been pointed out (Dubois, 1988) that they are initially cheap, easy to maintain and do not appear to react adversely with the vacuum system. Certainly, advances in the development of fluids with low vapour pressure and low backstreaming have helped them to maintain their importance. Nevertheless, future industrial and research activity in the development of advanced materials, thin films and information technology (super LSI devices, 3D memory devices) may need pumps that are cleaner and more convenient.

### 3.2.2 Turbomolecular pumps

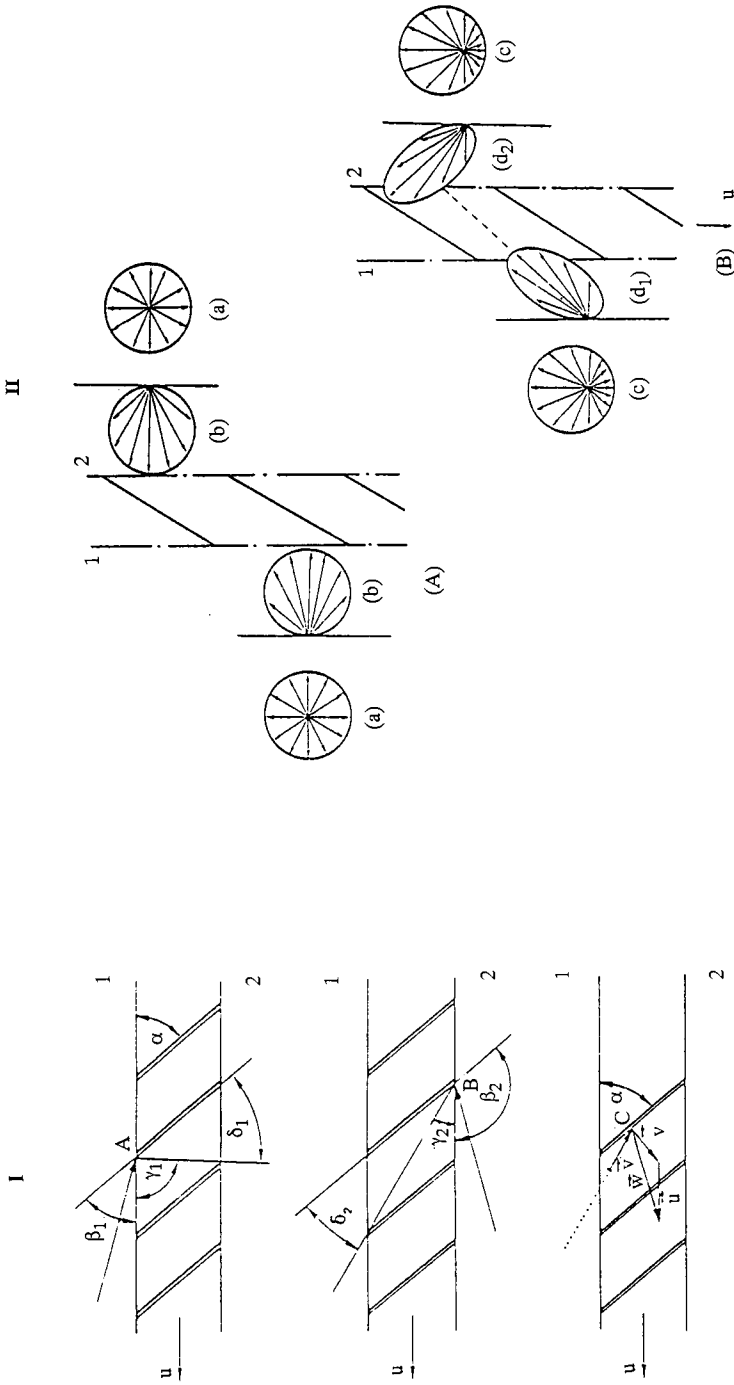
The turbomolecular pump was invented by Becker (see references in Hucknall and Goetz, 1987) and initially exploited commercially by A. Pfeiffer GmbH. The device is a multi-stage, bladed, axial flow turbine that compresses gas according to a mechanism that is gradually being established (Tu and Yang, 1987; Tu *et al.*, 1988). This process occurs most efficiently under conditions of molecular flow.

### 3.2.2.1 Theory

One of the first models to explain the pumping mechanism of a rotor stage in a turbomolecular pump was proposed by Kruger and Shapiro (1961). According to this model (Figure 3.6(I)), the velocity of the blade ( $u$ ) is large compared with the mean thermal velocity ( $\bar{c}$ ) of the gas particles. The limiting condition, where the ratio  $u/\bar{c}$  is very large, means that almost all the particles incident on the blade row would hit at points A or B, respectively, if they approach from side 1 or side 2. As a result, if it is assumed that particles are diffusely reflected, then the probability of transmission from side 1 to side 2 ( $P_{12}$ ) is greater than that from side 2 to side 1 ( $P_{21}$ ) resulting in pumping. (In Figure 3.6(I), the angles given in (a) and (b) can be assumed to reflect these probabilities.) For a multistage device, consisting of rotor and stator blades, Kruger and Shapiro (1961) assumed that particles passing in either direction (1→2 or 2→1) through a moving stage would contact a blade surface at least once and, therefore, have gained a velocity component in the same direction as the moving blades before being directed to an adjacent stationary stage (Figure 3.6 (I)(c)). Particles then hitting the stationary stage lose the velocity component and leave the stator with their original speed. Thus if the rotor and stator blades were geometrically identical, their pumping action would also be the same.

With actual turbomolecular pumps, the blade-to-molecular velocity ratio is significantly less than one. Calculations of  $u/\bar{c}$  for various gases at 20°C show that for a blade velocity of 250 m s<sup>-1</sup>, the ratio was 0.143 and 0.63 for H<sub>2</sub> and Ar, respectively. This represents a considerable deviation from the Kruger-Shapiro assumption. Tu and co-workers (1987, 1988) devised a model for single- and multiple-stage pumps with more typical  $u/\bar{c}$  ratios. In Figure 3.6(II)(A), gas particles on either side of a stationary stage are shown. Particles approaching a channel between blades have three possibilities: they may collide with the upper blade or encounter the lower blade or they may pass directly through. The probabilities of these events was estimated by Monte Carlo methods (Tu *et al.*, 1988) or by integral equation methods (Tu and Yang, 1987) assuming molecular flow, Maxwellian velocity distribution and other results from the kinetic theory of gases. Based on the distributions of velocities and incident molecular fluxes and the symmetry of the blades, there is no pumping action. When the particles encounter a moving stage (Figure 3.6(II)(B)), there are changes in both the velocity and flux distributions. From Figure 3.6(II)(B), it can be seen that a large part of the particles incident from the forward direction will pass through the blade channel without collision. In contrast, most of the particles incident on the channel from the reverse direction will be blocked by the upper blade and directed away from the channel. Thus, more particles pass from side 1 to side 2 than in the opposite direction. Some predictions are shown in Table 3.1.

In a more elaborate treatment, Tu *et al.* (1988) pointed out that with multi-stage pumps, each row of blades was almost a mirror image of the adjacent row which meant that gas particles leaving a blade channel with the predicted angular distribution will have a disadvantageous distribution for the next channel. Correction factors to the transmission probabilities then had to



**Figure 3.6** Diagram of a single pumping stage. (I) Model according to Kruger and Shapiro (1961).  $\alpha$  = blade pitch;  $\gamma_1$  = angle representing the probability that a particle will enter the blade channel and hit a surface;  $\delta_1$  = angle representing the probability that the particle will pass through, similar considerations for  $\gamma_2$  and  $\delta_2$ . (II) Model according to Tu et al. (1987, 1988). (A) Molecules incident on a stationary blade. (a) Maxwellian velocity distribution; (b) cosine distribution. (B) Molecules incident on a moving blade. (c) Velocity distribution; (d<sub>1</sub>, d<sub>2</sub>) distribution of incident molecules

**Table 3.1** *Calculated transmission probabilities for single blade rows according to Tu and co-workers (1987, 1988)*

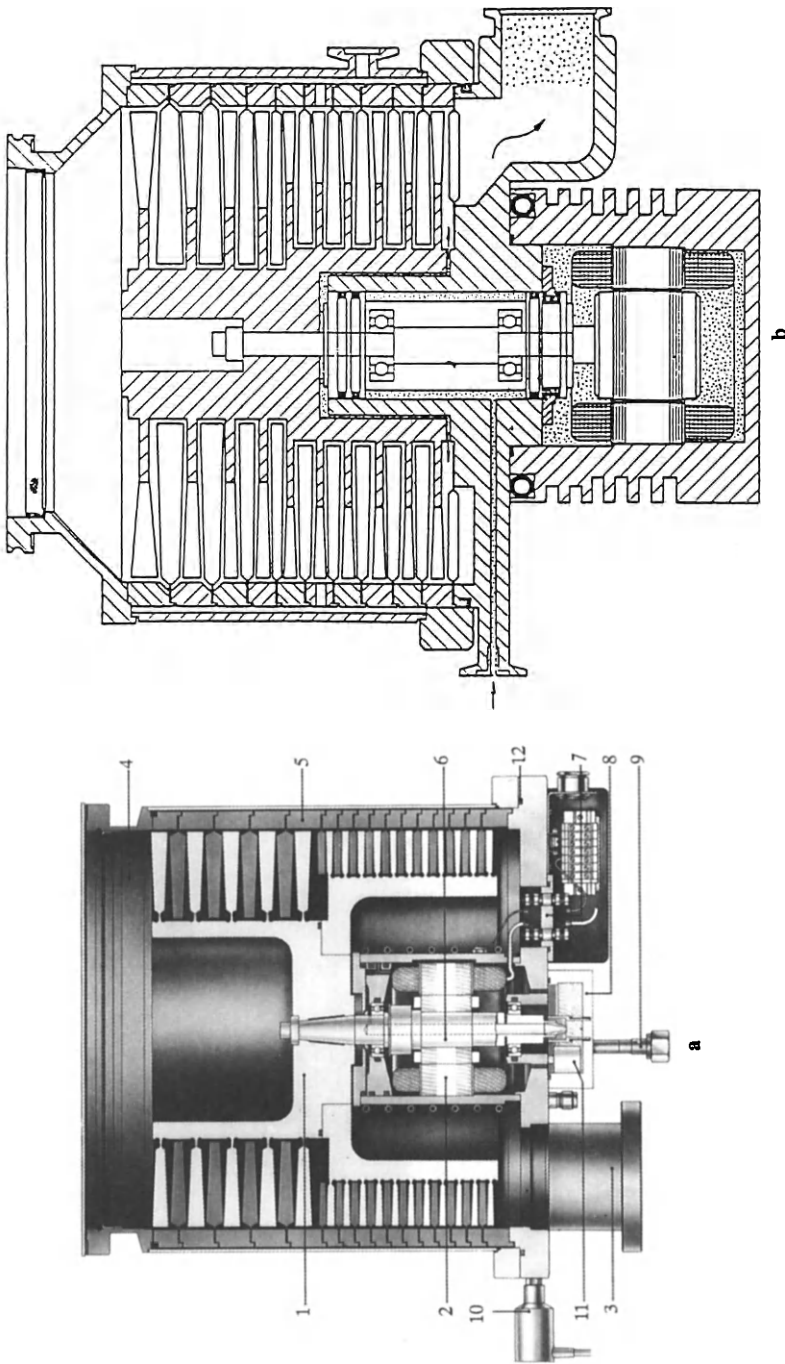
$\alpha = 40^\circ$	$\alpha = 20^\circ$
$u/c = 0.5^*$	$u/c = 0.5$
$P_{12} = 0.625$	$P_{12} = 0.403$
$P_{22} = 0.6786$	$P_{22} = 0.8753$

be applied in order to reproduce the pumping characteristics of multi-stage assemblies. Nevertheless, agreement between theory and experiment was encouragingly close.

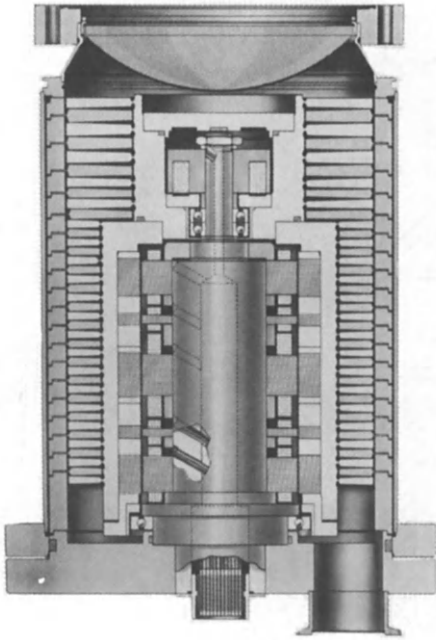
### 3.2.2.2 Design

According to a recent survey of commercially-available turbomolecular pumps (Hucknall and Goetz, 1987), vertical, single-flow devices are now the preferred configuration. Typical modern turbomolecular pumps are shown in Figure 3.7(a) and (b). The rotor is driven by a water-cooled three-phase motor which is located in the fore-vacuum space inside the pump body. The rotor is machined from a block of aluminium alloy and the individual blades are offset (angle  $\alpha$  in Figure 3.6).  $\alpha$  decreases from the high-vacuum to the fore-vacuum side of the pump. This reduction in blade angle brings about an increase in compression ratio but a decrease in pumping speed. The bladed stator assembly is made from semicircular discs (usually sheet aluminium) and each pair of discs is placed between a pair of rotor blades and separated by spacers from the next stator stage. The pumped gas is compressed along the rotor-stator assembly and is passed to the backing pump.

The bearings are critical to the efficient operation of a turbomolecular pump. In Figure 3.7(a), the bearings are lubricated with a suitable low-vapour-pressure oil. The method of lubricant delivery involves a hollow shaft tapered at the lower end and dipping into the oil reservoir. With the fore-vacuum port evacuated (and *only* then), the required amount of oil is drawn up through the shaft and discharged through ports in the vicinity of the bearings. As an alternative, grease lubrication has been employed (see Figure 3.7(b)). With this system, no lubricant can escape and the pump can be operated in any orientation. In recent developments, conventional steel bearings have been replaced by ceramic bearings which are lighter and more durable. On account of their very high reliability and the extremely low level of hydrocarbon contamination, turbomolecular pumps having the rotor suspended by magnetic bearings have been developed. The first turbomolecular pump with such bearings was introduced in the mid-1970s (Frank and Usselman, 1977) and is shown in Figure 3.8. This design incorporated fully active bearings. An active magnetic bearing consists of an electromagnet, powered and controlled by a suitable electronic control unit via a sensor. Bearings are required to stabilize the rotor against axial, radial and 'rocking' motion. Two dry-running ball bearings, not used in normal operation,



**Figure 3.7** (a) Diagram of a large ( $S_{N_2} = 5500 \text{ l s}^{-1}$ ) turbomolecular pump with oil-lubricated bearings. Inlet flange = DN 500 150-K; rotational speed = 18 000 r.p.m.; weight 280 kg (reproduced by kind permission of Arthur Pfeiffer Vakuumtechnik Weizlar GmbH) (b) Diagram of a vertical turbomolecular pump with purge gas facility for pumping corrosive gases and particulates



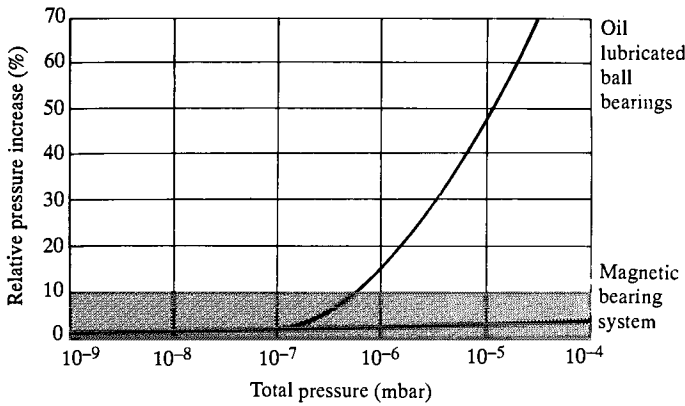
**Figure 3.8** *Cross-section of the world's first turbomolecular pump with magnetic bearings*

support the rotor when power energizing the magneto-bearings has been interrupted. Developments are continuing (Kabelitz and Fremerey, 1988)

If a pump with conventionally lubricated bearings is switched off or vented, there is the possibility of system contamination occurring. This is significantly minimized with magnetic bearing turbomolecular pumps (Figure 3.9). A further drawback with lubricated bearings may occur during the pumping of highly reactive compounds. Although the rotor and stator of the pump may be corrosion-resistant and unreactive fluorocarbon-based lubricants can be used, attack on steel bearings may occur. This problem has been lessened by the admission of a purge gas (see Figure 3.7(b)). In purged pumps, the flow of gas ( $N_2$ , Ar) must be adjusted so that the pressure in the motor housing exceeds that in the fore-vacuum port. This ensures a continuous flow of gas from the area of the motor to the port, thereby preventing the penetration of the bearings by corrosive gases.

### **3.2.2.3 Operation**

The pumping speed of a turbomolecular pump depends on the inlet pressure and the type of gas pumped. The pumping speed achieves a constant value at pressures less than about  $10^{-3}$  mbar but it declines significantly at greater pressures (Figure 3.10(a)). Its dependence on the gas arises because the



**Figure 3.9** Increase in hydrocarbon contamination during the deceleration of a turbomolecular pump

pumping probability for light gases is lower than that for N<sub>2</sub> (an important factor in the behaviour of the pump is the ratio  $u/c$  (see Section 3.2.2.1) and, for fixed  $u$ , the effectiveness declines as  $c$  increases). To a certain extent, there is compensation due to the increased conductance of the aperture for light gases and, in fact, the pumping speed for H<sub>2</sub> is between 80% and 90% of that for N<sub>2</sub>. The decrease in pumping speed at intake pressures above 10<sup>-3</sup> mbar may be explained by the transition from molecular flow conditions. Although the decrease is sharp, the speed of rotation will be maintained to about 1 mbar.

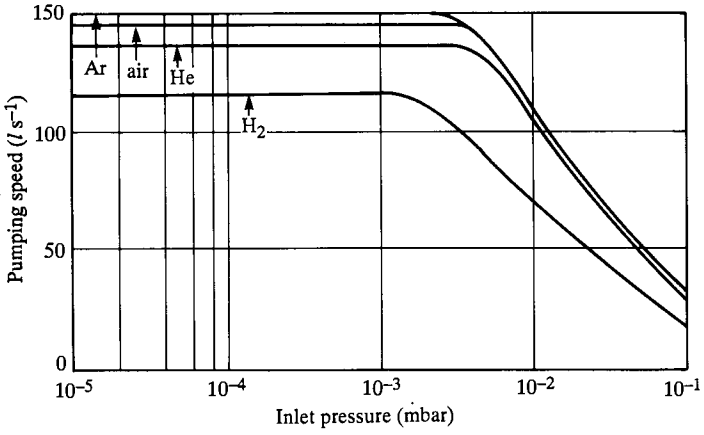
Being a gas transfer device unable to compress against atmosphere pressure, a turbomolecular pump requires backing. The speed of the backing pump should lie between 23 and 10% of that of the TMP for high vacuum operation. If the pump is used at intake pressures greater than 10<sup>-3</sup> mbar, then the backing pump must be chosen to cope with the throughput presented.

The compression ratio,  $K_{max}$ , is given by the expression:

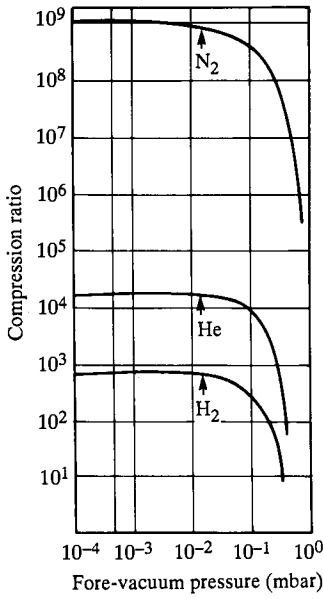
$$K_{max} = k_0 \exp(g\sqrt{M} u z)$$

where  $k_0$  is a constant,  $g$  is a 'geometric factor' (dependent on rotor geometry),  $u$  is the blade speed and  $z$  is the number of stages.  $K_{max}$  is defined as the ratio  $P_{out}/P_{in}$  for the turbomolecular pump at zero throughput. It is determined according to PNEUROP (1973) by fitting a test dome to the pump inlet. After the chamber has been evacuated to the ultimate pressure of the pump, test gas (N<sub>2</sub>, He, H<sub>2</sub>) is admitted via the backing line and inlet- and backing pressures measured. Typical values are shown in Figure 3.10(b). At 10<sup>-2</sup> mbar, the compression ratio for N<sub>2</sub> is almost 10<sup>9</sup>, whilst for He and H<sub>2</sub> the corresponding figures are considerably less. The dependence of  $K_{max}$  on relative molecular mass means that heavy gases are highly compressed and





a



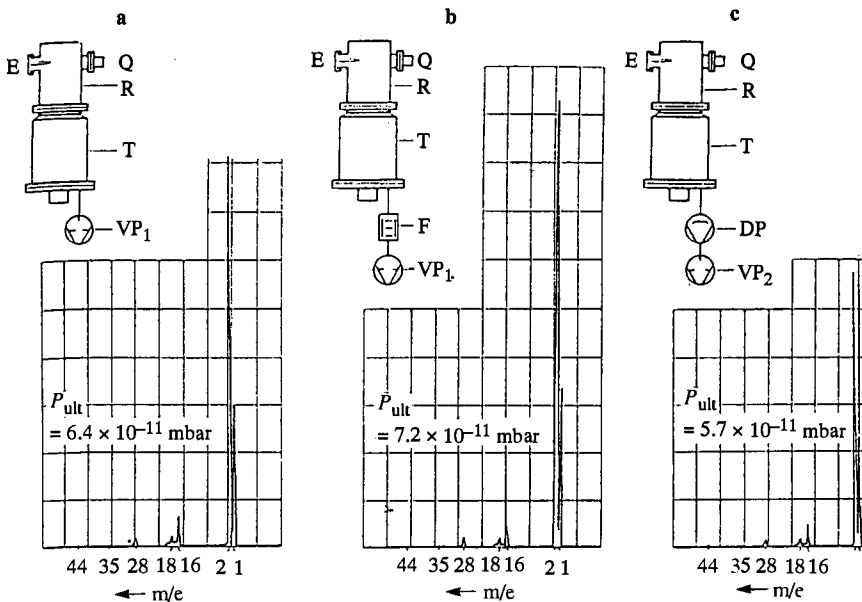
b

**Figure 3.10** (a) The variation of pumping speed with inlet pressure. (b) The variation  $K_{max}$  with forevacuum pressure for a turbomolecular pump ( $S_{N_2} = 150\ l\ s^{-1}$ )

have a lower probability of backflow than lighter species. This is reflected in the 'clean' vacua produced by turbomolecular pumps (Figure 3.11). The apparatus shown in Figure 3.11 consisted of a 5 litre chamber fitted with an extractor gauge (E) and quadrupole mass spectrometer (Q). Metal seals were used and the chamber and upper flange of the TMP were heated at 200°C for several hours in order to reach low pressures. The residual gas spectra show that there are no components with mass number greater than 44. Hydrogen, however, is the predominant gas. The peak at mass 16 was ascribed to atomic oxygen generated by decomposition of H<sub>2</sub>O. Frank (1989) concluded that the ultimate pressure obtained with a turbomolecular pump is, in general, independent of the choice of backing pump.

### 3.2.2.4 Applications

The obvious advantages of the turbomolecular pumps (production of high, clean vacua) have been exploited in many applications. In many industrial vacuum processes, such as the deposition of optical and protective coatings and the production of semiconductors, additional demands are made on pumping systems. These include rapid operational readiness, maintenance-



**Figure 3.11** Residual gas spectra for a small chamber evacuated by a turbomolecular pump ( $S_{N_2} = 450 \text{ l s}^{-1}$ ) backed by: (a) an oil-sealed rotary vane pump ( $VP_1$ );  $S = 30 \text{ m}^3 \text{ h}^{-1}$ ; (b) as (a) but with foreline adsorption trap (F); (c) a diffusion pump ( $s = 170 \text{ l s}^{-1}$ ) and oil-sealed rotary vane pump ( $VP_2$ )  $S = 10 \text{ m}^3 \text{ h}^{-1}$  (after Frank, 1989)

free operation, even in the presence of reactive or abrasive media, and the ability to accommodate large, constant gas throughputs at relatively high pressures. Turbomolecular pumps have been found to meet these requirements more than adequately with suitable modification in some cases. Indeed, certain processes can be realized only by the use of these components. In this section, the application of turbomolecular pumps in research and manufacturing industry will be described.

*(i) The use of turbomolecular pumps in nuclear technology*

Several highly important investigations in the field of nuclear fusion are being carried out currently (Joint European Torus (JET) at Culham, Tokamak Fusion Test Reactor (TFTR) at Princeton and others). Such projects require pumping systems with high gas throughputs producing clean high vacua and turbomolecular pumps have frequently been selected for use on the vacuum systems of these installations. Difficulties are encountered as a result of pumping radioactive material (such as tritium in the case of plasma fusion experiments). Apart from the risks to maintenance personnel, long-term exposure to radiation causes damage, particularly to the organic materials (lubricants, seals, insulators) used in vacuum systems. Further, semiconductor devices (transistors, diodes, etc.) are very susceptible to radiation (through the formation of lattice defects) and this may affect the control systems of components, for example, the frequency convertors on turbomolecular pumps. Tritium (a  $\beta$ -emitter) may not only contaminate through H-exchange but also induce deterioration by radiation.

Vacuum equipment can be designed for remote maintenance and repair but a simpler and less costly solution is to locate it outside the main shielding of the installation and provide some additional protection (Abbel *et al.*, 1982). In the specific case of turbomolecular pumps, susceptibility to radiation means that the frequency convertors may have to be located remotely from the pumps they supply. Duval and co-workers (1986), however, have described a range of pumps, the motors of which have power supply requirements less strict than is usual.

Pumps that can be used to handle tritium have been described in the literature and are commercially available (see Hucknall and Goetz, 1987). To minimize tritium release, modifications to standard pumps include the use of metal seals (CF-type flanges with copper gaskets) on the high- and fore-vacuum ports, the use of metal gaskets for the pump-body seal (leakage in the pump may thereby be reduced to  $10^{-9}$  mbar l s<sup>-1</sup> (using He)) and the use of suitable instrumentation to monitor rotor speed, vibration level, etc. and thereby prevent catastrophic failure. Since the available pumps fitted with magnetic bearings have relatively low pumping speeds, pumps used in radioactive environments are usually oil sealed. A minimum of fluid is used and the pump reservoir is made of stainless steel and fitted with valved drain and filling-ports. Radiation-resistant lubricants may be used, although perfluoropolyethers can decompose under the influence of radiation to yield highly reactive F atoms.

In applications involving plasma fusion reactors, turbomolecular pumps are exposed to strong external magnetic fields. Under these conditions, eddy currents may cause the pump rotor to heat up. The magnitude of this effect depends on several factors, including the thermal conductivity of the rotor material, the rotation frequency and the distribution of the magnetic field. The influence of static and pulsed fields has been investigated (Goetz, 1982; Bieger *et al.*, 1979) and results have shown that a non-shielded pump can be operated in homogeneous magnetic fields up to 6.5 mT perpendicular to the pump axis without causing unacceptable heating of the rotor. Murakami *et al.* (1987) have tested a small TMP with a ceramic ( $\text{Si}_3\text{N}_4$ ) rotor for use with fusion reactors.

### (ii) Electronics and electrical industry

Several stages are involved in the manufacture of semiconductors, including deposition, sputtering and etching. These processes often involve a high throughput of a range of gases, some of which may be toxic and explosive. Advances in semiconductor production will require cleaner surfaces. These constraints mean that refrigerator-cooled cryopumps and turbomolecular pumps are being used increasingly in the electronics industry. Both types of pump meet all the requirements, but cryopumps have the disadvantage that, in certain processes, the hazardous gases and vapours removed by the pump are re-evolved during regeneration.

One particularly demanding process in the manufacture of semiconductors is plasma etching. In this process, highly reactive species (ions, atoms, radicals) are generated from a suitable gas. This results in a range of aggressive materials being presented to the pumping system (see Section 7.2). This problem has been substantially overcome by the use of a purge-gas system and, in certain cases, by the application of coatings (PTFE,  $\text{Al}_2\text{O}_3$ , Ni, etc.) to the susceptible surfaces.

There are applications, both in the electrical and electronics industry, in which dusts/powders are either produced or used in the process. Coating television screens, for example, generates substantial amounts of solid material. The problem may be overcome by mounting a turbomolecular pump at right angles to the evaporation chamber (Goetz *et al.*, 1987).

### (iii) Other processes

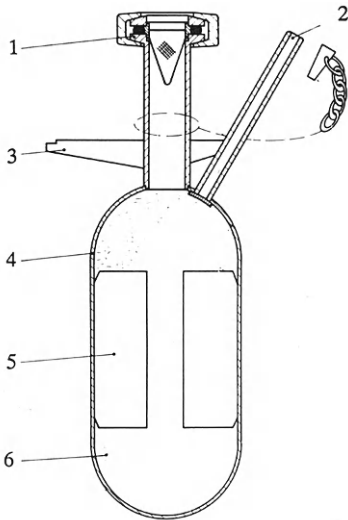
Turbomolecular pumps are widely used for coating systems, including plants for the optical industry (deposition of anti-reflexion and filter layers, for example) and the production of magnetic layers. They have the advantages that they provide a good-quality vacuum, allow short process times and allow a high gas throughput. Sputtering plants used in the manufacture of flat glass and in the deposition of protective coatings also involve a high throughput of gas at a pressure of  $10^{-2}$  to  $10^{-3}$  mbar. Turbomolecular pumps are also used in such systems. Some applications are discussed by Deters and co-workers (1987).

### 3.3 Entrapment pumps

#### 3.3.1 Adsorption pumps

The term ‘sorption pump’ is used rather imprecisely to describe a pump in which the gas is physically sorbed in a porous material cooled to liquid nitrogen temperatures. Strictly, the sorption process encompasses two mechanisms – adsorption and absorption (occlusion) – and the term ‘sorption pump’ could cover getter pumps, sublimation pumps, sputter ion pumps, etc. According to ISO 3529/II, the pumps that will be discussed in this section should be termed *adsorption pumps*.

The need for a hydrocarbon-free backing pump for the then newly developed ion pumps led to interest in adsorption pumps in the 1950s. An adsorption pump consists essentially of a vacuum-tight, cylindrical vessel, made of stainless steel and filled with the adsorbant (Figure 3.12). A series of heat-conducting fins are attached to the inside of the cylinder in order to dissipate the heat of gas adsorption. The pump is usually connected to the vacuum system with a valve. It is activated by heating to 200–300°C for several hours (with the vacuum valve closed) to drive off water vapour and adsorbed gases. Simultaneous baking and purging with nitrogen can increase performance. After regeneration, the pump is chilled with liquid nitrogen and is then ready for use.

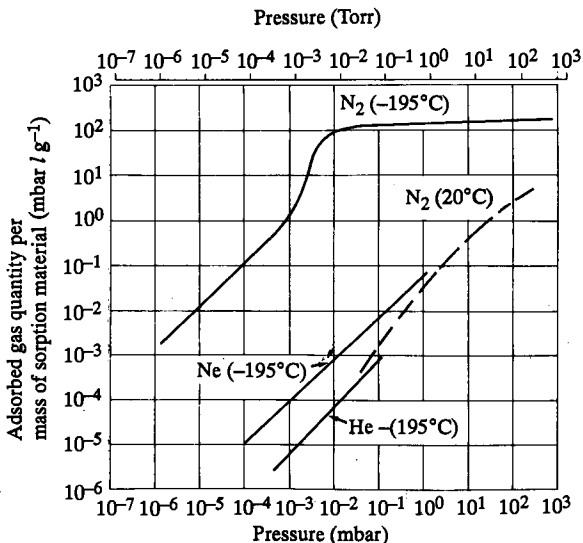


**Figure 3.12** Schematic diagram of an adsorption pump.  
1, inlet port; 2, degassing port/safety outlet; 3, support for Dewar;  
4, pump body; 5, heat-conducting fins; 6, adsorbant, e.g. molecular sieve

Generally, molecular sieves, in the form of pellets, are used as the adsorbant. Molecular sieves are synthetic zeolites (metal aluminosilicates). Types 5A (Ca aluminosilicate) and 13X (Na aluminosilicate) are commonly used. These materials have a very large surface area (several hundred  $\text{m}^2 \text{g}^{-1}$ ) and, therefore, have a considerable gas sorption capability. The pore size depends on the type of molecular sieve. Types 5A and 13X have pore diameters of 0.5 and 1.3 nm, respectively. Since the amount of gas adsorbed can be large, a safety-valve is provided to prevent a great pressure build-up in an isolated pump if the refrigerant is removed.

The design and performance of adsorption pumps is determined by various factors, including the type of gas being pumped and the capacity of the sieve. Isotherms for a type 5A molecular sieve (Figure 3.13) (Turner and Feinleib, 1962) show that, at liquid nitrogen temperature, larger quantities of nitrogen are adsorbed than Ne or He. A complete monolayer appears to be formed at about 100 mbar  $\text{l g}^{-1}$  and, thereafter, adsorption is significantly reduced. The adsorption of gas depends not only on the temperature but also on the pressure above the adsorbate surface. Because of the different adsorption properties, the pumping speed and ultimate pressure of an adsorption pump are different for different gases. The best performance is obtained when pumping  $\text{N}_2$ ,  $\text{CO}_2$ , water and other vapours. Light noble gases are hardly adsorbed at all.

From the isotherms, characteristic data can be obtained from which the performance of the molecular sieve as a pump can be calculated. This is usually expressed in terms of the pressure achieved when the system



**Figure 3.13** Adsorption isotherms for  $\text{N}_2$  ( $-195^\circ\text{C}$  and  $20^\circ\text{C}$ ),  $\text{Ne}$  ( $-195^\circ\text{C}$ ) and  $\text{He}$  ( $-195^\circ\text{C}$ ) on type 5A molecular sieve (From Turner and Feinleib, 1962)

(vessel + pump volume) at a particular starting pressure is exposed to the adsorbant which is subsequently chilled to liquid N<sub>2</sub> temperature. The procedure is detailed by Henning (1989). For example, for a system (volume =  $V$ , temperature =  $T_1$ , starting pressure,  $P_1$ ), the amount of gas in the system can be expressed as:

$$P_1 V \frac{T_n}{T_1} + m A_{T_1}^* P_1$$

where  $T_n \sim 273\text{K}$  and represents a 'standard' temperature against which to measure ( $PV$ ) terms,  $m$  is the mass of the adsorbant and  $A_T^*$  is obtained from the appropriate adsorption isotherm at  $T_1$ . It represents the slope of simplified isotherms (quantity adsorbed/unit mass of adsorbant/relevant pressure range).

When the adsorbant is chilled (to  $T_2$ ), the mass of gas remains the same but the pressure falls due to adsorption. The resulting pressure ( $P_2$ ) is obtained from:

$$P_1 V \frac{T_n}{T_1} + m A_{T_1}^* P_1 = P_2 V \frac{T_n}{T_1} + m A_{T_2}^* P_2$$

$$P_2 = P_1 \frac{V_0 + m A_{T_1}^*}{V_0 + m A_{T_2}^*} \text{ where } V_0 = V \frac{T_n}{T_1}$$

$$= P_1 \frac{\frac{V_0}{m} + A_{T_1}^*}{\frac{V_0}{m} + A_{T_2}^*}$$

If the pump is used several times without intermediate regeneration, then adjustments must be made to the above formula which take into account the quantity of gas previously adsorbed.

The ultimate pressure that can be obtained with an adsorption pump evacuating a system from atmospheric pressure is approximately  $10^{-2}$  mbar. By using two pumps, the situation can be improved somewhat. If the pumps are used in parallel, only a slight improvement is obtained. If the pumps are used successively then, depending on the procedure, quite low pressures can be achieved. The most satisfactory method with dual pumps appears to be:

1. With the valves to *both* pumps open, cool one pump down.
2. When the pressure ceases to fall, isolate the cold pump.
3. Chill the second pump.

Unfortunately, evacuation of a vessel initially containing atmospheric air using this technique can achieve only limited success due to the presence of neon and helium ( $p_{\text{Ne}}$  in air,  $2 \times 10^{-2}$  mbar;  $p_{\text{He}}$ ,  $5 \times 10^{-3}$  mbar). One method that will reduce the partial pressures of noble gas is to flush or back-fill the chamber with a gas such as dry N<sub>2</sub>.

A very large adsorption pump was designed and successfully operated some years ago for the continuous evacuation (down to  $10^{-2}$  mbar) of a flow system. Throughputs of up to  $10 \text{ mbar l s}^{-1}$  were maintained for several hours (Creek *et al.*, 1968).

### 3.3.2 Getter pumps

Getters take up gas by adsorption, absorption (diffusion into the interior of the getter) and chemical compound formation. The initial stage involves the interaction of the particle with the surface (measured by the 'sticking probability') and, for a getter area  $A$ , the pumping speed is given by:

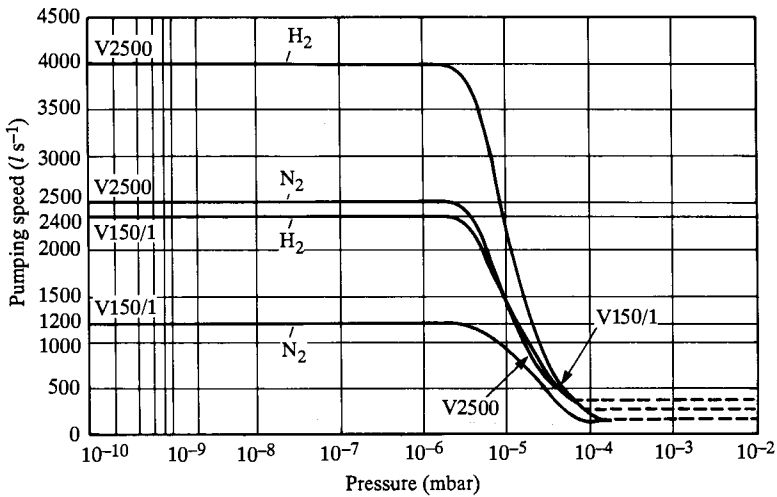
$$S = \alpha A \bar{c} / 4$$

where  $\alpha$  is the sticking probability and  $\bar{c}$  is the thermal speed of the gas molecules. The value of  $\alpha$  is very dependent on the conditions. It generally increases with decreasing temperature and decreases with the degree of coverage. Experimental observations suggest that surface coverage, in some cases, remains so low during gas adsorption that rapid diffusion into the bulk must be occurring. When the getter is saturated with gas particles,  $S$  is reduced to a very low level. The working temperature of the getter for maximum gas adsorption can also be different for each gas–solid system. For example, with Ba at  $50^\circ\text{C}$ , an evaporated deposit will pump oxygen for a considerably longer time than carbon monoxide, due possibly to the formation of a thin, protective layer which stops further interaction. At  $40^\circ\text{C}$ , a similar phenomena is observed with  $\text{O}_2$  but, at temperatures greater than  $80^\circ\text{C}$ , both gases react completely.

Almost any metal that reacts with gases such as  $\text{H}_2$ ,  $\text{N}_2$ ,  $\text{O}_2$ ,  $\text{H}_2\text{O}$  and  $\text{CO}_2$  can be used as a getter. Usually, however, the preferred material is restricted to a few. Two types of getter are available and these are termed evaporable and non-evaporable (bulk) getters. Usually the evaporable getter works at room temperature and below, while NEG (non-evaporable getters) are activated by heating and operate at relatively high temperatures. Commonly used evaporable getters include Ca, Ba, Ti, Th, Mo and Zr, whilst the NEGs are metals such as Ta, Ti, Zr and alloys such as Zr-Al, Zr-V-Fe, etc. A review of getters and gettering has been given by Giorgi *et al.* (1985).

Evaporable or sublimation getter pumps depend on the ability of a thin film of getter to adsorb gas. The pumping speed, as discussed at the beginning of this section, is high if the film has been freshly deposited and is cooled. The speed, however, gradually declines as the degree of surface coverage increases and the film of getter may have to be renewed. This may be achieved either by continuous or intermittent evaporation. The pumping speed–inlet pressure relationship is interesting for evaporation pumps (Figure 3.14). It is constant (as long as coverage  $\ll 1$ ) until pressures are reached where the mean free path of the evaporating getter particles is the same as the distance between the source and the collecting device for the film, and then it declines. Further pressure increase causes further speed reduction until pumping finally stops.





**Figure 3.14** Pumping speed–pressure characteristics of commercial Ti sublimation pumps for  $N_2$  and  $H_2$ .

Titanium sublimation pumps are fairly simple devices. They consist of a cylindrical, stainless steel pump body containing the evaporation source for the getter and, usually, a screen collector for the evaporated material. The pump has a flange to attach it to the vacuum system. Supports for the getter filament material and electrical leadthroughs are also incorporated (Figure 3.15(a)). The evaporation rate is an exponential function of temperature and the filament may have to be run close to its melting point. To prevent rapid burnout, the Ti is often alloyed with another metal (the preferred alloy is 85% Ti – 15% Mo) in order to raise the melting point. Pumps can be run under various conditions (constant current, constant voltage) but the most efficient way is to find the minimum evaporation rate to give the maximum pump speed. The manufacturer usually recommends ‘on/off’ intervals and currents for pumping at various pressures. The onset of crystal growth in the filaments, which leads to embrittlement, marks the end of the filament life.

The variation of sticking probability with getter temperature and its dependence on gas type is important. Some approximate data are shown in Table 3.2.

A Ti sublimation pump with facilities for  $LN_2$ -cooling of the screen collector is shown in Figure 3.15(b). Although  $LN_2$  cooling increases the pumping speed for  $N_2$ , there is no difference between water- and  $LN_2$ -cooling for  $H_2$ .

The Ti sublimation pump is used in conjunction with another pump. Any high vacuum pump is suitable as long as it has the capacity to remove gases not taken up by the getter. Sputter ion and turbomolecular pumps are often used in combination with TSP for clean pumping into the extreme UHV

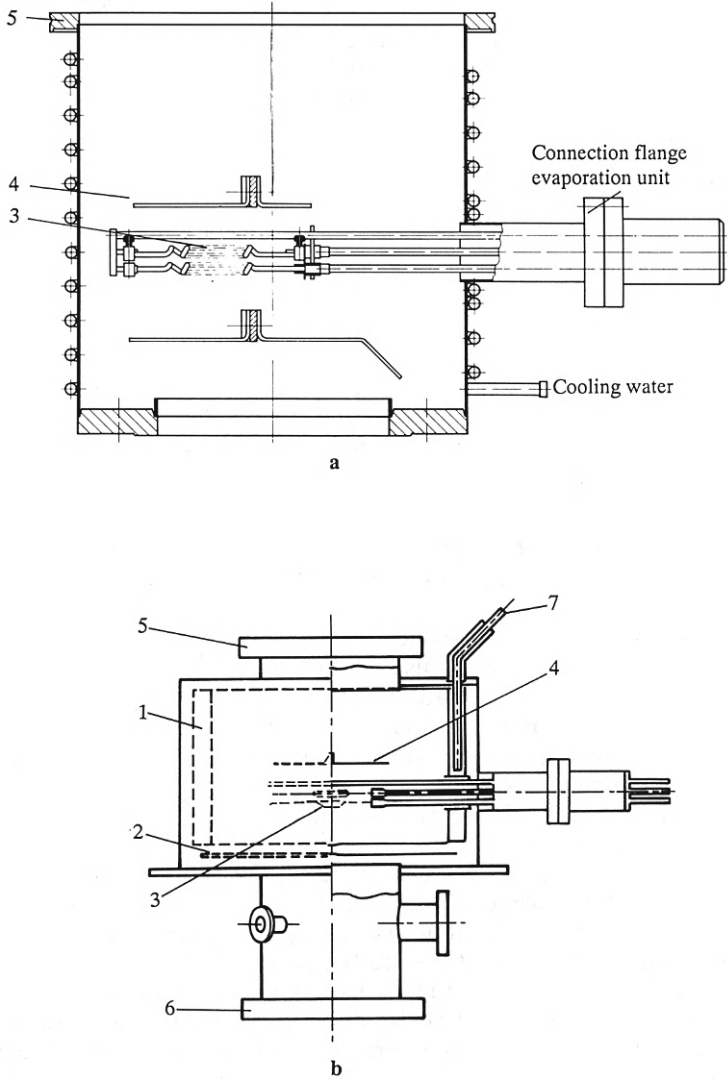
**Table 3.2** *Approximate sticking probability ( $\alpha$ ) for gases on Ti at various coverages ( $\theta$ ) (Gupta and Leck, 1975)*

Gas	Ti (77K)	Ti (300K)	$\theta$
N <sub>2</sub>	1	0.3	0.5
	0.005	0.001	1
	—	—	2
H <sub>2</sub>	0.06	0.04	0.5
	0.03	0.02	1
CO	1	1	0.5
	0.8	0.2	1
	0.1	—	2
O <sub>2</sub>	1	1	0.5
	1	1	1
	0.8	0.9	2

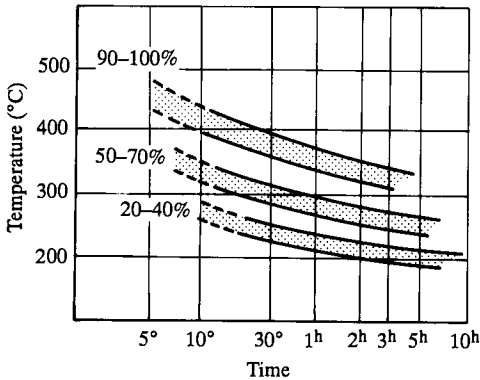
range. Because of the ability of the getter pump to remove H<sub>2</sub>, pressures of  $\leq 5 \times 10^{-12}$  mbar can be obtained with Ti sublimation + turbomolecular pumps.

Bulk getter or NEG pumps are based on materials that allow initial gas adsorption followed by its rapid diffusion into the bulk. Their speed for pumping gases is determined by the rate of this process and they are operated at relatively high temperatures. Various materials can be used in NEG pumps, including Ta, Nb, Ti, Th, etc. Binary (particularly 84% Zr – 16% Al) and ternary Zr-containing alloys (for example, 70% Zr – 24.6% V – 5.4% Fe) are, however, preferred. In order to obtain efficient gettering, the materials must be activated under vacuum.

Metals such as Ta, Ti and Zr have to be regenerated at quite high temperatures (600–2000°C), whereas alloys can be activated under less severe conditions. In Figure 3.16, for example, the efficiency (percentage of initial pumping speed compared with that of a fully-active getter) of regeneration for a Zr-V-Fe alloy is shown as a function of time and temperature. The function of the activation process is to drive any compounds (oxides, nitrides, carbides), which are formed during the pumping of some gases, more deeply into the bulk. NEGs are operated at fairly high temperatures (Ta, 700–1200°C; Zr-Al, 200–400°C) in order to prevent the formation of impervious surface films. Hydrogen and its isotopes appear to form solid solutions with the getter and, during activation, the gas is evolved and must be pumped away. Inert gases are not pumped. NEG may be manufactured in the form of pellets, powder, strips and rods and various configurations of pump are possible. The main criteria appear to be the need to activate the getter and maintain it at its operating temperature. For a given pump volume, the



**Figure 3.15** Versions of titanium sublimation pumps. 1, cylindrical, cooled getter screen; 2, screen plate cooled by heat conduction; 3, evaporation coil; 4, screening plate; 5, connection for vacuum chamber; 6, connection to the pump; 7, LN<sub>2</sub> supply



**Figure 3.16** Efficiency of activation of a Zr-V-Fe alloy as a function of temperature and time (Sciuccati et al., 1988)

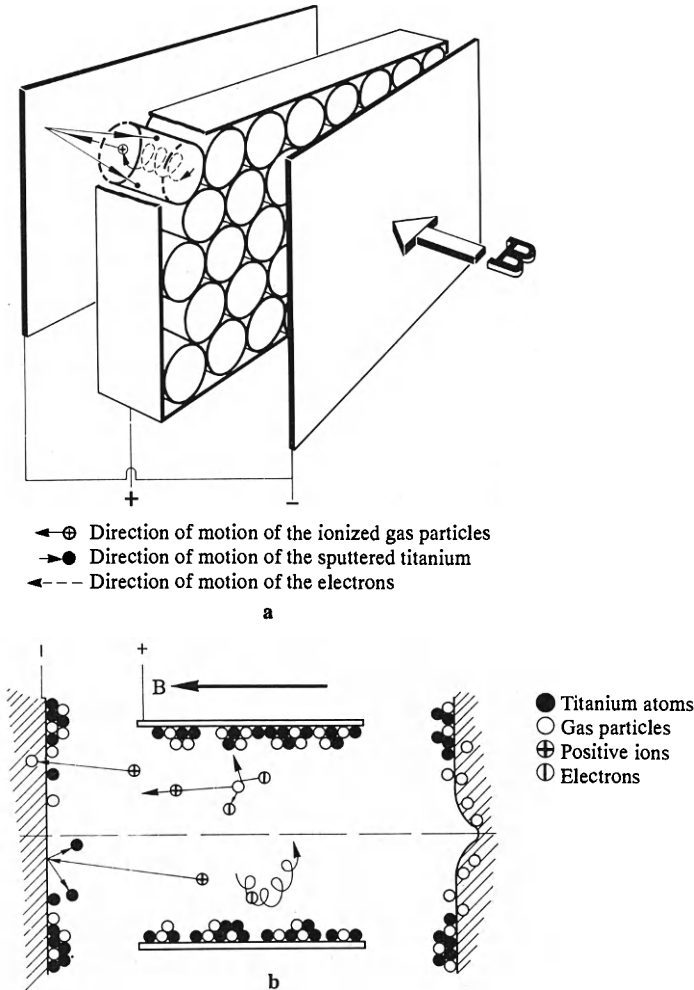
pumping speed of a NEG pump is less than for a titanium sublimation pump. The getter material must be changed when it is saturated but it lasts considerably longer than the filaments in a sublimation pump.

### 3.3.3 Sputter-ion pump

The getter pumps so far described cannot pump chemically inert gases. This can be achieved by the generation of ionized particles within the pump. On acceleration, these particles bury themselves deeply into solid surfaces and are, therefore, removed. The development of ion pumps has been reviewed recently by Audi and de Simon (1987). In this section, evaporation ion pumps will not be covered and discussion will be restricted to sputter-ion pumps.

The action of sputter-ion pumps is based on sorption processes initiated by ionized gas particles. Ions are produced in a gas discharge in what has been termed a Penning cell (Audi and de Simon, 1987). This consists of a cylindrical anode placed between two parallel cathodes. The cathodes are at negative potential (a few kV) relative to the anode and the entire electrode system is maintained in a strong, homogeneous magnetic field, parallel to the anode axis (for further details see Section 4.1.2.2). Electrons in the gas discharge are contained within the anode and the probability of ionizing collisions with neutral gas particles is high. In the basic sputter-ion pump, the anode is made of stainless steel and placed between two titanium cathodes. The electrodes are enclosed in a stainless steel body with the magnetic field being provided by an external permanent magnet. As a result of ion bombardment of the cathode, Ti is sputtered within the pump. Penning cells of radius 15–25 mm and length 10–40 mm are normally used (Audi and de Simon, 1987) which allow operation in a magnetic field of flux 0.1–0.15 T. A voltage of approximately 3 kV is necessary to ignite a discharge at low pressures. Current increases with voltage until a plateau is reached at

approximately 7 kV. Ion pumps are normally operated in this range. A single cell has a pumping speed between  $0.3$  and  $2 \text{ l s}^{-1}$ . It is usual to have a large number of cells within a pump (Figure 3.17(a)). Pumping in sputter-ion pumps involves three effects (Figure 3.17(b)). During bombardment, ions may penetrate and become implanted in the cathode. This mechanism is effective for all types of gas ion. The bombardment process also sputters cathode material onto surrounding surfaces. This can then remove 'getterable' gases ( $\text{O}_2$ ,  $\text{N}_2$ ,  $\text{H}_2\text{O}$ ,  $\text{CO}$ ,  $\text{CO}_2$ ). The third effect, responsible for the



**Figure 3.17** (a) Schematic diagram of a diode-type sputter-ion pump. (b) Schematic diagram showing pumping mechanisms. Discharge current ( $I$ ) is a function of  $n_0$  and can be used to measure  $P$ .

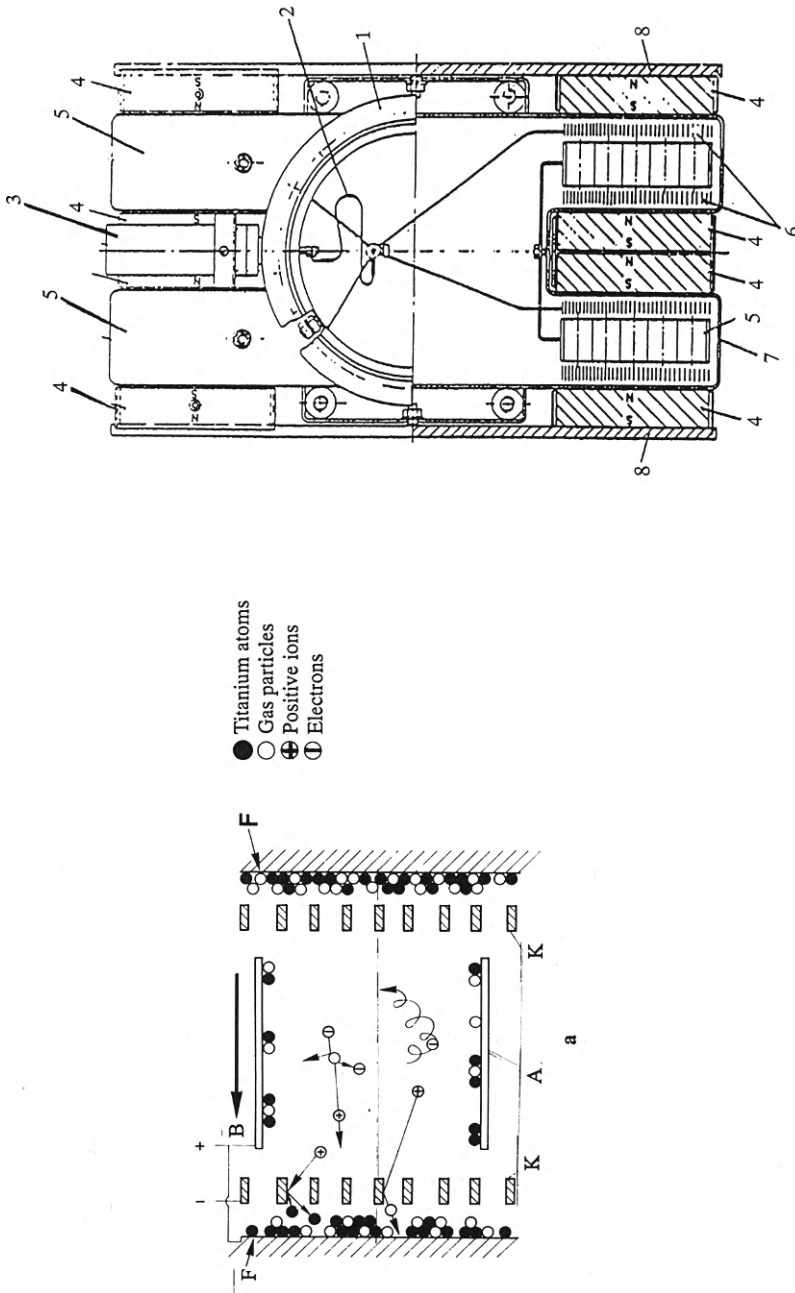
removal of noble gases, involves the rebounding of a neutralized gas ion from the cathode. This effect is a function of the angle of incidence of the ion and the relative masses of the target and ion. If the rebounding species retain their original energy, then they can bury themselves in the pump walls and the anode. Thereafter, they may be buried by sputtered material from the cathode. This mechanism is termed 'bounce-back'.

Diode-type pumps are not entirely successful for the removal of noble gases – the pumping speed is low ( $0.01\text{--}0.03 S_{N_2}$ ) and it is unstable. A phenomenon termed 'instability for noble gases' can arise when steep and sudden increases in pressure are observed after pumping large amounts of noble gas. This is due to the release of implanted gas particles during sputtering. Attempts have been made to increase 'bounce-back' and thereby improve both the stability and speed of pumps for noble gases. Increasing the molecular mass of the cathode helps and pumps with one Ta ( $M = 181$ ) cathode and one Ti cathode have been developed. This gives higher pumping speeds for noble gases ( $0.2 S_{\text{air}}$ ) and removes some instability. A more successful approach has been to increase the probability of glancing-angle collisions by using cathodes which are in the form of a grid (Figure 3.18(a) and (b)). The cathode in this case is semi-transparent and the inside wall of the pump housing is used as a 'third electrode'. This configuration is referred to as a triode pump. The anode and pump walls are at earth potential, while the cathodes are maintained at negative voltage.

With the triode pump, ions are accelerated out of the discharge towards the cathode which they strike with glancing incidence. Cathode material is sputtered, producing a getter deposit. During the collision, ions are neutralized without significant energy loss and may become implanted. Ions which have not lost their charge cannot move to the wall and return to the cathode and may cause further sputtering. The result of these effects is pumping speed for noble gases which is  $0.25\text{--}0.3$  that for  $N_2$ . A design variant on the triode pump uses cathode plates which are perforated in a complicated manner to yield finned cells (Starcell TM form; see Audi and de Simon, 1987).

A pressure of about  $10^{-3}$  mbar is required to confine the discharge in a Penning cell. It can be maintained down to very low pressures. The starting pressure for an ion pump is, therefore, in the range  $10^{-2}$  to  $10^{-3}$  mbar, depending on the type of pump, although the preferred operating range is below  $10^{-5}$  mbar. For pre-evacuation, 'clean' pumps should be used and turbomolecular pumps are frequently employed. The usual ultimate pressure reached with an ion-pumped system is in the range  $10^{-10}$  to  $10^{-11}$  mbar. An ion pump gives its best performance only when it is combined with a power supply with the appropriate characteristics (Weston, 1985).

Sputter-ion pumps are commercially available with nominal speeds up to  $500 \text{ l s}^{-1}$ . According to PNEUROP specifications the maximum of the pumping speed for  $N_2$  or air versus pressure curve is denoted as the 'nominal pumping speed'. The pressure at which  $S$  is quoted must be given. They produce a very clean vacuum and are used both in relatively small systems or in large-scale plants such as synchrotrons (Trickett, 1988) which require a large number of relatively small pumps rather than a few very large units.



**Figure 3.18** (a) A triode-type sputter-ion pump. A, anode cylinder (same as for diode-type pumps); K, cathode grid; F, target (wall of pump housing) forming the third electrode; B, Magnetic field. (b) Plan and cross-sectional views of a triode-type sputter-ion pump (Leybold IZ 270). 1, inlet flange; 2, band conductor; 3, current leadthrough; 4, permanent magnets; 5, anodes in frames (A in Figure 3.18(a)); 6, cathode grid; 7, target (F in Figure 3.18 (a))

### 3.3.4 Cryopumps

Cryopumps are entrapment pumps. The process of cryopumping involves the removal of gas particles from a system by means of surfaces cooled to temperatures below 120K. At sufficiently low temperatures, all gases, with the exception of He, condense to form a solid phase and this phenomenon is termed cryocondensation. The pressures obtainable by cryocondensation depend on the vapour pressure of the solid phase. A temperature of 20K (normal b.p. of  $\text{LH}_2$  is 20.3K) is sufficient to achieve UHV conditions for all gases except Ne, He, hydrogen and deuterium (Figure 3.19). In order to obtain these pressures with  $\text{H}_2$ , a temperature below 4K must be achieved (normal b.p., liquid  $^4\text{He} = 4.21\text{K}$ ). This presents a problem since hydrogen is readily released into a vacuum by many materials (see Chapter 6).

A phenomenon that increases the effectiveness of a cryopump very significantly is termed cryosorption. In cryosorption, a gas with a very low boiling point is adsorbed on a cooled solid at a higher temperature. In commercially available cryopumps, the adsorbant used is a solid such as activated charcoal or a molecular sieve. The effectiveness of this mechanism

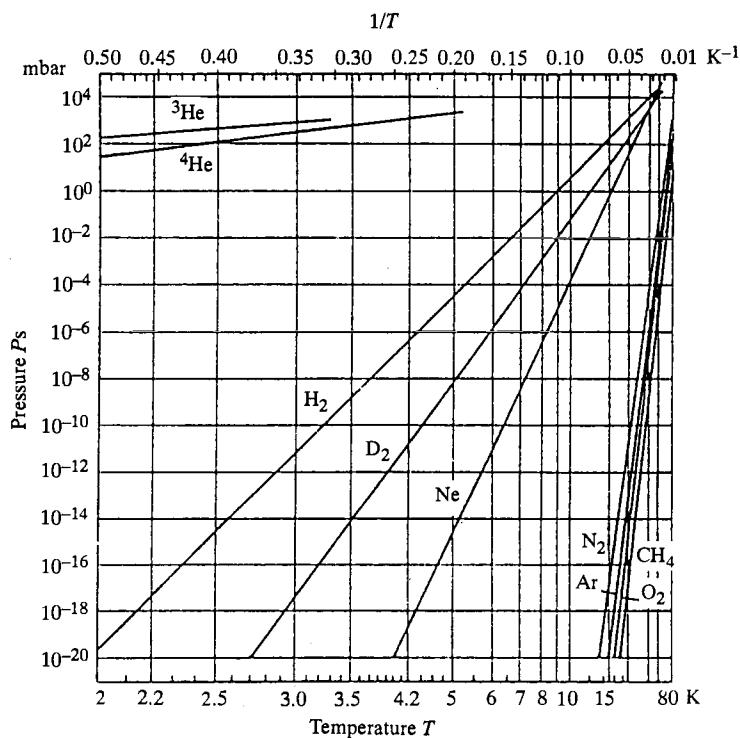


Figure 3.19 Cryocondensation



can be seen in Figure 3.20, which shows the adsorption equilibrium pressure of H<sub>2</sub> and He in the presence of cryocooled activated charcoal. Cryosorption may also occur at the surface of a gas condensate. Whereas cryocondensation can involve the formation of condensate layers several millimetres thick, cryosorption involves mono-layer formation, and solids with very large surface areas are required as the adsorbants.

A third mechanism that will inevitably occur during the cryopumping of gas mixtures is termed cryotrapping. This involves the condensation of a low-boiling-point gas in the presence of a higher-boiling species. Argon, ammonia and CO<sub>2</sub> have been used as co-condensates with hydrogen. With cryotrapping partial pressures of hydrogen several orders of magnitude less than the vapour pressure of pure hydrogen at the same temperature have been observed. Cryotrapping is rarely used as a method of pumping, however, since a second component must always be present. A schematic diagram of the mechanism of gas trapping at cold surfaces is shown in Figure 3.21.

In any cryogenic system, the heat load transferred to the cold surface determines the refrigeration capacity required to maintain the low temperature. Analysis has shown that the thermal loads received by a surface at cryogenic temperatures are due to:

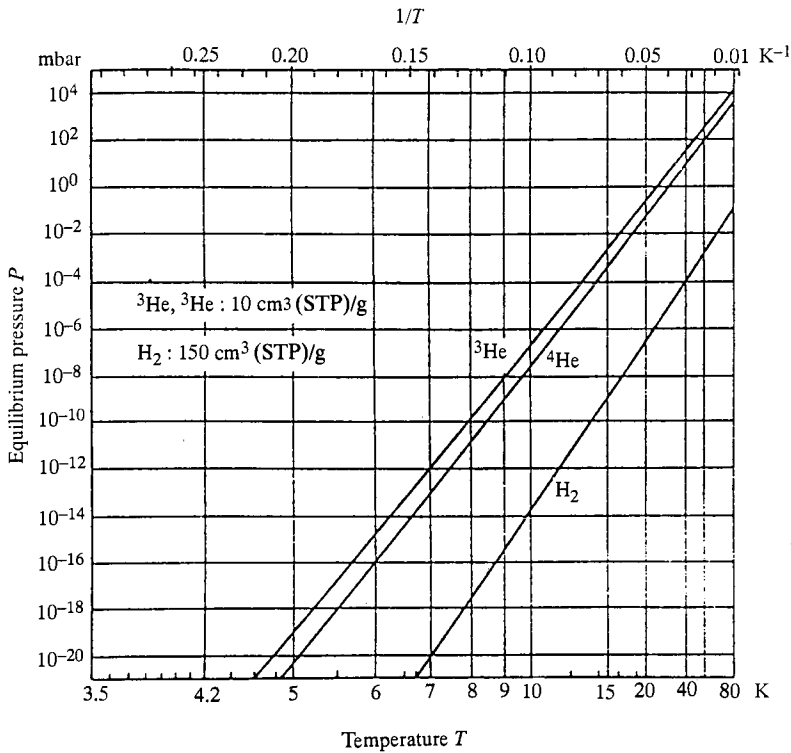
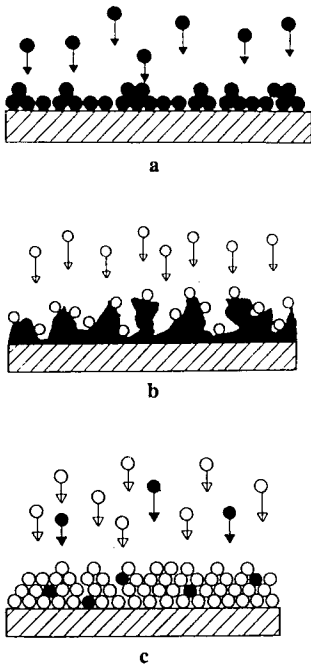


Figure 3.20 Effectiveness of cryosorption



**Figure 3.21** Mechanisms of gas trapping at cold surfaces (from Baechler, 1987). (a) cryocondensation; (b) cryosorption; (c) cryo-trapping

1. Thermal radiation ( $\dot{Q}_{\text{rad}}$ ) from a warm surface ( $T_R$ ) to the cold surface ( $T_C$ ). This is proportional to the area ( $A$ ) of the cryosurface, the relative emissivity ( $\epsilon$ ) and the temperature difference ( $T_R^4 - T_C^4$ ):

$$\dot{Q}_{\text{rad}} \sim A\sigma\epsilon(T_R^4 - T_C^4)$$

where  $\sigma$  is the Stefan–Boltzmann constant, and  $\dot{Q}_{\text{rad}}$  depends on the emissivity of the cold surface. It is convenient during the construction of cryoequipment to reduce  $\epsilon$  as much as possible by polishing or gold-plating ( $\epsilon \sim 0.03$ ). If a condensate film accumulates, however,  $\epsilon$  changes and, for films several millimetres thick, it can approach 0.9 ( $\epsilon$  for a black body = 1).

2. The heat load due to gas condensation ( $\dot{Q}_{\text{cond}}$ ). This involves the heat which has to be extracted from the gas to cool it to the trapping temperature and the enthalpy of condensation (or heat of adsorption). This quantity increases with gas throughput.
3. The heat load due to the thermal conductivity of the gas ( $\dot{Q}_{\text{th.cond}}$ ). There are gas particles between the cryosurface and the warm surroundings. This quantity is negligible at low pressures but must be taken into account above  $10^{-3}$  mbar.

$$\dot{Q}_{\text{TOT}} = \dot{Q}_{\text{cond}} (\dot{Q}_{\text{ads}}) + \dot{Q}_{\text{th.cond}} + \dot{Q}_{\text{rad}}$$

Of these terms,  $\dot{Q}_{\text{rad}}$  predominates. It is extremely high when the cryopanel is surrounded by surfaces at normal ambient temperatures but it can be reduced significantly by surrounding it with a shield at, say 77K, when the heat flux due to radiation decreases to about 1% of its room temperature value. Cooled radiation baffles are incorporated between the cryopanel and the area to be evacuated. Their design arises from the need to minimize the thermal load due to radiation whilst maintaining adequate conductance for the gas to be pumped. The geometrical arrangements that have evolved for small cryopumps are:

- (a) Chevron baffles
- (b) Louvres and modified chevrons

Data regarding the effectiveness of various cryopanel-baffle configurations are presented in the book by Haefer (1981). Very large cryopumps use an 'open structure' type of baffle (see Coupland *et al.*, 1982).

#### 3.3.4.1 Characteristics of cryopumps

Cryopumps have characteristics that greatly influence their usefulness and the manner in which they are operated. These include the starting pressure, pumping speed, ultimate pressure and capacity.

##### (i) Starting pressure

In principle, a cryopump can be started at atmospheric pressure. This would be undesirable, however, for two reasons. Firstly, at pressures above  $10^{-3}$  mbar,  $\dot{Q}_{\text{th.cond}}$  may be extremely large. The heat transfer per unit surface area by conduction of various gases over a range of pressures can be readily calculated. Secondly, a thick layer of condensate would form and reduce the capacity of pump. It is usual, therefore, to pre-evacuate the system to an acceptable pressure. The pump used for pre-evacuation should be large enough to allow the starting pressure to be achieved within a suitable time. All precautions should be taken to minimize contamination of the cryopump. An empirical relationship for a normally operating cryogenerator-cooled pump, separated from a vacuum chamber by a valve, suggests that the valve can be opened if:

$$pV\dot{Q}_2 \leq 30 \text{ mbar l W}^{-1}$$

where  $p$  is the starting pressure,  $V$  is the chamber volume and  $\dot{Q}_2$  is the cooling power of the second stage of the cryogenerator (see Section 3.3.4.3).

##### (ii) Ultimate pressure

The ultimate pressure ( $p_{\text{ult}}$ ) that can be obtained in a cryopump depends, in the case of cryocondensation, on the saturation vapour pressure ( $p_{\text{sat}}$ ) of the gas or gases to be pumped, the temperature ( $T_c$ ) of the cryopanel and the wall temperature ( $T_w$ ) of the pumped system. It is given by the equation:

$$p_{\text{ult}} = p_{\text{sat}} \sqrt{\frac{T_w}{T_c}}$$

**Table 3.3** Variation of vapour pressure (mbar) with T(K)

Gas	$10^{-10}$	$10^{-8}$	$10^{-6}$	$10^{-4}$	$10^{-2}$	$10^1$	$10^3$
Ar	23.5	26.6	30.3	35.4	42.7	61.3	87.2
H <sub>2</sub>	2.98	3.47	4.17	5.22	6.78	11.4	20.3
Ne	6.42	7.28	8.40	9.93	12.13	18.1	27.1
N <sub>2</sub>	21.0	23.5	26.8	31.1	37.0	53.0	77.3
O <sub>2</sub>	25.0	28.0	31.6	36.3	42.8	61.3	90.1

Table 3.3 gives the vapour pressures for some gases at the appropriate temperatures which can be used in the above expression.

For example, the ultimate pressure that can be obtained in a chamber at 300K containing H<sub>2</sub> with a cryopump maintained at 4.2K with liquid He is:

$$p_{\text{ult}} \sim 10^{-6} \times \sqrt{\frac{300}{4.2}} \sim 8.5 \times 10^{-6} \text{ mbar}$$

If the chamber contained Ne, for example, and was pumped by a cryogenerator at 10K, then:

$$p_{\text{ult}} \sim 10^{-4} \times \sqrt{\frac{300}{10}} \sim 5.5 \times 10^{-4} \text{ mbar}$$

Much lower ultimate pressures can be achieved with cryosorption and cryotrapping but these are difficult to calculate.

### (iii) Pumping speed

The theoretical pumping speed for a surface that is so cold that the probability of particles condensing on it is unity, can be calculated in terms of the molecular conductance of an aperture:

$$S \text{ (l s}^{-1}\text{)} = 3.64 \sqrt{\frac{T_w}{M}} \left( 1 - \frac{p_{\text{sat}}}{p} \sqrt{\frac{T_w}{T_c}} \right) \text{ per cm}^2 \text{ of aperture as } p \rightarrow p_s.$$

At much higher pressure, the terms in brackets can be ignored.

In this expression,  $M$  is the relative molecular mass of the gas,  $p$  is the pressure of the gas in the vessel being evacuated and  $T_w$ ,  $T_c$ ,  $p_{\text{sat}}$  have been defined above.

Since the first term ( $3.64 (T_w/M)^{1/2}$ ) is determined by the average speed of gas molecules at  $T_w$ , we obtain the maximum pumping speed at 300K and 77K for various gases, given in Table 3.4. If a cryopanel has an area  $A_c$ , then the theoretical pumping is  $SA_c$ . Using this expression, it can be shown that, for a panel of 300 cm<sup>2</sup> and a gas temperature of 300K,  $S$  for O<sub>2</sub>, Ne and H<sub>2</sub> are 3300, 4170 and 13320 l s<sup>-1</sup>, respectively. When the cryopanel is shielded by a

**Table 3.4** Maximum pumping speed (s) for some gases ( $l\ s^{-1}\ cm^{-2}$ )

Gas ( $T_w/K$ )	H <sub>2</sub>	O <sub>2</sub>	N <sub>2</sub>	Air	H <sub>2</sub> O
300	44.5	11.1	11.9	11.7	14.9
77	22.6	5.7	6.0	5.9	–

baffle, with a transmissivity ( $t_B$ ), the pumping speed decreases by an appropriate factor:

$$S_{\text{eff}} = S \times \frac{\alpha t_B}{\alpha + t_B - \alpha t_B} \quad \text{where } \alpha \text{ is the sticking coefficient}$$

For a louvre baffle,  $t_B = 0.5$ ; for a chevron baffle,  $t_B = 0.25$ . Thus, in the example above,  $S_{\text{eff}}$  for O<sub>2</sub> would be  $1650\ l\ s^{-1}$  (louvre) and  $825\ l\ s^{-1}$  (chevron)

(iv) 'Stay-down' time

This refers to the time that a cryopump can operate with a constant pressure in the chamber before 'saturation' is reached. When cryocondensation is the mechanism responsible for gas trapping, multilayers build up and deposits several millimetres thick can form. The limits to this process arise for two reasons. Either, with increasing thickness, the surface temperature of the condensate rises to the point where no further condensation can occur; or the structure of the deposit is such that it breaks away from the cryopanel and falls onto warmer surfaces where it evaporates. The 'stay-down' time is a function, therefore, of the thermal conductivity of the deposit and the layer thickness ( $x$ ) or the growth rate of the condensate. It can be estimated from the expression:

$$\text{Time} = x \frac{\Delta x}{\Delta t} \quad \text{at pressure } p$$

where  $x$ , based on practical experience, is 0.5 cm.  $\Delta x/\Delta t$  can be obtained from graphs of the dependence of condensate growth rate on pressure at an appropriate gas temperature (say 293K).

Approximate values for the stay-down time are:

$$\text{N}_2 : t = 1.1 \times 10^{-2}/p \quad \text{where } t \text{ is in h and } p \text{ in mbar}$$

$$\text{Ar} : t = 1.5 \times 10^{-2}/p$$

(v) Capacity

The capacity of a cryopump is the maximum amount of gas that can be pumped by cryocondensation or sorption before the pumping speed is significantly reduced. The mass of gas corresponding to this can be obtained from the expression:

$$C_m = \rho \times A_c \times x$$

where  $\rho$  is the density of the condensate and  $A_c$  and  $x$  are as previously defined. In terms of the  $(pV)$  value, it is given by:

$$C_{pV} = S \times p \times t$$

where  $S$  is the speed of the pump,  $p$  is the pressure which is being maintained and  $t$  is the 'stay-down' time.

The pumping capacity is measured experimentally as the quantity of gas (in mbar l) that has been pumped up to the moment when  $S$  has been reduced to 50% of its initial value. The test is run with a dome and a constant throughput so that the 50% decrease in the volume rate of flow is indicated by a corresponding doubling of pressure in the system. The pumping capacity depends on the nature of the gas, and PNEUROP recommends that  $H_2$  should be used as a typical cryosorbed gas and Ar should be used to represent a typical condensable gas.

#### (vi) Others

Refrigerator-cooled cryopumps have additional, important characteristics, including the cool-down time, cross-over point and maximum throughput. These will be discussed in Section 3.3.4.3.

#### 3.3.4.2 Bath and evaporator cryopumps

Some cryopumps may contain a cryogen to achieve temperatures low enough for effective gas removal. The simplest form of cryopump, termed a bath cryopump, consists simply of a surface chilled to the required temperature. Some common liquid cryogens are listed in Table 3.5.

By the use of liquid He, temperatures in the range 4.2–1.5K can be obtained. Consumption of liquid cryogen can be high. For example, the volume of liquid boiled off by the dissipation of 1 W into the fluid at its boiling point is 1.38 and 0.12 l h<sup>-1</sup> for liquid He and H<sub>2</sub>, respectively. To reduce the consumption of a cryogen such as liquid He, a liquid-nitrogen-cooled radiation shield is used.

Cryopumps based on cryogens are frequently used to handle large throughputs of gas with high pumping speed (Coupland *et al.*, 1982). A comparison between refrigerator-cooled pumps and those using cryogens is given in Table 3.6.

**Table 3.5** Cooling potential of various cryogens

Fluid	Normal boiling point (K)	Enthalpy difference between saturated liquid and vapour	
		kJ/kg	kJ/l
He	4.21	20.9	2.6
H <sub>2</sub>	20.3	443	31.4
N <sub>2</sub>	77.4	199.3	160.9
Ar	87.3	161.9	225.7

**Table 3.6** *Comparison between cryogenes and refrigerators for use in cryopumps*

<i>Parameter</i>	<i>Cryogen</i>	<i>Refrigerator</i>
Temperature	Depends on available cryogen, about 1K possible	Down to 5K with appropriate system
Capacity	Limited only by storage/distribution	Depends on size of cryogenerator
Control	Regulation of cryogen flow required Stability can be poor	Achieved by simple manipulation of power input
Reliability	Good	Good if well maintained
Capital costs	Moderate/low per unit of heat extracted	High per unit cooling capacity
Running costs	Depends on cryogen and whether recovery system used	Low
Applications	Very wide	Only where moderate cooling capacity required.

### 3.3.4.3 *Refrigerator-cooled cryopumps*

#### (i) *Cryocoolers*

For routine use in vacuum technology, cryopumps with pumping speeds comparable with other high- and ultra-high-vacuum pumps are required. For this purpose, pumps cooled with fairly low-powered refrigerators, often known as cryocoolers, are used. Most low-power refrigerators use gas compression–expansion cycles. Generally, the work done on the working fluid by compression is rejected to the surroundings via a heat exchanger. The fluid is then expanded in a separate chamber and extracts heat from the chamber to achieve cooling that can be used for refrigeration. Various types of closed-cycle machines have been devised including:

1. The Stirling refrigerator.
2. The modified Solvay refrigerator.
3. The Gifford–McMahon refrigerator.

The refrigeration cycles of these devices have been described by Nambudripad (1986). A large number of commercially available cryopumps are based on the two-stage Gifford–McMahon refrigerator (McMahon and Gifford, 1960), which is capable of producing useful refrigeration down to about 7K. In the Gifford–McMahon process, the working fluid (5N or 6N He) is moved

cyclically through a regenerator located inside a displacement piston. A schematic diagram of a one-stage Gifford–McMahon process is shown in Figure 3.22. Compressed He (20–25 bar) at room temperature is introduced via a rotary valve into a thin-walled cylinder, which forms the main part of the cryocooler, and into a regenerator connected across the hot and cold ends. Initially, high-pressure helium enters the cylinder through the valve and, since a significant force is required to move the displacer, an isochoric compression occurs ( $P_L \rightarrow P_H$  at  $V_{\min}$ ). The valve continues to supply high pressure helium to the system and isobaric expansion through the regenerator takes place ( $V_{\min} \rightarrow V_{\max}$  at  $P_H$ ). At this point, the position of the valve is such that the low-pressure (5–7 bar) side of the compressor is now connected to the system. Gas expands and, in doing so, cools the regenerator ( $P_H \rightarrow P_L$  at  $V_{\max}$ ). Finally, with the low-pressure side still connected, movement of the displacer causes an isobaric decrease in volume ( $V_{\max} \rightarrow V_{\min}$  at  $P_L$ ).

The cycle is now complete and the next one begins. The only difference is that the regenerator is now cooler than before. It is not possible to represent the thermodynamic changes of the gas on a single temperature versus entropy diagram because various portions of the gas follow slightly different paths (Hands, 1987). In two-stage refrigerators (Figure 3.23), the first stage provides pre-cooling for the second stage. The relationship between the performance of the two stages depends on the mass of the working fluid used in each cycle (i.e. on the relative dimensions of the two stages). This is fixed at the design stage. The first stage is cooled to a temperature of 30–80K with a refrigerating capacity between 10 and  $10^2$  W, depending on the type of refrigerator and the gas load. The second stage has a refrigerating capacity from 2 to 10 W, at a temperature between 8 and 20K again depending on the load. The Gifford–McMahon cycle is inherently thermodynamically less efficient than the Stirling cycle. Nevertheless, Gifford–McMahon refrigerators are popular because the compressor works independently on the displacer. This means that the cold head can be mounted in any orientation and standard, commercial, oil-lubricated compressors, used for air-conditioning and refrigeration, can be used. Further, under some circumstances, more than one head can be run from a single compressor.

Regenerator losses are mainly responsible for the low efficiency of small cryocoolers. Typically, they have thermal efficiencies greater than 0.95 but the inefficiency represents a heat flux into the cold end and is often a significant fraction of the useful cooling power. In such systems, longitudinal thermal conduction from the hot to the cold end of the regenerator may occur and thin-walled cylinders and displacers made of suitable materials must be used. Displacers may be made of a suitable resin and in a two-stage unit, the first-stage regenerator consists of hundreds of discs of fine, bronze wire mesh. Alternate stainless steel spacers and punched copper discs have also been used to reduce longitudinal heat conduction. In the second stage regenerator/displacer lead powder is used because it has a higher specific heat than copper-based alloys at low temperature.

The helium compressor unit must maintain the purity of the working fluid and, because of this, stringent precautions are taken. Helium from the



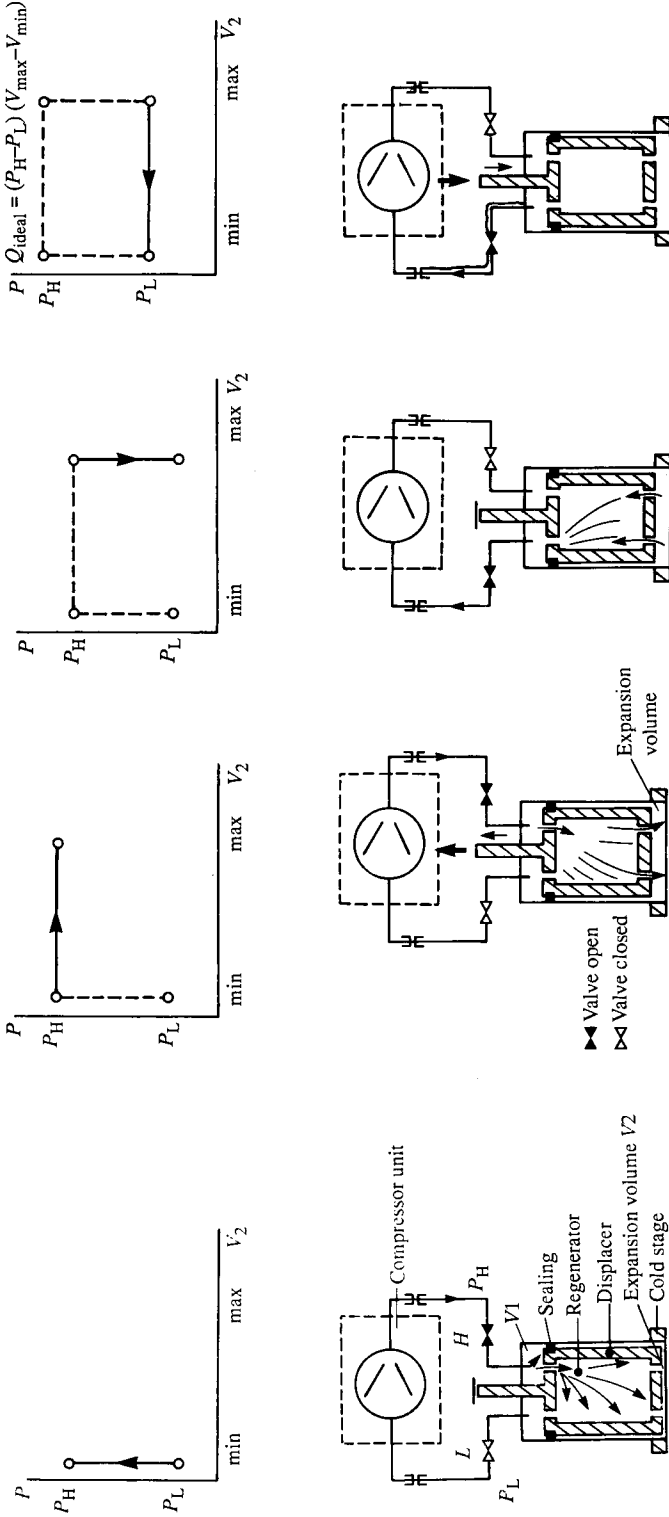
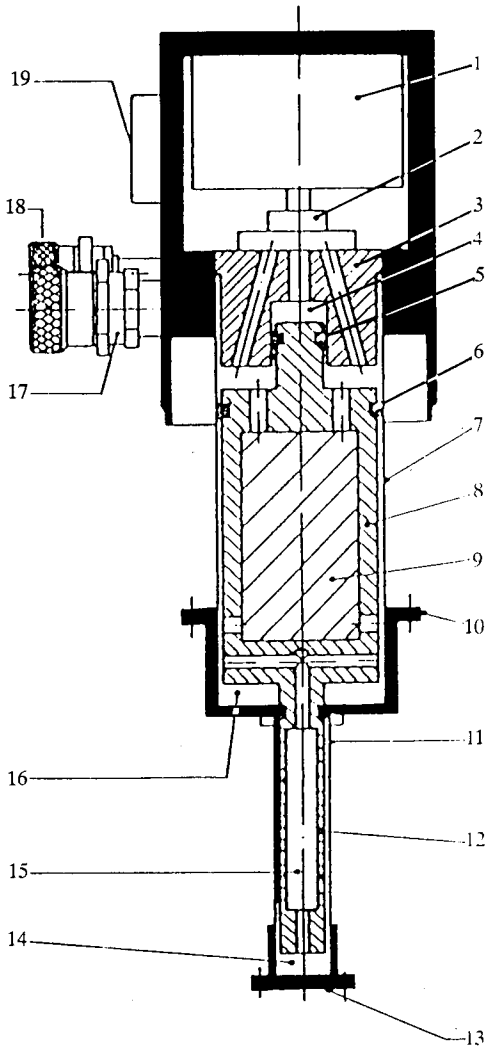


Figure 3.22 Schematic diagram of the Gifford-McMahon refrigeration cycle



**Figure 3.23** Schematic diagram of a two-stage Gifford-McMahon cold head. 1, synchronous motor; 2, control valve; 3, control disc; 4, control chamber; 5, gasket on control piston; 6, gasket for first stage; 7, cylinder; 8, displacer, first stage; 9, regenerator, first stage; 10, first stage; 11, gasket for second stage; 12, displacer, second stage; 13, second stage; 14, expansion volume, second stage; 15, regenerator, second stage; 16, expansion volume, first stage; 17, He low-pressure; 18, He high-pressure; 19, current leadthrough with socket for electric lead

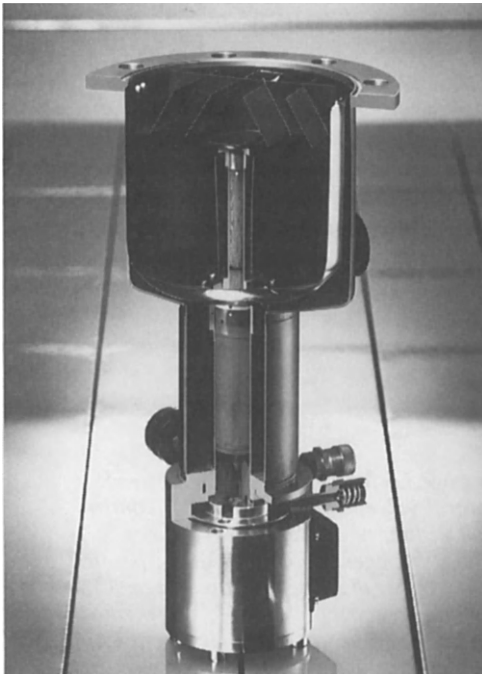
cryocooler is adiabatically compressed and heat extracted in a water-cooled heat exchanger. Thereafter, the gas is passed through an oil separator, containing glass wool, and charcoal adsorbers before passing to the cold head.

The vacuum committee of PNEUROP in 1987 published a procedure to assess the refrigeration capacity (cooling power) of the cold head. This is measured for each stage at a particular temperature, with the other stage maintained at a typical temperature. For two-stage cold heads, the refrigeration capacities are those that maintain steady temperatures at  $T_{1\text{st stage}} = 80\text{K}$  and  $T_{2\text{nd stage}} = 20\text{K}$  when simultaneously loaded.

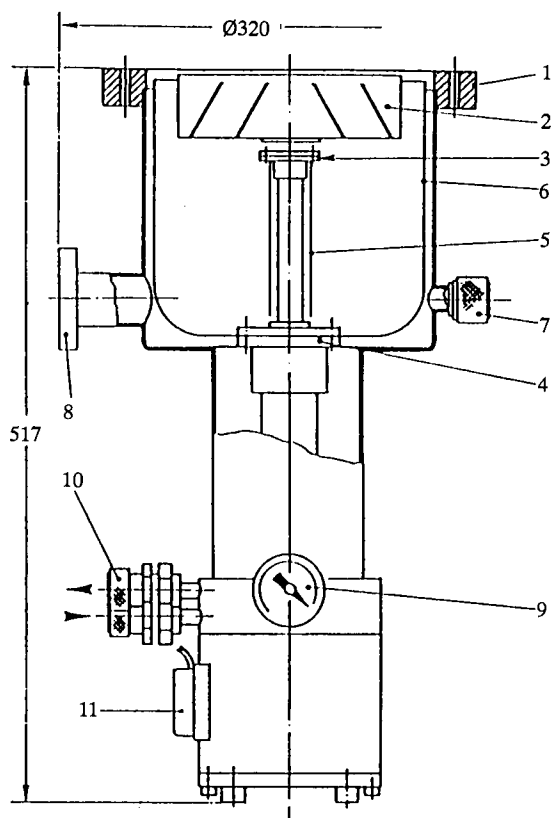
According to the procedure, electrical heaters (allowing well-defined thermal loads) and suitable temperature sensors are fitted to the stages. The cold head is placed in a suitable vacuum housing, protected by super-insulation against radiation. In order to minimize thermal conductivity due to gas, the housing is evacuated to under  $10^{-4}$  mbar for the duration of the test. The stages are cooled and when they have reached a steady operational temperature, the heaters are set and adjusted until the first and second stages can maintain 77K and 20K, respectively.

*(ii) Cryopumps*

The two-stage Gifford–McMahon cryocooler is the basis of most standard cryopumps. A typical vertical pump is shown in Figures 3.24 and 3.25. A



**Figure 3.24** *Cut-away cryopump based on two-stage Gifford–McMahon cold head*



**Figure 3.25** Schematic diagram of a cryopump based on a two-stage Gifford–McMahon cold head. 1, high-vacuum flange; 2, baffle; 3, second stage flange; 4, first stage flange; 5, cryopanel; 6, radiation shield; 7, safety valve; 8, fore-vacuum connection; 9, hydrogen-filled vapour pressure thermometer; 10, He gas connection couplings; 11, electrical connection

cup-shaped radiation shield is attached to the first cold-stage with good thermal contact via an indium gasket. A louvred radiation baffle is placed at the entrance to the cup, attached again using indium metal seals. The cryopanel (Figure 3.25), covered on one side with an adsorbant such as activated charcoal, are bolted to the second stage with the adsorbant facing inwards. In more specialized pumps, designed to have higher pumping speeds and capacities for  $\text{H}_2$ , the configuration of the cryopanel may be *significantly* different from that shown in order to present larger amounts of adsorbant more immediately to the gas (see Figure 3.27).

Standard refrigerator-cooled cryopumps are available with pumping speeds for  $\text{N}_2$  ranging from 400 to 18 000  $\text{l s}^{-1}$ . The cold heads used in these pumps

range in cooling capacity from 12 to 80 W for the first-stage (80K) and from 2 to 10 W for the second stage (20K). They may be attached to the vacuum equipment with CF or LF flanges, the diameters of which can range from 100 to 630 mm. A typical cryopump attached to a compressor is shown in Figure 3.26.

From an operational point of view, refrigerator-cooled cryopumps have certain characteristics in addition to those discussed in Section 3.2.4.1. These include the cool-down time, crossover and maximum throughput. The cool-down time is defined as the time elapsed between starting the pump at room temperature (and a defined pressure) and the point when the second stage reaches 20K. This can vary from 1 to 3 h. The time to attain 10K at the second stage can be relatively long. Crossover is a measured characteristic

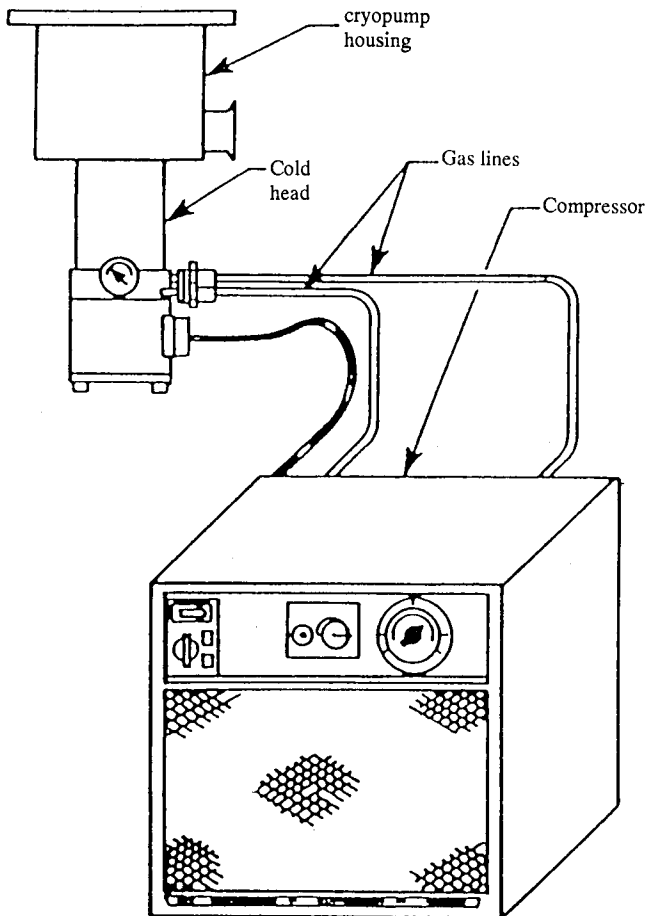


Figure 3.26 *Typical cryopump system*

(PNEUROP (1987) 'Vacuum Pumps, Rules of Acceptance V. Refrigerator-cooled Cryopumps', Draft acceptance specification) and it is defined as the maximum amount of  $N_2$  (in mbar l) that can be admitted to the pump in a short time (98% should be admitted in 3 s) and still allow the second stage to remain at  $\leq 20K$ . Maximum throughput is defined as the maximum quantity of gas flowing through the pump inlet that the pump can withstand whilst maintaining a second-stage temperature of  $20 \pm 1K$ .

At some stage during the operation of a cryopump, it will cease to function efficiently and have to be regenerated. This condition can arise, as discussed earlier, when a cryocondensed deposit is so thick that it fouls the inlet or it touches a warm part of the pump. For cryosorbed gases, regeneration may be more frequent, since the capacity of a pump is significantly less than that for condensable gases, such as  $N_2$  and Ar. Regeneration does not present a problem and three methods are available:

1. The pump is switched off and allowed to warm up.
2. The pump can be purged with warm, dry, chemically inert gas ( $N_2$ , Ar).
3. Electrical heaters are attached to the first and second cold stages.

Regeneration by methods (2) and (3) can only be carried out if the appropriate devices are fitted to the pump.

During regeneration it is always advisable to connect the cryopump to an auxiliary vacuum pump. Release of gas can occur very suddenly and must be handled quickly and efficiently (to prevent a rapid pressure rise in the pump). All standard cryopumps are fitted with safety valves but it is certainly not good practice to allow uncontrollable venting to occur. One must always be aware during regeneration of the gases which have been pumped. High concentrations of highly toxic substances may accumulate. The possibility of fire or explosion must always be considered and it is unwise to operate any energy source (ion gauge, heater) on the chamber during the process.

### (iii) Applications

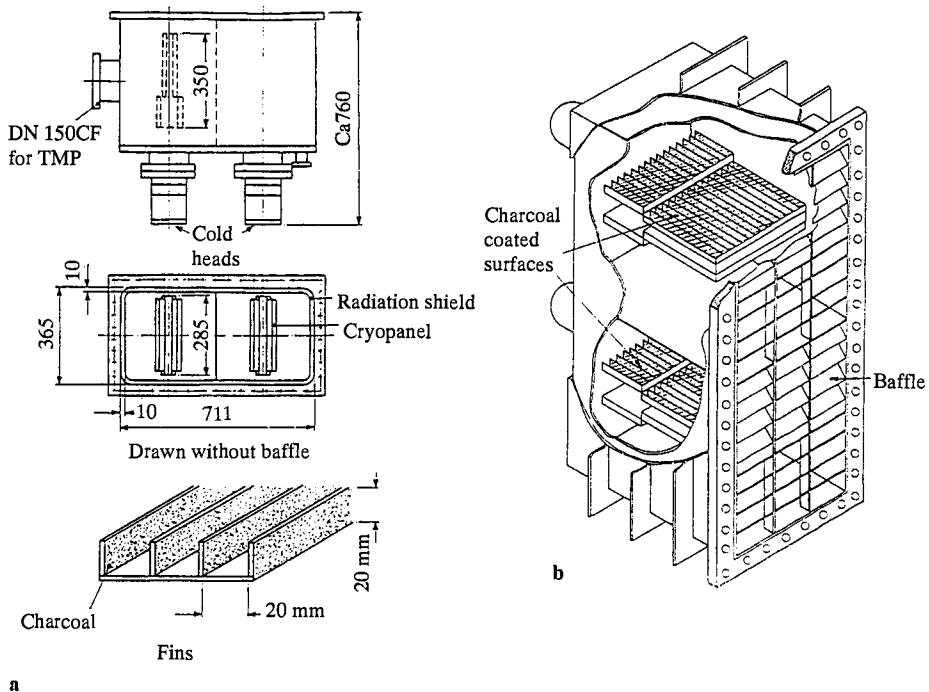
Cryopumps of all types (bath, refrigerator) can produce clean vacua in the high- and ultra-high vacuum range. They have a high, effective pumping speed for all gases and they can be built to whatever size is necessary. Traditionally, they have been used on large-scale projects such as nuclear fusion reactors, space-simulation chambers, particle accelerators, beam lines, etc. More recently, however, they are being used fairly routinely on equipment for the production of high-quality optical coatings and in the semiconductor industry. An interesting recent development is the use of cryopumps for the evacuation of large (tens of  $m^3$ ) working chambers for electron beam (EB) welding.

#### (a) Nuclear fusion technology

Many aspects of fusion technology demand pumps which will handle large throughputs of hydrogen and have pumping speeds for the gas in excess of  $10^6 \text{ l s}^{-1}$ . The economical way of providing this usually involves liquid helium condensation cryopumps (Coupland *et al.*, 1982). Recently, compact, high

throughput refrigerator-cooled pumps have been designed for use on some of the plasma diagnostic equipment. Coupland and co-workers (1987), described a pump, based on a commercially available two-stage cold head, used for the evacuation of a system designed to generate a high-brightness beam of hydrogen atoms. In order to achieve speeds for  $H_2$  of  $30\,000\text{ l s}^{-1}$ , a pump based on two cold heads was designed with a baffled inlet area of approximately  $2600\text{ cm}^2$ . Charcoal covered cryopanel (area =  $3990\text{ cm}^2$ ), much larger than usual, were incorporated, having the charcoal attached to the outside of the second-stage surfaces (Figure 3.27).

During the operation of cryopumps for hydrogen, the maximum amount of hydrogen that can be pumped is set by the explosive limit of  $H_2$ /air mixtures that can be created by the accidental admission of air to the pump. The maximum allowable partial pressure of  $H_2$  is 17 mbar which, in the system of Coupland and co-workers (1987) (volume = 400 l), corresponded to a hydrogen loading of 6800 mbar l (about one day's operation). Regeneration was performed by switching off the cold heads, and  $H_2$  required a finite time (about 1 h) to desorb from the capillary structure of the charcoal. During regeneration, the pump was evacuated using turbomolecular pumps.



**Figure 3.27** A large-scale, refrigerator-cooled cryopump ( $S_{H_2} = 30\,000\text{ l s}^{-1}$ ) (from Coupland et al., 1987). (a) Pump dimensions. (b) Configuration of cryopanel and louvre baffle

(b) Space simulation facilities

Because of the sensitivity of satellite surfaces to contamination, large space simulation chambers must be pumped cleanly down into the high-vacuum range. The chambers are large. For example, the IABG simulation facility at Ottobrunn near Munich, has a chamber which has a length of 13 m and a diameter of 7 m ( $V = 500 \text{ m}^3$ ). The pumping system consists of oil-sealed rotary pumps, Roots vacuum pumps and turbo-pumps and cryopumps. The rotary pumps evacuate the system from atmospheric pressure to 65 mbar; the Roots pumps then evacuate to  $10^{-1}$  mbar. A cryopump with a nominal speed for  $\text{N}_2$  of  $55\,000 \text{ l s}^{-1}$  pumps the system down to  $10^{-3}$  mbar, whilst six such pumps ( $S_{\text{eff},\text{N}_2} = 150\,000 \text{ l s}^{-1}$ , taking into account conductances) evacuate the chamber from  $10^{-3}$  down to the required pressure (below  $10^{-5}$  mbar) within 2 h. Details of an IABG cryopump is shown in Figure 3.28. It consists of two, two-stage cold heads but the radiation shield and baffle are cooled with liquid  $\text{N}_2$ , provided separately.

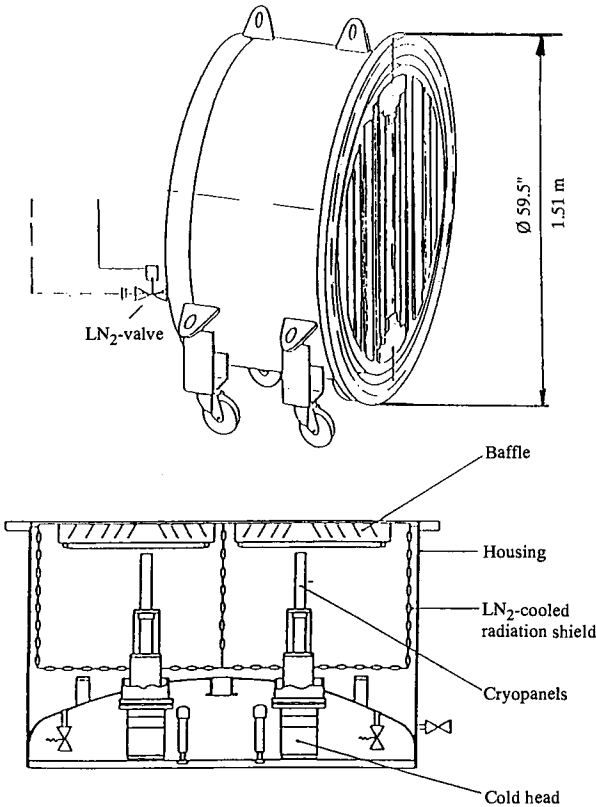


Figure 3.28 Refrigerator-cooled cryopump ( $S_{\text{N}_2} = 55\,000 \text{ l s}^{-1}$ ) based on commercial cold heads



## (c) Semiconductor applications

Refrigerator-cooled cryopumps are used in various areas of semiconductor processing, including sputtering, ion implantation, plasma etching and molecular beam epitaxy (see Chapter 7). The main application, however, appears to be sputtering in order to remove contaminants. Pumps for sputtering must have a high throughput and capacity for Ar. In a typical sequence, the process chamber is evacuated to less than  $10^{-6}$  mbar. Argon is then admitted up to  $10^{-2}$  to  $10^{-3}$  mbar and sputtering commences. After the process has been completed, the chamber is quickly re-evacuated to the base pressure. During the sputtering process, the thermal load must not exceed the cooling capacity of the pump. Further, the pump must have a capacity for both Ar and H<sub>2</sub> (evolved during sputtering) large enough to maintain continuous operation for 1 week. An extremely ingenious solution to these problems is to hinge the radiation baffle. This minimizes the thermal load on the second stage, restricts the Ar throughput during sputtering and maintains the speed of the pump for water vapour.

When using cryopumps on systems containing corrosive gases, such as Cl<sub>2</sub>, F<sub>2</sub>, HF, etc., protective coatings must be considered for susceptible surfaces. Materials that have been used include polymers (polyethylene, PTFE) and metals such as silver and gold. Problems have been encountered with polymer layers owing to possible mismatch of the coefficients of linear expansion between the substrate and the coating. Metals such as silver do not show this problem but because of the different emissivities of coated surfaces, the thermal balance inside the pump may be disturbed excessively.

## References

- Abbel, K., Henning, J. and Lotz, H. (1982) *Vacuum*, **32**, 623  
 Audi, M. and de Simon, M. (1987) *Vacuum*, **37**, 629  
 Baechler, W.G. (1987) *Vacuum*, **37**, 21  
 Bieger, W., Dippel, K.H., Richter, F. and Usselman, E. (1979) *Vakuum Technik*, **28**, 34  
 Coupland, J.R., Hammond, D.P. and Obert, W. (1982) *Vacuum*, **32**, 613  
 Coupland, J.R., Hammond, D.P., Baechler, W. and Klein, H.H. (1987) *Journal of Vacuum Science and Technology*, **A5**, 2563  
 Creek, D.M., Petty, R. and Jonathan, N. (1968) *Journal of Scientific Instruments (Journal of Physics E)*, **1**, 582  
 Deters, L., Goetz, D.G. and Schwartz, W. (1987) *Journal of Vacuum Science and Technology*, **A5**, 2367  
 Dubois, L.H. (1988) *Journal of Vacuum Science and Technology*, **A6**, 162  
 Duval, P., Saulgeot, C. and Raynaud, A. (1982) *Vacuum*, **32**, 623  
 Duval, P., Saulgeot, C. and Raynaud, A. (1986) *Vacuum*, **36**, 281  
 Florescu, N.A. (1960) *Vacuum*, **10**, 250  
 Frank, R. (1989) In *Theory and Practice of Vacuum and Technology* (eds M. Wutz, H. Adam and W. Walcher) (English translation W. Steckelmacher), F. Vieweg and Son, Braunschweig/Wiesbaden, p. 227

- Frank, R. and Usselman, E. (1977) In *Proceedings of the 7th International Vacuum Congress and 3rd International Conference on Solid Surfaces*, Vienna, p. 49
- Giorgi, T.A., Ferraro, B. and Storey, B. (1985) *Journal of Vacuum Science and Technology*, **A3**, 417
- Goetz, D.G. (1982) *Vacuum*, **32**, 703
- Goetz, D.G., Schaefer, G. and Rufus, J. (1987) *Journal of Vacuum Science and Technology*, **A5**, 2421
- Gupta, A.K. and Leck, J.H. (1975) *Vacuum*, **25**, 362
- Haefler, R.A. (1981) *Kryo Vakuumtechnik*, Springer-Verlag, Berlin
- Hands, B.A. (1987) *Vacuum*, **37**, 621
- Henning, H. (1989) In *Theory and Practice of Vacuum Technology*, (eds M. Wutz, H. Adam and W. Walcher) (English translation W. Steckelmacher), F. Vieweg and Son, Braunschweig/Wiesbaden, p. 254
- Hucknall, D.J. and Goetz, D.G. (1987) *Vacuum*, **37**, 615
- Kabelitz, H.P. and Fremerey, J.K. (1988) *Vacuum*, **38**, 673
- Kruger, C.H. and Shapiro, A.H. (1961) In *Rarified Gas Dynamics* (ed. L. Talbot), Academic Press, New York, p. 117
- Laurenson, L. (1987) *Vacuum*, **37**, 609
- McMahon, H.O. and Gifford, W.E. (1960) *Advances in Cryogenic Engineering*, **5**, 354
- Murakami, Y., Abe, T., Morii, S., Nakaisha, N. and Hata, S. (1987) *Journal of Vacuum Science and Technology*, **A5**, 2599
- Nambudripad, N. (1986) In *Cryogenic Engineering* (ed. B.A. Hands), Academic Press, London, p. 43
- Nuss, H.E. (1988) *Vacuum*, **38**, 617
- Pfeiffer, A., GmbH. (1967) German Patent 1,015,573
- PNEUROP (1973) Acceptance Specifications Part III, No. 5608
- Power, B.D. and Crawley, D.J. (1954) *Vacuum*, **4**, 415
- Power, B.D., Dennis, N.T.M., Oswald, R.D. and Colwell, B.H. (1974a) *Vacuum*, **24**, 117
- Power, B.D., Dennis, N.T.M., Oswald, R.D. and Colwell, B.H. (1974b) *Japanese Journal of Applied Physics*, Suppl. 2, Pt. 1, **13**, 33
- Sciuccati, F., Ferrario, B., Gasparini, G. and Rosai, L. (1988) *Vacuum*, **38**, 765
- Trickett, B.F. (1988) *Vacuum*, **38**, 607
- Tu, J.-Y. and Yang, N.-H. (1987) *Vacuum*, **37**, 831
- Tu, J.-Y., Yang, N.-H., Pang, S.-J. and Zu, Y. (1988) *Journal of Vacuum Science and Technology* **A6**, 2535
- Turner, F.T. and Feinleib, M. (1962) In *Transactions of the 8th National Vacuum Symposium and 2nd International Congress*, Vol. 1, Pergamon Press, Oxford, p. 300
- Van Atta, C.M. (1965) *Vacuum Science and Engineering*, McGraw-Hill, New York, p. 219
- Vekshinsky, S.A., Menshikov, M.I. and Rabinovich, I.S. (1959) *Vacuum*, **9**, 201
- Weston, G.F. (1985) *Ultra-high Vacuum Practice*, Butterworths, Guildford

# 4

## *Pressure measurement*

---

A gas exerts a pressure on the walls that enclose it. By definition, pressure is the ratio of the force ( $F$ ) which is exerted perpendicular to a plane area ( $A$ ) of the wall. A force of 1 newton (N) applied to an area of  $1 \text{ m}^2$  gives the basic unit of pressure which is called the pascal (Pa).

$$P \text{ is defined as } \frac{F}{A}; [P] = \frac{\text{N}}{\text{m}^2} = \text{Pa}$$

Other units of pressure that are used are:

$$1 \text{ bar} = 10^5 \frac{\text{N}}{\text{m}^2} = 10^5 \text{ Pa}$$

$$1 \text{ millibar (mbar)} = 10^{-3} \text{ bar} = 10^2 \text{ Pa}$$

The so-called 'standard atmosphere' is exactly  $101\,325 \text{ N m}^{-2}$  (1013.25 mbar) although, for convenience, atmospheric pressure at sea level may be regarded as 1000 mbar. The standard atmosphere should not be used as a unit of pressure. Other units of pressure that may now be regarded as obsolescent are the Torr ( $1 \text{ Torr} \approx 1.33 \text{ mbar}$ ) and the micron ( $\mu$ ) ( $= 10^{-3} \text{ Torr}$ ).

The measurement of pressure in vacuum technology is based on techniques involving either:

1. The measurement of the actual force per unit area (direct pressure measurement); or
2. The measurement of particle number density ( $n$  = the number of particles (atoms, molecules) per unit volume of gas) which is related to pressure by the relationship:

$$P = nkT$$

or a physical quantity which is proportional to  $n$  (indirect pressure measurement).

Obviously, at very low pressures, the forces are low and direct pressure measurement is carried out with difficulty. Highly sensitive direct gauges do exist, however. For example, the McLeod gauge will allow measurements to be performed down to  $10^{-6}$  mbar, whilst a suitable capacitance manometer will give satisfactory results to  $10^{-3}$  mbar and just below. Much lower pressures require the use of indirect methods for pressure measurement (Leck, 1988).

To operate a vacuum process successfully, it is essential to measure and, often, to control the total pressure and the following sections will describe the gauges available. Although total pressure measurement is a useful guide to

the general performance of a system it is insufficient to allow detailed investigation and development of the process. For this, measurement of the partial pressures, the combined effects of which produce the total pressure, provides considerably more insight into the process and may stimulate improvements. In the latter part of this chapter, residual gas analysis and partial pressure measurement will be discussed in detail.

## 4.1 Total pressure measurement

### 4.1.1 Direct methods

#### 4.1.1.1 Liquid level manometers

A liquid level manometer consists of a U-tube filled with liquid. One end of the tube is connected to the system in which the pressure is to be measured. The other end may be exposed to some reference pressure or evacuated and closed off (Figure 4.1). In other versions of the U-tube manometer, the tubes are inverted and placed in a reservoir of manometric liquid. A valve is fitted at an appropriate point to isolate the measuring/reference sides and a suitable connection is made to the vacuum system. The measured quantity  $\Delta h$  is proportional to the pressure difference between the legs of the manometer:

$$\Delta h = \frac{1}{\rho g} \Delta p$$

where  $\rho$  is the density of the manometric liquid at the temperature of measurement ( $[\rho] = \text{kg m}^{-3}$ ) and  $g$  is the acceleration due to gravity at the point of observation ( $g = 9.81 \text{ N kg}^{-1}$ , usually). Pure mercury ( $\rho, 20^\circ\text{C} = 13.546 \text{ kg m}^{-3}$ ) is commonly used as the liquid in the U-tube and the lower limit of pressure measurement is a few mbar. Under some circumstances other liquids (such as silicone oil) may be used.

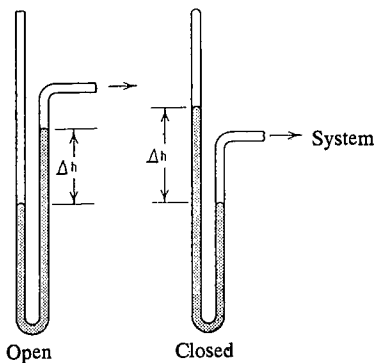


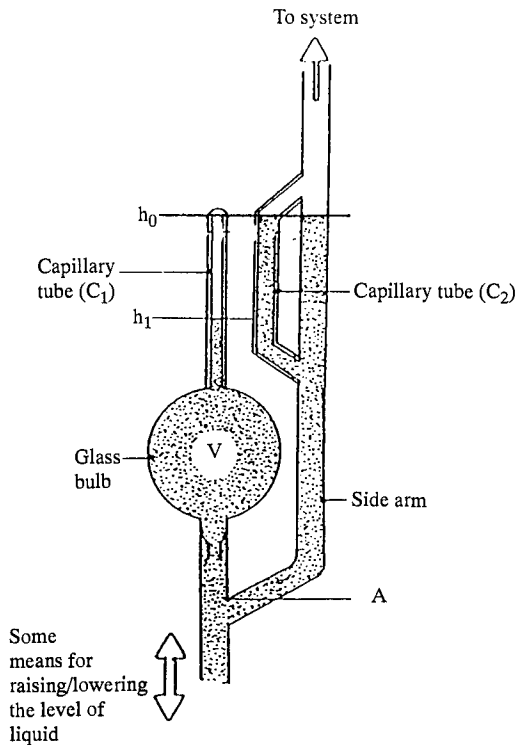
Figure 4.1 Liquid level manometers with open and closed ends

**4.1.1.2 Compression vacuum gauges**

The measuring range of liquid level manometers is limited at low pressures because of the difficulties in the precise measurement of  $h$ . If the gas to be measured is compressed, however, the original pressure can be increased to a point where it is easily measured by means of a U-tube manometer. For example, if  $P_i$  and  $V_i$  are the pressure and volume, respectively, of the original sample of gas, significant compression at constant temperature will give a gas with pressure and volume  $P_f$  and  $V_f$ :

$$P_i \times V_i = P_f \times V_f$$

In order to yield a measurable value for  $P_f$ , a suitable compression ratio (here defined as  $V_i/V_f$ ) must be achieved. A very familiar type of compression vacuum gauge is the McLeod gauge (Figure 4.2), the essentials of which will now be described. The gauge is made of glass and consists of a large spherical volume to which is attached a capillary tube. There is a connection to the vacuum system and some means of raising and lowering the level of mercury (the manometric liquid) in the gauge. In operation, when the mercury is below point A in Figure 4.2, the gas in volume  $V$  has the same pressure as that



**Figure 4.2** McLeod-type gauge

in the system. On raising the mercury level to point A, gas is isolated in volume  $V$  and the attached capillary ( $C_1$ ). Capillary tube  $C_2$  is parallel to and has the same diameter as  $C_1$  to ensure that the capillary depression in both is approximately the same. The difference in level of mercury in  $C_1$  and  $C_2$  is due to the pressure difference resulting from compression of the original sample of gas from volume  $V$  to its volume within  $C_1$ . The mercury is allowed to rise until its meniscus within capillary  $C_2$  has reached a level corresponding to the closed end of  $C_1$ . If the system contained permanent gas only then:

$$P_i V_i = P_f V_f$$

where  $V_i = V$  and  $V_f = (h_0 - h_1)a$

and  $a =$  cross-sectional area of the tube

and  $P_f = P_i + \rho g (h_0 - h_1)$

The last equation represents the pressure due to the mercury column and the gas pressure ( $P_i$ ) exerted on the column in  $C_2$ . The pressure is therefore related to the measured distance ( $h_0 - h_1$ ) by the equation:

$$P_f = \frac{\rho g a}{(V - (h_0 - h_1))a} \times (h_0 - h_1)^2$$

if  $(h_0 - h_1)a \ll V$ , then:

$$P_f = \frac{\rho g a}{V} (h_0 - h_1)^2$$

This shows that the lowest pressure that can be measured in a McLeod gauge is determined by volume  $V$  and, in some cases, a gauge may contain  $2000 \text{ cm}^3$  of mercury. Experience has shown that 1 mm may be the minimum recommended bore of capillary  $C_1$ . As an indication of the pressure range of a McLeod gauge, with  $V = 300 \text{ cm}^3$  and  $C_1 = 150 \times 1 \text{ mm}$ ,  $(h_0 - h_1) = 1 \text{ mm}$  and 150 mm represent  $2 \times 10^{-6}$ , and  $6 \times 10^{-2}$  mbar, respectively (Van Atta, 1965).

The McLeod gauge is cumbersome and fragile. In practice, accuracy (defined as the closeness of agreement between the result and the true value of a property) is limited due to a number of causes. These include sticking of mercury, and uncertainty in the determination of the zero point ( $h_0$ ) of the gauge. Another potentially serious source of error arises when the vacuum system contains vapours that will partially condense during compression. Generally, however, water vapour originating from normal atmospheric air will not cause a problem.

Kammerer compression gauges use the same principle. Adjustment of the mercury level involves turning a hand wheel that operates a flexible diaphragm forming the base of the mercury reservoir. Compared with McLeod gauges, they are simple, compact and relatively robust. They can be used for routine measurements but, as with the McLeod gauge, the working principle

does not allow continuous measurement and, for each reading, one or more minutes may be required.

#### **4.1.1.3 Mechanical vacuum gauges**

The general principle behind mechanical vacuum gauges is as follows. If a pressure difference exists across a thin, tensioned barrier such as a metal or elastomer diaphragm, then the net force will give rise to a deflection of the barrier:

$$F = (P_1 - P_2)A$$

where  $A$  is the barrier area and  $P_1$  and  $P_2$  are the pressures on either side.

In mechanical vacuum gauges, the barrier divides the pressure-sensing head into measurement and reference sides. Any deflection may be observed by having attached to the barrier either a lever system connected to a pointer or an electrical displacement-sensing device. Several variants of the basic design are used in commercially available gauges. For example, if the reference side of the gauge is evacuated to a pressure significantly below (two orders of magnitude, at least) the lowest that can be measured with the gauge, the system pressure will be obtained directly from the deflection. If the system pressure is measured against a known reference pressure of comparable magnitude, then the gauge is a differential device. Attention must also be paid to the positioning of the deflection-sensing system. It is obviously preferable to have it located in the reference rather than the measuring side. An extremely important characteristic of such gauges is that their readings are independent of the type of gas being measured.

##### *(i) Bourdon tube gauge*

The essential feature of this gauge is a vacuum-tight, bent expansion tube which can be attached to the vacuum system. The reference pressure is the external, atmospheric pressure and differences cause alterations in tube curvature that are transferred mechanically to a pointer. The indication depends on the ambient pressure and this type of gauge is suitable only for the approximate measurement of pressure in the range 10 to  $10^3$  mbar.

##### *(ii) Capsule vacuum gauge*

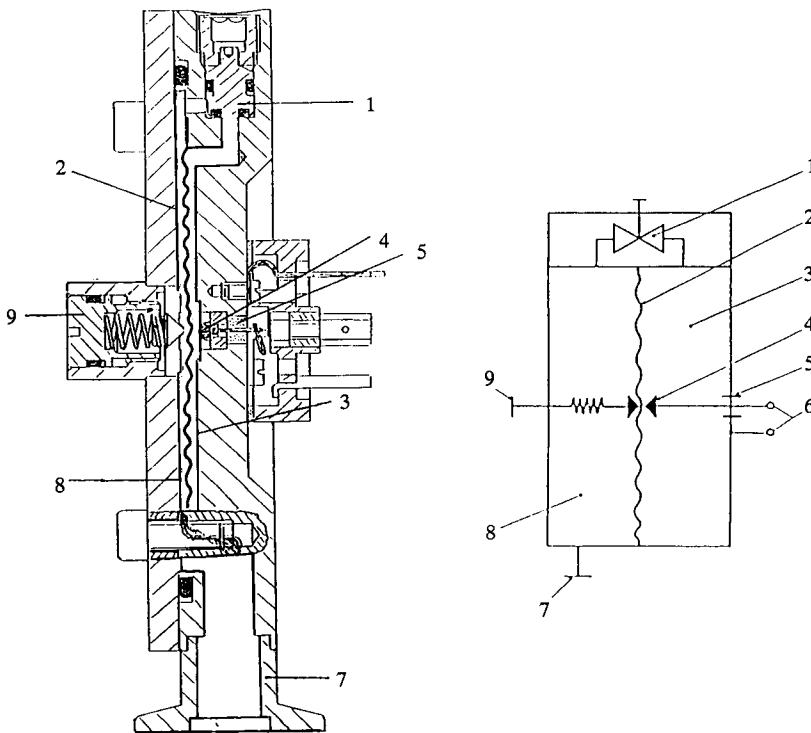
The pressure-sensing element in this case is an evacuated (to about  $10^{-2}$  mbar), sealed Cu-Be alloy capsule, mounted to the system to be monitored. Distortion of the capsule due to pressure changes is transmitted through a lever system to a pointer on an appropriate linear scale. Capsule gauges are available with full-scale readings of 20, 100 and  $10^3$  mbar and an uncertainty of  $\pm 1$  scale division. This represents readings  $\pm 10$  mbar and  $\pm 1$  mbar with the 1000 and 100 mbar versions, respectively. One obvious disadvantage with the capsule gauge is that reactive gases or vapours that may be present are in direct contact with the movement-sensing system.

Pressure switches are used in the operation of vacuum equipment in order to initiate certain actions when an appropriate pressure has been reached. They are based on the principles discussed above. A diaphragm switch

(Figure 4.3) consists of a membrane dividing the device into measuring/reference chambers. On the reference side of the switch there is an electrically insulated contact rod and the opposing contact consists of disc attached to the diaphragm. The required switching point is adjusted using a small valve (1) built into the system. Thus, with this valve open, the pressures in measuring (8) and reference (3) sides are equal and the diaphragm is not deflected. Under this condition, the diaphragm is moved by means of the adjustment screw (9) until contact is made between (9) and (4). In the case of the commercial pressure switch shown in Figure 4.3, the diaphragm (Cu-Be) has a diameter of 70 mm and a pressure difference of 1 mbar can be shown to cause a deflection of 0.05 mm. With this device, long-term stability and accuracy ( $\pm 0.1$  mbar) can be achieved. The switch-on circuit incorporates a delay of 0.5 s.

(iii) *Diaphragm vacuum gauge*

The deflection of a diaphragm is proportional to pressure difference over a wide range. For many applications, however, it is important to have an



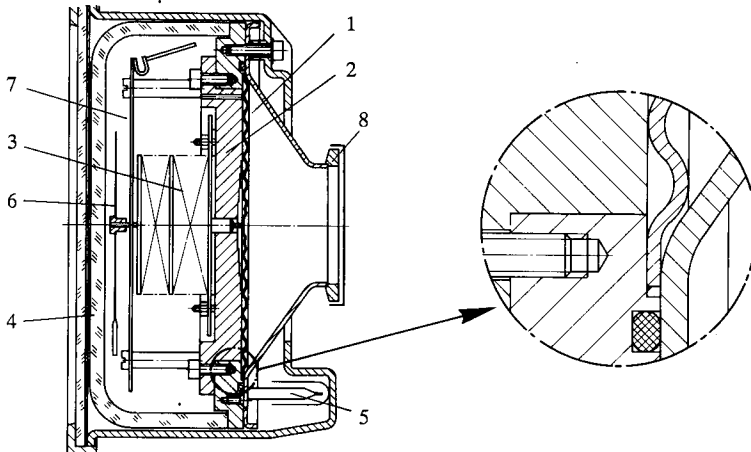
**Figure 4.3** Diaphragm pressure-sensitive switch (Leybold PS 111). 1, by-pass valve; 2, diaphragm; 3, reference side; 4, contact rod; 5, current leadthrough; 6, electrical connection; 7, system connection point; 8, measuring side; 9, Adjustment screw



extended pressure scale in the range 1–10 mbar. The precision diaphragm vacuum gauge shown in Figure 4.4 fits this requirement. It consists of a disc-shaped, corrugated diaphragm made of suitable material (stainless steel, Au- or Ni-coated Cu-Be) dividing the reference side from the measuring side. The reference volume consists of a glass volume evacuated to  $P < 10^{-3}$  mbar within which the diaphragm deformation-sensing system is located.

Under conditions of approximately equal pressure on either side (up to about 10 mbar), the whole area of the diaphragm is available for response. As the measuring-side pressure is increased (say, 10–15 mbar), the first corrugation rests on an internal contour disc, shaped to match the diaphragm. This reduces the area available for sensing. Further pressure changes gradually cause more of the diaphragm to rest on the disc, thereby reducing the sensitivity significantly between 100 and  $10^3$  mbar. The uncertainty in pressure measurements in the range 1–10 mbar is only about 0.2 mbar with such a gauge.

For a display of the pressure, remote from the sensing head, diaphragm vacuum gauges incorporating electrical displacement-sensing devices may be used. In a direct adaptation of the precision gauge described earlier, the pressure-dependent variation of the diaphragm displacement is converted to an electrical signal by means of a precision slide resistor located within the reference chamber. The accuracy of the gauge is not adversely influenced and it is also possible to have a variable trigger point which can energize a relay when a desired threshold has been reached. With other types of mechanical gauges, mechanical deformation can be converted into an electrical signal either piezoresistively or by means of a bending beam and attached strain gauges.



**Figure 4.4** *Schematic diagram of a precision diaphragm vacuum gauge.*  
 1, corrugated diaphragm; 2, base plate; 3, diaphragm movement transmission; 4, sealed glass volume ( $P < 10^{-3}$  mbar); 5, sealed-off point; 6, pointer; 7, scale; 8, connection point to system

*(iv) Capacitance manometers*

The modern capacitance manometer contains a tensioned metal diaphragm (inconel) which is exposed to the gas to be measured. The reference side of the manometer contains two capacitance electrodes deposited on a ceramic disc in close proximity to the diaphragm. In an absolute gauge, the sealed reference chamber is evacuated to  $10^{-7}$  mbar and maintained at this pressure using a chemical getter. Applied pressure deflects the diaphragm towards the electrode assembly causing a capacitance change which is greater in the vicinity of the centre electrode than the outer one. This unbalances a suitable capacitance bridge and by amplification and demodulation of the output, a high level dc output signal (usually 0–10 V) is generated. The various techniques that have been used to obtain suitable signals from variable capacitance pressure transducers have been discussed by Sullivan (1985).

Modern capacitance manometers are designed to operate over four decades of pressure, at intervals between 1 and  $2 \times 10^4$  mbar full-scale indication. The full-scale reading of any transducer is the highest pressure at which valid measurements can be made. In modern devices, at pressures of about 10% above full scale, the diaphragm touches the electrode. This protects it up to a pressure difference of approximately 1.3 bar or 125% full-scale, whichever is the larger. Like all transducers, they are subject to errors resulting from temperature fluctuations and some attempt is usually made to compensate for this by choice of suitable materials of construction. For example, forsterite (a magnesium silicate) is chosen for the electrode substrate because of the closeness of its temperature expansion coefficient to that of inconel. They are not identical, however, and even small changes in sensor temperature may cause changes in the signal output. These effects can be minimized by the attachment to the sensor of a device which can compensate the output appropriately for temperature. A better method involves locating the entire sensor in a temperature-regulated enclosure, normally at 45°C, to minimize the effects of variations in ambient temperature (zero coefficient = 0.0004% full scale/°C according to Sullivan (1985)). If a capacitance manometer has a measuring head at a temperature above ambient then, in precise work, an error can arise due to thermal transpiration. Thus, if the system and gauge head pressures and temperatures are  $P_1$ ,  $T_1$  and  $P_2$ ,  $T_2$ , respectively, then if the mean free path of gas molecules ( $\bar{l}$ ) is greater than the diameter ( $d$ ) of the gas connecting tube, then:

$$P_1 = P_2 \times (T_1/T_2)^{1/2}$$

Although temperature variation is the most disturbing factor for a high-accuracy pressure transducer, rate of change of temperature also affects performance. For this reason, careful consideration must be given to the location of the sensor (away from sources of heat, moving air currents, etc.). For systems where elevated temperatures are used to prevent condensation (e.g. steam-traced lines in the chemical industry), high temperature sensors (regulated to 150°C) are commercially available.

Finally, most capacitance manometers are capable of responding to pressure transients in milliseconds but, due to conductance and dead volume limitations, response times of 10–30 ms are more usual.

### 4.1.2 Indirect methods

#### 4.1.2.1 Thermal conductivity vacuum gauges

Thermal conductivity is defined according to the equation:

$$\dot{Q}_{\text{heat conduction}} = kA \frac{T_1 - T_2}{d}$$

where  $\dot{Q}$  is the thermal flux (quantity of heat/time interval) flowing through material of thermal conductivity ( $k$ ) from a temperature ( $T_1$ ) to a lower temperature ( $T_2$ ) and  $A$  is the area through which heat flows perpendicularly,  $d$  is the distance between the surfaces.

For a gas in the pressure range where the mean free path of particles ( $\bar{l}$ ) is greater than or approximately equal to the distance between the warm surface and the surroundings, thermal conductivity depends on pressure. Under these circumstances, for a heated (to  $T_1$ ) wire (radius  $r$  and length  $l$ ) within a cylindrical, gas-containing tube (wall temperature  $T_2$ ):

$$\dot{Q}_{\text{heat conduction}} = a_E \times \frac{n\bar{c}}{4} \frac{C_{\text{molar},v}}{N_A} \times 2\pi r l \times (T_1 - T_2)$$

$$\therefore k = a_E \frac{n\bar{c}}{4} \frac{C_{\text{molar},v}}{N_A} \quad (\text{compare the expressions for } \dot{Q})$$

where  $C_{\text{molar},v}$  is the molar heat capacity of the gas at constant volume,  $\bar{c}$  is the mean gas particle speed,  $n$  is the gas particle number density and  $a_E$  is an 'accommodation factor' which takes into account that, because of their relative dimensions, gas particles will be in excellent thermal equilibrium with the tube wall but in less good thermal equilibrium with the heated wire.

Further manipulation of the expression for  $k$  yields:

$$k = a_E \frac{\bar{c}}{4} \frac{C_{\text{molar},v}}{RT} \times P$$

Hence  $k$  depends on  $P$  and its variation can be used to measure  $P$ .

At high pressure, it can be shown that  $k$  is only temperature dependent. This means that the temperature assumed by an electrically heated wire in a system containing gas will be related to a gas pressure under the appropriate conditions. Thermal conductivity gauges operate on this principle and will now be discussed.

A thermal conductivity gauge, such as a Pirani gauge, consists essentially of a fine wire of circular cross section ( $d = 5\text{--}20 \mu\text{m}$ ) supported inside a tube ( $d \approx 20 \text{ mm}$ ). The length of the wire can be 50–100 mm. In principle, the rate of heat transfer between the wire (temperature  $T_1$ ) and its surroundings (temperature  $T_2$ ) is measured. The filament is heated by an electrical current to a temperature approximately 100K above the surroundings. Heat loss from the wire is due predominantly to three mechanisms (Reich, 1989):

1. Thermal conduction through the gas between the wire and its surroundings. This is expressed as:

$$\dot{Q}_{\text{heat cond}} = \text{const. } (S) \times \frac{P}{1 + gP}$$

where  $S$  is a function of the gas properties ( $\bar{c}, C_{\text{molar},v}$ , etc.),  $P$  is the pressure and  $g$  is a geometrical factor.

2. Thermal radiation ( $\dot{Q}_{\text{rad}}$ ) from the wire to its surroundings.
3. Thermal conduction through the ends of the wire to the connectors ( $\dot{Q}_{\text{end}}$ ).

$\dot{Q}_{\text{end}}$  and  $\dot{Q}_{\text{rad}}$  are pressure independent but they simulate a 'zero pressure' ( $P_0$ ).

$$\dot{Q}_{\text{end}} + \dot{Q}_{\text{rad}} = S \times P_0$$

which defines the pressure that can be measured. If the electrical heating power ( $\dot{Q}_{\text{elec}}$ ) maintains the wire at a constant temperature and ambient temperature remains constant then:

$$\begin{aligned} \dot{Q}_{\text{elec}} &= \dot{Q}_{\text{heat cond}} + \dot{Q}_{\text{end}} + \dot{Q}_{\text{rad}} \\ &= V^2 I / R \end{aligned}$$

where  $V$  is the voltage,  $I$  is the current and  $R$  is the resistance of the wire

$$= S \left( P_0 + \frac{P}{1 + gP} \right)$$

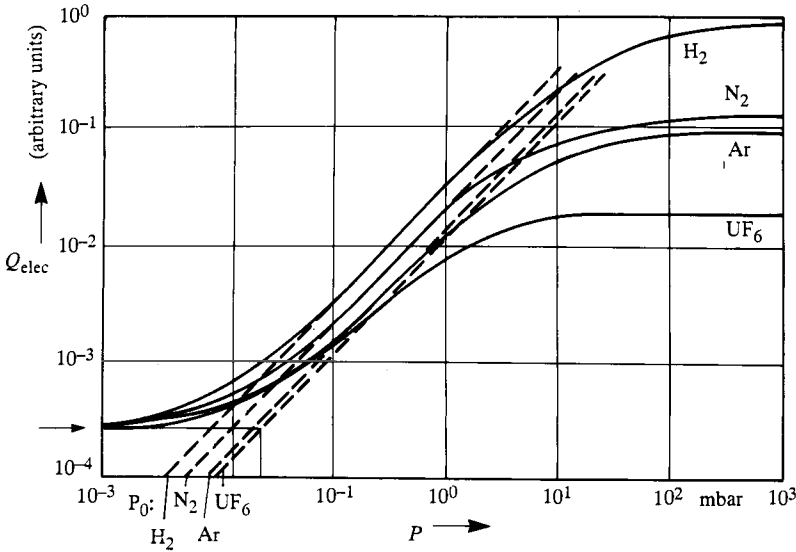
In Figure 4.5,  $\dot{Q}_{\text{elec}}$  is plotted against  $P$  for several gases. From this it can be seen that the sensitivity ( $S$ ) is characterized by the position of the curve. If  $P_0$  is regarded as the point of intersection between the broken lines and the indicated horizontal then it has a value between 9 and 20  $\mu\text{bar}$ . The upper limit for  $\text{UF}_6$  (relatively large molecular mass) is about 10 mbar, whereas for  $\text{H}_2$  it is approximately 500 mbar. The region where thermal loss is proportional to pressure is established when:

$$0.01 < \frac{\bar{l}}{Z} < 10$$

where  $Z$  is the distance between the wire and the wall. For  $\text{N}_2$  and 298K, this covers the range between 0.68 and  $6.8 \times 10^{-4}$  mbar.

The thermocouple vacuum gauge is a thermal conductivity gauge in which the temperature of a heated tungsten filament is measured using a fine thermocouple attached to its mid-point. The filament is heated by a constant electrical current which is maintained no matter what the temperature of the filament. As the gas pressure changes, heat conduction increases and the filament temperature falls. The thermocouple temperature can be calibrated against gas pressure. Some details of thermal conductivity gauges are given by Van Atta (1965) and O'Hanlon (1980).

The term Pirani gauge usually refers to a gauge in which the heated wire is incorporated into a Wheatstone bridge circuit. There are two modes of operation which involve a constant filament temperature or constant heating power. In Figure 4.6(a), the operation of a Pirani gauge at constant heating



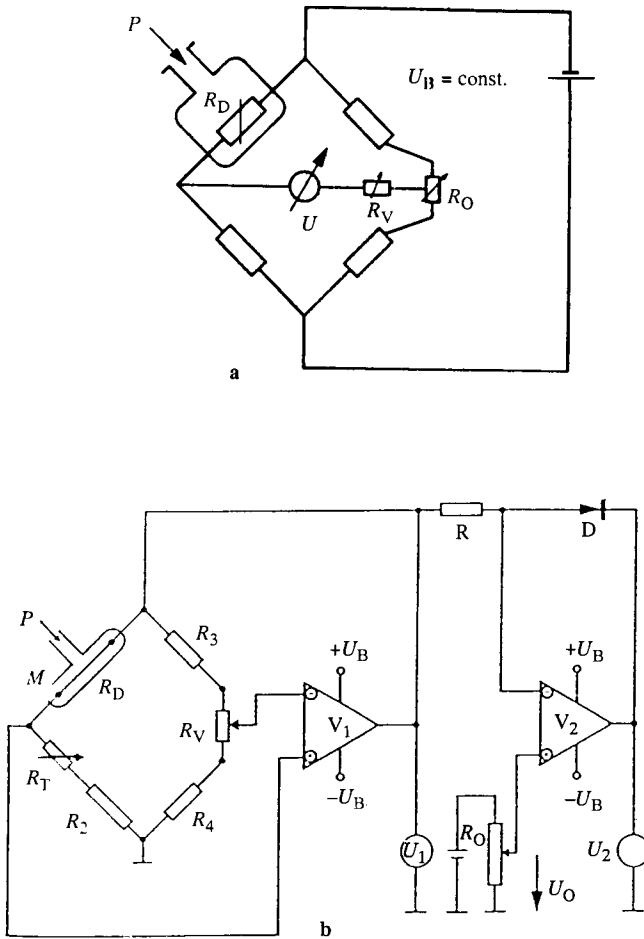
**Figure 4.5** Plot of  $Q_{elec}$  required to maintain a constant wire temperature ( $T_1$  where  $T_1 - T_2 = 100K$ ) in the presence of pressures of various gases (after Reich, 1989).  
 Actual conditions: W wire ( $l = 60\text{ mm}$ ;  $d = 7.7\ \mu\text{m}$ )

power is shown. The wire is a branch of a Wheatstone bridge operated at a constant voltage. As the temperature of the filament changes with pressure, its resistance changes. This unbalances the bridge circuit which is indicated as the voltage  $U$ . With suitable calibration, this can be registered directly in terms of pressure:

$$U = AU_B \frac{P}{P + B(d/l)}$$

where  $A$  and  $B$  are constants and  $d$  and  $l$  represent the filament diameter and length, respectively. The measuring range of this type of Pirani gauge is rather restricted (often  $10^{-3} - 1$  mbar). Increasing the ratio of wire diameter to length, however, shifts the range towards higher pressures (say,  $10^{-2}$  to 10 mbar). Over a period of time, variations in the filament characteristics will occur. Compensation for this can be carried out using two calibration potentiometers ( $R_o$  and  $R_v$  in Figure 4.6(a)).  $R_o$  is adjusted *only* with the gauge head evacuated to a pressure approximately two orders of magnitude below its lowest value.  $R_v$  is adjusted to full-scale deflection with the head exposed to atmospheric pressure. A Pirani gauge operated in this way has, unfortunately, a long response time.

Thermal conductivity gauges may operate at constant resistance (and, therefore, constant wire temperature). The electrical circuit for this mode of



**Figure 4.6** Schematic diagrams showing the electrical circuits for Pirani gauges. (a) Constant heating power. (b) Constant filament temperature

operation is shown in Figure 4.6(b). The wire is one arm of a Wheatstone bridge circuit consisting of  $R_D \approx R_2 \approx R_3 \approx R_4$ . A temperature-compensating (up to 40°C) resistance  $R_T$  is also included which is located within the sensor head. The voltage applied to the bridge ( $U_B$ ) is controlled by amplifier  $V_1$  in order to maintain  $R_D$  at a constant value.

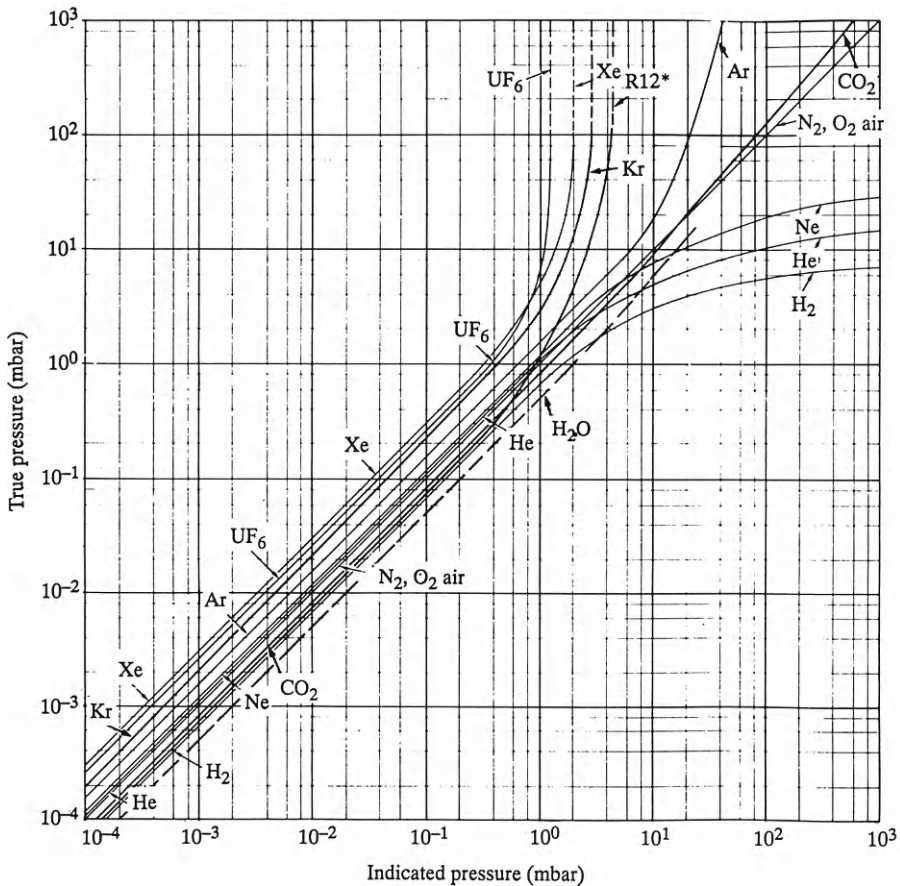
In practice, the bridge is not precisely balanced and the gauge meter indicates voltage  $U$ , applied to the bridge by a suitably calibrated voltmeter:

$$U_1 = 2 \sqrt{R_D S (P + P/(1 + gP))}$$

A non-linear scale is thus obtained where  $P_0$  is about  $10^{-2}$  mbar but more complex electronics (to the right-hand side of line  $U_1$ ) make the region  $10^{-3}$  to

$10^{-2}$  mbar accessible. The gauge head also incorporates a potentiometer ( $R_v$ ) and an adjustment for the compensating voltage  $U_0$  at  $R_0$  to take care of variations in the surface of the sensing wire which affect its heat transfer characteristics. These changes may be the result of oil contamination, for example.

Pirani gauges operated on the constant resistance principle are used largely for pressure control in the appropriate range since their response time is very short (20–50 ms). They are usually calibrated by the manufacturers using dry air or  $N_2$ . Although gases with similar molecular mass ( $O_2$ ,  $CO_2$ ) present no problems, adjustments may have to be made to the gauge reading if the predominant gases are significantly lighter or heavier. This can be carried out using a calibration curve (Figure 4.7).



**Figure 4.7** Curves indicating the relationship between indicated and true pressure measured using a Pirani gauge calibrated with dry  $N_2$  or air

#### 4.1.2.2 Ionization gauges

An ionization gauge measures the pressure in a system by ionizing a fraction of the gas particles and then, depending on the precise method of ionization, measuring either the ion current or a gas discharge current. Ionization is usually accomplished by means of thermionic electrons ('hot cathode gauges') or using a magnetically sustained glow discharge. The relationship between ion or discharge current and pressure cannot be calculated satisfactorily from first principles and must be established by calibration.

##### (i) The cold cathode gauge

The principle of the cold cathode gauge is the establishment of a discharge in a relatively low pressure of gas by the application of a high d.c. voltage between metal electrodes (anode and cathode). Because the production of charge carriers is too low, such a discharge is extinguished at pressures of approximately  $10^{-3}$  mbar.

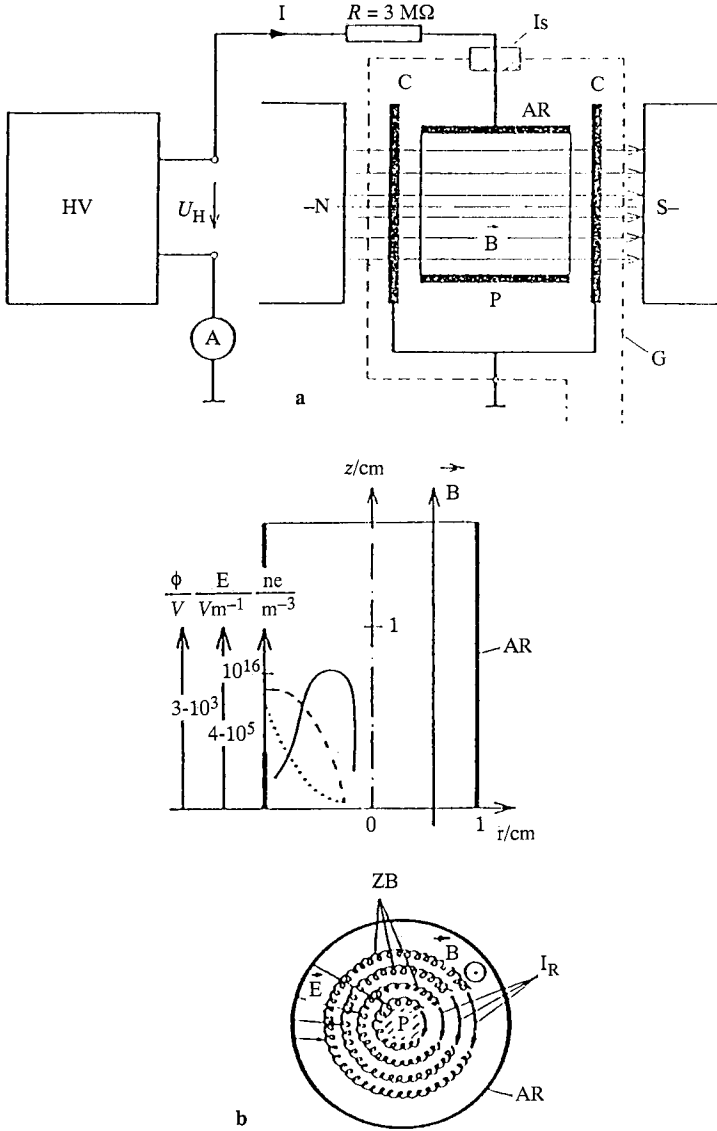
Experiments by Penning (1936) using magnetically confined cold-cathode discharges, however, showed that the discharge current was proportional to pressure in the range  $10^{-3}$  to  $10^{-5}$  mbar. Below that pressure, however, the discharge became erratic. Developments by Redhead eventually allowed the construction of gauges based on this effect which could measure pressures as low as  $10^{-12}$  mbar. A brief history of the cold cathode ionization gauge has been presented by Redhead (1988).

Various configurations of the cold cathode gauge are possible including the Penning cell, magnetron and inverted-magnetron types. A schematic diagram of a cold cathode gauge is shown in Figure 4.8(a). A high d.c. voltage is applied to a ring-shaped anode. The outer housing and the cathode are at earth potential. The electric field in most of the discharge (which, at pressures below  $10^{-4}$  mbar can be regarded as a pure electron plasma) volume is orthogonal to the magnetic field. The discharge current ( $I$ ) is measured. Special precautions are required to avoid spurious currents due to cable and internal leakage, etc. also registering.

The types of discharge that can occur in crossed fields have been described by Schuurman (1967). According to this work, in the high magnetic field region, most of the anode voltage appears across a cylindrical electron sheath (first demonstrated experimentally by Knauer (1962)) and an approximately neutral plasma occupies the region near the axis of the anode ring at a potential near to the cathode potential and an electron charge density much below that in the sheath. The electrons in the space charge ring follow cycloidal paths resulting from the crossed fields and only reach the anode in stages following collisions with gas atoms. If a gas is present in the space then, in addition to the 'diffusion' of electrons, ionizing collisions also occur. The electrons produced enter the space-charge cloud while the ions are accelerated by  $\vec{E}$  towards the inside and reach the cathode fairly quickly after several oscillations through the centre.

Because the ionization rate and the diffusion rate across the magnetic field are proportional to the number of gas particles/unit volume ( $n_g$ ), an equilibrium is established between carrier production and loss. Thus the electron





**Figure 4.8** (a) Schematic diagram of a vacuum gauge based on a magnetically-confined cold-cathode discharge. C, cathodes; AR, ring-shaped anode; G, gauge housing;  $I_s$ , insulated, high voltage leadthrough;  $N_1S$ , poles of permanent magnet; B, 0.1–0.2T;  $U_H$ , 3 kV. (b) Discharge in the cell according to Knauer and Lutz (1963). B, magnetic field (crossed field); E, electric field (crossed field);  $I_R$ , electron ring current; ZB, cycloidal trajectories of electrons; P, plasma (approximately neutral); ———, charge density; - - - -, electric field strength; ..... , actual anode potential

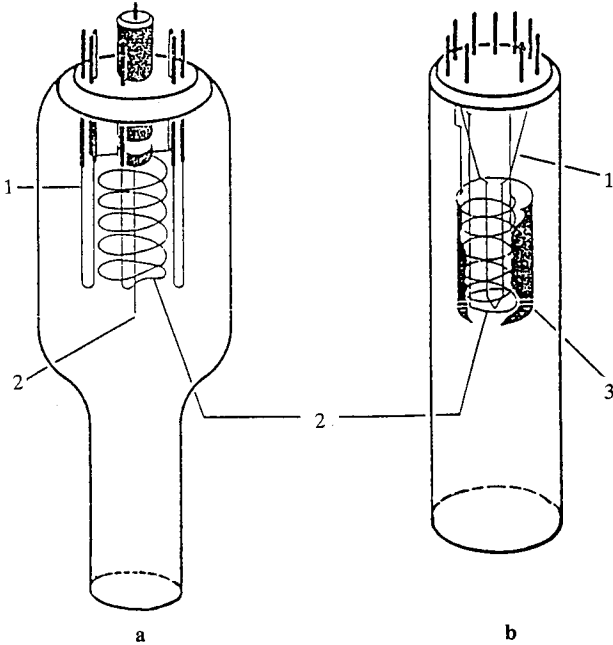
density in the ring (current  $I_R$ ) remains independent of  $n_g$ ; the external current will be proportional to pressure down to  $10^{-12}$  mbar. With cold cathode gauges, a considerable discharge current can be obtained, a typical value being  $2\text{--}5 \text{ A mbar}^{-1}$  for  $I_D/P$ . This means that pressure measurement can be carried out down to  $10^{-6}$  mbar without amplification and the gauge is more economical and simpler to operate than the hot-cathode ionization gauge.

Observations of the variation of discharge current ( $I_D$ ) with pressure have indicated that non-linearity and discontinuities in the curves occur (Lange *et al.*, 1966). For example, over the pressure range  $10^{-4}$  to  $10^{-12}$  mbar, Lange and co-workers observed a decrease in  $I_D/P$  by a factor of 35. It appears that such behaviour is very sensitive to the condition of the electrodes, small changes in mechanical alignment and anomalous electron diffusion (oscillations). The accuracy of measurements using cold cathode gauges is not particularly good, particularly at higher pressures (a *clean* Penning gauge is inaccurate by a factor of 2; a *dirty* gauge is inaccurate by a factor of 10). Discharge instabilities, non-linearity of the  $I_D$  versus  $P$  characteristics and pumping action are the principal difficulties preventing precise pressure measurement. Nevertheless, because of its cheapness, simplicity and ruggedness, this type of gauge has been widely used in applications where it is more important to control pressure rather than measure it precisely.

At approximately  $10^{-4}$  mbar, the nature of the discharge begins to change from that described. A plasma extends throughout the anode cylinder and controls the discharge mechanism. A point is reached where the ion current is no longer proportional to pressure. At sufficiently high pressures, when the electron mean free path approaches the gauge dimensions, the magnetic field no longer has an effect and a glow discharge or arc occurs. Combined pressure measuring instruments incorporating both Pirani and Penning gauges are now commercially available. The advantage of the combined instrument is that there is automatic switching between the Penning and the Pirani gauge which allows continuous pressure indication from  $10^{+3}$  to  $10^{-6}$  mbar. The Penning gauge is automatically switched on when the pressure decreases below  $5 \times 10^{-3}$  mbar and switched off again as the pressure increases. This avoids Penning gauge errors at  $10^{-2}$  mbar and above.

### (ii) Hot cathode ionization gauges

The basic hot cathode ionization gauge is shown in Figure 4.9. It consists of a heated cathode which emits a current of electrons that is accelerated through a modest voltage (150–200 V) between the cathode and anode (grid). Energetic electrons collide with, and may ionize, gas particles. Ions are attracted to the collector which is negatively biased with respect to the cathode and the grid. The ion current is proportional to pressure in that, the higher the pressure the greater the probability of occurrence of electron impact ionization. The concentric triode gauge (Figure 4.9(b)), was a development of the thermionic triode amplifier radio valve. The large area of the collector unfortunately gave residual currents equivalent to an  $N_2$  pressure of  $1 \times 10^{-6}$  to  $3 \times 10^{-6}$  mbar, thereby restricting the useful measuring range of the gauge. Bayard and Alpert (1950) made significant alterations to the triode gauge. To reduce the residual currents, the filament



**Figure 4.9** Schematic diagram of the hot cathode ionization gauge.  
 (a) Bayard–Alpert.  
 (b) Concentric triode. 1, Cathode; 2, anode; 3, collector

was moved outside the grid structure and the collector became a fine wire located on the axis of the grid (Figure 4.9(a)). These modifications reduced the residual current by several orders of magnitude (Tilford, 1985).

The principle of the hot cathode ionization gauge is that electrons emitted from the cathode (current,  $I^-$ ), collide with gas particles, ionizing some. Ions travel to the collector where they are measured as a current  $I^+$ . The ion and electron currents are proportional according to the relationship;  $I^+ = S(I^-P)$  or, strictly,  $(I^+ - I_r^+) = S(I^-P)$  where  $I_r^+$  is the pressure-independent residual current.  $S$  is termed the ‘relative sensitivity’ of the gauge (or gauge constant). Its value is usually provided by the manufacturer. Typically, for  $N_2$ ,  $S = 10 \text{ mbar}^{-1}$ . It is gas-dependent and should be determined by calibration.

For a constant electron current, the ‘absolute sensitivity’ ( $K$ ) is given by:

$$K = I^+/P$$

It is usual practice to keep  $I^-$  constant, in the range 10 mA to 10  $\mu\text{A}$ , by controlling cathode heating. If  $S = 10 \text{ mbar}^{-1}$  and  $I^- = 10^{-3} \text{ A}$ , then  $I^+/P = 10 \text{ mbar}^{-1} \times 10^{-3} \text{ A} = 10^{-2} \text{ A mbar}^{-1}$ . This means that, at  $10^{-7} \text{ mbar}$ , the ion current would be 1 nA.

Ion current is proportional to the efficiency of ion ionization during gas-electron collisions. This is a function of electron energy (typically 150 eV) and the nature of the gas taking part in the collision. At electron energies

typical of ionization gauges, there is a very large variation in the collision cross-section for gas ionization. This is reflected in the large variation in the correction factor for different gases for ionization gauge readings by which the indicated pressure is converted to the true pressure. It is not, however, possible to obtain accurate, theoretical gas sensitivities for ionization gauges from data on the variation of ionization cross-sections with electron energy.

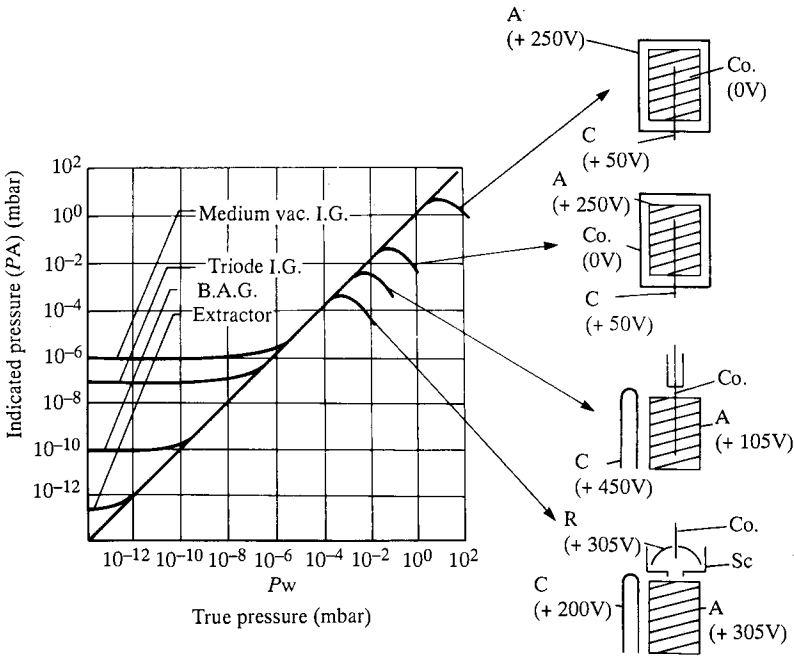
The performance of ion gauges depends on many factors including electrode geometry, electrical parameters, the emission characteristics of the filament, space and surface charges, etc. Filaments have been constructed of various types of materials. Tungsten filaments, for example, operate at 1800°C and show good performance. In a conventional Bayard–Alpert gauge with tungsten cathodes 180°C apart, mean ( $\pm$ SD) values of  $S$  of  $7.5 \pm 2.4\%$   $\text{mbar}^{-1}$  were reported (Tilford, 1985). With tungsten filaments relatively close together (8 mm apart),  $S$  was  $7.5 \pm 8.8\%$   $\text{mbar}^{-1}$ . Tungsten filaments have certain disadvantages. They have a short life at high operating pressures and they are reactive, particularly with hydrocarbons. Further, dissociation of certain molecules can occur readily on the W surface. Thoriated iridium cathodes, which operate at temperatures between 1000 and 1200°C, are used extensively. They are resistant to burn-out but are destroyed by halogens and silicones. Tilford (1985) assessed their performance as ‘relatively poor’ ( $S = 7.5 \pm 25.5\%$   $\text{mbar}^{-1}$ ) and ascribed this to the variable thermal contact between the iridium and the Th(IV) oxide coating. Cathodes made of rhenium (operating temperature, about 1800°C) are insensitive to halogens, O<sub>2</sub>, hydrocarbons and hydrogen. Its vapour pressure, particularly in the UHV region, may present problems.

Electrodes in hot cathode gauges may be constructed from tungsten, molybdenum and nickel. Recently, interest has been taken in the long-term stability of gauges as indicated by gauge sensitivities (for example, Wood and Tilford, 1985). Although changes in sensitivity of about 10% over a period of 1 year are typical for carefully handled gauges (Harten *et al.*, 1988), sudden jumps of up to 20% have been observed. Harten *et al.* (1988) investigated the influence of secondary electron emission from the gauge grid and ion collector on stability and concluded that it was enhanced by 10–20% through this effect. Secondary electron emission was altered by surface contamination, particularly with Mo and W (widely used materials of construction for ion gauges). The development of gauges with gold-plated electrodes (Gentsch *et al.*, 1985) has given devices with excellent long-term stability (3% change in 1 year). According to Wood and Tilford (1985), however, the largest change in sensitivity appears to result from operating or baking the gauge at pressures above  $10^{-3}$  mbar.

Several variants of the hot cathode ionization gauge are available (Figure 4.10). The conventional triode has already been described briefly but the other important types will now be discussed.

### High-pressure gauges

At very high pressures, the filament will burn out but ‘medium vacuum’ gauges (range 1 to  $10^{-6}$  mbar) are manufactured. The problem with conven-



**Figure 4.10** Variations on the triode ionization gauge with their appropriate pressure ranges. A, Anode; C, cathode; Co., collector; R, reflector; Sc, extractor

tional triodes is that the gauge becomes non-linear above  $10^{-3}$  mbar owing to multiple collisions (electron energy lost in non-ionizing processes) and space-charge effects. As the ion and electron currents become comparable, the true emission current may vary due to the contribution of the electron current from ionized gas particles. The latter will have a reduced probability of ion formation. Further, as the rate of ion formation increases, so a positive space charge may develop that impairs the efficiency of ion collection. With the development of 'non-burnout' filaments, attention was paid to these problems. The gauge characteristics of the triode at 'high' pressures were improved considerably by interchanging the positions of the anode and collector and reducing the separation between electrodes. With these modifications, measurements up to 1 mbar were possible. High-pressure gauges are not normally used for accurate work since other devices, such as the capacitance manometer, work better in this range. They operate, however, over a wide pressure range which is commonly encountered in industrial processes.

### Bayard-Alpert Gauge

When discussing the conventional triode gauge it was pointed out that the measurable pressure was determined by the pressure-independent residual

current. This is caused by the electron-stimulated desorption of ions from the anode and, particularly, by the so-called X-ray effect. The latter arises owing to collisions of electrons with anode in which soft X-rays are produced. If these encounter the ion collector, photo-electrons are emitted. To the ion-current amplifier, this event is indistinguishable from the arrival of an ion. It is pressure independent but proportional to the electron current ( $I^-$ ). To reduce the X-ray limit, Bayard and Alpert (1950) altered the electrode configuration of the conventional triode to that shown in Figure 4.10. The reduction in collector area decreases significantly the chances of X-rays striking it and the lower limit of measurement is reduced to about  $10^{-9}$  mbar. Gauges with very fine collectors ( $d=10 \mu\text{m}$ ) are claimed to measure 'well below'  $10^{-12}$  mbar (Benvenuti and Hauer, 1977).

Gauges measuring below  $10^{-9}$  mbar

Attempts to reduce further the low-pressure limit led to the development of the modulator gauge (Redhead, 1960) and the extractor gauge (Redhead, 1966).

In a Bayard-Alpert gauge with a modulator, a second wire (the modulator) lies within the anode. It is switched between anode and collector potentials and the collector current that results is noted. For example, if the modulator is at anode potential then the gauge is unaffected:

$$I_{\text{TOT}}^+ = I^+ + I_r^+$$

If the modulator is at collector potential, then some ions are attracted to it. The residual current will be unaffected:

$$I_{\text{mod}}^+ = (1 - k) I^+ + I_r^+$$

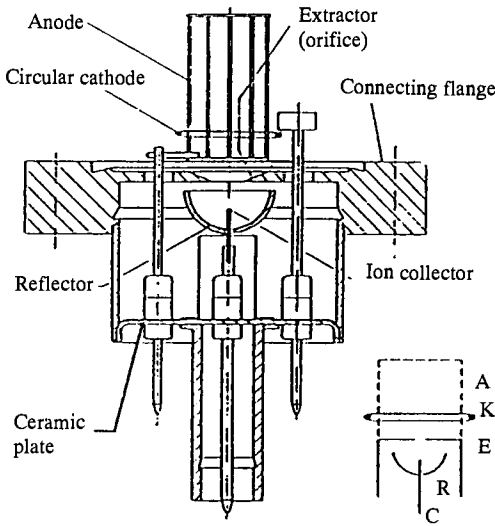
where  $I_{\text{mod}}^+$  is the modulator current and  $k$  is termed the modulator coefficient. The latter can be determined experimentally at about  $10^{-6}$  mbar where  $I_r^+$  is insignificant:

$$I^+ = \frac{(I_{\text{TOT}}^+ - I_{\text{mod}}^+)}{k}$$

The assumption that  $I_r^+$  is unaffected by gauge modulation is incorrect (Nash, 1987) and a gain of only 10–100 is possible by the method.

With the extractor gauge, the ion collector is 'hidden' from the X-radiation. A version of the gauge is shown in Figure 4.11 from which it can be seen that the anode is a cylindrical cage, encircled at its lower end by the cathode. A plate with an orifice extracts ions from the region of ionization. The ion collector, in the form of a wire tip, is situated below the extractor surrounded by a reflector at anode potential.

Due to the geometry of the system, as well as the potentials of the electrodes, the influence of both X-rays and ion desorption are almost eliminated and the gauge lower limit is approximately  $10^{-12}$  mbar. Recent developments with the extractor principle include the point collector gauge (Watanabe, 1987). In this device, the collector is the tip of a tungsten needle ( $d = 0.03 \text{ mm}$ ,  $l = 0.05 \text{ mm}$ ) projecting from a thin, tapered sleeve. The



**Figure 4.11** *Extractor ionization gauge*  
( $p = 10^{-4}$  to  $10^{-12}$  mbar)

anode is a spherical grid made of finely woven Mo. A circular filament encircles the grid at its equator. It is claimed that pressures below  $10^{-13}$  mbar can be measured.

In conclusion, some additional comments must be made concerning hot cathode ionization gauges generally. They are frequently available as 'nude' gauges or as gauges mounted within a glass envelope. With the former, the electrodes are mounted directly on a connecting flange (usually CF, but also KF – see Chapter 6). Nude gauges can be immersed completely in the system to be measured but they are fragile and care must be exercised not to cause damage during installation. The cleanliness of an ionization gauge affects its performance considerably and, to avoid problems, the head must be degassed. Degassing may be carried out by bombardment of the grid and collector (suitably biased) with electrons from the filament at an emission current of a few tens of milliamps. With some gauges, degassing is performed by direct resistance heating of the anode.

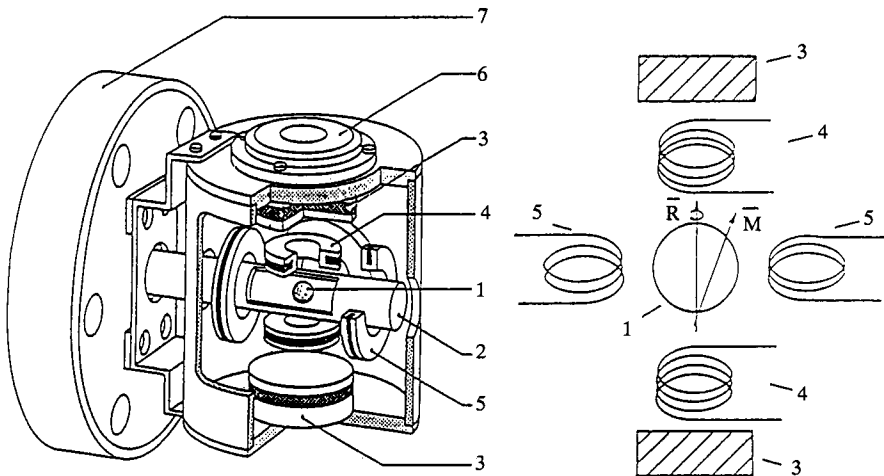
Usually, 30 minutes is sufficient to clean a gauge thoroughly and degassing is usually carried out whilst the rest of the system is baking or immediately afterwards, as it is cooling. This minimizes the adsorption of degassed materials on the system walls.

#### **4.1.2.3 Spinning rotor gauge**

Gas friction (measured in terms of the dynamic viscosity) is almost independent of pressure at high pressures. At low pressures, however, it is proportional to the particle number density ( $n$ ) and hence the pressure ( $P = nkT$ ). If

gas friction can be measured, pressure can be determined but initial attempts to develop a gas friction vacuum gauge proved unsuccessful. Beams and co-workers (1962) suggested that gas friction could be measured by observations of the deceleration of a magnetically suspended spinning ball. A vacuum gauge based on this principle was developed by Fremerey and co-workers at KFA, Juelich (Fremerey, 1985). Commercial spinning rotor gauges are produced by Leybold AG and MKS Instruments under licence from KFA.

A diagram of a commercial spinning rotor gauge is shown in Figure 4.12. A small ball bearing (steel or stainless steel) is housed in a non-magnetic finger and suspended by permanent magnets. Electromagnetic coils support the ball if it moves up and down or laterally. They are energized by a d.c. amplifier controlled by a sensing voltage proportional to the deviation from the equilibrium position. Coils connected to the output of a two-phase a.c. generator provide a rotating magnetic field to spin the ball about a vertical axis. It achieves a rotational speed of about 400 Hz within 1 minute before cutting out and allowing the ball to coast. The relative deceleration of the ball is given by  $-\dot{\omega}/\omega$  where  $\omega$  is the angular velocity of the ball and  $\dot{\omega}$  is the time derivative of the angular velocity. This is obtained in the following way. Because of the local conditions, the ball becomes magnetized. However, magnetization is not uniform and the ball has an external magnetic field similar to that of the earth. Because the field is not axially symmetrical, it produces an inductive voltage in two 'pick-up' coils arranged in the horizontal



**Figure 4.12** Schematic diagram of a commercial spinning rotor gauge (Viscovac VM 211). 1, ball ( $d = 4.5$  mm); 2, gauge tube (i.d. = 7.5 mm); 3, permanent magnets (0.05 T at ball) to suspend ball; 4, coils to stabilize ball vertically; 5, driving coils (4) to spin rotor about a vertical axis; 6, spirit level; 7, connection flange. The pick-up coils required to determine the deceleration rate are not shown



plane. This voltage alternates with a frequency that decreases as the ball slows. The Viscovac gauge shown in Figure 4.12 operates between 415 and 405 Hz. When measurement commences, the ball is accelerated to 415 Hz. Measurement of deceleration then starts. When the rotational frequency falls to about 405 Hz, measurement is automatically interrupted and the ball is accelerated again.

According to the equation of Beams *et al.* (1962), it can be shown that, in the molecular flow region, the pressure  $P$  is given by:

$$P = \frac{\pi r \rho \bar{c}}{10\sigma} \left( -\frac{\dot{\omega}}{\omega} \right) - B$$

where  $r$  and  $\rho$  are the radius and density, respectively, of the ball,  $\sigma$  is the tangential momentum transfer coefficient,  $\omega$  and  $\dot{\omega}$  have been defined and  $\bar{c}$  is the mean velocity of the gas particles ( $= 8RT/\pi M_{\text{molar}})^{1/2}$ . The numerical algorithms used to calculate  $(-\dot{\omega}/\omega)$  are given by Fremerey (1985). Provided that the composition of the gas, the pressure of which is to be measured, is known,  $\sigma$  and  $B$  (the residual drag) are the only quantities that are either not known or cannot be readily measured. Work at the National Physical Laboratory has indicated that  $\sigma$  is close to unity and does not vary with gas species for typical ball bearings. Careless handling of the rotor balls may, however, cause irreversible changes in the gauge characteristics (Messer *et al.*, 1987).

The ball also experiences a pressure-independent residual drag arising from several sources (asymmetries in the suspension field, incorrect positioning of the sensing head, vibration, etc.) and the above equation must be appropriately modified. Investigations into this effect have been carried out by Redgrave and Downes (1988).

Finally, with commercial spinning rotor gauges, pressures between  $10^{-1}$  and  $10^{-6}$  mbar can be measured with a stability of about 1% per year and an uncertainty of 4%. The gauge is used as a transfer standard gauge in some systems used for the calibration of vacuum gauges (see below).

### 4.1.3 Calibration of vacuum gauges

As with any other instrument, vacuum gauges require calibration. This gives the ratio of the gauge reading to the pressure. There are three possible calibration procedures (Steckelmacher, 1987):

1. Comparison of the gauge reading with an absolute gauge where both sensing heads are mounted on a suitable calibration chamber and are exposed to the calibration gas under identical conditions.
2. Installation of the gauge on a calibration chamber, within which an accurately known pressure has been generated.
3. Comparison of the gauge reading with that of another gauge previously calibrated in a manner traceable to an internationally recognized standards laboratory.

The absolute gauges used in direct comparisons and as primary calibration manometers have been listed by Steckelmacher (1987) and include manometers and compression gauges of the McLeod type. With manometers, the accuracy of measurement depends on the precision with which the height of the surface of the manometric liquid can be determined (Simpson, 1991). Conventional manometers can be used in the pressure range  $10^3$  to 1 mbar but for great precision (about 0.1% at  $10^{-1}$  mbar), micromanometers are employed. According to NPL publications, in principle the McLeod gauge is fundamental in its operation. In practice, however, it is best regarded as a reference instrument requiring calibration against a suitable standard. The pumping action of mercury vapour streaming into a cold trap fitted to the system to prevent contamination (Gaede–Ishii effect; see Reich, 1989) causes uncertainty.

To establish a known, low pressure in a system, the controlled expansion of a gas is an accepted technique (NPL, 1984). A series expansion apparatus consists of several large and small vessels separated from each other by valves (Figure 4.13). A final pressure  $P_4$  is calculated from an accurately known starting pressure  $P_1$  by the technique shown in Figure 4.13.  $P_1$  is accurately measured on a U-tube manometer or by means of a calibrated Bourdon tube. Calculation of the final pressure is based on Boyle's law, so:

$$P_4 = \frac{V_1}{(V_1 + V_2)} \times \frac{V_2}{(V_2 + V_3)} \times \frac{V_3}{(V_3 + V_4)} \times P_1$$

Error in  $P_4 \leq 1\%$  and  $10\%$  at  $10^{-2}$  and  $10^{-6}$ , respectively. The equipment must be capable of being evacuated to at least two orders of magnitude below the pressure to be generated. Apparatus at the NPL cover the pressure ranges  $10^{-3}$  to  $10^{-8}$  and  $10$  to  $10^{-3}$  mbar. The former is a bakeable system, with all-metal seals, whilst the latter uses elastomer seals. A small computer calculates the generated pressure and makes corrections of temperature and departures from Boyle's law.

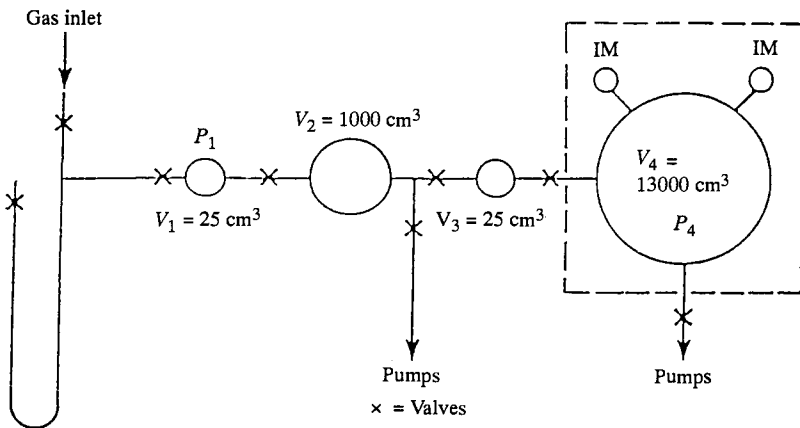
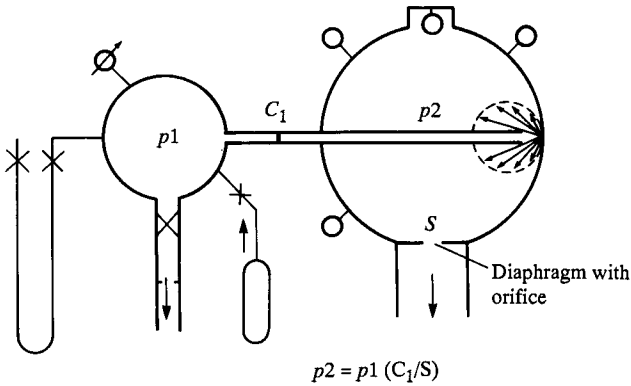


Figure 4.13 Schematic diagram of an apparatus for series expansion of gas



**Figure 4.14** *Dynamic method for gauge calibration*

For calibration at pressures from  $10^{-5}$  to  $10^{-9}$  mbar, dynamic methods can be used. The principle is shown in Figure 4.14. The gauges to be calibrated are attached to a chamber into which a known gas flux is admitted:

$$Q = C_1 (P_1 - P_2)$$

The gas is simultaneously evacuated via an orifice of known conductance:

$$Q = P_2 S$$

If the pumping speed is very large and the gas flux is low, then:

$$P_2 = P_1 (C_1/S)$$

When the lowest possible uncertainty is not required, vacuum calibration by comparison is an acceptable technique (Nash and Thompson, 1983). Reference gauges (which themselves are regularly calibrated) are mounted on a suitable vacuum system, together with the gauge to be calibrated. Typically, this system consists of a bakeable chamber having a volume that is large compared with the total volume of the gauges to be calibrated. These are arranged around the chamber, radially and equally spaced, on elbows so that they interact to the minimum. Calibration gas ( $< 0.1\%$  impurities) is introduced so that it is in thermal equilibrium with the vessel walls and pressure around the gauge ports is uniform. The apparatus should be maintained at a constant temperature ( $\pm 1^\circ\text{C}$ ). The required pressures at the high end of the range may be obtained dynamically by balancing the flow of gas into the system (via a leak valve) against the amount removed by the pumps.

Detailed descriptions of calibration systems appear in the literature. Nash and Thompson (1983) discussed that used by the NPL for the range 1 to  $10^{-6}$  mbar. Simple triode hot cathode gauges were used over the lower part of the pressure range and capacitance manometers outside this range. All gauges are calibrated regularly using the series expansion method. The gauge

outputs (ionization currents or voltages) are measured and a computer used to calculate the corresponding pressure by curve-fitting). Reich (1980) described an apparatus built by Leybold that is used to provide calibrations, traceable to German national standards held by the PTB (Physikalische Technische Bundesanstalt), in the range  $10^3$  to  $10^{-9}$  mbar. This equipment is shown in Figure 4.15(a). In the Leybold-DKD system, reference gauges are capacitance manometers (1 and  $10^3$  mbar full scale), a spinning-rotor gauge and a Gentsch ion gauge. The uncertainty in calibration is shown in Figure 4.15(b).

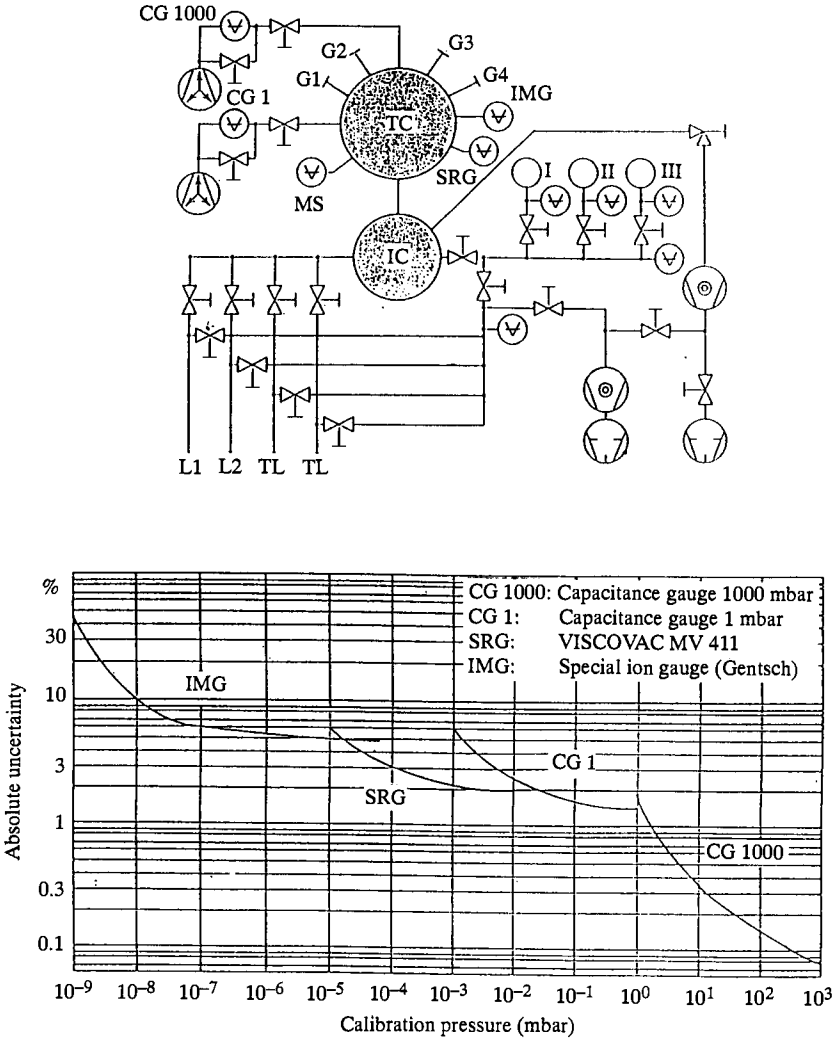
Commercial systems are also available, designed for gauge calibration by the comparison method. The Leybold CS 1000 system, for example, covers the range from  $10^3$  to  $10^{-5}$  mbar and consists of an appropriately sized chamber pumped by a turbomolecular pump. A high vacuum valve permits isolation for static calibration in the coarse range and also the dynamic balancing of a gas flow in the lower range. Reference standards are capacitance manometers ( $10^3$  and 1 mbar FSD) and a spinning rotor gauge ( $10^{-2}$  to  $10^{-5}$  mbar). Since capacitance manometers perform best if they are kept under vacuum, the equipment has facilities for their separate evacuation and isolation when not in use.

#### 4.1.4 Connection of gauges

Particular care must be paid to the location and use of vacuum gauges if measuring errors are to be avoided. Some precautions are general whilst others apply to certain gauge types. The basic rules, however, are:

1. Avoid positioning a gauge where there is a strongly-preferred direction of gas flow (e.g. adjacent to pumps, traps; opposite gas inlet valves).
2. Place the sensor as close as possible to the point where measurement of the pressure is required.
3. Protect the sensor from dirt, corrosion and other disturbing influences. The devices that can be used depend on the source of the problem. For example, if solid particles are generated in the process then protection may involve the use of sinter filters or connectors that incorporate bends, chicanes, etc. In the case of corrosive gases, the sensor may require flushing after use and careful elimination of dead volumes. Pressure pulses may have to be damped (sinters) whilst elimination of vibration will involve decoupling the sensor from the system.
4. Keep the connecting tubing between gauges and the system as short and as wide as possible.

With certain gauges, specific problems may arise. For example, capacitance manometers are often maintained at a controlled, elevated temperature. Thermal transpiration must then be corrected for. With ionization gauges, it is important to avoid stray electrical and magnetic fields (from, for example, EB guns, HF sputtering equipment, etc.).



**Figure 4.15** (a) Schematic diagram of a gauge calibration system and (b) the uncertainty of the calibrations obtained. TC, test chamber; MS, mass spectrometer; CG 1, transfer standard capacitance manometer; CG 1000, transfer standard: capacitance manometer; IMG, transfer standard: ionization gauge; SRG, transfer standard: Spinning rotor gauge; G1 to G4, calibration flanges; I to III, calibration gases; IC, inlet chamber; TL, transfer standard: calibrated leaks; L1 and L2, leaks to be calibrated

## 4.2 Partial pressure measurement

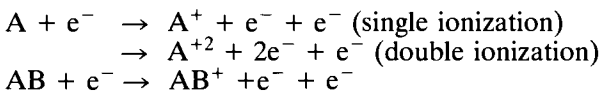
The first systematic application of partial pressure measurement to the improvement and understanding of a vacuum process came in the 1940s. It was used at the Lawrence Radiation Laboratory on a uranium isotope separation system. A simple Dempster-type mass spectrometer was used, in which ions of the various gases present in the system were produced in a Penning-type discharge. They were then extracted through a narrow slit using an electric field and deflected through  $180^\circ$  by a magnetic field normal to the direction of motion. For appropriate values of the ion-accelerating voltage and magnetic flux density, all ions of a given mass/charge ratio were focused on a receiver slot through which they passed to impinge on a collector electrode. After this pioneering use of magnetic deflection mass spectrometry, improvements were made quickly and analytical applications, particularly in the petroleum industry, led to commercial development of the technique. Until the 1950s, however, mass spectrometry remained a specialized art and apparently irrelevant to many potential users in engineering and chemistry.

Attention turned to the development of 'dynamic' analysers in which ion separation is based on the time-dependence of one of the system parameters. In the 1950s, W. Paul and his colleagues at the University of Bonn recognized that an electrodynamic quadrupole field has great potential as a mass analyser. The important merits included sensitivity and moderate resolution, compactness and lightness. Paul's work coincided with a demand for a compact partial pressure analyser in fields as diverse as research into the chemistry of the upper atmosphere and general monitoring of vacuum conditions and gas purity. In the intervening years, it has been recognized that the quadrupole is indeed the best general purpose mass analyser available and its applications will be discussed later. Initially, residual gas analysis in general will be reviewed, with specific reference to quadrupole mass spectrometers.

### 4.2.1 Residual gas analysers

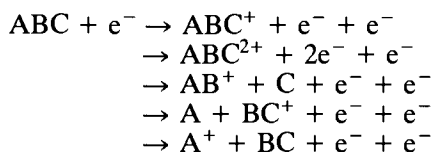
A residual gas analyser is essentially a mass spectrometer, consisting basically of an ion source, a mass analyser, an ion detector and a display system. The ion source produces ions from the gas to be analysed. The mass analyser then separates the ions according to their mass-to-charge ( $m/e$ ) ratio. Ions from the mass analyser are finally detected and the resultant ion currents measured.

A technique extensively applied to the generation of positive ions in commercial residual gas analysers (RGAs) is electron impact ionization. This is shown for very simple species:



The energy of the initial electrons influences the number and type of ions formed. Ionization begins at an appropriate electron energy (the ionization

potential of the atom or molecule) and, thereafter, the number of ions formed grows rapidly with increasing energy. After passing through a maximum (in the range 50–160 eV), the number decreases slowly. Most RGAs operate in this energy range. When complex molecules are ionized, the number of ion species that are formed is increased. The more complex the molecule, the more fragments may be produced:



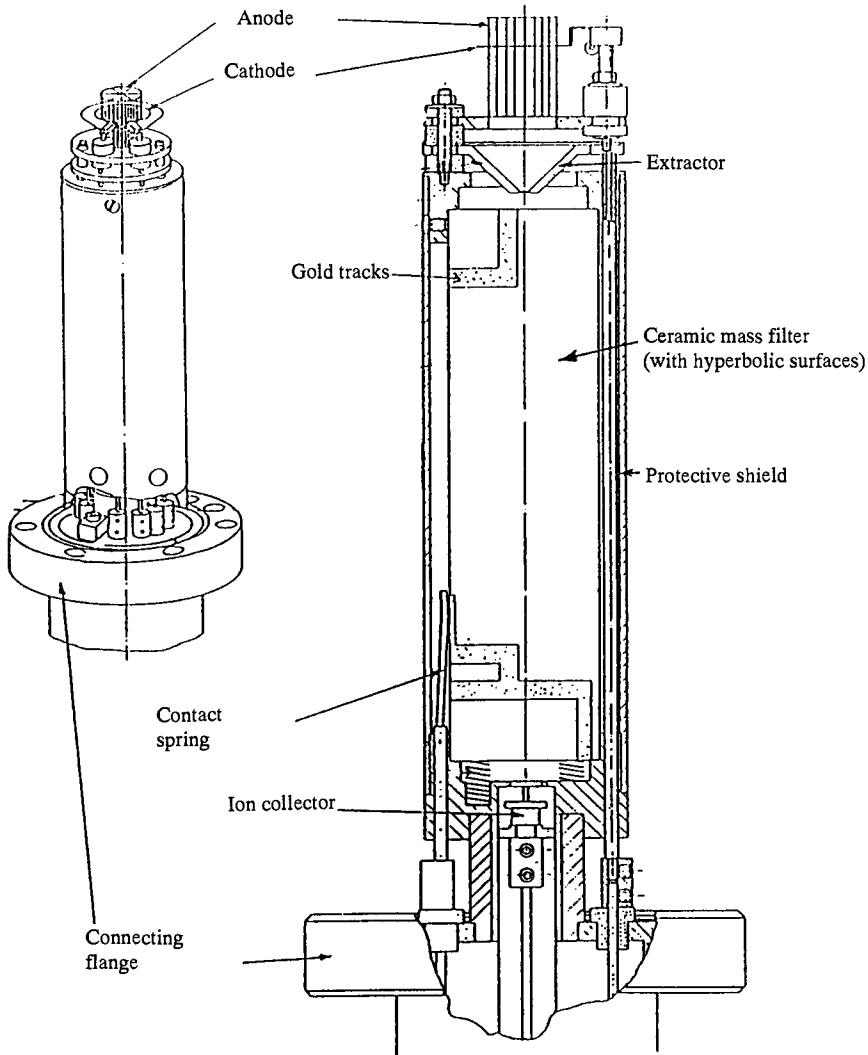
The occurrence and relative abundance of various kinds of ions are characteristic of the parent molecule and typical spectra are contained in data collections (see, for example, Cornu and Massot, 1966).

#### 4.2.1.1 Ion sources

Three different types of electron impact (EI) ion source are available. They are known as the axial, cross-beam and grid types. In the axial source, electrons and ions travel along the same axis. It is a general purpose source with a high sensitivity. In the cross-beam source, electrons are generated from either of two filaments at 90° to both the ion extraction and gas-inlet systems. Radially-symmetric, extractor-type ion sources which include the grid type, are frequently used (Figure 4.16), which, in the 'nude' configuration, are attached directly to the equipment being monitored. Such a source is 'open' and is suited to general analysis in the HV/UHV pressure range. 'Closed' sources may be preferred for sampling at  $P > 10^{-3}$  mbar or for the analysis of small amounts of certain impurities in a high-purity gas. Other factors that have to be taken into consideration are the influence of the filament material, the occurrence of adsorption or degassing in the source and the pressure dependence of these effects. It is always important to define the object of an analysis to select the most suitable ion source for the application.

The material from which the filament is constructed can enhance the performance of an RGA. Tungsten is suitable for relatively unreactive gases at pressures of  $10^{-5}$  mbar or below. However, they operate at high temperatures (over 2000K) and react chemically with hydrocarbons to yield tungsten carbide. Subsequent reaction with water vapour produces metal (together with oxides of carbon) again but the resulting recrystallization leads to embrittlement and premature failure. Thoriated iridium filaments operate at much lower temperatures (1300–1500K) and have longer lifetimes. They react readily with halogens and halogen-containing compounds, however, and failure is rapid. Rhenium filaments operate at intermediate temperatures and, because of some evaporation, are self-cleaning. There is evidence to suggest that mass analysers with Re cathodes are less stable (significant sensitivity changes) in operation (Blanchard *et al.*, 1986).

It is important, particularly in the UHV pressure range, that the contribution of the RGA to the composition of vacuum should be insignificant. The potential for degassing must be minimized by the selection of suitable



**Figure 4.16** *Sensor head of a commercial, general-purpose quadrupole mass spectrometer*

materials and the minimization of dead volumes. A facility for ion source degassing (by raising its temperature significantly) is often provided. Even after prolonged bake-out, peaks are sometimes observed in a mass spectrum which are due to electron-induced desorption. They occur typically at 12, 16, 19 and 35 amu and can be distinguished from those generated by EI ionization because of their different energies. Plating the ion source with gold reduces both adsorption and EID.



**4.2.1.2 Mass filter**

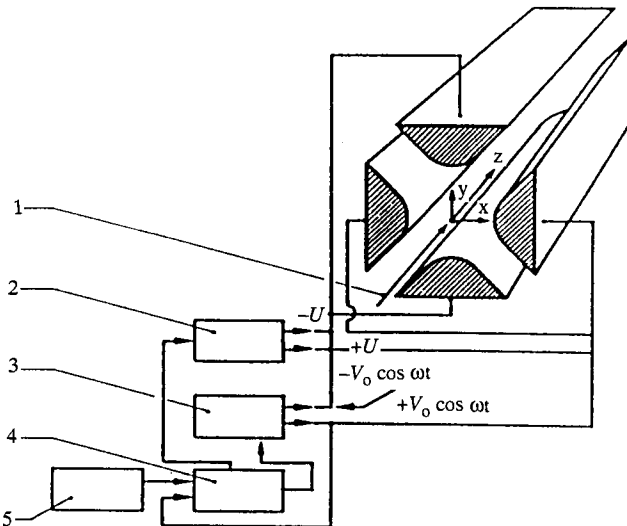
The quadrupole mass filter is a very complex device in spite of its apparent mechanical simplicity. It consists of four parallel rods (ideally hyperbolic in cross-section but often cylindrical) between opposite pairs of which a continuous ( $U$ ) and an RF-voltage ( $V \cos \omega t$ ) are applied. The principle of operation of the quadrupole has been excellently reviewed by Dawson (1976, 1986).

A schematic diagram of the filter is shown in Figure 4.17. The quadrupole uses a strongly focusing, alternating gradient field. ‘Strong focusing’ means that the restoring force ( $Ee$ ) on an ion injected axially down the centre of the mass filter increases with its displacement from the axis. The force depends on the electric field ( $E$ ) and this is given by  $E = -\nabla\phi$  where  $\phi$  is the potential and is proportional to square of the displacement from the axis.  $\phi$  is given by:

$$\phi = \phi_0 \frac{(x^2 - y^2)}{2r_0^2}$$

and this does not vary along the  $z$ -direction. The equations of motion of an ion, mass =  $m$  and charge =  $e$ , are given by appropriate equations such as  $m\ddot{x} = eE_x$  where  $E_x$  is equal to  $-(\partial\phi/\partial x)$ . The best way to examine the quadrupole is to consider opposite pairs of rods in turn.

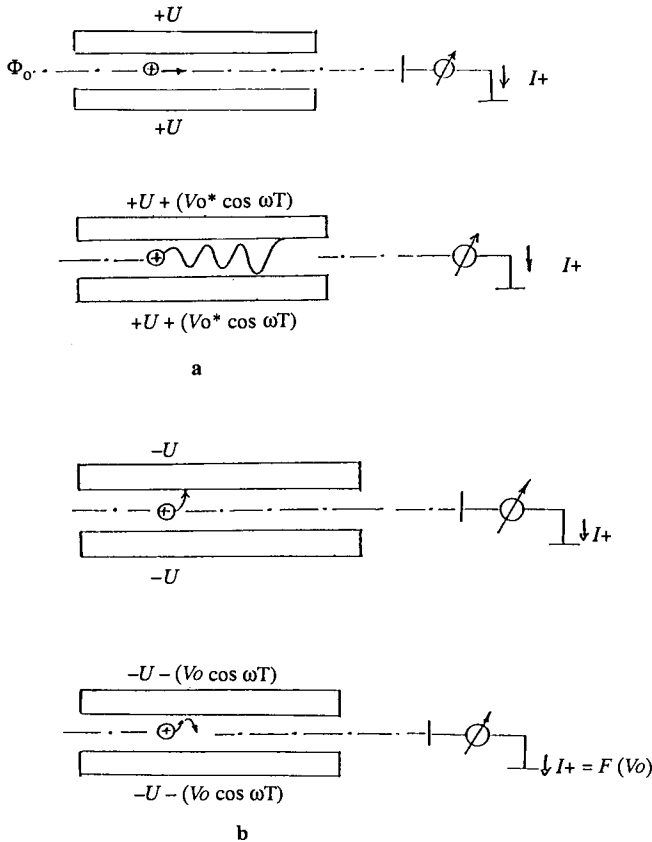
Consider the separation system in the  $x$ - $z$  plane of the quadrupole (Figure 4.18(a)). In the equation for  $\phi$ , if  $\phi_0$  is constant and is equal to  $U$ , then *all* ions and trajectories will be stable in the  $x$ -direction (perfect focusing) but defocusing (unstable trajectories with sharply increasing amplitude) will occur



**Figure 4.17** Diagram of a quadrupole analyser with hyperbolic surfaces. 1, ion beam; 2, d.c. generator; 3 and 4, RF generators; 5, saw-tooth generator

in the  $y$ -direction. If, however,  $\phi_0$  is a periodic function of time, i.e.  $\phi_0 = (U + V_0 \cos \omega t)$ , the trajectories in both planes will be deflected alternately towards and away from the zero. Stability in both planes can exist if the periodicity is short enough and the ion is so heavy that it can't respond during defocusing. For example, if  $\phi_0 = U + V_0 \cos \omega t$ , light ions can follow the alternating component and oscillate with ever-increasing amplitude. The  $x$ -direction is, therefore, equivalent to a high-pass mass filter (only high masses get through the electrode system).

In the  $y$ - $z$  plane (Figure 4.18(b)), heavy ions are defocused. Some lighter ions will be stabilized by the alternating component if its magnitude and frequency can correct the ions' trajectory when it tends to increase. The  $y$ -direction is, therefore, a low-pass mass filter. A combination of the two systems gives a mass filter with a certain pass-band.



**Figure 4.18** Ion trajectories under the influence of pairs of surfaces in a mass filter. (a)  $x$ - $z$  plane (Figure 4.17). (b)  $y$ - $z$  plane

The stability of the trajectories in the  $x$ - and  $y$ -directions can be expressed as a function of two parameters,  $a$  and  $q$  where:

$$a_x = -a_y = \frac{4eU}{m\omega^2 r_0^2}$$

$$\text{and } q_x = -q_y = \frac{2eV_0}{m\omega^2 r_0^2}$$

Mathematical stability can be plotted on a 'stability diagram' (Figure 4.19(a)). In the conventional quadrupole, mass separation is obtained by choosing a constant ratio  $a/q$  (equivalent to the ratio  $2U/V$ ). To produce a mass spectrum,  $V$  is scanned with  $U$  following so that a 'mass scan line' is traversed (Figure 4.19(b)). A particular mass is transmitted by the filter only if  $V$  and  $U$  lie within the stability line for that mass. If the current for transmitted ions is monitored whilst  $V$  and  $U$  are scanned, a mass spectrum results. It is usual to operate with a line such as 'B' in Figure 4.19(b) which is parallel to the tips of the stability regions but is displaced downwards by an amount that gives a convenient peak width. An inherent property of the quadrupole system is the dependence of mass peak intensity (transmissivity) on mass. This is because slow ions are resident in the filter for a longer time and are forced to oscillate more in the RF field. Slow ions are more resolved but suffer more transmission losses than light ions. In the interpretation of a mass spectrum, the mass dependence of sensitivity on mass must be recognized. By electronic correction of  $U/V$ , however, it is possible to compensate for the decrease in transmission (with a loss of resolution at heavy masses). This is achieved by ensuring that the sensitivity for two gases, with masses at appropriate positions in the mass range, is the same.

#### 4.2.1.3 Ion detection

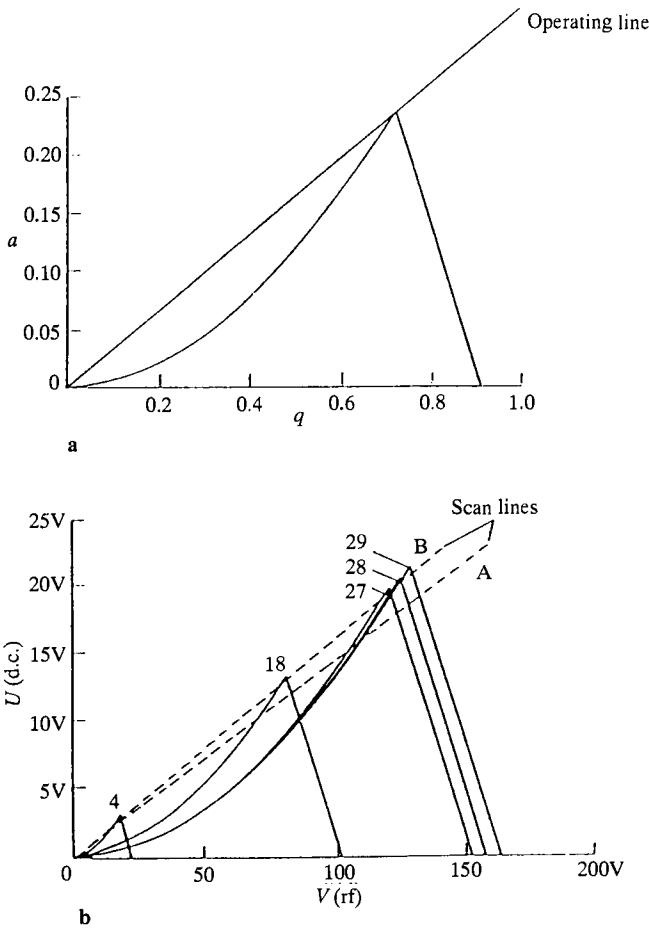
Ions, having passed through the mass filter, must be detected. The simplest system consists of a plate at ground potential followed by a stable, low-noise FET amplifier. Such a device is termed a Faraday cup. It has a gain of one, assuming the geometry is selected to minimize charge loss due to reflected ions. Assuming an absolute sensitivity for  $N_2$  of  $10^{-4}$  A mbar $^{-1}$ , the ion current levels can be low. The smallest detectable partial pressure using a Faraday cup can be calculated as follows:

If the noise is  $5 \times 10^{-14}$  A and the absolute sensitivity is as indicated, then:

$$P_{\min} = \frac{5 \times 10^{-14} \text{ A}}{10^{-4} \text{ A mbar}^{-1}} = 5 \times 10^{-10} \text{ mbar}$$

For a Faraday cup, the amplifier time constant must be enough to keep the signal/noise ratio over 10. A slow response must be expected from the detector.

Both the signal/noise ratio and the response time can be improved by the replacement of a Faraday cup with an electron multiplier. The principle of



**Figure 4.19** (a) The  $a$ - $q$  stability diagram for a mass filter showing the stability region. (b) Stability regions for various masses. ( $V$  is scanned with  $U$  following so that they follow a 'scan line') (see Batey, 1987)  
 Radio frequency = 2 MHz; Quadrupole  $r_0 = 2.75$  mm

operation is that ions are accelerated and strike a 'dynode'. This emits secondary electrons which are accelerated towards a second dynode. The process is repeated until a large number of electrons emerge from the multiplier to strike a Faraday plate. The multiplier gain ( $G$ ) is given by:

$$G = G_1 \times G_2^n$$

where  $G_1$  is the number of secondary electrons generated per incident ion and  $G_2$  is the number of secondary electrons generated per incident electron from

each of  $n$  dynodes. Values of  $G_1$  and  $G_2$  depend on the energy and nature of the incident ion and on the dynode material. It is usual to operate the entrance to the multiplier at a high negative potential ( $-1$  to  $-3$  kV), giving an overall gain of  $10^4$  to  $10^8$  (Batey, 1987). This means that, for an incident ion current of  $10^{-17}$  A, the output current from the multiplier can be  $10^{-11}$  A, which is readily measurable. Three types of multiplier are in common use with residual gas analysers:

1. Discrete dynode multiplier.
2. Continuous channel electron multiplier (CEM).
3. Microchannel plate.

As the name implies, type (1) consists of a number of separate dynodes, often made of a Cu-Be alloy. Different arrangements are available ('Venetian blind'; 'box-and-grid'). The problem with such multipliers is that they degrade rapidly if exposed to ambient air. O'Hanlon (1980), however, has pointed out that the gain can be restored after suitable treatment. The continuous channel electron multiplier consists of a finely drawn tube ( $\text{PbO-Bi}_2\text{O}_3$ ; O'Hanlon, 1980) with a high voltage applied between the ends. The high resistivity of the material (80–100 M $\Omega$ ) establishes a potential gradient. Charge amplification is similar to that taking place in a discrete dynode multiplier. The advantage of the CEM is its tolerance to ambient air and small size. They saturate at a lower current than Be-Cu multipliers and cannot yield a linear output at high pressures unless the operating voltage or mission current is reduced. The microchannel plate works in a similar way to the CEM. Generally, the material used to make microchannel plates has a much higher resistance than that for CEMs, and the output current is lower (Batey, 1987).

#### 4.2.1.4 Characteristics

Mass range and resolution are two extremely important characteristics of a quadrupole. They are determined by five basic parameters:

1. Rod length.
2. Rod diameter.
3. Maximum available RF voltage.
4. Frequency of RF supply.
5. Ion injection energy.

Mass range is determined by rod diameter, the RF voltage and the frequency of the RF supply. According to Austin *et al.* (1976), the maximum mass to which an instrument can be tuned is given by:

$$M_{\max} = \frac{7 \times 10^6 V_m}{f^2 r_0^2}$$

where  $V_m \cos 2\pi ft$  is the RF voltage applied between adjacent rods and  $r_0$  ( $[r_0] = \text{m}$ ) is the inscribed radius of the rods. It was pointed out that  $V_m$  is limited because of the problems associated with the manufacture of very

stable, high voltage a.c. generators and  $V_m = 3$  kV is a typical value.  $r_0$  is limited by the problem of maintaining a high accuracy in the manufacture of the rod assembly and  $r_0 = 3$ – $10$  mm are usual. A value of  $f$  between 500 kHz to 6 MHz is sufficient to cover a mass range up to 1000 amu.

The resolution ( $R$ ) of a residual gas analyser is given by:

$$R = M/\Delta M$$

where  $M$  is the mass number ( $m/e$ ) and  $\Delta M$  is the width of the mass peak at an appropriate height.  $\Delta M$  is usually measured at a point equal to 10% of the peak height. Other definitions are given by O'Hanlon (1980). The resolution of a quadrupole is determined by the number of cycles of RF field to which the ions are exposed (Austin *et al.*, 1976). A precise relationship is not possible but a good approximation is:

$$M/\Delta M = \frac{1}{K} N^n$$

where  $N$  is the number of RF cycles and  $n$  is about 2.  $K$  is not known precisely but it can be assumed to have a value of 20. For a given instrument,  $N$  can be calculated from the rod length ( $L$ ), the RF frequency ( $f$ ) and the ion injection energy ( $V_z$ ) (Austin *et al.*, 1976):

$$\frac{M}{\Delta M} = \frac{0.05f^2L^2M}{2eV_z}$$

$$\text{or } \Delta M = \frac{40eV_z}{f^2L^2}$$

In amu, this expression becomes:

$$\Delta M = \frac{4 \times 10^9 V_z}{f^2 L^2}$$

Taking  $L = 0.2$  m,  $f = 2$  MHz and  $V_z = 5$  eV, the best possible value for  $\Delta M$  is 0.125 amu. In practice, this cannot be achieved for various reasons. One factor is the use, in many analysers, of circular rods to form the electrode assembly because of the difficulty of manufacturing a filter with hyperbolic surfaces. According to Austin *et al.* (1976), a consistent improvement (by a factor of two) in resolution had been observed when hyperbolic, rather than cylindrical, surfaces are used in the electrode assembly.

Mechanical misalignment and contamination of the electrode assembly significantly affect the performance of a quadrupole. Circular rods must be straight and parallel in the assembly and this alignment must remain after baking, cleaning, etc. Experimental evidence showing the effect of misalignment was reported by Austin *et al.* (1976). 'Precursor' peaks are formed and sensitivity is altered. Mao and Leck (1987) have also shown that distortions in the ion source-analyser system significantly reduce sensitivity. They pointed out that multi- or split-peak structures were also a good indication of electric field distortion but this could be caused not only by mechanical misalignment

but also by the accumulation of charge on a contaminated surface. Contamination of surfaces in the ion source, analyser and ion detection system brings about a decline in the sensitivity of the RGA. Sensors normally require cleaning after a period of use but the interval between cleaning varies widely with the conditions of use. For slight contamination, baking under high-vacuum conditions may suffice. Thorough cleaning requires the complete dismantling of the analyser.

According to Mao *et al.* (1987), 'Typical users of small mass spectrometers have no requirement for precise measurement of the residual gas atmosphere'. The small quadrupole is now very widely accepted as the most convenient device for routine gas analysis in vacuum systems. Mao *et al.* (1987) pointed out that, having ensured a resolution adequate for the required task, the user of a residual gas analyser should ensure the following:

1. The stability of the instrument's characteristics over an acceptable period of time.
2. The linearity of the output current over the chosen pressure range.
3. Adequate sensitivity and stability of sensitivity over the specified mass range.
4. A fixed 'cracking pattern' for common gases which is independent of both pressure and instrument resolution setting.

The sensitivity of a residual gas analyser is usually given as  $I^+(28)/p_{N_2}$  or  $I^+(40)/p_{Ar}$  A mbar<sup>-1</sup> where  $I_{(M)}^+$  is the ion current at mass number  $M$  produced from the gas. As has been mentioned, for a Faraday cup, this is of the order of  $10^{-4}$  A mbar<sup>-1</sup>. This is a factor of approximately 100 times less than a Bayard-Alpert gauge and is explained by the relatively inefficient transmission (about 10%) of ions through the analyser. Probably of greater importance to the user are the changes in stability that can occur. These can be ascribed to small changes in system geometry and electrical supplies. Sensitivities are known to change unpredictably over a period of time, and Mao and Leck (1987) recommended setting an analyser to the minimum acceptable resolution to obtain a higher and more stable sensitivity. Ideally, there should be a linear relationship between  $I_{(M)}^+$  and the partial pressure of the gas giving rise to  $M$ . Every gas has a characteristic pressure beyond which deviations from linearity occur. In many commercial instruments, this limit is about  $10^{-4}$  mbar but space- and surface-charge effects can cause significant deviations at lower pressures. With regard to the overall performance, ion current, transmission, 'cracking pattern', etc. should be stable. Long-term instability ('drift'), either on the position of a peak or its amplitude, can only be avoided by the constancy of the d.c./RF voltage and amplifier drift. Usually, unstable peaks are caused by the former.

#### **4.2.1.5 Qualitative analysis with quadrupoles**

The aim of qualitative gas analysis by quadrupole mass spectroscopy is to identify the types of gas present in the quadrupole head. The procedure for the generation of a mass spectrum involves:

1. Admission of the gas mixture, at a pressure below  $10^{-4}$  mbar, to the analyser either via a pressure converter or by direct immersion.
2. Indication of the ion fractions in a constant transmission mode.
3. Preparation of a mass spectrum.
4. Evaluation of data.

The basic procedure for interpretation of data in the case of a pure gas does not present any problem. The following steps can be followed:

1. Identification of the molecular peak. This may be the peak with the highest mass number although care must be taken with isotopes. Generally, the largest peak in the group of peaks with the highest mass is assumed to be the molecular peak.
2. Location of the first few peaks according to mass number and their arrangement according to their intensities.
3. Comparison of the peak sequence with reference spectra. The peak sequence of all substances, the molecular weight of which is equal to the mass number of the established molecule, is compared with the sequence obtained.
4. Selection of the most probable substance.

Qualitative evaluation of the mass spectra is shown in Figure 4.20 for two simple examples, with gas A, the relative intensity ratios are related to the peak with the highest mass. Comparison of these data with those given in Cornu and Massot (1966) shows that of the gases with molecular mass 44 (including ethanol, propane, nitrous oxide, ethylene oxide, etc.), only  $\text{CO}_2$  has a fractional distribution that compares with that given. In the second example, gas B gives a cluster of peaks which is symptomatic of a substance with several isotopes. Again, the mass peaks have been arranged in order of decreasing intensity but, in this case, related to the sum of the peaks. Consultation of a table of isotopes reveals that the gas can only be xenon.

#### ***4.2.1.6 Quantitative measurements with quadrupoles (partial pressure measurement)***

The quadrupole mass spectrometer may be regarded as an ionization gauge fitted with a mass separation system. Both the ionization gauge and the mass spectrometer must be correctly calibrated to give an accurate measure of pressure.

If quantitative analysis is to be undertaken with a vacuum system, the analyser must be located in a position where the relevant information may be obtained. As was discussed earlier, it is also essential to consider effects that may be induced by the analyser head itself. These include chemical reactions with the cathode (dissociation, cracking, etc.) and physical effects such as electron stimulated desorption and degassing. Having eliminated these factors as far as possible, the aim of quantitative analysis is to relate the amplitude of the signal obtained for a peak with the component from which it was produced and, thence, to its partial pressure.



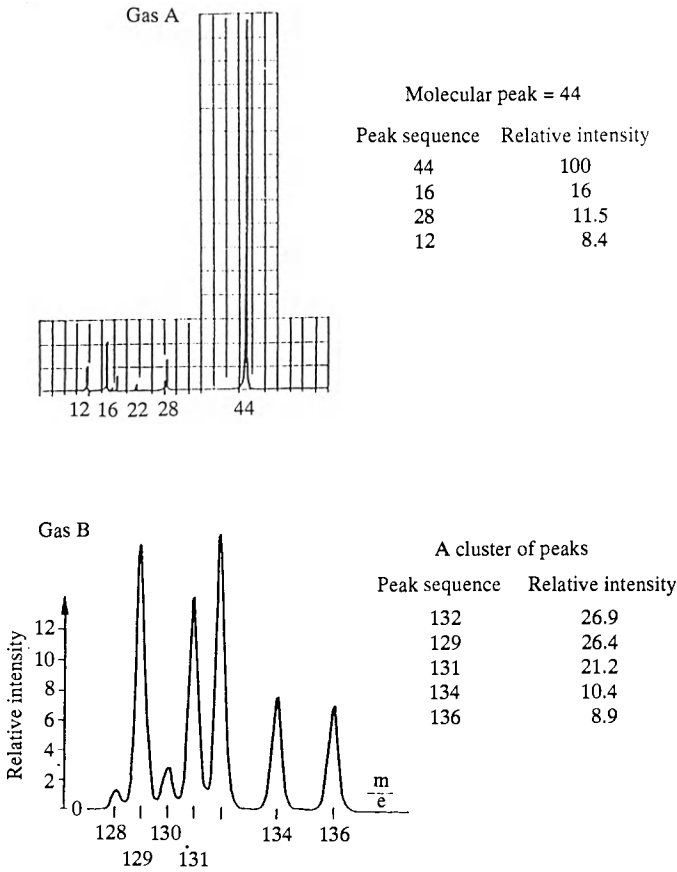


Figure 4.20 Mass spectra of two pure gases A and B

The procedure for obtaining quantitative data can be described in terms of certain characteristics of the analysis system. These can either be obtained experimentally or from tabulated data. Thus if the partial pressure of a gas  $G$  is to be measured, then *total* ion current for *all* the fragments into which  $G$  can break must be measured, and related to the sensitivity of the system to  $G$ :

$$p(G) = I^+(G)/S(G)$$

It is a considerably simpler procedure, however, to select some fragment (mass =  $M$ ) which is characteristic of  $G$  and measure *its* ion current:

$$p(G) = I^+(G,M)/S(G,M)$$

where  $S(G,M)$  is now the sensitivity for  $G$  measured by evaluation of the peak at mass  $M$ .

It is usual to establish the sensitivity of the mass analyser by using  $N_2$  where:

$$S(N_2) = \frac{I_{N_2}^+}{P_{N_2}}$$

$S(N_2)$  may be established by taking  $N_2$  of the highest purity, measuring its pressure ( $P_{meas}$ ) with a calibrated (ion) gauge located in a position equivalent to the ion source and obtaining the total ion current of all the species from  $N_2$ .

Another technique is to obtain

$$S(N_2) = \frac{I_{N_2(28)}^+}{BF_{N_2(28)} \times p_{N_2}}$$

where  $BF_{N_2(28)}$  is the fragmentation factor and gives the fraction of the total ion current due to mass 28 in this case and mass  $M$  generally.

The sensitivity to  $G$  is then:

$$S(G) = S(N_2) \times IP(G)$$

where  $IP(G)$  is the ionization probability of  $G$  relative to  $N_2$ .

It can be shown that:

$$S(G, M) = S(N_2) \times IP(G) \times BF(G, M) \times T(M)$$

where  $T(M)$  is the transmission factor of the system for mass  $M$  from which

$$P(G) = \frac{I^+(G, M)}{S_{N_2} \times IP(G) \times BF(G, M) \times T(M)}$$

In these expressions  $T(M)$  represents the number of ions of mass  $M$  passing to the collector compared with ions of mass 28, with identical pressures in the source. In the mode of constant transmission,  $T(M)$  can be taken as unity. Further, instead of  $S(N_2)$ , the expression given above for  $I^+_{N_2(28)}/BF_{N_2(28)} \times p_{N_2}$  is used. The quotient  $I^+_{N_2(28)}/p_{N_2}$  is termed the nominal sensitivity of the mass spectrometer.

For the most precise work,  $I^+(G, M)$  should be replaced by  $(I^+(G, M) - I_0^+(M))$ , where  $I_0^+(M)$  is the off-set current at mass  $M$  not due to the observed mass peak. Further, fragmentation factors for a gas should be determined for the particular mass analyser by obtaining a spectrum for the purest available sample of the gas and determining the ion currents corresponding to each peak:

$$I^+(G) = \sum I^+(G, M); \quad BF_{G(M)} = I^+(G, M)/I^+(G).$$

Ionization probabilities may also be measured experimentally.

For analyses to within 20%, the definitive equation can be simplified by taking tabulated values for the fragmentation factors and ionization probabilities and also assuming typical, well-documented values for  $I^+(28)/p_{N_2}$ .

#### 4.2.1.7 Applications

The development of the quadrupole mass spectrometer was spurred on by features such as speed of analysis, sensitivity and compactness which made it an ideal device for research into fundamental processes in surface science and

gas-phase reactions (Todd, 1976; Hucknall, 1985). Use of the quadrupole mass spectrometer has continued to expand and it is now used routinely to monitor vacuum conditions, gas purity, surface effects in fusion reactors (Dietz, 1988; Blanchard *et al.*, 1986; Hasler and Rettinghaus, 1988) and storage rings and accelerators (Becker, 1988). Recently, further applications have been indicated including their use for respiratory gas monitoring during anaesthesia to obtain an immediate indication of clinical problems (Holme *et al.*, 1988). Koprio *et al.* (1988) have used quadrupole mass spectrometry during thin-film deposition both for control of the evaporant source and monitoring of the flux.

## References

- Austin, W.E., Holme, A.E. and Leck, J.H. (1976) In *Quadrupole Mass Spectrometry and its Applications*, (ed. P.H. Dawson), Elsevier, Amsterdam
- Batey, J.H. (1987) *Vacuum*, **37**, 659
- Bayard, R.T. and Alpert, D. (1950) *Reviews of Scientific Instruments*, **21**, 571
- Beams, J.W., Spitzer, D.M., Jr. and Wade, J.P., Jr. (1962) *Reviews of Scientific Instruments*, **33**, 151
- Becker, U. (1988) *Vacuum* **38**, 597
- Benvenuti, C. and Hauer, M. (1977) *Nuclear Instruments and Methods*, **140**, 453
- Blanchard, W.R., McCarthy, P.J., Dylla, H.F., La Marche, P.H. and Simpkins, J.E. (1986) *Journal of Vacuum Science and Technology*, **A4**, 1715
- Cornu, A. and Massot, R. (1966) *Compilation of Mass Spectral Data*, Heyden, London
- Dawson, P.H. (1976) In *Quadrupole Mass Spectrometry and its Applications*, (ed. P.H. Dawson), Elsevier, Amsterdam, p.9
- Dawson, P.H. (1986) *Journal of Vacuum Science and Technology*, **A4**, 1709
- Dietz, K.J. (1988) *Vacuum*, **38**, 591
- Fremerey, J.K. (1985) *Journal of Vacuum Science and Technology*, **A3**, 1715
- Gentsch, H., Tewes, J. and Messer, G. (1985) *Vacuum*, **35**, 137
- Harten, U., Grosse, G., Jitschin, W. and Gentsch, H. (1988) *Vacuum*, **38**, 167
- Hasler, E. and Rettinghaus, G. (1988) *Vacuum*, **38**, 777
- Holme, A.E., Parris, M. and Purdy, S.J. (1988) *Vacuum*, **38**, 787
- Hucknall, D.J. (1985) *Chemistry of Hydrocarbon Combustion*, Chapman and Hall, London
- Koprio, J.A., Peter, G. and Fischer, H. (1988) *Vacuum*, **38**, 783
- Knauer, W. (1962) *Journal of Applied Physics*, **33**, 2093
- Knauer, W. and Lutz, M.A. (1963) *Applied Physics Letters*, **2**, 109
- Lange, W.J., Singleton, J.H. and Eriksen, D.P. (1966) *Journal of Vacuum Science and Technology*, **3**, 338

- Leck, J.H. (1988) *Total and Partial Pressure Measurement in Vacuum Systems*, Blackie and Son Ltd., Glasgow
- Mao, F.M. and Leck, J.H. (1987) *Vacuum*, **37**, 669
- Mao, F.M., Yang, J.M., Austin, W.E. and Leck, J.H. (1987) *Vacuum*, **37**, 335
- Messer, G., Roehl, P., Grosse, G. and Jitschin, W. (1987) *Journal of Vacuum Science and Technology*, **A5**, 2440
- Nash, P.J. (1987) *Vacuum*, **37**, 643
- Nash, P.J., and Thompson, T.J. (1983) *Journal of Vacuum Science and Technology*, **A1**, 172
- National Physical Laboratory (1977) *Measurement Services Pressure and Vacuum*. NPL, London
- National Physical Laboratory (1984), *Calibration of Vacuum Gauges by the Series Expansion Method*. NPL, London
- O'Hanlon, J.F. (1980) *A User's Guide to Vacuum Technology*, Wiley-Interscience, New York
- Penning, F.M. (1936) *Physica*, **3**, 873
- Penning, F.M. (1937) *Philips Technical Review*, **2**, 201
- Redgrave, F.J. and Downes, S.P. (1988) *Vacuum*, **38**, 839
- Redhead, P.A. (1960) *Reviews of Scientific Instruments*, **31**, 343
- Redhead, P.A. (1988) *Vacuum*, **38**, 901
- Redhead, P.A. (1965) *Journal of Vacuum Science and Technology*, **3**, 173
- Reich, G. (1980) In *Proceedings of the 8th International Vacuum Congress*, Cannes, vol. II, p.222
- Reich, G. (1989) In *Theory and Practice of Vacuum Technology* (eds M. Wutz, H. Adam and W. Walcher), F. Vieweg and Son, Braunschweig/Wiesbaden, p.393
- Schuurman, W. (1967) *Physica*, **36**, 136
- Simpson, D.I. (1991) Paper presented at the Institute of Physics Symposium, 'Vacuum Gauge Calibration and the Calibration of Standard Leaks', March 1991
- Steckelmacher, W. (1987) *Vacuum*, **37**, 651
- Sullivan, J.J. (1985) *Journal of Vacuum Science Technology*, **A3**, 1721
- Tilford, C.R. (1985) *Journal of Vacuum Science Technology*, **A3**, 546
- Todd, J.F.J. (1976) In *Quadrupole Mass Spectrometry and its Applications* (ed. P.H. Dawson), Elsevier, Amsterdam, p. 241
- Van Atta, C.M. (1965) *Vacuum Science and Engineering*, McGraw-Hill, New York, p. 63
- Wood, S.D. and Tilford, C.R. (1985) *Journal of Vacuum Science and Technology*, **A3**, 542
- Watanabe, F. (1987) *Journal of Vacuum Science and Technology*, **A5**, 242

# 5

## *Leak detection*

---

### 5.1 Introduction and principles

The first systematic application of 'vacuum analysis' in order to improve the performance of a system was made at the Lawrence Radiation Laboratory in 1943/44 during work on methods of U-isotope separation. A system was assembled based on a mass spectrometer designed by Dempster in 1918. Using this equipment, it was found that leak detection could be carried out effectively by probing the external surface of the vacuum system with a gas not normally present and looking for a response on the appropriately tuned mass spectrometer. Helium was found to be the ideal search gas.

So effective was the method that a simplified, portable mass analyser was developed which had a self-contained vacuum system. Helium leak detection thus became simple and effective. Many improvements were subsequently made (particularly developments at the University of Minnesota) until a commercially exploited leak detector emerged. By today's standards, they were crude instruments being evacuated with diffusion pumps with dry-ice-cooled traps. Photomultiplier tubes were used extensively.

Leak detection has progressed to such an extent that it is carried out whenever necessary:

1. To prevent loss of material from a system when that would either interfere with the operation of the system or contaminate the surroundings.
2. To detect unreliable components.

It is also no longer confined to vacuum systems and is nowadays applied routinely to a wide range of industries and products such as:

1. Electronic components:
  - (a) Encapsulated devices.
  - (b) Integrated circuit (IC) enclosures.
  - (c) Image converter tubes.
2. Precision instruments:
  - (a) Pressure sensors.
  - (b) Altimeters.
  - (c) Infra-red detectors.
3. Sheet metal fabrications:
  - (a) Barrels.
  - (b) Cans and cases.
  - (c) Bellows/corrugated tubes.
4. Vessels and tanks:
  - (a) Heat exchangers.

- (b) Cryogen tanks/containers.
  - (c) Pressure vessels.
5. Components for refrigeration/air conditioning:
- (a) Compressors.
  - (b) Thermostats.
  - (c) Heat pumps.

### 5.1.1 Definitions, formulae and units

Gas leaks are flow paths in the boundary of a system that allow material to pass from a region of higher pressure to one of lower pressure. Leaks may be holes or cracks or areas of general porosity and the flow of gases through a leak follows the same laws of flow as indicated in Chapter 1. Thus the flow-rate or throughput is determined by the pressure difference across the boundary although the actual length of the leak is generally greater than the thickness of the boundary.

It is extremely difficult to calculate from the equations derived in Chapter 1, the mass flow-rate ( $q_m$ ) or the PV-throughput for a leak because the precise dimensions of the leak are not known. Nevertheless, an approximate value may be obtained, as can be seen in the following example.

#### Example 1

A leak with a diameter of  $1 \mu\text{m}$  ( $1 \times 10^{-4} \text{ cm}$ ) has a length of  $0.2 \text{ cm}$ . Suppose that on one side of the leak there is a pressure of air of  $1 \text{ bar}$  and, on the other side, there is a 'vacuum', calculate the PV-throughput at  $20^\circ\text{C}$ .

For viscous, laminar flow involving air

$$q_{\text{PV}} \text{ at } 20^\circ\text{C} = 135 \frac{d^4 (P_o^2 - P_i^2)}{l \cdot 2} \text{ mbar l s}^{-1}$$

where  $l$  and  $d$  are in  $\text{cm}$  and  $P_o$  and  $P_i$  (the outer and inner pressures, respectively) are in  $\text{mbar}$ .

$$\begin{aligned} \text{Thus } q_{\text{PV}} &= \frac{135 \times (10^{-4} \text{ cm})^4 (1000^2 - 0^2)}{0.2 \text{ cm} \cdot 2} \text{ mbar l s}^{-1} \\ &= \frac{1.35 \times 10^8 \times 10^{-16}}{0.2 \times 2} \text{ mbar l s}^{-1} \\ &= 3.38 \times 10^{-8} \text{ mbar l s}^{-1} \end{aligned}$$

The possibility of 'choked' flow may also exist. For air, the critical pressure ( $P^*$ ) at which this could occur is given by the relationship:

$$\frac{P^*}{P_0} = 2.3 \times \frac{d^2}{l} \times P_0$$

$$\begin{aligned} \text{whence } P^* &= \frac{2.3 \times (10^{-4})^2 \times 10^6}{0.2} \\ &= 1.15 \times 10^{-1} \text{ mbar} \end{aligned}$$


---

At this pressure, the mean free path of air is such that molecular flow conditions will prevail somewhere inside this 'ideal' cylindrical leak. Thus air passing through will experience a change in flow conditions from viscous laminar to molecular. According to Wilson and Beavis (1976), flows in leaks and in most vacuum systems seldom achieve rates high enough for choked flow to be considered. Calculations, however, indicate contrary results (Sydow, 1989).

In leak detection, the magnitude of the leak is specified in terms of the leak rate ( $q_L$ ), which is itself given in terms of the PV-throughput ( $q_{PV}$ ) flowing through the leak. The pressures on either side of the leak and the temperature should also be defined. The usefulness of PV-throughput in describing a leak can be appreciated when it is considered that the leak brings about a pressure rise in an evacuated system (volume  $V$ ) isolated from its pumps:

$$q_L = q_{PV} = V \frac{\Delta P}{\Delta t}$$

Leaks are often quantified by carrying out pressure-rise measurements. The unit extensively used in practice is:

$$[q_L] = \text{mbar l s}^{-1}$$

Using the equation of state for an ideal gas ( $PV = (m/M) RT$ ), it can be shown that:

$$\dot{m} = q_L \frac{RT}{M}$$

Leak rates in various units are given in Table 5.1. In practice, with leaking system, one is concerned mainly with the in-leakage of air. When the magnitude of these leaks is being assessed, however, they may be probed by a very different gas (He, for example). Leak rates for two different types of gases (assuming identical temperatures) are given by the expressions:

$$\frac{q_{L,\text{gas1}}}{q_{L,\text{gas2}}} = \sqrt{\frac{M_{\text{molar,gas2}}}{M_{\text{molar,gas1}}}} \quad (\text{molecular flow})$$

$$\frac{q_{L, \text{gas1}}}{q_{L, \text{gas2}}} = \frac{\eta_{\text{gas2}}}{\eta_{\text{gas1}}} \quad (\text{laminar, viscous conditions})$$

( $\eta$  is the dynamic viscosity)

The appropriate constants for some gases are given in Table 5.2.

**Table 5.1** Leak rates

$\text{Pa m}^3 \text{ s}^{-1}$	$\text{mbar l s}^{-1} (T_n)$	$\text{cm}^3 (\text{NTP}) \text{ s}^{-1}$	Air (kg/year (20°C))
1	10	10*	377
0.1	1	1	37.7
$10^{-2}$	$10^{-1}$	$10^{-1}$	3.8
$10^{-3}$	$10^{-2}$	$10^{-2}$	0.38
$10^{-5}$	$10^{-4}$	$10^{-4}$	$3.8 \times 10^{-3}$

NTP corresponds to  $T=273.15\text{K}$  and  $P=1.01325 \text{ bar}$

\* Conversion factor:  $1 \text{ mbar l s}^{-1} = 9.869 \text{ cm}^3 (\text{NTP}) \text{ s}^{-1}$

**Table 5.2** Properties of gases

Gas	Molar mass ( $\text{kg kmol}^{-1}$ )	Dynamic viscosity ( $\eta \cdot 10^6$ )( $\text{kg m}^{-1} \text{ s}^{-1}$ )*
H <sub>2</sub>	2.016	8.8
He	4.003	19.6
H <sub>2</sub> O(v)	18.015	ca.9
N <sub>2</sub>	28.013	17.5
air†	28.96	18.2
C Cl <sub>2</sub> F <sub>2</sub> (R12)	120.914	13.2

\* At 20°C and  $P = 1 \text{ bar}$ .

† Air = 0.78 N<sub>2</sub> + 0.21 O<sub>2</sub> + 0.01 Ar.

### Example 2

A guarantee is to be given for refrigerators over a period of 5 years. During this period, 10% of the refrigerant (Freon 12) may escape through leaks. The cooling system is charged with 300 g of the Freon and operates with pressures of 17 bar and 0.6 bar in the high-pressure and low-pressure sides, respectively. If pure helium is to be used as



the search gas in a vacuum leak check (see Section 5.1.2.2), what is the maximum permissible leak rate?

Charge = 300 g. 10% of this is permitted to leak away in 5 years. This is equivalent to 6 g yr<sup>-1</sup>.

$$\text{Now } PV = \frac{m}{M} RT$$

$$\begin{aligned} \therefore q_{PV} &= \frac{6[\text{g}] \times 83.14 [\text{mbar l mol}^{-1} \text{K}^{-1}] \times 293[\text{K}]}{121 [\text{gmol}^{-1}] \times 3.15 \times 10^7 [\text{s yr}^{-1}]} \\ &= 3.83 \times 10^{-5} \text{ mbar l s}^{-1} \end{aligned}$$

In order to convert the CF<sub>2</sub>Cl<sub>2</sub> leak rate into a He leak rate, the relationship:

$$q_{\text{He}} \times \eta_{\text{He}} = q_{\text{R12}} \times \eta_{\text{R12}}$$

is used

$$\begin{aligned} \therefore q_{\text{He}} &= \frac{3.85 \times 10^{-5} [\text{mbar l s}^{-1}] \times 13.2 \times 10^{-6} [\text{kg m}^{-1} \text{s}^{-1}]}{19.6 \times 10^{-6} [\text{kg m}^{-1} \text{s}^{-1}]} \\ &= 2.59 \times 10^{-5} [\text{mbar l s}^{-1}] \end{aligned}$$

To modify this leak rate, which would apply to the situation where He (17 bar) leaked across a boundary to 0.6 bar, to a situation where 1 bar He was probing an evacuated object, allowance must be made for the pressure:

$$q_{\text{He,HP}} = 2.59 \times 10^{-5} \text{ mbar l s}^{-1} = 135 \frac{d^4}{l} \left\{ \frac{(17\,000)^2 - (600)^2}{2} \right\}$$

$$\begin{aligned} q_{\text{He,vac}} &= 2.59 \times 10^{-5} \times \frac{[(1000)^2 - 0^2]}{2} \times \frac{2}{[(17\,000)^2 - (600)^2]} \\ &= \frac{2.59 \times 10^{-5} \times 10^6}{2.89 \times 10^8} \\ &= 8.96 \times 10^{-8} \text{ mbar l s}^{-1} \end{aligned}$$

No pressurized or evacuated system is entirely leak-tight, nor does it have to be. Demands for 'zero leakage', 'no leakage' and so on, are impossible to implement. What is required is elimination of leaks to a point where they no longer interfere with the efficient running of the system and the successful completion of the required operation. For example, equipment used in medium-vacuum work should be leak-tight to  $10^{-3}$  mbar l s<sup>-1</sup>. For high-vacuum system, if the overall leak rate is  $10^{-6}$  mbar l s<sup>-1</sup> or below, then it is very leak tight. At  $10^{-5}$  mbar l s<sup>-1</sup>, the leak rate is acceptable but should it increase to  $10^{-4}$  mbar l s<sup>-1</sup>, leak location must be carried out. With ultra-high-vacuum equipment, the leak rate must be very low indeed.

### 5.1.2 Methods of leak detection

To establish the presence of leaks in equipment and then possibly localize and eliminate them, procedures may be followed that can be classified as:

1. Pressure methods.
2. Vacuum methods.

In the former, the object to be tested is filled with a fluid at a pressure suitably above ambient. Escape of material from the object may allow the leak to be located and quantified. In the vacuum method, the object under consideration is evacuated and gas (air or a suitable test gas) entering through the leak is detected.

#### 5.1.2.1 Pressure leak testing

Various methods have been used although many have been superseded by the use of commercial leak detectors.

##### 5.1.2.1.1 Pressure drop method

A gas is admitted to the object under test until a suitable pressure has been achieved. The time interval required for the pressure to decrease by an appropriate amount is then obtained. The *total* leak rate may then be calculated from:

$$q_L = V \frac{\Delta P}{\Delta t}$$

The actual pressure used in the test depends on the construction and material of the object but it should attempt to reproduce as closely as possible the conditions under which the object is normally used.

For test purposes, air at 1 bar overpressure may be used and it is recommended (Sydow, 1989) that the decrease in pressure should be very much less than the starting pressure. The minimum detectable leak rate using this test is about 1 mbar l s<sup>-1</sup>.

#### 5.1.2.1.2 *Bubble tests*

Having established an overpressure in the object to be tested, it is immersed in water. The outer surface is then observed for the formation of bubbles. Leak rates may be quantified by collecting the bubbles in a water-filled, calibrated cylinder placed over the leak. It is claimed that, by using warm water, suitably treated to reduce surface tension, leak rates in the range  $10^{-4}$  to  $10^{-5}$  mbar l s<sup>-1</sup> may be detected. Unfortunately, equipment tested in this way has to be subsequently dried. There are also problems involved in the immersion of very large objects.

Leak testing using soap solution is a variation on this technique. The suspect region on the pressurized equipment is painted with the solution and the area observed for the production of bubbles. The formation of a bubble of radius 1 mm within 5 minutes against atmospheric pressure corresponds to a leak rate of about  $10^{-5}$  mbar l s<sup>-1</sup>.

Gross leaks in sealed items may also be detected by immersion in hot (120°C) per fluorocarbon liquids and the observation of bubble formation.

#### 5.1.2.1.3 *Tests with gas-phase tracers*

Leak localization using a reactive gas pressure test may be performed. Ammonia has been used for this purpose. The equipment under test is pressurized and paper impregnated with the dye bromocresol purple is applied externally. In the presence of ammonia, there is a colour change from yellow to purple. The use of ammonia is not to be recommended. There is a risk of corrosion and such a test is usually restricted to equipment that will be used subsequently with ammonia.

Pressurization of systems with search gases such as He or halogen-containing compounds is a widely applied technique. Escape of the search gas through the leaks can be detected using selective He and halogen detectors in conjunction with 'sniffers' and the procedure will be discussed in great detail in Section 5.1.2.1.4. The preferred halogen-containing tracer gases are usually refrigerants. Examples are Refrigerant-12 (dichlorodifluoromethane, CF<sub>2</sub>Cl<sub>2</sub>) and Refrigerant-22 (chlorodifluoromethane, CHClF<sub>2</sub>). R12, for example, is an inert (until it reaches the upper atmosphere), non-toxic, readily available compound. The equipment is filled with the refrigerant (or a refrigerant/air mixture) at a slight excess pressure and suspected areas are probed with a 'sniffer'.

Leaks of halogen-containing gases may be detected with a 'halide torch'. In this, a halogen-free fuel such as propane is burned in an enclosure containing a copper tube or plate. Some of the air for combustion is drawn into the flame through a tube and a flexible extension to this may be used as the sniffer. In the presence of halogens, the flame changes from its normal blue colour to green. This may be observed visually or by means of a suitable detector. The lowest detectable limits are claimed to be  $10^{-4}$  (visual detection) to  $10^{-5}$  mbar l s<sup>-1</sup> (spectrophotometric detection).

#### 5.1.2.1.4 *Pressure leak-testing using He and a 'sniffer'*

After prior preparation (including cleaning and drying), the equipment under investigation is pressurized with He or a He + air mixture, either after

evacuation to about 10 mbar or by the addition of He is such a way that a good mixture is obtained. The external surface is then investigated for the escape of helium using a sniffer which continuously aspirates air and transfers it to the detector (a He-specific mass spectrometer; see Section 5.3). Depending on the size of the test object and whether an integral or a partial leak check is to be carried out, the surface is either completely surrounded or partially covered by a hood prior to the test in order to restrict the volume of air being sampled.

The covering must have as small a volume as convenient (this may have to be determined for quantitative work) and its edges must be tightly sealed. As can be seen from Figure 5.1, plastic foil or a bag may be used, the appropriate configuration being decided by the experience of the investigator. Very elaborate systems may be used in some circumstances. Pidduck (1986), for example, described measurements of the escape of helium from satellite propulsion systems. The spacecraft transportation container ( $V = 33 \text{ m}^3$ ) was the test volume and, after carrying out tests to assess helium loss within the container itself, tests were performed, by injecting  $100 \text{ cm}^3$  He, in order to measure the sensitivity of the procedures (Figure 5.2).

Under conditions of laminar flow through a leak, the flux into the surroundings at atmospheric pressure ( $P_{\text{at}}$ ) from a chamber filled with pure helium is proportional to  $(P_{\text{He}}^2 - P_{\text{at}}^2)$ . By increasing the pressure of helium in the system, therefore, an increase in the sensitivity of the test arrangement (expressed as  $(P_{\text{He}}^2 - P_{\text{at}}^2)/[(2P_{\text{at}})^2 - P_{\text{at}}^2]$ ) will be obtained.

The sniffer (here denoted as a 'Quick-Test' sniffer) consists of a metal capillary probe fitted with a sinter and a flexible plastic tube (5–50 m) through which air is drawn continuously by means of a diaphragm gas-transfer pump (Figure 5.3). This is connected directly to the test port of the leak detector (Figure 5.4) and the sampled gas delivered via a throttle to the mass spectrometer.

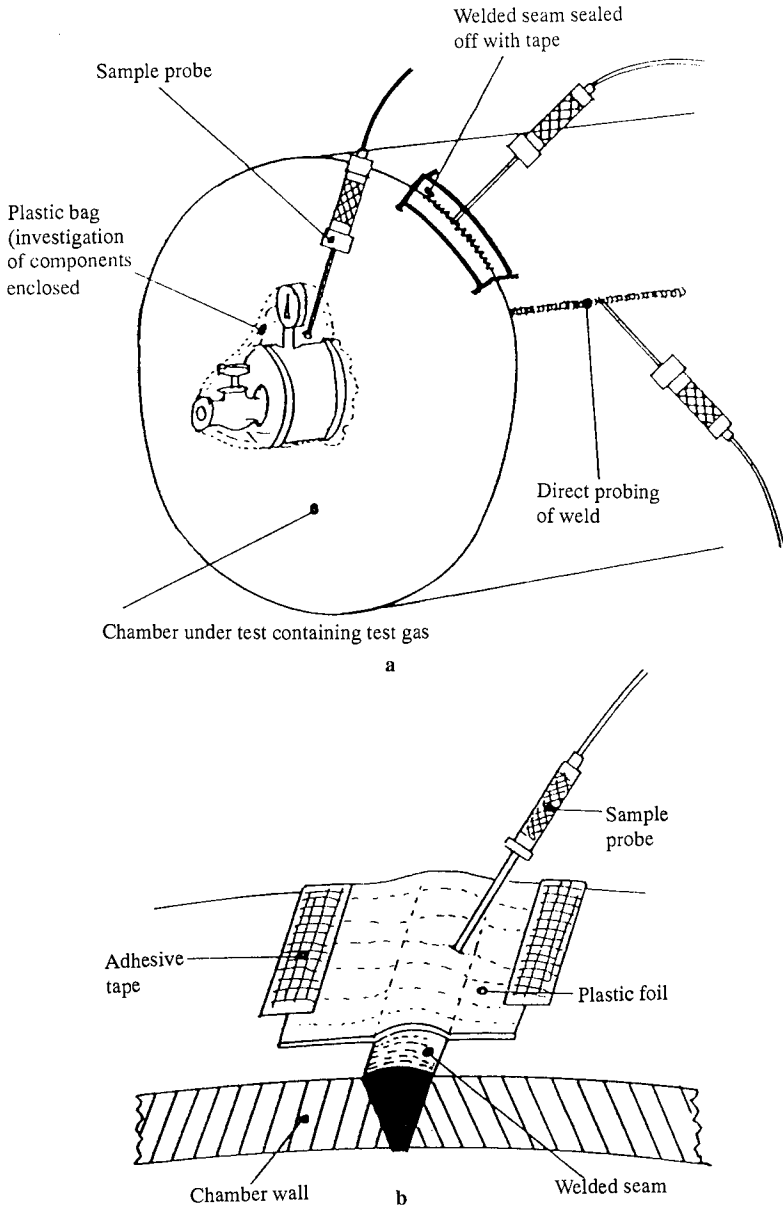
The 'Quick-Test' sniffer allows a fast response time, even for probe tubes of great length (cf. 15 s and 270 s for the same length of tubing (50 m) for sample systems with and without the 'quick' probe).

Using a sniffer with He as the test gas, the sensitivity of the method is limited by:

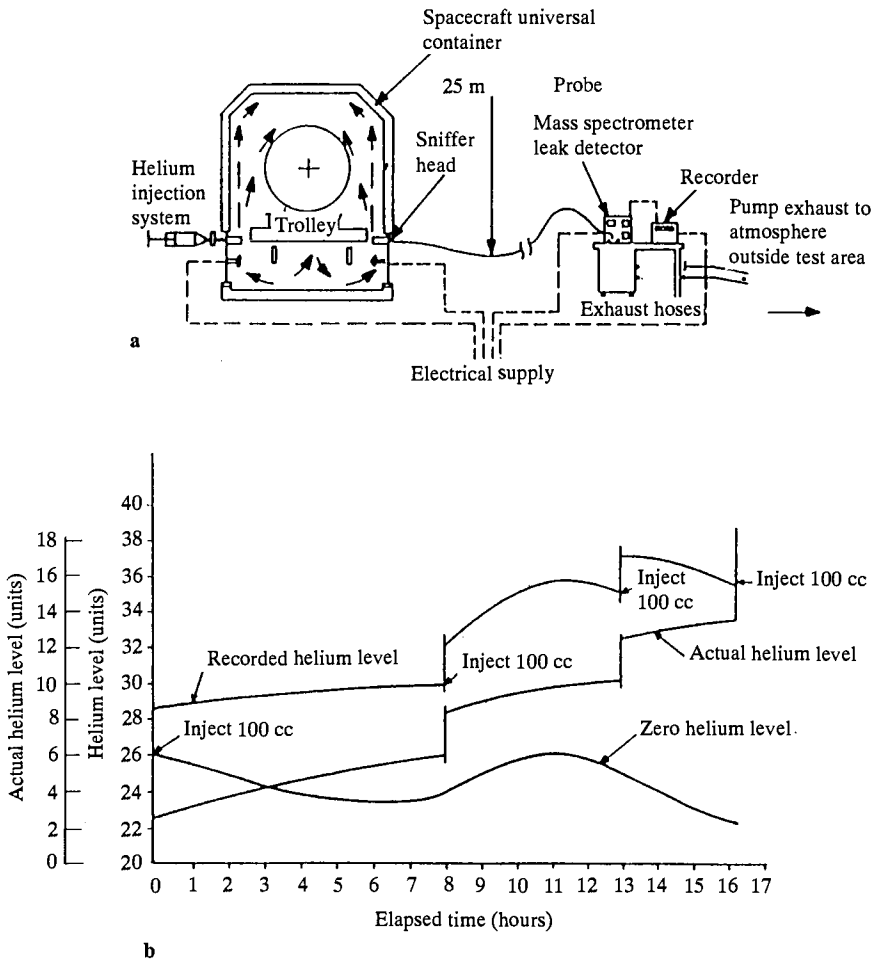
1. The He concentration in the ambient air.
2. The He concentration at the point of escape from the leak.
3. The residence time of the probe tip at the point of leakage.

In principle, the sniffer measures He concentration. This is only a measure of the true leak rate when experimental conditions are defined and a relevant calibration has been performed. With the probe tip stationary in front of a leak, the detection limit using this method is restricted by the ability of the detector to measure changes in helium concentration in the presence of the 5 ppm He that is always present in air. It is essential, of course, that there are no other emissions of He in the vicinity.

Assuming there are no air draughts to disperse the gas, helium emerging from a leak will diffuse uniformly into the surrounding air (Figure 5.5). The variation in the indicated leak with distance of the probe tip from the leak is



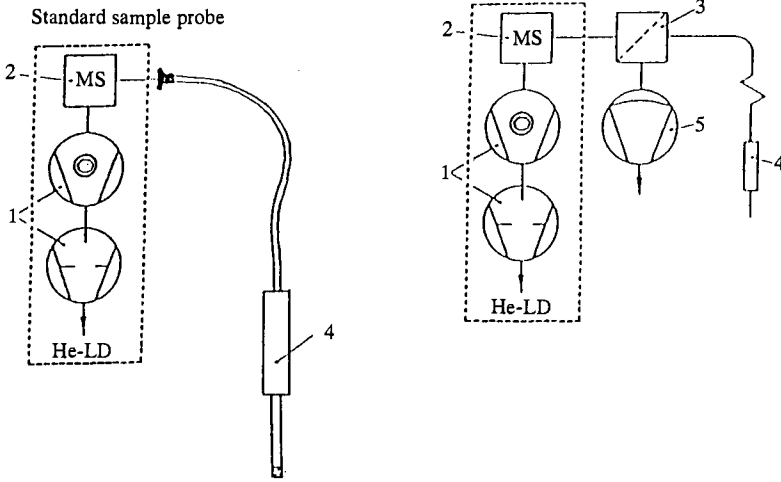
**Figure 5.1** Preparation for leak testing with a 'sniffer'. (a) a vessel (b) welded seams



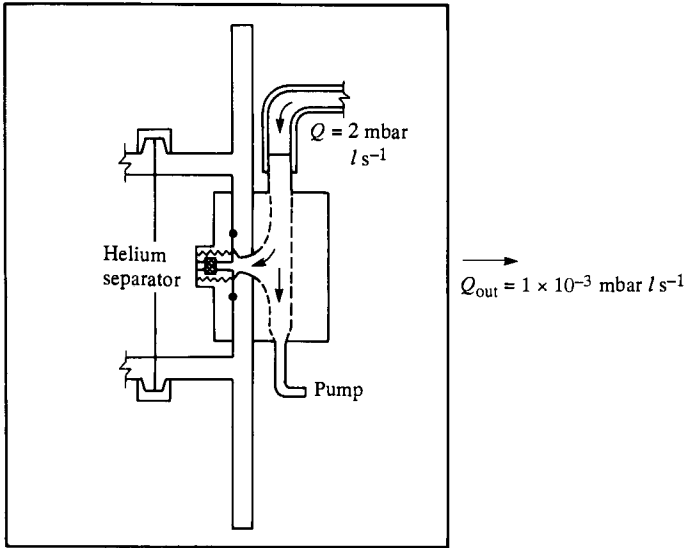
**Figure 5.2** Layout of equipment for use in leak checking satellite propulsion system. (a) System for measurement of helium loss from the CPS module. (b) Plots of He levels against time in order to assess sensitivity and the duration of the test

also shown in Figure 5.5. Finally, maintaining the probe tip directly above the leak for a suitable length of time, will give an indication of the maximum amount of helium emerging from the leak. Moving the tip over the leak will decrease the amount of helium entering the tip and the greater the sniffer speed, the lower the displayed leak.

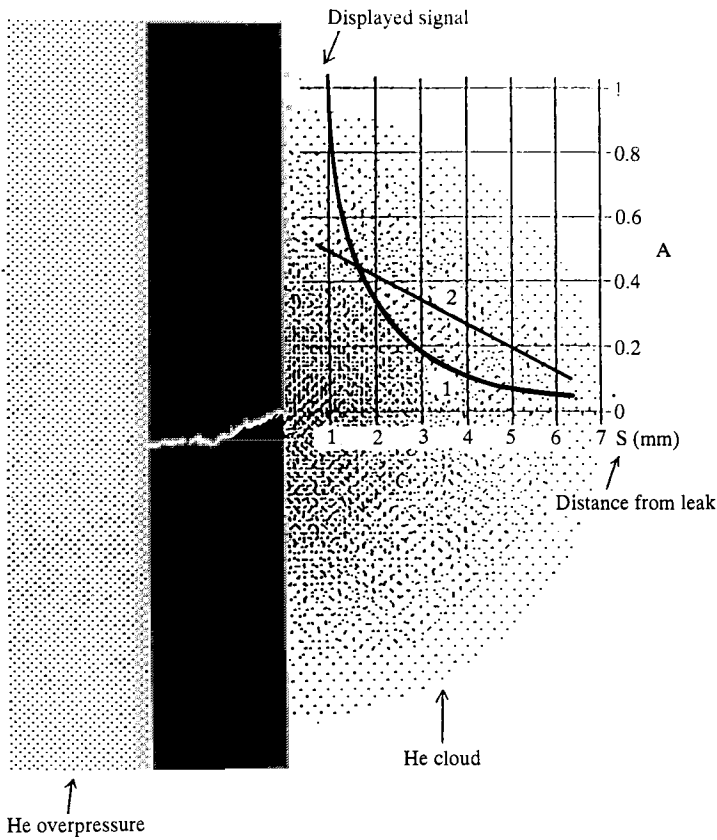
In practice, for leak localization, the leak detector is set to its most sensitive range and areas suspected of leakage are explored by moving the probe at



**Figure 5.3** Helium sample probes. 1, LD vacuum pumps; 2, mass spectrometer; 3, separator; 4, sampling probe; 5, displacement pump; LD, leak detector



**Figure 5.4** Details of He sample probe



**Figure 5.5** Emission of helium from a leak in still air showing the decrease in the displayed signal for a standard probe (1) and a 'quick' probe (2)

moderate speed with the tip kept as near as possible to the surface. If an increase in He concentration is detected, then the precise location of the increase is established by slowly approaching the area several times with the probe. The area is marked, repaired and then retested.

#### 5.1.2.1.5 Pressure leak-testing using halogen-containing compounds

A halogen detector can be used in the same way as the helium leak detector for the external sniffing of objects pressurized with a suitable gas. The set-up consists of a sniffer tube, a detector and a pump. Air to be tested is aspirated through the sniffer tube and passes to the detector. Halogen sniffer detectors can locate leak rates down to  $10^{-6}$  mbar  $l s^{-1}$ .

#### 5.1.2.2 Vacuum leak detection methods

In principle, any gas-dependent pressure measuring device can be used as a leak detector. For example, total pressure measuring gauges such as ioniza-



tion gauges and thermal conductivity gauges are calibrated using dry N<sub>2</sub> or air. If other gases, varying significantly in the relevant properties, are predominant in the vacuum system then differences can be observed between the true and indicated pressures. This effect can be exploited for the purposes of leak detection by spraying suspect areas with propanone, alcohol, He, CO<sub>2</sub>, etc. and observing any changes in the pressure gauge.

Use of a quadrupole mass spectrometer to analyse the composition of residual gas within the vacuum system is a highly reliable method of detecting an air leak, for example. With examination of the intensity of the lines in the spectrum associated with mass numbers 14 (N<sup>+</sup>), 28 (N<sub>2</sub><sup>+</sup>) and 32 (O<sub>2</sub><sup>+</sup>), one may conclude that air has entered the system.

In practice, however, use of a dedicated leak detector is a much more reliable and effective method of locating and quantifying leaks.

#### 5.1.2.2.1 Pressure rise method

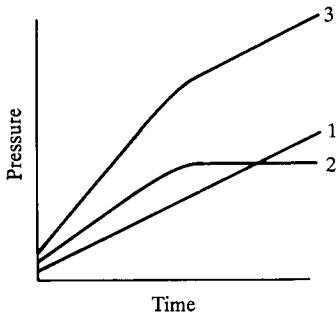
Before proceeding with a leak test, it may be useful to assess the magnitude of any leaks in the system. This may be carried out by evacuating the system (volume,  $V$ ), isolating it from the pumps and observing the pressure rise ( $\Delta P$ ) measured over a time interval ( $\Delta t$ ) using a vacuum gauge on the chamber:

$$Q_{\text{IN}} = V \frac{\Delta P}{\Delta t} \text{ (for constant system volume)}$$

Unfortunately, this method assesses all gas flux into the system, including leaks and degassing. It is also time consuming and may be unreliable.

To identify the gas sources that have given rise to the pressure increase, it is necessary to repeat the observations of  $\Delta P$  with  $\Delta t$  several times and in different pressure regions. For example, if at pressures below 10<sup>-1</sup> mbar, a pressure rise is observed which decreases with increasing pressure before levelling off, degassing is the problem. If the rate of pressure rise remains constant up to higher levels, then there is probably a leak in the system. Usually, however, both effects occur simultaneously. General pressure versus time curves for vacuum systems isolated from their pumps are shown in Figure 5.6. Curve 3 shows the most common type of pressure rise. At lower pressures, the gas flux consists of leakage and degassing, the latter decreasing with pressure. When a certain pressure has been reached, only leakage flux remains (linearly increasing, lower rate section of curve 3).

With the pressure rise method, particularly when small leak rates ( $\leq 10^{-4}$  mbar l s<sup>-1</sup>) are involved, the observation time in the rough vacuum range can be extremely long. For example, if a volume of 1 m<sup>3</sup> was examined for leaks using a diaphragm vacuum gauge ( $P_{\text{range}}$  1–10 mbar for an accurate determination of  $\Delta P = 1$  mbar), then for leaks of about  $2 \times 10^{-2}$  mbar l s<sup>-1</sup>, measurements would require at least 50 000 s (13.9 h). Shorter times are available if the test is carried out at a lower pressure.



**Figure 5.6** Pressure rise in a chamber after isolating the pump (schematic diagram). 1, pressure rise due to a real leak; 2, pressure rise resulting from outgassing of the chamber walls and any inserts; 3, summation of both effects

### Example 3

A vacuum chamber ( $V = 1 \text{ m}^3$ ;  $q_L = 2 \times 10^{-2} \text{ mbar l s}^{-1}$ ) is isolated from its pumps. Within what time interval would the pressure rise from  $1 \times 10^{-3}$  to  $7 \times 10^{-3}$  mbar?

$$q_L = V \frac{\Delta P}{\Delta t}$$

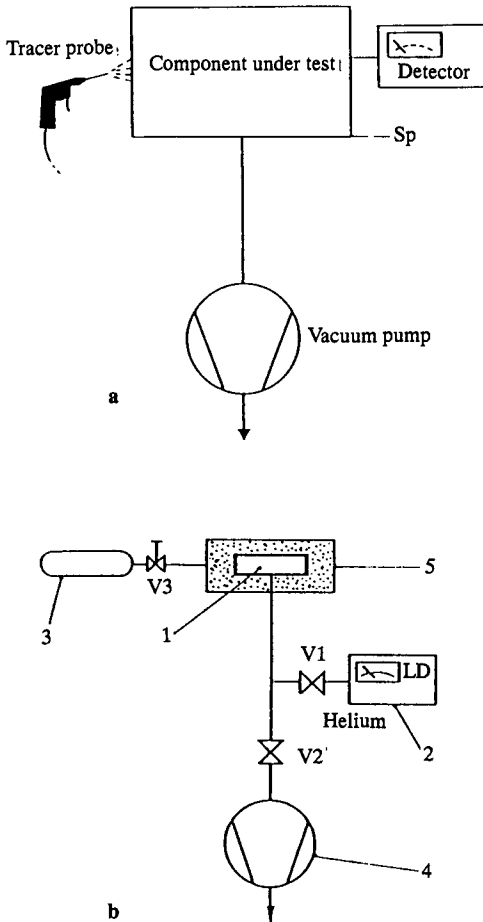
$$2 \times 10^{-2} \text{ mbar l s}^{-1} = \frac{1000 \text{ l} \times (6 \times 10^{-3} \text{ mbar})}{\Delta t \text{ (s)}}$$

$$\therefore \Delta t = 300 \text{ s}$$

Performance of pressure rise tests at relatively low pressures may, however, give results complicated by degassing. Only by performing tests over a large pressure range can the two effects be separated.

#### 5.1.2.2.2 Vacuum leak detection with search gases

In the vacuum method of leak detection, using search gases and selective detectors, the object to be tested is connected to the vacuum pumping system and the leak detector is also incorporated into the vacuum line at an appropriate point. The outer surface of the system is then probed with search gas (Figure 5.7). By using the method shown in Figure 5.7(a), leak localization can be carried out. By surrounding the whole of the object with an



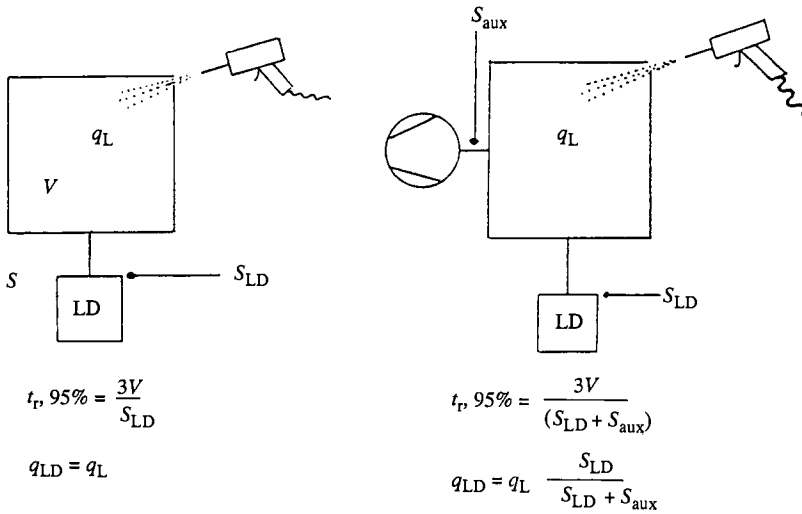
**Figure 5.7** Leak detection by the vacuum method using a search gas.

(a) Leak localization.

(b) Integral (overall) leak test. 1, test piece evacuated by pump 4; 2, leak test instruments (choice of types); 3, test gas reservoir; 4, vacuum pump; 5, hood filled with test gas

envelope filled with search gas (Figure 5.7(b)), an integral (overall) estimate of the leak-tightness can be made.

It is possible to use halogen leak detectors (see Section 5.2) for vacuum leak testing although use of a He-specific mass-spectrometer leak detector (see Section 5.3) is more common. To perform leak detection by the vacuum method (Figure 5.8) efficiently and effectively the characteristics of the leak detector and the influence of its location on the system being tested must be taken into consideration, and these factors will now be discussed.



**Figure 5.8** Vacuum method of leak localization.  
 (a) Without additional pumping.  
 (b) With additional pumping.  
 The relationship between  $S$  and  $S_{LD}$  depends on the conductance of the pipework between the system and the leak detector inlet

The partial pressure ( $p_{Tr}$ ) of the search gas accumulating within the test object is determined by the size of the leak ( $q_L$ ) in the system under test and the volume rate of flow of the vacuum pump at the point of connection to system:

$$p_{Tr} = \frac{q_L}{S}$$

The sensitivity ( $C$ ) of such an arrangement is defined as:

$$p_{Tr} = q_L C$$

where

$$C = \frac{1}{S}$$

Thus the sensitivity increases with decreasing volume flow rate of the pump.

The response time of this arrangement (i.e. the time elapsed between the search gas entering the leak and a certain fraction of the final reading being indicated on the detector) depends on the ratio between the volume of the object and  $S$ .

The time constant is given by:

$$\tau = \frac{V}{S} = VC$$

The response time ( $t_r$ ) of such an arrangement is  $VC$  and  $3VC$ , for 63% and 95% of the final signal, respectively. This implies that a high sensitivity is always related to long response time, especially for large objects.

The response time can, of course, be improved but only at the expense of a loss in sensitivity. For example, if an auxiliary pump is present (Figure 5.7(b)), the response time decreases as indicated although the indicated leak rate is less than the true leak-rate by a factor  $(S_{LD}/(S_{LD} + S_{aux}))$ .

Vacuum systems, particularly large plants, always have their own pump sets (Figure 5.9). Among the problems that can be encountered are:

1. The sensitivity of a particular leak detector-plant arrangement may be too low.
2. The response time may be excessive.
3. The pressure in the plant may be too high for the direct connection of a leak detector.

It is necessary to be aware of the characteristics of a leak detector (minimum detectable leak rate, maximum inlet pressure, etc.) before a connection point is chosen. For example, in arrangement 1 of Figure 5.9 the volume flow rate of the high vacuum pump may be so large that the amount of test gas from the

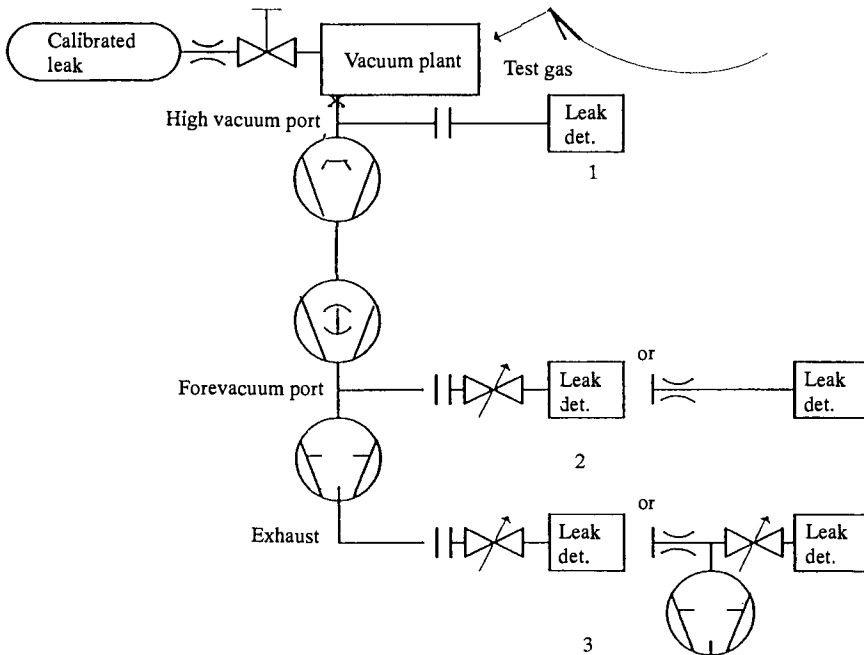
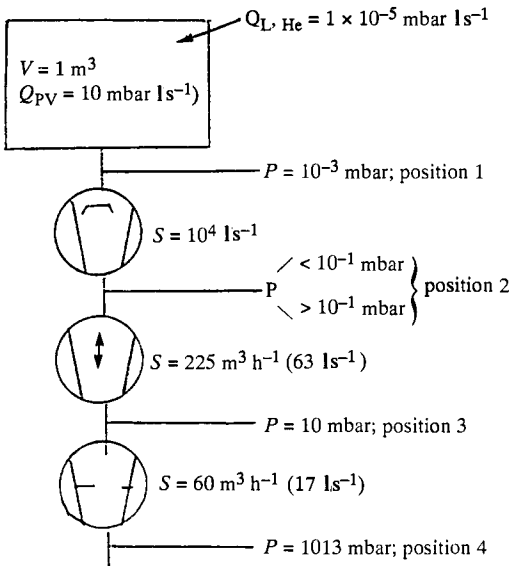


Figure 5.9 Leak detection by the vacuum method on a large plant

leak entering the detector may either be extremely low or below the detectable limit. In this situation, the partial flow ratio must be adjusted so that more search gas enters the detector. This can be achieved either by throttling the volume flow rate of the plant or by connecting the detector at a point where the flow rate is lower (positions 2 or 3 in Figure 5.9). As regards response time, this should always be checked by using a calibrated leak mounted at a point as far away as possible from the detector. Improvements in response time can be achieved by various methods including reducing the distance between the detector and the suspected leak and reducing the time constant by positioning the detector at a point where  $V/S$  is suitable (the adverse effect on sensitivity must be borne in mind). In the situation where the pressure at an appropriate point is too high for direct connection to a leak detector, a fixed (capillary, orifice) or variable throttle must be inserted so that the maximum inlet pressure for the detector is not exceeded.

**Example 4**



A high-vacuum system has a leak equivalent to  $1 \times 10^{-5} \text{ mbar l s}^{-1}$  ( $Q_{L,He}$ ). Various ports exist where a helium leak detector may be connected (Positions 1–4). Based on the data given in the diagram and those given for the leak detector ( $q_{L,min} = 1 \times 10^{-9} \text{ mbar l s}^{-1}$ ;  $q_{max} = 3 \times 10^{-2} \text{ mbar l s}^{-1}$ ;  $P_{max, inlet} = 10^{-1} \text{ mbar}$ ;  $S_{LD,He} = S_{LD,air} = 0.3 \text{ l s}^{-1}$ ), calculate approximately the indicated leak rate

and response time (95% signal) for the detector connected to positions 1–3.

$$q_{\text{indicated}^*} = 1 \times 10^{-5} \times \frac{0.3}{(10^4 + 0.3)} \text{ mbar l s}^{-1} = 3 \times 10^{-10} \text{ mbar l s}^{-1*}$$

\* This is less than minimum detectable leak rate

$$t_{95\%} = \frac{3V}{S} = \frac{3 \times 1000 \text{ (l)}}{(10^4 + 0.3) \text{ l s}^{-1}} = 0.3 \text{ s}$$

### Position 2

Two situations may arise:

1. pressure at the connection port is below  $10^{-1}$  mbar
2. pressure at the connection port exceeds  $10^{-1}$  mbar

$$(1) q_{\text{indicated}} = 1 \times 10^{-5} \times \frac{0.3}{63 + 0.3} \text{ mbar l s}^{-1} = 4.7 \times 10^{-8} \text{ mbar l s}^{-1}$$

If the volume of the diffusion pump is 30 l and that of the intermediate line is 10 l

$$t_{95\%} = 0.3 + \frac{3 \times 40}{(63 + 0.3)} = 0.3 + 1.9 \text{ s} = 2.2 \text{ s}$$

- (2) A throttle must be inserted between the system and the detector such that the maximum admissible flow ( $3 \times 10^{-2}$  mbar l s<sup>-1</sup>) is passed to the detector. Under these circumstances, the volume rate of flow *before* the throttle is not known precisely. The partial flow ratio ( $\gamma$ ) is, however:

$$\gamma = \frac{3 \times 10^{-2} \text{ (mbar l s}^{-1}\text{)}}{10 \text{ (mbar l s}^{-1}\text{)}}$$

$$q_{\text{indicated}} = 1 \times 10^{-5} \times 3 \times 10^{-3} \text{ mbar l s}^{-1} \\ = 3 \times 10^{-8} \text{ mbar l s}^{-1}$$

If the leak detector is connected to the throttle valve by a 1 m NW16 connection ( $V = 0.2$  l).

$$t_{95\%} = 0.3 + 1.9 + \frac{3 \times 0.2}{0.3} = 4.2 \text{ s}$$

**Position 3**

A throttle must be inserted between the system and the detector. The partial flow ratio is as before

$$q_{\text{indicated}} = 1 \times 10^{-5} \times \frac{3 \times 10^{-2}}{10} \text{ mbar l s}^{-1} = 3 \times 10^{-8} \text{ mbar l s}^{-1}$$

If the volume of the line between the pumps is 5 l and the leak detector is connected to the throttle valve by a 1 m NW16 connection

$$t_{95\%} = 0.3 + 1.9 + 3 \times \frac{5}{17} + 3 \times \frac{0.2}{0.3} = 5.1 \text{ s}$$

**5.1.3 Leak detectors**

The use of indirect pressure gauges and mass spectrometers has been mentioned earlier. Instruments responding selectively to appropriate search gas (for example halogen and helium leak detectors) have also been introduced briefly but will be discussed in greater detail in the following sections. High-frequency vacuum testers (Tesla coil detectors) have also been extensively used for checking glass apparatus in the pressure range  $100\text{--}10^{-3}$  mbar. The Tesla coil detector consists of a hand-held unit with a probing electrode and a power supply for the coil. As the electrode approaches an evacuated glass system, a high-frequency discharge is established in the system. If a leak exists in the glass envelope, a bright capillary discharge occurs between the electrode and the hole. Care should be taken, however, with thin-walled equipment since extensive sparking can itself produce a leak.

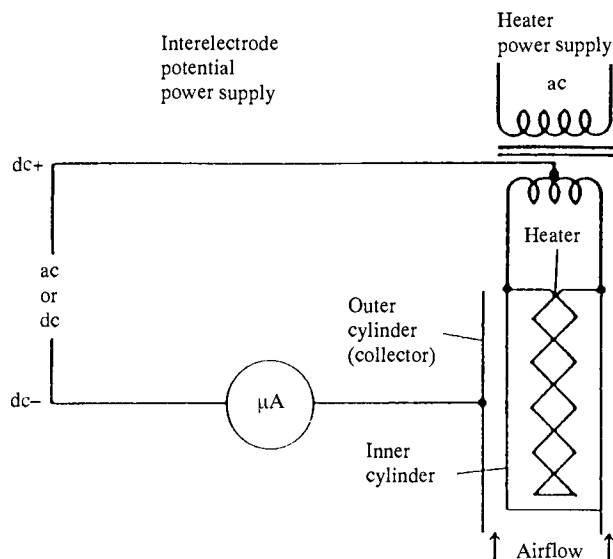
**5.2 Halogen leak detector****5.2.1 Heated anode detector**

Halogen leak detectors detect gaseous halogen compounds. The sensor (Figure 5.10) consists of a cylindrical electrode, impregnated with a mixture of potassium hydroxide and iron (III) hydroxide. This is maintained at  $800\text{--}900^\circ\text{C}$  either by an internal heater or by an external spiral platinum heater. This gives rise to a basic ion emission ( $I_B$ , few  $\mu\text{A}$ ). Ions are collected on a concentric outer cylinder.

In the presence of halogens, positive-ion emission may increase markedly and the change in ion current is proportional to the partial pressure of the halogen-containing gas ( $p_{\text{Hal}}$ ). Thus, if the collector current is  $I_C$ , then:

$$I_C = I_B (1 + \epsilon p_{\text{Hal}})$$





**Figure 5.10** Basic circuit of heated anode halogen leak detector, showing two-element heated anode sensing structure (see McMaster, 1982)

where  $\epsilon$ , the sensitivity, may have values in the range  $100\text{--}10^4 \text{ mbar}^{-1}$ . If a mean sensitivity of  $10^3 \text{ mbar}^{-1}$  is assumed, then in the presence of  $p_{\text{Hal}} = 10^{-3} \text{ mbar}$ , the basic ion emission will double.

Halogen leak detectors are usually not very sensitive to halogens themselves ( $\text{F}_2$ ,  $\text{Cl}_2$ ,  $\text{Br}_2$ ) and their response to halogenocarbons is also dependent on the gas. This is shown in Table 5.3.

Halogen leak detectors, or rather 'leak detection tubes' can be connected directly to the vacuum system to be tested. To obtain a good response, it is

**Table 5.3** Relative sensitivity of a commercial halogen leak detector (Inficon HLD 3000) to various halogenocarbons

Designation	Formula	Response relative to R12
R12	$\text{CCl}_2\text{F}_2$	1.0
R11	$\text{CCl}_3\text{F}$	3.8
R13 B1	$\text{CBrF}_3$	0.47
R14	$\text{CF}_4$	very low
R23	$\text{CHF}_3$	very low
R114	$\text{ClF}_2\text{CCF}_2\text{Cl}$	0.94
R503	$\text{CHF}_3 + \text{CClF}_3$	0.22

usual to make the connection in the backing line of the pump set where there will be a high concentration of search gas. In this position, precautions must be taken to prevent back-streaming pump oil entering the detector, thereby destroying its sensitivity. It is usual to connect the halogen leak detector vertically via a pipe with a bend.

They can also be used for 'sniffing'. For this application, a sniffer tube and a pump are attached to the sensor (Figure 5.11). Gases to be tested are aspirated through the detector. Halogen sniffer detectors can detect halogen concentration as little as 0.1 ppm under some circumstances.

Heated anode halogen leak detectors are easy to use, portable and relatively cheap. Their disadvantages are, however:

1. The emitter is hot. They are obviously potentially dangerous near flammable materials.
2. With prolonged exposure to search gas, the leak indication tends to disappear. This phenomenon arises due to the depletion of available ions at the emitter surface. Significant time is required for  $K^+$  to diffuse from the bulk and restore the sensor.
3. The sensing element deteriorates with time or with excessive exposure to search gases. Under normal operating conditions, an average lifetime of 800–1000 h may be expected. In order to achieve a quick, sensitive response from the sensor the continual admittance of a small amount of oxygen is desirable. This can be achieved by introducing a small leak (about  $10^{-4}$  mbar  $l s^{-1}$ ; a trapped hair, for example) across the sealing ring.

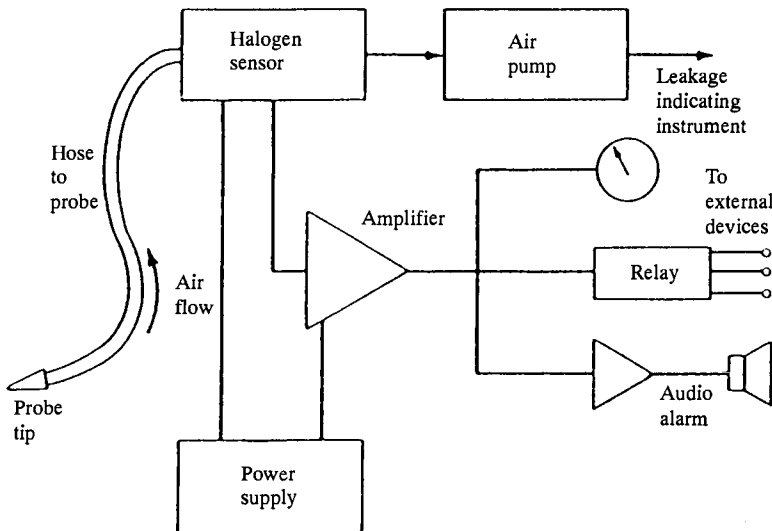


Figure 5.11 Schematic diagram of a halogen leak detector

4. Sensors will respond to any halogen-containing gas (cleaning fluids, aerosol propellants, etc.). Because it contains  $K^+$ , cigarette smoke can also induce a response on a halogen leak detector.

Finally, the use of halogen-containing search gases has drawbacks in leak detection. Among these can be listed:

1. *Low diffusion rate* – in order to produce a repeatable signal, the gas within a system under examination must have a uniform composition. Halogenocarbons have a relatively low rate of diffusion.
2. *Significant adsorption* – Experience has shown that they ‘cling’ to surfaces for several minutes and may be responsible for a sluggish recovery of halogen leak detector.
3. *Relatively high density* – Halogenocarbons may accumulate within a system. This can give rise to ‘ghost’ leak indications up to 24 h after the original leak has been repaired. Forced ventilation after leak checking will prevent this.

### 5.3 Helium-specific mass spectrometer leak detector

Helium is an ideal search gas. It is inert, adsorbed to a very small extent and is present in very small quantities (5 ppm) in air. It is also unlikely to be used as a process gas. Magnetic sector field mass spectrometers tuned to detect low molecular masses ( $m/e = 2,3,4$  usually) are excellent helium detectors. The leak rate is obtained from measurements of the helium partial pressure ( $p_{\text{He,MS}}$ ) in the mass spectrometer entering at a defined volume rate of flow ( $S_{\text{He,MS}}$ ). The helium leak rate is then:

$$q_{\text{L,He}} = p_{\text{He,MS}} \cdot S_{\text{He,MS}}$$

The lowest detectable helium leak can be calculated from the expression:

$$q_{\text{L,He,min}} = p_0 S_{\text{He}} + C_{\text{He,min}} \cdot P_{\text{T}} \cdot S_{\text{He}}$$

where  $C_{\text{He,min}}$  and  $p_0$  are the lowest detectable He concentration and partial pressure, respectively and  $P_{\text{T}}$  is the total pressure in the detector.  $C_{\text{He,min}}$  and  $p_0$  depend on the specifications of the mass spectrometer.

If  $C_{\text{He,min}} \cdot P_{\text{T}} \ll p_0$ , then  $q_{\text{L,He,min}} = p_0 S_{\text{He}}$ .

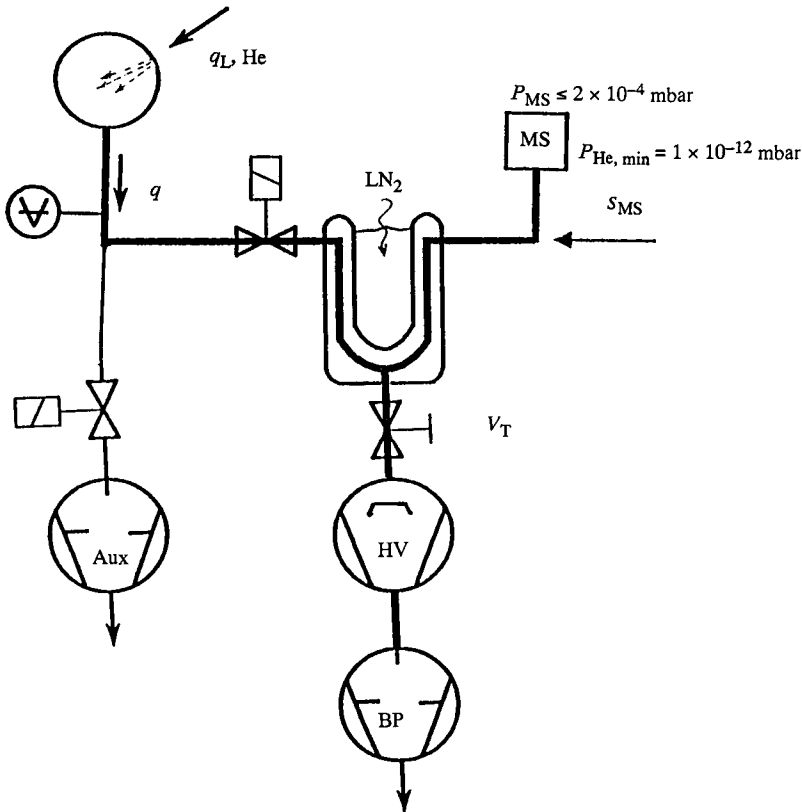
With  $p_{0,\text{He}} = 10^{-12}$  mbar and  $S_{\text{He}} = 21 \text{ l s}^{-1}$  it is possible to detect leak rates of  $2 \times 10^{-12}$  mbar l  $\text{s}^{-1}$ .

A helium-specific leak detector consists of a mass spectrometer and a pumping system. Magnetic sector field mass spectrometers are normally used in helium leak detectors. Only in one particular model, as far as the author is aware, is a quadrupole mass spectrometer used. The mass spectrometer itself consists of an ion source, deflection system and an ion collector. As the maximum permissible total pressure in the mass spectrometer is approximately  $2 \times 10^{-4}$  mbar (Reich, 1987), a high vacuum pumping system is required and its main function is to achieve this limit after a short time and

maintain at least this pressure thereafter. Only a limited volume rate of flow is usually available to evacuate the object under test.

Two configurations may be used for He leak detectors. These have been designated: main flow leak detector and counter-flow leak detector. Schematic diagrams for the two types are shown in Figures 5.12 and 5.13.

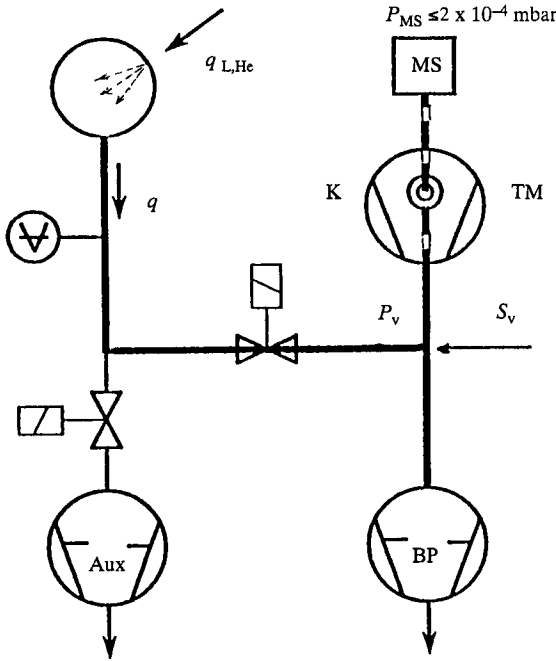
In the main-flow leak detector (Figure 5.12) the mass spectrometer is evacuated by an appropriate high vacuum pump via a liquid-nitrogen-cooled (LN<sub>2</sub>) trap. Gas from the system being checked for leaks enters the detector at a point between the mass spectrometer and the pump inlet and initial concern about contaminants from the system entering the former led to the fitting of LN<sub>2</sub> traps. This was a sensible precaution but the trap also serves a



**Figure 5.12** Schematic diagram of a main flow leak detector (after Reich, 1987). Indicated leak rate:

$$q_{ind} \sim P_{He, MS} = \frac{q_{He}}{S_{MS, He}}$$

HV, high-vacuum pump; BP, backing pump; Aux, auxiliary roughing pump; LN, liquid-nitrogen-cooled trap ( $S_{vap} = 11 \text{ l s}^{-1} \text{ cm}^{-2}$ ; typical dimensions,  $l = 30 \text{ cm}$ ;  $d = 10 \text{ cm}$ );  $V_T$  = throttle valve

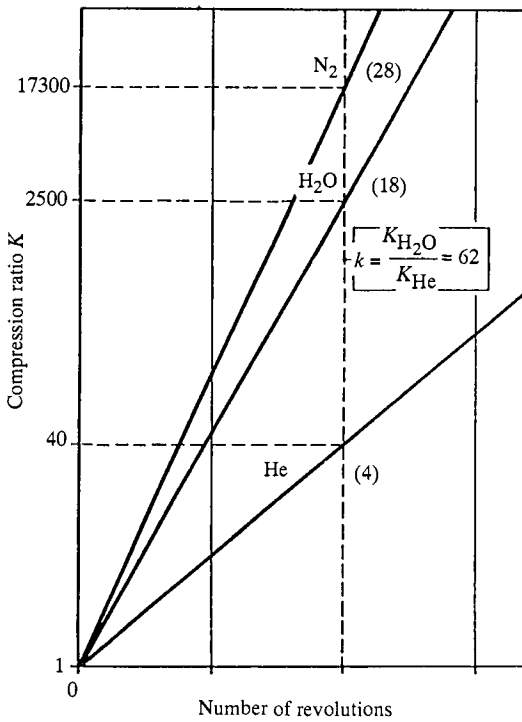


**Figure 5.13** Schematic diagram of counterflow leak detector (after Reich, 1987).  
 Indicated leak rate,  $q_{ind} \sim P_{He, MS} = q_{He} / K_{He} S_{v, He}$ .  
 TM, turbomolecular pump of compression ratio  $K$  (TM may also be replaced by a diffusion pump); BP, backing pump; Aux, auxiliary pump;  $S_v$  and  $P_v$  indicate the pumping speed and the pressure in the backing line

very useful function in ‘freezing out’ water vapour, which is often the most significant residual gas. As an indication of the effectiveness, it can be shown that a trap of the dimensions given in Figure 5.12 has a very large (several  $10^3 \text{ l s}^{-1}$ ) effective speed for water vapour. Not only does the trap increase considerably the He concentration but it reduces significantly the pump-down time until the system is ready for leak detection.

The fact that molecular pumps (turbomolecular and diffusion pumps) have a compression ratio which is dependent on the molecular weight of the gas being pumped, is exploited in the counter-flow leak detector (Figure 5.13). The dependence of  $K$  on molecular mass as a function of rotational speed is shown in Figure 5.14.

Figure 5.14 shows that whilst  $K_{He} = 40$ , the corresponding values for water and  $N_2$  are 2500 and 17 300, respectively.  $K$  for higher molecular masses is even greater (see Section 3.1.2). Obviously, the mass spectrometer must be placed close to the high vacuum port to maintain the mass spectrometer in an appropriate state for leak detection but considerable enrichment of light gases



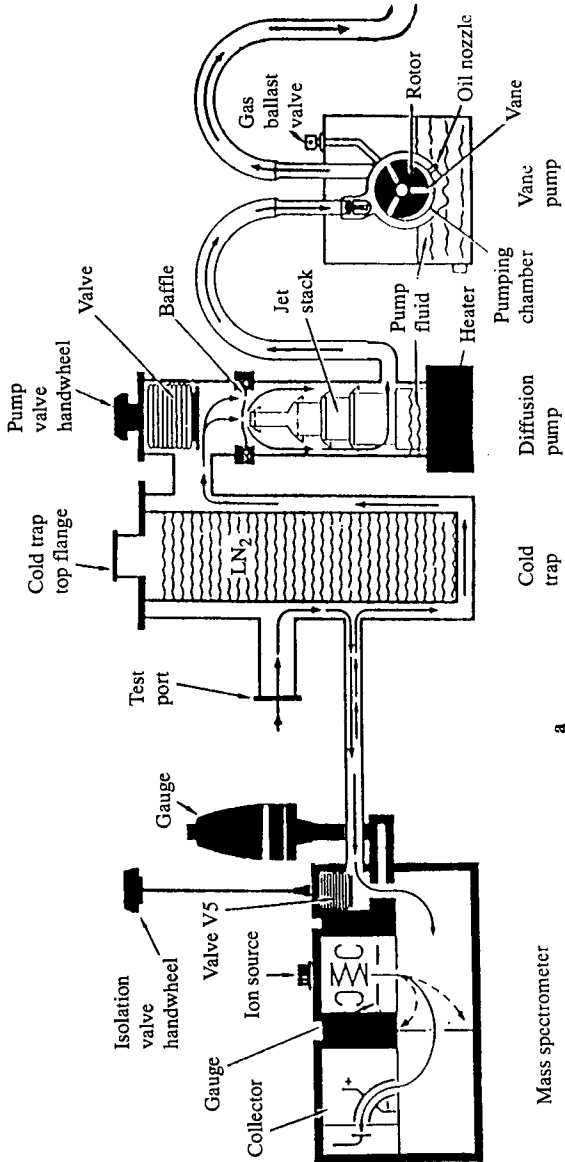
**Figure 5.14** Variation of the compression ratio of a turbomolecular pump with rotational speed for different gases (after Reich, 1987)

(such as He) on the high-vacuum side occurs if gases from the system under investigation are admitted on the fore-vacuum side of the turbomolecular pump.

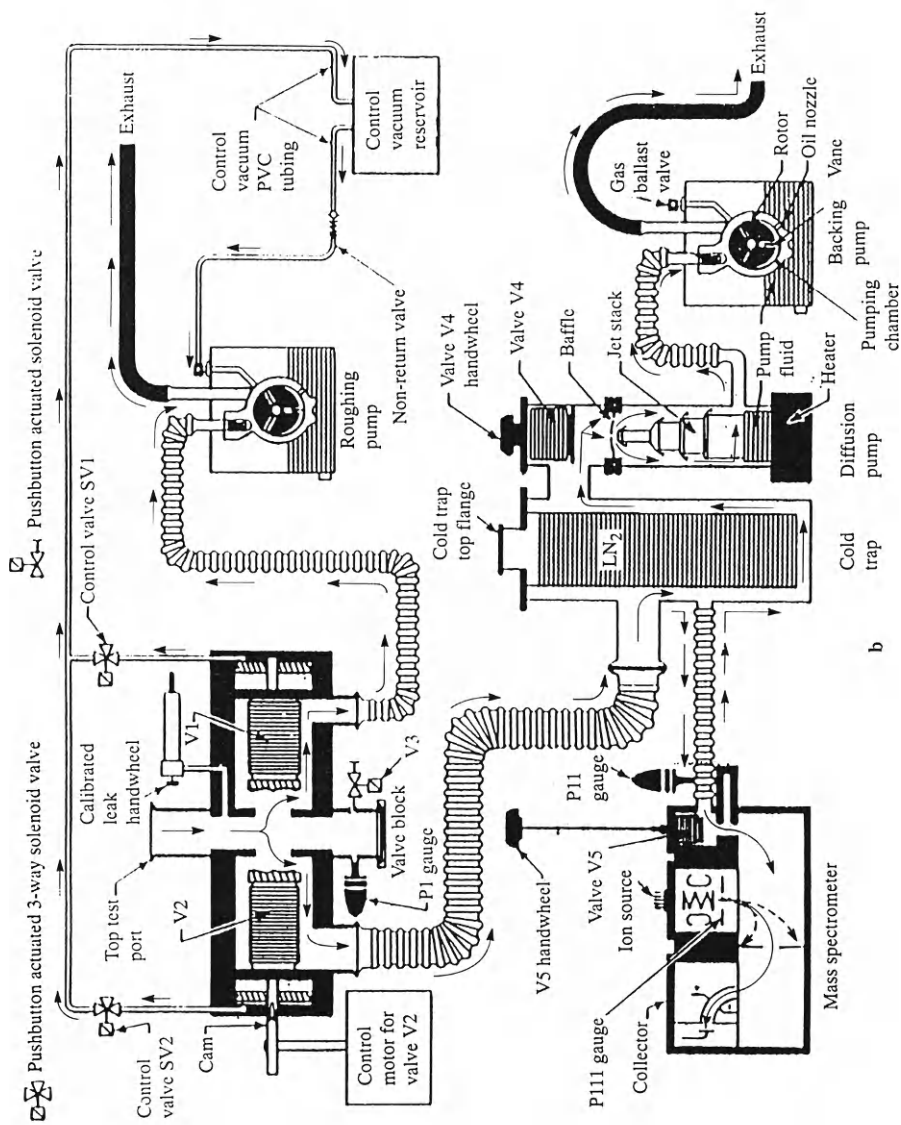
### 5.3.1 Lay-out

A conventional, commercial, main-flow leak detector is shown in Figure 5.15.

The pumping system for the mass spectrometer consists of a  $150 \text{ l s}^{-1}$  oil-diffusion pump backed with a two-stage rotary vane pump ( $4 \text{ m}^3 \text{ h}^{-1}$ ). An auxiliary single-stage pump ( $16\text{--}60 \text{ m}^3 \text{ h}^{-1}$ , depending on the application) is provided in order to evacuate the object prior to a leak test by the vacuum method. Gauges (marked  $P_{II}$  and  $P_{III}$  in Figure 5.15(b)) monitor the pressure in the mass spectrometer.  $P_{II}$  is indicated, from  $10^{+3}$  to  $10^{-3}$  mbar, by a Pirani gauge while  $P_{III}$ , assessed from measurements of the total ion current in the mass spectrometer ion source, can be within the range  $10^{-3}$  to  $10^{-6}$  mbar. If the mass spectrometer is allowed to operate at a pressure over  $2 \times 10^{-4}$  mbar, the leak reading will be inaccurate and the ion source will rapidly deteriorate.



**Figure 5.15** Simplified diagram of a commercial, conventional, main-flow leak detector (Leybold Ultratest F). (a) Mass spectrometer and pumping system. (b) Complete vacuum system. NOTE: This figure shows valve V1 open and valve V2 partially open; the ready lamp would be flashing ON and OFF in this mode of operation



b

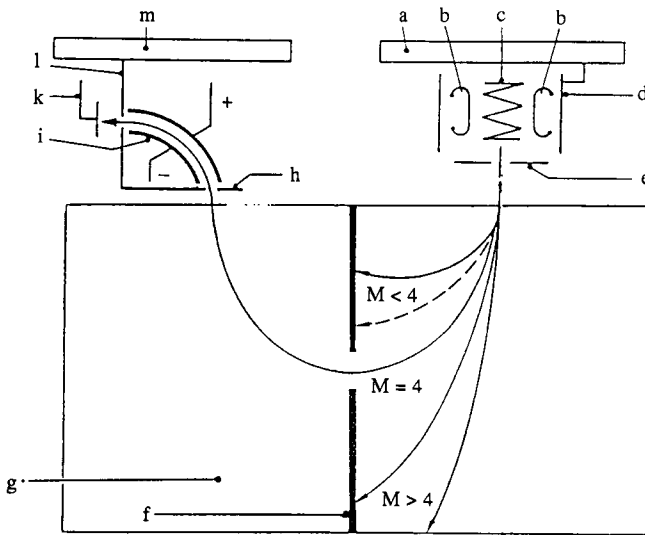


For leak detection applications, magnetic sector field mass spectrometers (Figure 5.16; in this, sector angle = 180°) are preferred. In such systems, ions are formed, accelerated and extracted. Under the influence of a homogeneous magnetic field, perpendicular to the path of the ions, they are deflected in circular orbits of radius  $r$ (m) given by:

$$r = \frac{1}{B} \sqrt{2 \frac{m}{ze} \cdot V_{acc}}$$

- where  $m$  = mass of ion [kg]
- $V_{acc}$  = ion-accelerating voltage [volts  $\equiv$   $m^2 \text{ kg s}^{-3} \text{ A}^{-1}$ ]
- $e$  = electronic charge [ $1.6021 \times 10^{-19}$  As]
- $z$  = number of charges carried by the ion
- $B$  = magnetic flux density [Tesla =  $\text{kg s}^{-2} \text{ A}^{-1}$ ]

By selecting values for  $B$  and  $V_{acc}$ , the path followed by ions of given  $m/e$  values can be predicted. Insertion of a slit at an appropriate point in the ion trajectory will enable ions to pass to the ion collector. The mass spectrometer shown in Figure 5.16 is of the double-focusing type. After magnetic mass



**Figure 5.16** *A double-focussing mass spectrometer for the detection of masses 3 and 4 at high sensitivity. a, ion-source flange; b, cathodes (thoriated iridium); c, anode (heated); d, ground shield; e, extractor plate and ion collector for pressure measurement (PIII); f, intermediate slit; g, 180° magnetic deflection field; h, inlet slit to 90° electrostatic field; i, electrostatic deflection plates; k, ion collector; l, ground slit; m, ion collector flange*

separation has taken place, further filtering (electrostatic) takes place to remove 'stray' ions, which may have entered the field, reaching the ion collector. Because of this second stage of focusing, the minimum detectable partial pressure is lowered and the background considerably reduced. With this spectrometer, the lowest detectable partial pressure of helium ( $p_{\text{He,min}}$ ) is  $2 \times 10^{-12}$  mbar. Depending on the pumping speed  $S_{\text{MS,He}}$ , typically within the range  $5 - 20 \text{ l s}^{-1}$ , minimum leak rates from  $1$  to  $5 \times 10^{-11}$  mbar  $\text{l s}^{-1}$  can be detected. By throttling the pump, an improvement in sensitivity of 10 can be obtained.

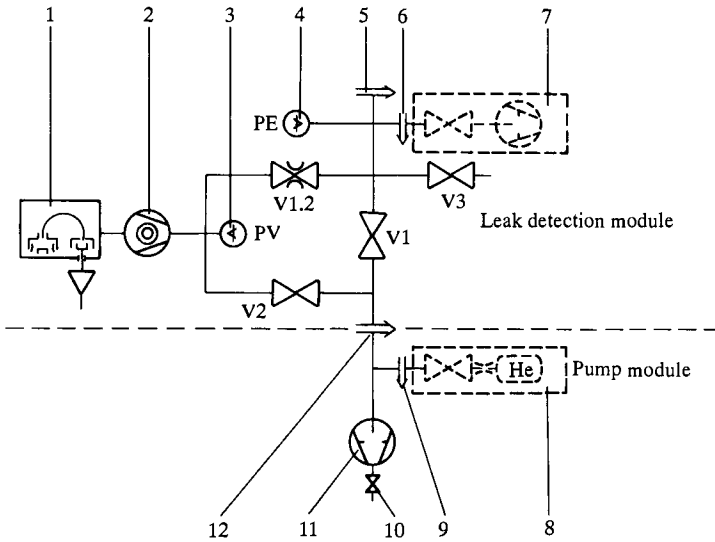
In the magnetic sector field mass spectrometers, permanent magnets can be made of material such as ferrite or  $\text{CoSm}_5$ . The magnetic flux density of the latter material is significantly less sensitive to temperature fluctuations. Ions are formed by electron-impact ionization. Thoria-coated iridium and tungsten have both been used for the cathodes. In the presence of halogen-containing compounds, however the thorium coating is rapidly removed.

With regard to the detector, a Faraday cup or plate used in conjunction with a sensitive amplifier represents the simplest, cheapest and most reliable means of ion detection. When a Faraday cup collector is used in this way, optimum performance is obtained only when the connection with the amplifier is very short. To reduce spurious signal pick-up to a minimum, the electrostatic shielding must be near perfect and vibration must be eliminated. With good-quality components and due attention to interference prevention, ion currents from about  $10^{-9}$  down to  $10^{-15}$  A can be detected.

A commercially available counter-flow He leak detector is shown in Figure 5.17. Ions are produced in an extractor-type source with Ir/ThO<sub>2</sub> cathodes. The mass separation system involves magnetic deflection in an inhomogeneous field and it allows selection of masses 2, 3 and 4. In this leak detector, the mass spectrometer is connected directly to the inlet of the turbomolecular pump via a gasket that minimizes both helium adsorption and permeation.

The use of a turbomolecular pump has many advantages, including the fact that once the correct rotational speed has been attained, the pumping speed is predictable and extremely stable. This has obvious advantages for the quantification of leaks close to the limit of detection. With diffusion pumps, unless precautions have been taken, instabilities in the boiler can give rise to uncertainties in the indicated leak rate under the same conditions.

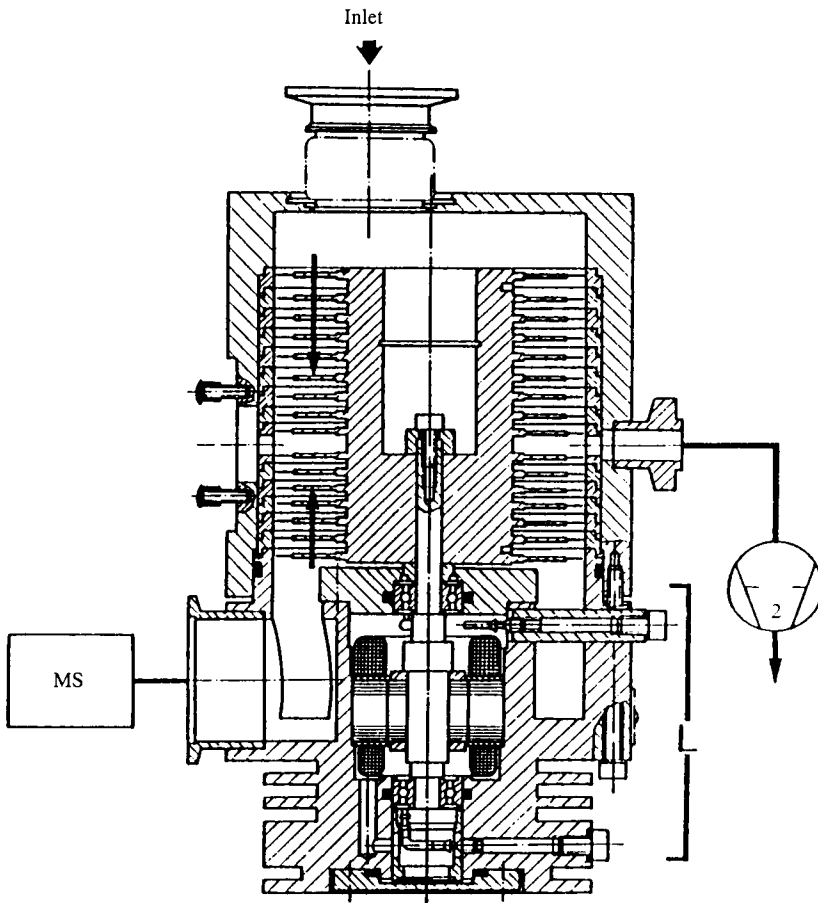
With modern leak detectors such as that shown in Figure 5.17, the complete leak-testing cycle, including signal processing and conversion is controlled by microprocessor. All operational steps from evacuation of the test port to leak testing to switching off are fully automated and the sequence of valve actuation is controlled in such a way that misoperation is impossible. The microprocessor monitors both the inlet and the fore-vacuum pressure and the rotational speed of the TMP. Should the appropriate conditions for leak detection *not* be established then the microprocessor takes suitable action and indicates this in the form of fault codes. For example, if the inlet pressure exceeds a safe level, the ion source is switched off and an error message displayed. Actions are also taken in the event of failure of the pressure sensors, cathodes or turbomolecular pump.



**Figure 5.17** Schematic diagram of a commercial counterflow leak detector  
 1, magnetic sector field mass spectrometer; 2, turbomolecular pump ( $S^* = 50 \text{ l s}^{-1}$ ); 3, Pirani gauge (fore-vacuum line); 4, Pirani gauge (leak detector inlet); 5, test port; 6, second test port; 7, roughing pump for gross leak testing; 8, optional calibrated leak, 9, port for attachment of 8; 10, outlet shut-off valve; 11, two-stage oil-sealed rotary vane pump ( $S^* \sim 2 \text{ m}^3 \text{ h}^{-1}$ ); 12, connection/disconnection port; V1, V2, etc., valves

An extremely useful development of the counterflow leak detector has been the increase in the volume rate of flow at the inlet that has been achieved by the use of a twin inlet turbomolecular pump (Figure 5.18). The advantage of this system is that, after a relatively short pre-evacuation, using an oil-sealed pump of fairly high volume rate of flow, the object under test is evacuated cleanly by the 'split' turbomolecular pump.

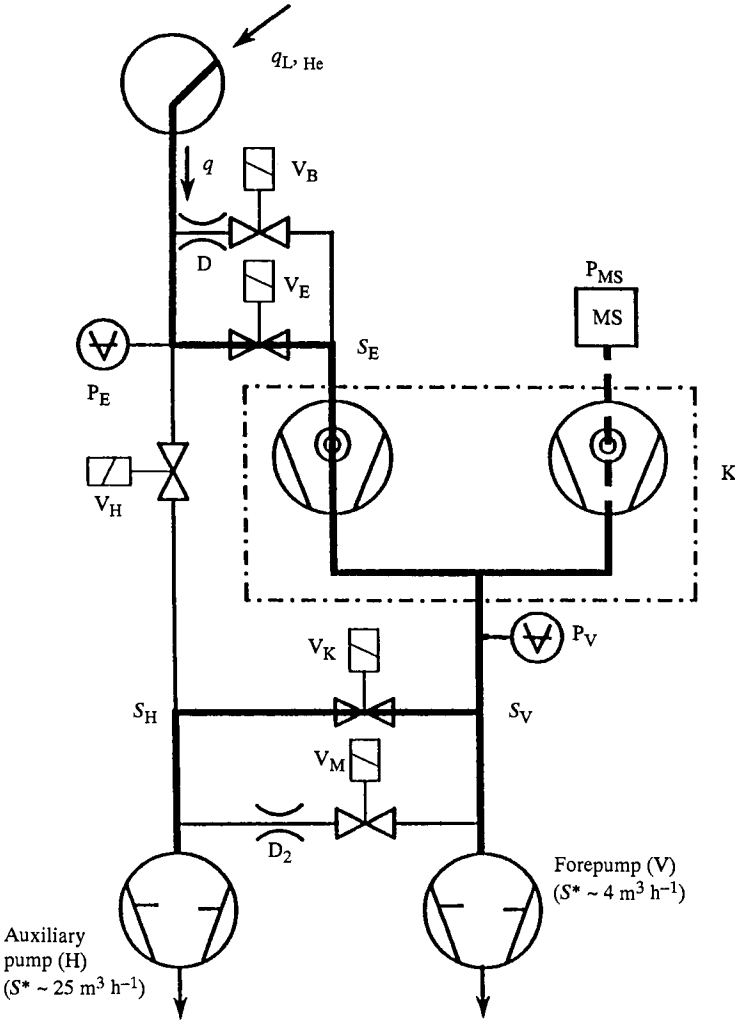
Further, the combination of this type of pump with an auxiliary pump ensures rapid, sensitive leak detection. For example, a schematic diagram of a commercial leak detector having a split turbomolecular pump (Leybold UL500) is shown in Figure 5.19. After having obtained an inlet pressure ( $P_E$ ) that is approximately equal to  $P_{V,\text{max}}$ , valve  $V_H$  is closed and valves  $V_E$  and  $V_K$  are opened. This connects the object to the turbomolecular pump. The pumping time prior to leak testing is significantly reduced but this is offset by a reduction in sensitivity by the same factor. However, leak checking for larger leaks can proceed at this point. During this period,  $P_v$  will continue to fall until, when it reaches  $P_{V,\text{max}}/10$ ,  $V_K$  is closed and the sensitivity increases appropriately.



**Figure 5.18** Modified turbomolecular pump having twin inlets and a common fore-vacuum connection (from Reich, 1987)

### 5.2.2 Operation

The operation of a non-automated, conventional, liquid-nitrogen-cooled leak detector can appear to be complex. Before leak detection proceeds, the detector must be suitably set up and adjusted. This involves allowing the diffusion pump to warm up, filling the liquid-nitrogen-cooled trap and adjusting the mass spectrometer (when a pressure less than  $10^{-4}$  mbar has been obtained). The best way to carry out adjustment is by using a known standard such as a calibrated He leak (see Section 5.4). Thus with the calibrated leak open and the mass spectrometer switched to detect 'mass 4', the emission current in the ion source and the accelerating and deflection



**Figure 5.19** Schematic diagram of a commercial counterflow leak detector fitted with a split turbomolecular pump (Leybold UL 500)

voltage of the ions are adjusted according to the manufacturer’s procedure. The emission is set until the correct leak-rate reading is obtained. When the calibrated leak is shut off, the reading should fall to zero. With such leak detectors, it is important to prevent contamination of the mass spectrometer during shut-down. This involves switching off the emission and, by closing the appropriate valve, isolating the spectrometer from the rest of the system. In the case of long-term shut-down (over 1 week), the liquid-nitrogen-cooled trap must be emptied and any trapped gas pumped away before closing the high vacuum valve and switching off the system.

The operation of microprocessor-controlled leak detectors is extremely simple, usually involving only switching on the system. Thereafter, the microprocessor performs self-checks, switches on the turbomolecular pump and monitors pressures and holds the mass spectrometer in stand-by until further instructions are given. Even with an automated leak detector, however, unless a standard leak has been built into the system, calibration must be carried out before leak quantification can be performed with confidence.

## 5.4 Calibrated leaks

As with an ionization gauge, a helium leak detector does not perform absolute measurements and it has to be calibrated against a known standard. Calibrated or standard leaks are available which are essential for checking the leak-rate indication of the detector and are invaluable to check the performance (response time, detection sensitivity) of the detector-system configuration. A calibrated leak supplies a known gas flow at a particular temperature.

### 5.4.1 Capillary leaks

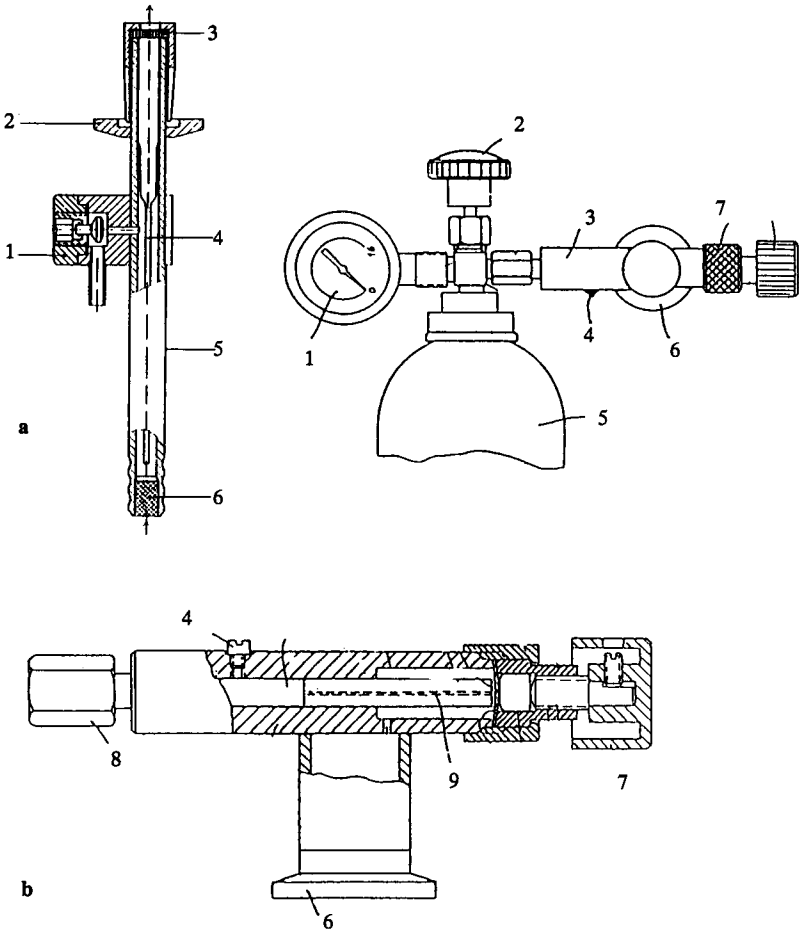
Capillary leaks are available with or without gas reservoirs. A calibrated leak without a gas reservoir is shown in Figure 5.20. It consists of a glass capillary contained within a housing. Both the gas inlet and exit are fitted with filters to protect the capillary. Leaks without a reservoir are available in the range  $10^{-4}$  to  $10^{-6}$  mbar  $l s^{-1}$ . Smaller leaks (down to  $10^{-8}$  mbar  $l s^{-1}$ ) require finer capillaries which are easily blocked. For certain leak detectors (for example, the Leybold UL100), however, a standard capillary leak of about  $10^{-7}$  mbar  $l s^{-1}$  is fitted for tuning and calibration. With such a leak, although the He loss is less than 2% per year, recalibration of the leak is necessary every 3 years. A standard leak with a high-purity He gas reservoir is shown in Figure 5.20(b). Depending on the pressure of gas at the entrance to the capillary, a leak within the range  $10^{-4}$  to  $10^{-6}$  mbar  $l s^{-1}$  can be obtained. For this purpose, the leak is fitted with a vent screw so that suitable pressures from that of the gas in the reservoir down to 1 bar can be set. The actual leak rate is obtained from a calibration curve of leak rate against He gas pressure.

Capillary leaks have an advantage that they are relatively insensitive to temperature changes. For example, their temperature coefficient is  $\leq 0.5\%$  per  $^{\circ}C$  change from the temperature of the original calibration of the test leak.

If test gases other than He are used with capillary leaks, suitable correction factors must be applied to the nominal value of the leak to obtain the actual value. The conversion factor used depends on the flow region involved. For example, to convert a He nominal flow rate in the laminar region to that for a test gas,  $x$ , the factor is given by:

$$\frac{q_x}{q_{He}} = \frac{\eta_{He}}{\eta_x}$$

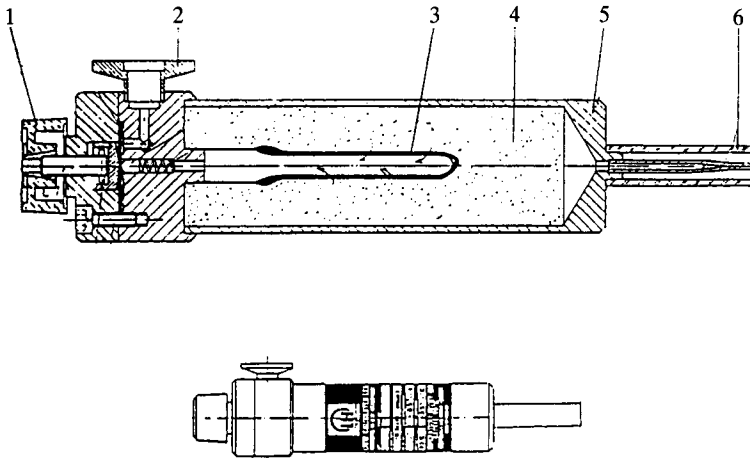
where  $\eta$  is the dynamic viscosity at the temperature of the test.



**Figure 5.20** Standard capillary leaks (a) Without gas reservoir. 1, flushing out valve; 2, small flange connection DN10; 3, outlet filter; 4, capillary leak; 5, stainless steel housing. 6, gas inlet filter. (b) With gas reservoir. 1, pressure gauge; 2, shut-off valve; 3, leak body; 4, vent screw; 5, He (5N) reservoir; 6, connecting flange; 7, diaphragm shut-off valve; 8, connecting flange to reservoir; 9, capillary

**5.4.2 Diffusion leaks**

To carry out quantification with leaks of about  $10^{-8}$  mbar l s<sup>-1</sup> or less, diffusion or permeation-type gas leaks must be used. A diffusion test leak (Figure 5.21) consists of a He reservoir (filled with either 3 bar (abs.) He or 300 mbar (abs.) for  $q_{L,He} \approx 10^{-8}$  or  $10^{-9}$  mbar l s<sup>-1</sup>, respectively). He from



**Figure 5.21** Diffusion test leak. 1, shut-off valve; 2, connection port (NW10 KF); 3, diffusion leak; 4, He reservoir; 5, stainless steel body; 6, filling port

the reservoir passes, via a diffusion barrier, to the connection flange. The leak is also fitted with a shut-off valve having a Teflon diaphragm to prevent He emission during zero checking. As helium passes continuously through the barrier, the leak is normally stored with the shut-off valve open. Closing the valve causes helium accumulation and an artificially high initial reading at the start of calibration.

Diffusion is an activated process and for this reason temperature changes have a more significant effect than with capillary leaks. Diffusion leaks are normally calibrated by the manufacturer at 23°C; their temperature coefficients are given by:

$$\frac{\Delta q_L}{q_L} \cdot \Delta T = 0.03\text{--}0.04 \text{ K}^{-1}$$

Changes in leak rate with time are miniscule and amount to:

$$\frac{\Delta q_L}{q_L} \cdot \Delta t = 0.005 \text{ year}^{-1}$$

## 5.5 Practical aspects of leak detection on vacuum plants

Some aspects of leak detection on plants fitted with several vacuum pumps have already been discussed (see Example 4, this chapter). Several problems can be encountered and these are listed below.

(a) Sensitivity of the arrangement is too low



With large system, any problems that may arise through an unsatisfactory time constant, can usually be overcome by locating the leak detector at an appropriate point in the pump train. This aspect is dealt with adequately in Section 5.1.2.2.2.

(b) The pressure is too high for the direct connection of the leak detector

This problem has again been reviewed in Section 5.1.2.2.2. Possible solutions involve the attachment of a throttle valve or a fixed throttle (capillary, orifice) to the plant or connection of the detector at a position where the volume range of flow of the system is greater.

### Example 5

A line in a chemical plant is to be leak tested. It has a diameter of 100 mm and is fitted with test ports (NW 40) at 10 m intervals. Within the line the working pressure is 10 mbar and the effective volume flow rate is  $120 \text{ m}^3 \text{ h}^{-1}$ ; the permissible leak rate is  $5 \times 10^{-2} \text{ mbar l s}^{-1}$ . Using a commercial leak detector ( $S_{\text{inlet}} = 10 \text{ l s}^{-1}$ ,  $q_{\text{max}} = 2 \times 10^{-3} \text{ mbar l s}^{-1}$ ) connected via a valve and a long line:

1. Should the valve be located near the line or near the detector?
2. What will be the indicated leak rate?
3. After what time can a signal be expected?

1. The diffusion time to 99% of the final indication is given by

$$t = L^2/2D$$

where  $L$  is the distance for diffusion and  $D$  is the diffusion coefficient, given by:

$$D = \bar{l} \bar{c}/3$$

where  $\bar{l}$  is the mean free path and  $\bar{c}$  is the mean speed. For helium in air at 1 mbar,  $D = 0.024 \text{ m}^2 \text{ s}^{-1}$ . The shortest response time will be obtained if the valve is placed near the line.

2. The volume throughput for the line is:

$$q_{\text{PV}} = P \times S$$

$$= 10(\text{mbar}) \times \frac{120}{3.6} (\text{mbar l s}^{-1})$$

$$= 333.3 \text{ mbar l s}^{-1}$$

The partial flow ratio to the leak detector is:

$$\begin{aligned} &= \frac{2 \times 10^{-3} \text{ mbar l s}^{-1}}{333.3 \text{ mbar l s}^{-1}} \\ &= 6 \times 10^{-6} \end{aligned}$$

For a permissible leak rate of  $5 \times 10^{-2} \text{ mbar l s}^{-1}$ , the displayed leak rate will be:

$$\begin{aligned} q_L &= (5 \times 10^{-2}) \times (6 \times 10^{-6}) \text{ mbar l s}^{-1} \\ &= 3 \times 10^{-7} \text{ mbar l s}^{-1} \end{aligned}$$

$$\begin{aligned} \text{3. Volume of the system} &= \pi \times (0.05)^2 \times 10 \text{ m}^3 \\ &= 0.0785 \text{ m}^3 \end{aligned}$$

$$\begin{aligned} t_{95\%} &= \frac{3V}{S} \\ &= \frac{3 \times 78.54(1)}{33.3 \text{ (l s}^{-1}\text{)}} \\ &= 7 \text{ s} \end{aligned}$$

(c) The response time is too large

Determination of the response time is particularly important for complex equipment having a large volume. By positioning them as far as possible from the leak, calibrated leaks, particularly those without reservoirs, can be used to establish this. Response time can be improved by either positioning the detector at a point where the ratio  $V/S$  (where  $V$  and  $S$  have their usual meanings) is most favourable or by reducing the distance between the detector and the suspected leak.

(d) Contamination of the leak detector

Depending on the nature of the system under investigation, the possibility exists that the leak detector will be contaminated with dust, gases and vapours from the system, etc. The risk can be reduced by introducing a trap (dust filter, cold trap) at the detector inlet or by using a counter-flow leak detector.

(e) Contamination of the plant by the leak detector

In some situations, it is obviously not desirable to connect a clean system to an oil-sealed pump for extended periods of time. By means of a leak detector

with a double-inlet turbomolecular pump, the situation can be significantly improved. Other possible devices include the incorporation of a cold or sorption trap between the detector and the system and the use of the mass spectrometer alone. A further possibility could be to connect the leak detector to the system via a turbomolecular pump. In this situation the leak detector backs the turbomolecular pump and the correct backing pressure must be assured.

## References

- McMaster, R.C. (ed.). (1982) In *Non-Destructive Testing Handbook*, 2nd edn, Vol. 1, *Leak Testing*, American Society for Non-Destructive Testing/ American Society for Metals
- Pidduck, P.J.H. (1986) Leak testing bi-propellant communication satellites. Presented at the Institute of Physics Symposium, *New Developments in Leak Detectors and Application to Large Systems*, January
- Reich, G. (1987) *Vacuum*, **37**, 691
- Sydow, L. (1989) In *Theory and Practice of Vacuum Technology* (eds M. Wutz, H. Adam and W. Walcher), F. Vieweg and Son, Braunschweig/ Wiesbaden, p. 465
- Wilson, N.G. and Beavis, L.C. (1976) *Handbook of Vacuum Leak Detection*, American Vacuum Society Monograph Series, American Vacuum Society

# 6

## *Vacuum system construction*

---

### **6.1 Materials and fabrication**

Vacuum systems must be constructed from correctly selected and fabricated materials. The subject has been reviewed fairly extensively (see, for example, Weston (1985), Halliday (1987a) and Adam (1989)). Essentially, materials for vacuum use should be mechanically strong over the pressure and temperature range required and be capable of being machined, welded, formed, etc. They should not prevent the pressure required by the process from being attained and should, therefore, be free of cracks and pores and have a low vapour pressure, even at the highest operating or baking temperature for the system. It is also essential that the materials chosen are suitable for joining to other materials in the system.

In this chapter, discussion will be restricted to those solids (pure metals, alloys, and non-metals such as polymers, elastomers and ceramics) that are used for the construction and operation of vacuum equipment. This includes materials used in the fabrication of the vacuum chamber, pipes, valves, etc. and material used for lead-throughs (electrical, mechanical, coolants and other fluids). It does not include, however, substances used, for example, in the assembly of vacuum gauges or material used in the construction of pumps such as sputter-ion pumps.

#### **6.1.1 Materials**

##### ***6.1.1.1 Pure metals and alloys***

The atoms of metals are arranged in a regular pattern giving rise to structures that are hexagonal close-packed, face-centred cubic, etc. It is rare for the crystal lattice to be maintained throughout the material and in their usual form metals consist of crystallites, the form and size of which determine their mechanical properties. Metals and alloys are used for a very large number of tasks in vacuum engineering. They invariably form the chamber itself and the attached valves and fittings but they are also used as internal components on account of their electrical, mechanical and thermal properties.

The properties of materials required in vacuum engineering are generally similar to those considered in other areas of engineering:

1. Adequate yield and ultimate tensile strength.
2. Adequate toughness and fatigue strength.
3. Other appropriate chemical and physical properties (corrosion resistance, magnetic characteristics, etc.).

Obviously, vacuum equipment must be able to withstand atmospheric pressure. For this reason, it should be suitably shaped and have walls of an

adequate thickness to withstand an external pressure of 1 bar. Vacuum vessels are generally cylindrical or spherical in shape with domed doors and ends; plane surfaces may be used for small blanking plates but large surfaces are liable to distort. Wall thicknesses are calculated bearing in mind the elastic modulus and the plastic behaviour of the metal, according to the procedure outlined by Anderson and Cohen (1989). Other constraints are also imposed. For example, the vapour pressure of the metal, within the range of temperatures covered, must be less than the desired ultimate pressure. The permeability of the material to gas and the emission of gas into the vacuum must also be considered. These factors must now be discussed.

#### 6.1.1.1.1 Vapour pressure

Data concerning the saturated vapour pressure of materials relevant to vacuum technology, as a function of temperature, have been compiled by Touloukian (1989) and show that the use of cadmium, magnesium and zinc should be avoided. Temperatures corresponding to a vapour pressure of  $1 \times 10^{-5}$  mbar are 143, 208 and 273°C, for Cd, Zn and Mg, respectively. These metals are also constituents of certain alloys and can evaporate into the system according to the prevailing temperature. For example, at 200°C, large amounts of Zn will be lost from brasses containing 5–45% of the metal.

Evaporation in a vacuum depends on the vapour pressure of the volatile species and the temperature. The area-related rate of mass evaporation is given (Adam, 1989), by the expression:

$$(j_m)_{\max} = 0.438 \sigma_K \sqrt{\frac{M_r}{T}} p_s (T)$$

where  $\sigma_K$  is the probability for condensation;

$$[j_m] = \text{kg m}^{-2} \text{s}^{-1}; [T] = \text{K}; [p_s] = \text{mbar}$$

#### 6.1.1.1.2 Degassing

During the manufacture of materials (melting, casting, etc.), a considerable amount of gas can be taken up by the material through absorption, occlusion and dissolution. Further, solids may take up gases such as  $\text{N}_2$ ,  $\text{O}_2$  and water vapour either by storage in or by exposure to ambient air (say, after venting a vacuum system).

Under vacuum conditions, adsorbed gas is released at a rate that depends on the energy of desorption,  $E_{\text{des}}$ , in a process known as 'desorption'. Under identical conditions, gas incorporated within the solid is also released, but with a considerably longer time constant. This is known as 'outgassing'. The complete process (desorption + outgassing) is known as degassing.

#### Desorption

Gas particles adsorbed on the surface require a certain energy,  $E (\geq E_{\text{des}})$ , before they leave. The area-related desorption rate is given by:

$$j_{\text{des}} = \nu_0 n \exp(-E_{\text{des}}/RT)$$

where  $n$  is the number of particles,  $\nu_0$  is the frequency at which they oscillate perpendicularly to the surface ( $\nu_0 \approx 10^{13} \text{ s}^{-1}$ ; oscillation period,  $\tau_0 = 10^{-13} \text{ s}$ ) and  $T$  is the temperature of the surface.

Of a group of particles present on the surface, some will remain there for a long time until they desorb while others will leave more quickly. This can be expressed as a mean residence or 'sojourn' time:

$$\tau = \tau_0 \exp(E_{\text{des}}/RT)$$

The influence of desorption energy and wall temperature on the evolution from the surface of adsorbed gases is shown in Table 6.1.

The tabulated values are calculated from the equation for mean residence time by the insertion of appropriate values for  $E_{\text{des}}$  and  $T$ . The previous equation for the area-related desorption rate shows that an increase in temperature and/or a decrease in pressure will enhance desorption. Physisorbed layers (relatively small  $E_{\text{des}}$ ) are 'readily' removed while chemisorbed layers ( $E_{\text{des}}$  relatively high) are considerably more tightly bound. A rule-of-thumb that may be assumed is that, for every  $100^\circ$  temperature rise, gas emission after heating will be reduced by a factor of 10. The nature of the adsorbing surface is never uniform. It may have dislocations, grain boundaries, etc. which give rise to different values of the desorption energy. Further, the presence of any pre-adsorbed material (e.g. oxide layers) gives rise to completely different conditions.

Depending on the base pressure required, the construction material of the system, time available and the nature of processes to be carried out within the system, some limitations may be placed on the bake-out procedure used to remove adsorbed material. According to Duesing (1987), only physisorbed species such as  $\text{H}_2\text{O}$ ,  $\text{N}_2$  or  $\text{CO}_2$  are removed, and further cleaning is required to remove chemisorbed impurities. Armour (1987) pointed out that with ultra-high vacuum systems containing complex, highly precise mating surfaces (e.g. goniometers used in surface science), however, baking at temperatures in excess of  $200^\circ\text{C}$  leads to a rapid increase in the frequency of 'seizures'. For most applications with stainless steel systems, however,  $200^\circ\text{C}$  for 48 h is

**Table 6.1** Variation of the mean residence time ( $\tau$ ) with surface temperature and desorption energy ( $E_{\text{des}}$ ) (according to Adam, 1989). Results are given as  $\tau \text{ s}^{-1}$

$E_{\text{des}}$ (kJ mol <sup>-1</sup> )	Temperature		
	77K	298K	773K
4.2	$7 \times 10^{-11}$	$5.4 \times 10^{-13}$	$1.9 \times 10^{-13}$
42	$3 \times 10^{15}$	$2.2 \times 10^{-6}$	$6.8 \times 10^{-11}$
210	—	$6.7 \times 10^{23}$	16

adequate for a base pressure of  $10^{-11}$  mbar to be achieved. Mohri and co-workers (1984) desorbed  $H_2O$ ,  $H_2$ ,  $CO$  and  $CO_2$  by heating an aluminium alloy vacuum chamber at temperatures of  $170^\circ C$  or below. Above this temperature, the physical characteristics of the alloy were changed irreversibly.

Outgassing

Most gases are taken up by pure metals and alloys whilst the latter are in the molten state. They are commonly gases such as  $H_2$ ,  $N_2$ ,  $CO$  and  $CO_2$  and arise by interaction of the metal with the furnace gases during melting and/or by the incorporation of ambient gas during casting at atmospheric pressure. They may also diffuse into the metal although the latter process is relatively slow at room temperature.

To treat the process quantitatively, but relatively simply, outgassing has been considered for a *thin* (thickness small compared with the length) sheet of metal (Adam, 1989). At the start of degassing it is assumed that the sheet contains a uniform distribution of particles and the process, which involves diffusion, is initiated by a temperature rise. Under these conditions, a diffusion flux ( $j_{diff} \times A$ ) emerges symmetrically from both sides of the sheet:

$$j_{diff} = - D \cdot dn/dx$$

where  $n$  is the number density of dissolved particles and  $D$  is the diffusion coefficient:

$$D = D_0 \exp (- E/RT)$$

$E$  is an energy term that takes into account the mechanism by which the gas penetrates or leaves the solid.

A characteristic parameter,  $t_{out}$  (the outgassing time constant), may be defined which is given by the expression:

$$t_{out} = 4d^2/\pi^2 D$$

where the thickness of the sheet =  $2d$ . Since  $D$  is temperature dependent, so is  $t_{out}$ . For example, the diffusion coefficient of  $N_2$  in steel can, according to Barrer (1951), be denoted by the empirical relationship:

$$D(T) = 10^{-5} \exp (-17\ 000K/T) \text{ m}^2 \text{ s}^{-1}$$

Diffusive mass flux density can be calculated from:

$$j_{mass,0} = \frac{2D}{d} \cdot \rho_{diss.gas,initial}$$

where  $\rho_{diss.gas,initial}$  = mass density of dissolved gas

( $W_{diss.gas}$  = content of dissolved gas expressed in p.p.m.;  
 $\rho_{solid}$  = density of solid)

leading to  $j_{diff} = j_0 \cdot \exp (-t/t_{out})$  ( $t$  = outgassing time)

for  $t > 0.5t_{out}$  · For  $t < 0.5t_a$ ,

$$j_{\text{diff}} = j_0 \sqrt{\frac{t_a}{16t}}$$

At relatively low temperatures (300–600K), the long period of outgassing of the vacuum chamber walls and components therein, has the characteristics of a leak. Vacuum systems can be degassed by baking under vacuum for an appropriate length of time. However, because outgassing is significantly temperature dependent, metals for certain applications may be outgassed prior to assembly. For example, Lindblad *et al.* (1987) have removed hydrogen from stainless steel by ‘vacuum firing’ (1000°C at  $10^{-5}$  mbar).

With particle accelerators and storage rings, gas desorption may be brought about by interaction of the confined beam with the vacuum system. With electron beams, synchrotron radiation (visible  $\rightarrow$  hard X-rays) brings about the electron-stimulated desorption of gases such as H<sub>2</sub>, CO, CO<sub>2</sub> and CH<sub>4</sub>. With proton beams, desorption involves the formation of ions by interaction with residual gas molecules. The former then induce gas desorption through their collisions with the wall. An effective cleaning method that can be used (Ding and Williams, 1989; Benvenuti *et al.*, 1987) involves a glow discharge in Ar following a high-temperature pre-bake-out. A review of glow discharge techniques in the conditioning of large high and ultra-high vacuum systems has been presented by Dylla (1988).

#### 6.1.1.1.3 Permeation

This is a strongly temperature-dependent process and describes the transmission of gas through the solid by a mechanism involving adsorption at the high-pressure side, diffusion through and desorption from the surface of the permeable barrier and into the low-pressure region. Metals and alloys normally used for vacuum applications, and having the appropriate wall thickness, may be regarded as being impermeable to air, even at elevated temperatures. The highest permeability through metals is usually observed with hydrogen. The permeation of H<sub>2</sub> through palladium is particularly pronounced at temperatures of a few hundreds of degrees and it is used as a method for the production of very pure hydrogen. The permeation of oxygen through silver can also be high and increases with temperature.

The permeability of a barrier to gas is expressed quantitatively in terms of the ‘permeation gas flux’ (Adam, 1989). This is proportional to the wall surface area ( $A$ ) and inversely proportional to the wall thickness ( $d$ ). It also depends on the temperature ( $T$ ) of, and the pressure across, the barrier:

$$q = f(T) f'(P_1, P_2) \frac{A}{d}$$

The permeation gas flux is usually given in terms of PV-throughput ( $[q_{\text{PV}}] = \text{mbar l s}^{-1}$ ). A reference permeation gas flux is given in the form:

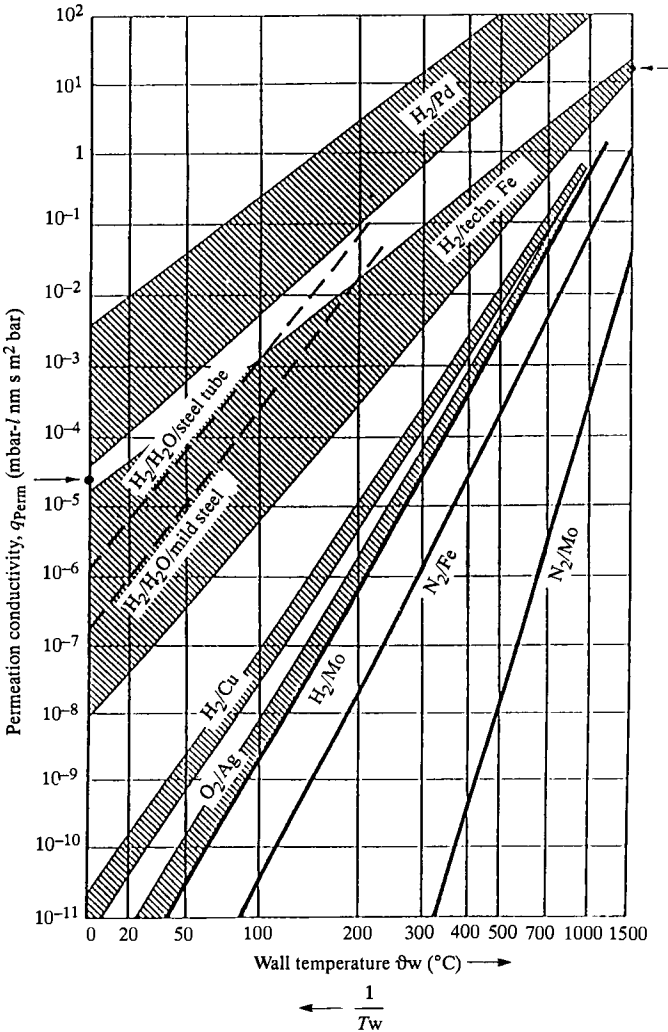
$$\bar{q}_{\text{perm}} = q_{\text{PV}} \cdot \frac{d}{A(P_1 - P_2)}$$



where, with  $A = 1 \text{ m}^2$ ,  $d = 1 \text{ mm}$  and  $P_1 - P_2 = 1 \text{ bar}$ ,

$$[\bar{q}_{\text{perm}}] = \text{mbar l s}^{-1} \left( \frac{\text{mm}}{\text{m}^2_{\text{bar}}} \right)$$

By analogy to thermal conductivity, Adam (1989) introduced the expression 'permeation conductivity' for  $\bar{q}_{\text{perm}}$ . Data showing the permeation conductivity for various metal-gas combinations are shown in Figure 6.1.



**Figure 6.1** Variation of the permeation conductivity of some gas-metal combinations with barrier temperature (from Adam, 1989)

### Mild steel (carbon steel)

This material is used in the construction of vacuum equipment only when pressures in the rough–medium range have to be maintained in the presence of non-corrosive gases and vapours. The area-related outgassing rates for mild steel after being pumped for 1 hour is in the range  $5.4\text{--}6.0 \times 10^{-7}$  mbar l s<sup>-1</sup> cm<sup>-2</sup> (the latter value is quoted for ‘slightly rusty’ steel). These data are according to Elsey (1975).

### Stainless steels

Austenitic stainless steels (AISI 300-series) are widely used for high and ultra-high vacuum systems on account of their strength and corrosion resistance. Their chemical composition is given in Table 6.2.

The degassing rates for unbaked stainless steel have been collected by Elsey (1975) and cover a range of values. Mechanically-polished steel gives a rate of  $1.7 \times 10^{-9}$  mbar l s<sup>-1</sup> cm<sup>-2</sup>; electropolished steel has a value of  $4.3 \times 10^{-9}$  mbar l s<sup>-1</sup> cm<sup>-2</sup>. Cleanliness of the steel affects outgassing rate. For example, Tohyama *et al.* (1989) measured the outgassing rate of electropolished, baked (850°C, 10<sup>-9</sup> mbar) type 316L steel containing various amounts of gas and non-metallic inclusions. As may be expected, H<sub>2</sub> outgassing decreased with decreasing content of hydrogen and non-metallic inclusions. The outgassing of (CO + N<sub>2</sub>) and CO<sub>2</sub> were reduced with decreasing carbon and nitrogen. Modification of the surface has also been found to reduce outgassing. Fujita and Homma (1988), for example, examined stainless steels which had been either electropolished, S-segregated or covered with a thin layer of precipitated (heating, 1000–1100K) boron nitride. On heating to 800°C, the latter material evolved the least amount of gas. Ishikawa and Odaka (1990) observed a reduction in outgassing by the surface oxidation (at 100–250°C) of a vacuum remelted type 316L steel. Following

**Table 6.2** Composition of austenitic stainless steels

AISI type (British type)	Composition (%)					
	Cr	Ni	C (max)	Mo	Si (max)	Other
304 (EN58E)	18–20	8–10.5	0.08	–	1.0	–
304 L	18–20	8–12	0.03	–	1.0	–
304 LN	18–20	8–12	0.03	–	1.0	N(0.1–0.16)
316	16–18	10–14	0.08	2–3	1.0	–
316 L	16–18	10–14	0.03	2–3	1.0	–
316 LN	16–18	10–14	0.03	2–3	1.0	N(0.1–0.16)
321 (EN58B)	17–19	9–12	0.08	–	1.0	Ti (5×C)
347 (EN58F)	17–19	9–13	0.08	–	1.0	Nb (10×C)

'baking', a rate of  $10^{-11} \text{ Pa m}^3 \text{ s}^{-1} \text{ m}^{-2}$  ( $\equiv 10^{-14} \text{ mbar l s}^{-1} \text{ cm}^{-2}$ ) was determined. Kato *et al.* (1990) reduced the rate of water vapour degassing from a 316 steel by the plasma deposition of carbon on the surface. After 1 h in vacuum, the rate for a treated surface was  $7.6 \times 10^{-11} \text{ mbar l s}^{-1} \text{ cm}^{-2}$ . Erikson *et al.* (1984) have measured room temperature degassing for a chamber made of 304 steel as  $2 \times 10^{-9}$  and  $2.3 \times 10^{-10} \text{ mbar l s}^{-1} \text{ cm}^{-2}$  after 1 h and 10 h respectively.

### Nickel and nickel-containing alloys

These materials have excellent corrosion resistance and are superb for vacuum use. They are, however, expensive. The addition of nickel to iron confers extra toughness. It also stabilizes the austenitic phase. Three nickel steels, containing 3.5, 5 and 9% are in commercial production. The 36% Ni-Fe alloy (Invar, Dilavar, Nilo 36) has a thermal expansion, over the temperature range from room temperature to 0K, that is an order of magnitude smaller than those of other structural alloys. For specialist applications, high Ni alloys have been used (Duesing, 1987). The composition of some of these materials is given in Table 6.3.

### Aluminium and its alloys

Pure aluminium and its alloys are used extensively in vacuum technology. Although relatively weak, the pure metal is light, comparatively cheap, has a high thermal conductivity, low thermal emissivity and is completely non-magnetic. It is used, for example, with particle accelerators and storage rings where the beam pipe must be non-magnetic in order not to disturb the external beam guidance system (Benvenuti *et al.*, 1987). Aluminium and its alloys have also been used in UHV system fabrication on account of their low degassing rates (see, for example, Miyamoto *et al.*, 1986; Ishimaru, 1984; 1989; Chen *et al.*, 1985; Poncet, 1987). Published degassing rates for widely used alloys are given in Table 6.4.

**Table 6.3** *Composition of some high Ni alloys*

Name	Composition (%)								
	Ni	Cr	Fe	Ti	Al	Mo	Nb	Co	Other
Inconel alloy 600	76.0	15.5	8.0	–	–	–	–	–	–
Nicrofer 7216 LC	74 min	16–17	6–8	–	–	–	–	–	–
Inconel alloy 601	60.5	23.0	14.0	–	1.4	–	–	–	–
Nimonic alloy 75	80.0	19.5	–	–	–	–	–	–	–
Inconel alloy X-750	73.0	15.5	7.0	2.5	0.7	–	1.0	–	–

Table 6.4 Degassing rates for some Al alloys

Alloy	Degassing rate ( $\text{mbar l s}^{-1} \text{cm}^{-2}$ )	Treatment	Reference
Type 6061	$< 1.3 \times 10^{-14}$ (20°C)	Firing (340°C; 4 h, $10^{-3}$ mbar) Baking (200°C; 24 h) Ar/O <sub>2</sub> discharge	Halama and Herrera (1976)
4 nm oxide layer/Al	$10^{-11}$	Prior to baking	Miyamoto <i>et al.</i> (1986)
Type 6063	$4 \times 10^{-13}$	Baking (150°C; 24h)	Ishimaru (1984; 1989)
6063 extrusion	$10^{-13} - 10^{-14}$	Baking (150°C; 24 h)	
6063 with inner 1050 cladding	$1.5 \times 10^{-10}$ (10 h) $1.5 \times 10^{-13}$ (10 h)	Unbaked Baking (150°C; 24 h)	Chen <i>et al.</i> (1985)
6063 (air, 1 month)	$5 \times 10^{-10}$ (10 h) $5 \times 10^{-12}$ (10 h)	Unbaked Baking (150°C; 24 h)	Chen <i>et al.</i> (1985)
6063 EX*	$2 \times 10^{-10}$ $5 \times 10^{-13}$	Room Baking (130–150°C; 24 h)	Chen <i>et al.</i> (1985)
6063 – T4 extruded; cooled in Ar/O <sub>2</sub>	$\leq 10^{-13}$	Baking (150°C; 24 h)	Dylla, Manos <i>et al.</i> (1990)
Type 6061	(0.4–0.8 W% Si, 0.7 W% Fe, 0.15–0.4 W% Cu, 0.15 W% Mn, 0.8–1.2 W% Mg, 0.04–0.35W% Cr, 0.25 W% Zn, 0.15 W% Ti, 0.05 W% others)		
Type 6063	(0.2–0.6 W% Si, 0.35 W% Fe, 0.1 W% Cu, 0.1 W% Mn, 0.45–0.9 W% Mg, 0.1 W% Cr, 0.1 W% Zn, 0.1 W% Ti, 0.05 W% others)		
Type 1050	99.5% Al, 0.2 W% Si, 0.4 W% Fe		

\* EX process involves fabrication in O<sub>2</sub>/Ar to give a thin (3nm), dense oxide layer.

Erikson and co-workers (1985) have also studied the degassing characteristics of optically black solar absorbing coatings on aluminium (anodized Al, black chrome on Al, black paint on Al). In all cases, the degassing rate is approximately  $10^{-6}$  to  $10^{-7}$  mbar l s<sup>-1</sup> cm<sup>-2</sup>.

### Copper and copper alloys

Oxygen-free, high-conductivity (OFHC) copper is excellent for use in vacuum equipment. It has good corrosion resistance, high electrical and thermal conductivity and is easily machined. It is unsuitable, however, for the vacuum envelope where the system requires baking since heavy oxidation and scaling may occur. OFHC is used in gaskets for demountable seals (e.g. Conflat flanges). It has been observed, however, that prolonged heating (550°C, 200 h) of copper-gasketed stainless-steel joints causes significant diffusion bonding between the materials (Garwin *et al.*, 1986). This problem can be overcome by the deposition of a diffusion barrier (TiN, 5 nm) on the flange.

#### 6.1.1.2 *Polymers*

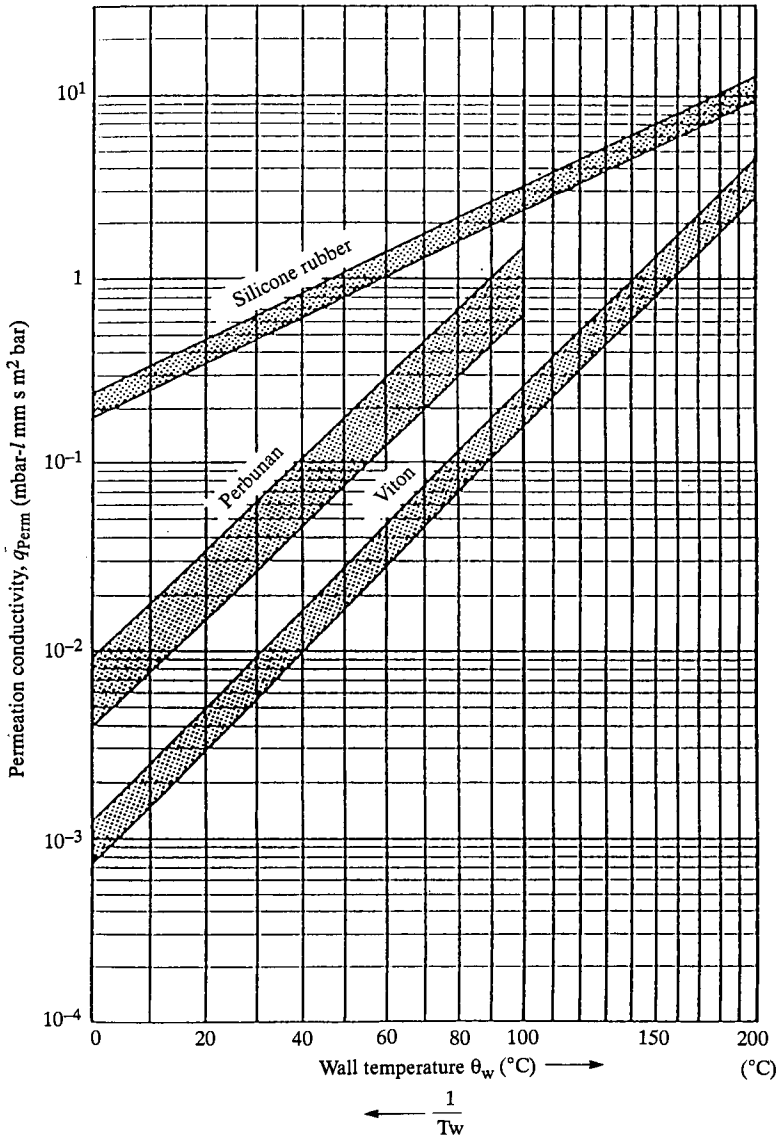
Polymers have a combination of properties such as low mass, low heat capacity, thermal and electrical insulation, that makes them suitable for many applications in vacuum technology. They can be subdivided into three broad classes of material:

1. *Thermoplastics* (e.g. PTFE, polyethylene, polypropylene). These are linear or branched polymers which are hard at room temperature but which soften or flow under the application of heat and pressure.
2. *Rubbers*. These are polymers with low interchain forces so that the material deforms readily under load but returns to the original shape when the load is removed.
3. *Thermosetting plastics* are normally liquid at some stage during processing but react to form a cross-linked structure that doesn't subsequently soften on heating.

Elastomers are materials with rubber-like properties which are particularly useful for O-rings and gaskets in vacuum technology. They are formed by grinding together the polymer with various amounts of plasticizers, filling agents, etc. to achieve the desired property, before they are vulcanized. Mechanical properties that are particularly important with elastomers used for demountable seals are the Shore hardness and the elasticity. The former is a measure of the resilience of the material, controlling the extent of deformation required to achieve a leak-tight seal while the latter determines the extent of permanent flattening that occurs in service. Other properties that are particularly important for polymeric materials are their permeability and outgassing.

All plastic materials such as elastomers allow the permeation of gas. Permeation is much larger than it is for glass and metal and depends markedly on the type of material and the additives used in manufacture. The permeability for atmospheric air increases significantly with humidity. Some permea-

tion data for silicone rubber, Viton (a copolymer of hexafluoropropylene and vinylidene fluoride) and perbunan (acrylonitrile-butadiene polymer) are shown in Figure 6.2 (from Adam, 1989). Laurenson and Dennis (1985) have measured the permeability of Viton, Aflas<sup>R</sup> (a copolymer of tetra-



**Figure 6.2** Permeation conductivity for some elastomers towards atmospheric air (relative humidity = 60%) (from Adam, 1989). Wall area = 1 m<sup>2</sup>, wall thickness = 1 mm; pressure difference = 1 bar

fluoroethylene and propene; <sup>R</sup>Asahi Glass) and a homopolymer of epichlorohydrin for several gases over a range of temperatures.

Degassing is a complex process and the rates for various materials have been collected by Diels and Jaeckel (1966). Adam (1989) has indicated that the process has an outgassing component (based on a model in which an air-saturated polymer of thickness  $d$  has a vacuum on both sides) and a permeation component (based on a fully degassed plastic having a vacuum on one side and atmospheric air on the other) in a process similar to that described in Section 6.1.1.1(b). Over a period of time, gas evolution due to outgassing decreases but a point is reached where increasing permeation becomes noticeable. Thereafter, gas desorption into the vacuum is determined almost exclusively by the permeation gas flux. Although the outgassing model described by Adam (1989) is based on air-saturated material, outgassing of unbaked elastomers may be dominated by water vapour evolution. Heating under vacuum for a few hours at about 150°C may reduce this considerably. A summary of the properties of some polymers and elastomers is given in Table 6.5.

### 6.1.1.3 *Ceramics (glasses, pure oxides, etc.)*

Glasses and ceramics have a range of uses in vacuum technology. They can be used for the construction of the main chamber, for windows on all-metal systems, electrical insulators, etc. Soft glasses (such as soda glass: SiO<sub>2</sub>, 65–70; Na<sub>2</sub>O, 5–15%; CaO, 5–15%) are excellent electrical insulators and have a particularly low permeability for hydrogen and helium. They have, however, a poor resistance to thermal shock and great care must be taken during heating and cooling.

Hard glasses (borosilicate glass such as Pyrex) contain at least 70% SiO<sub>2</sub> and their thermal stability is good. Although adsorption of water on glass can be a problem, Pyrex glass has been found to have a very low rate of outgassing ( $1-7 \times 10^{-9}$  mbar l s<sup>-1</sup> cm<sup>-2</sup> after 1 h in vacuum) (Elsey, 1975).

Quartz glass is pure silica. It has a high thermal stability and can be used for continuous operation at temperatures of about 1000°C. Quartz has a high permeability towards helium (the permeation conductivities are  $5 \times 10^{-5}$  and  $4 \times 10^{-2}$  mbar l s<sup>-1</sup> (mm m<sup>-2</sup> bar<sup>-1</sup>) at 20 and 1000°C, respectively. The room temperature permeability of quartz glass for air is determined by the helium content of the air and the PV throughput can be calculated from published values (Adam, 1989) of the permeation conductivity as a function of temperature. As the silica content of the glass is decreased, so is the permeability towards helium. Data for Pyrex are approximately  $2.5 \times 10^{-6}$  to  $4 \times 10^{-2}$  mbar l s<sup>-1</sup> (mm m<sup>-2</sup> bar<sup>-1</sup>) at 20 and 1000°C, respectively.

Ceramic materials are basically of three types: silicates, pure oxides, and special ceramics which contain carbides, nitrides and borides. They have some advantages over glass in that they are mechanically stronger and have better mechanical and electrical properties. A limited range of ceramics is available for vacuum applications. Historically, ceramics based on steatite (a magnesium metasilicate) were developed in the USA and Germany for use as insulators in vacuum systems. Enrichment of steatite with magnesium yields

**Table 6.5** *Some characteristics of polymeric materials*

<i>Polymers</i>	<i>Characteristics</i>
PTFE	Low outgassing ( $3 \times 10^{-7}$ mbar l s <sup>-1</sup> cm <sup>-2</sup> after 1 h (Eley, 1975)) Good electrical insulator
PVC	High outgassing ( $5 \times 10^{-7}$ mbar l s <sup>-1</sup> cm <sup>-2</sup> after 1 h (Diels and Jaeckel, 1966)) High water absorption
Polyethylene	Outgassing = $2.3 \times 10^{-7}$ mbar l s <sup>-1</sup> cm <sup>-2</sup> after 1 h (Eley, 1975) Good electrical insulator
Neoprene (polychloro- butadiene)	Significant outgassing, $(3-30) \times 10^{-6}$ mbar l s <sup>-1</sup> cm <sup>-2</sup> (1 h) (Eley, 1975)
Viton	Low outgassing ( $1.14 \times 10^{-6}$ mbar l s <sup>-1</sup> cm <sup>-2</sup> (1 h; Eley, 1975) as manufactured; $0.4 \times 10^{-8}$ mbar l s <sup>-1</sup> cm <sup>-2</sup> (after 'degassing'; Eley, 1975); $8 \times 10^{-8}$ mbar l s <sup>-1</sup> cm <sup>-2</sup> (20 h; Laurenson and Dennis, 1985) Good permeation resistance; Good resistance to oil; temperature resistant (-10°C to +200°C)
Aflas	Outgassing ( $1 \times 10^{-7}$ mbar l s <sup>-1</sup> cm <sup>-2</sup> (20 h; Laurenson and Dennis, 1985)) Excellent chemical resistance
Perbunan	Significant outgassing ( $3.5 \times 10^{-6}$ mbar l s <sup>-1</sup> cm <sup>-2</sup> (1 h; Eley, 1975)) Good permeation resistance; Poor resistance to oil.

forsterite (a magnesium orthosilicate) which has improved characteristics, particularly lower dielectric loss and a high coefficient of thermal expansion that closely matches those of titanium and inconel. Steatites and forsterites can be used to about 1000°C. Pure oxide ceramics based on the oxides of aluminium, magnesium, zirconium and beryllium have also been used but, in vacuum applications, those based on aluminium oxide are predominant.

Compared with silicate-based ceramics, Al<sub>2</sub>O<sub>3</sub> has a far higher operating temperature (up to 1800°C), good thermal stability and better mechanical and electrical properties. Insulating material containing 92–98% Al<sub>2</sub>O<sub>3</sub> has been used, as ceramic-metal seals, for high-temperature current lead-throughs in the construction of vacuum chambers for particle accelerators. In this application, the ceramic that has to be joined to the metal is premetallized with either molybdenum or titanium. Thereafter, a nickel layer is deposited



which is then heat treated in hydrogen (1000°C) to bring about penetration into the first layer. This layer can then be brazed to the appropriate metal component.

Vacuum processes taking place in metal systems may be observed through view ports. Bakeable, leak-tight windows are usually made of hard glass sealed into a flange with an appropriate glass-to-metal seal. The glass surface may be coated to reduce surface reflection or to prevent the build-up of electrical charge. For special applications, where high transmission of infrared and ultraviolet radiation is required, sapphire (pure  $\text{Al}_2\text{O}_3$ ) is used for inspection ports or windows. The procedure involves initial metallization of the sapphire (see above) followed by joining to a thermally compatible metal which can then be welded to the steel flange.

The permeation of gases through ceramics takes place by a mechanism similar to that for glasses. Since this involves passage of gas through the pores, the permeation conductivity depends on the nature of both the gas and the ceramic. Data are not extensive (Weston, 1985) and the manufacturer of the material may have relevant information. With regard to degassing, silicate ceramics reportedly behave rather like glass. Water vapour and the oxides of carbon are the main gases evolved through desorption and outgassing (Weston, 1985). In general, silicate ceramics having a high proportion of glassy phase material contain the most absorbed gas. Steatite, forsterite and high-alumina ceramics show less gas emission. When ceramic components form an appreciable part of the vacuum system, Weston recommends vacuum baking at 1000°C prior to assembly and heating at 450°C for several hours in the final system in order to reduce outgassing.

### 6.1.2 Cleaning

Cleaning is carried out in order to reduce to an acceptable level degassing from the vacuum system during operation. The subject has been reviewed by Halliday (1987b). Some gas sources are obvious and include deposits of oils, greases and tars left on the surfaces that will be exposed to vacuum. The surfaces themselves adsorb gases, and this process is increased significantly if they are covered by layers of porous oxide or show the effects of rusting and corrosion. Water vapour, introduced to the vacuum system by exposure to ambient air, is particularly difficult to remove and its effects can be minimized by venting the system with a dry, inert gas before opening.

The function of the cleaning process is to remove material that may cause problems whilst ensuring that the fabric of the vacuum system is left clean and uncontaminated. (It should be noted that discrete components can be more easily cleaned than assemblies.) Cleaning involves a number of steps carried out sequentially so that the greater the degree of cleanliness required, the more stages will be involved (for details, see Halliday, 1987b). The precise procedure depends on the material to be cleaned but it usually comprises:

1. *Removal of gross contamination* – This may involve scraping, brushing, wiping, etc. A suitable solvent can be used to remove deposits of tars, oils and similar material.

2. *Removal of deposits remaining from (1)* – Further cleaning can be achieved by blasting the surface, either with a suspension of minute glass beads in water or with an abrasive powder. Rinsing with water may be necessary to remove the debris produced.
3. *Degreasing* – Irrespective of whether steps (1) and (2) have been carried out, degreasing is an essential part of the cleaning procedure. The object to be cleaned may be treated either by immersion in a bath of liquid solvent (such as inhibited 1,1,1 – trichloroethane) or in a vapour degreasing bath of the same compound. In the former case, cleaning is enhanced by ultrasonic agitation.
4. Degreasing is followed by treatment to remove the solvent. This can be achieved by rinsing with acetone or, preferably, high purity ethanol and, finally, with distilled water.
5. At the end of the sequence, the object is dried in a stream of hot, dust- and oil-free air.

Chemical cleaning is rarely recommended for vacuum equipment (Halliday, 1987b) since aggressive chemicals such as dilute acids can affect dimensional accuracy and roughen the surface. There are, however, circumstances where chemicals may be used. These range from chemical decontamination by means of diluted organic acids to the production of a polished surface by non-mechanical means (for example, electropolishing). Such procedures must, however, be followed by rigorous washing and drying to remove any trace of the chemicals.

The cleaning processes indicated so far will leave a surface free of most adherent material. It will not, however, remove gas adsorbed on the surface or incorporated within the solid. Various aspects of degassing have already been discussed but, as Duesing (1987) pointed out, only physically bound impurities are removed by vacuum baking. For particular applications such as fusion reactors, particle accelerators and storage rings, glow discharge cleaning (using discharges in high-purity Ar or Ar/O<sub>2</sub> mixtures) is often necessary to remove chemically bound species (Hseuh *et al.*, 1985; Dylla, 1988). Grunze *et al.* (1988) have also indicated that gaseous contaminants in stainless steel UHV systems, for example, can be removed by the admission of a stream of nitric oxide during bakeout.

### 6.1.3 Fabrication

The chamber, connections, etc. having been designed and fabricated from appropriate material, must be assembled to form the vacuum system. The joints and interconnections within the system should be made in such a way that the possibility of leaks and trapped volumes is minimized. They may be classified as either permanent or demountable and, wherever possible, permanent joints are to be preferred.

The techniques used in making permanent joints are determined by the characteristics of the materials to be joined. Metals, for example, may be welded or soldered together while glass-to-glass seals are made by fusing the components together without inducing lasting stresses in the joint. With

glass-to-metal seals, combinations must be selected such that their coefficients of thermal expansion are similar over a wide range of temperatures.

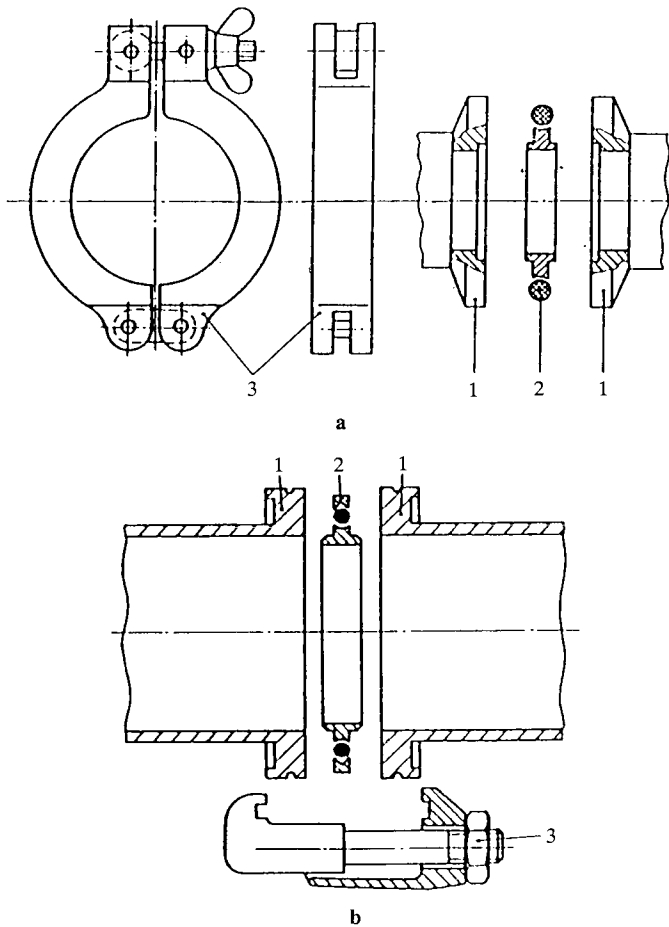
For vacuum system construction, the AC-TIG (tungsten-inert gas) method is usually used (see Davies, 1977). As long as the objects to be joined are thoroughly cleaned and degreased, uniform, scale-free seams can be produced. For thin-walled (up to 3 mm) sheets, no additives are required although fillers may be required under certain circumstances (Ishimaru, 1984). Vacuum technology places demands on welding practice not encountered in conventional applications and particular attention must be paid to the elimination of trapped volumes of gas and areas where dirt may accumulate. Comparisons of conventional welds with those suitable for vacuum practice are given by Kronberger (1958). Apart from the argon-arc process, microplasma and electron-beam welding offer some advantages in the fabrication of vacuum equipment. The former technique allows very thin sheets to be joined whilst the latter permits precise and distortion-free welding of both thin and thick material in any combination. Electron-beam welding has many attractive features including low contamination, a high rate of welding and a small heat-affected area. It also allows extremely narrow, deep-penetration welds to be made.

A second technique for joining metals is hard-soldering or brazing. Hard-soldered joints are usually made under vacuum at temperatures that depend on the solder. Those based on noble metals (for example Au-Cu (80/20), Cu-Au-Ni (65/35/3)) can be worked at lower temperatures than those with a substantial Ni content (Cu-Ni (70/30), Ni-Cr-Si-B-Fe (87/7/4.5/2.9/3)). Further details of brazing are given by Kaiser (1989).

In the fabrication of glass-to-metal seals, materials are chosen that have coefficients of thermal expansion that are matched as closely as possible. For example, the alloys NILO 475 (47% Ni, 5% Cr, remainder Fe) and VACON 10 (28% Ni, 18% Cr, remainder Fe) have mean coefficients of thermal expansion ( $52 \times$  and  $5 \times 10^{-7} \text{ K}^{-1}$  respectively) that are close to that of hard glasses such as the Schott Type 8250 ( $30\text{--}50 \times 10^{-7} \text{ K}^{-1}$ ).

Demountable joints are usually unavoidable on vacuum systems and involve those that can be broken and resealed. They are usually incorporated to facilitate dismantling or the connection of gauge heads or the introduction of samples. For pressures outside the UHV range, the seal is usually made by the deformation of a trapped O-ring. For small-diameter connections (up to DN50), a typical connector with quick-release couplings is shown in Figure 6.3(a).

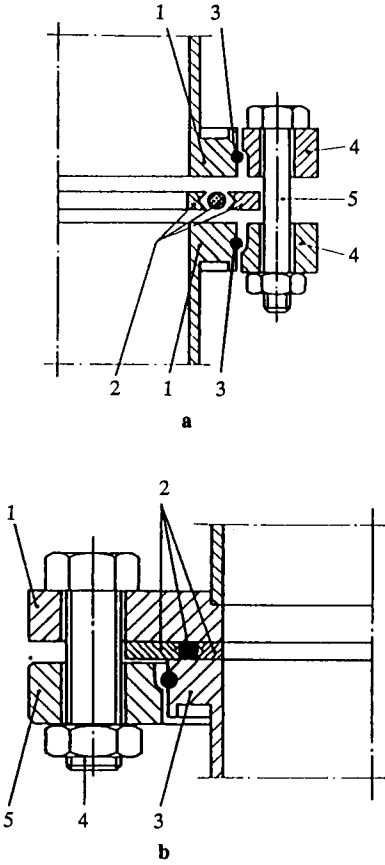
It consists of the flanges to be connected, a centring ring with an O-ring gasket (adapting centring rings are available for, say, DN10-16, DN20-25 and DN32-40 connections) and a suitable clamp. Connections with diameters greater than DN50 may have the flanges bolted together or they may be clamped together by the method shown in Figure 6.3(b). Clamp flanges have a locating groove running around the flange. A metal centring ring fitted with an O-ring which is held in position with an outer ring is placed between the flanges and clamps are fixed at appropriate positions round the groove on the flange and tightened to form the seal. For fixing bolted and clamped flanges together, so-called collar ring flanges can be used (see, for example, Figure



**Figure 6.3** Flanges and seals. (a) KF small flange connection. 1, small flanges; 2, centring ring with O-ring gasket; 3, clamping ring. For Al components, Perbunan O-rings are mainly used. (b) ISO-K clamp flange connection. 1, ISO-K flanges; 2, centring ring and O-ring gasket with outer ring; 3, clamp. Perbunan or Viton gaskets can be used. Al gaskets are also available for more demanding applications

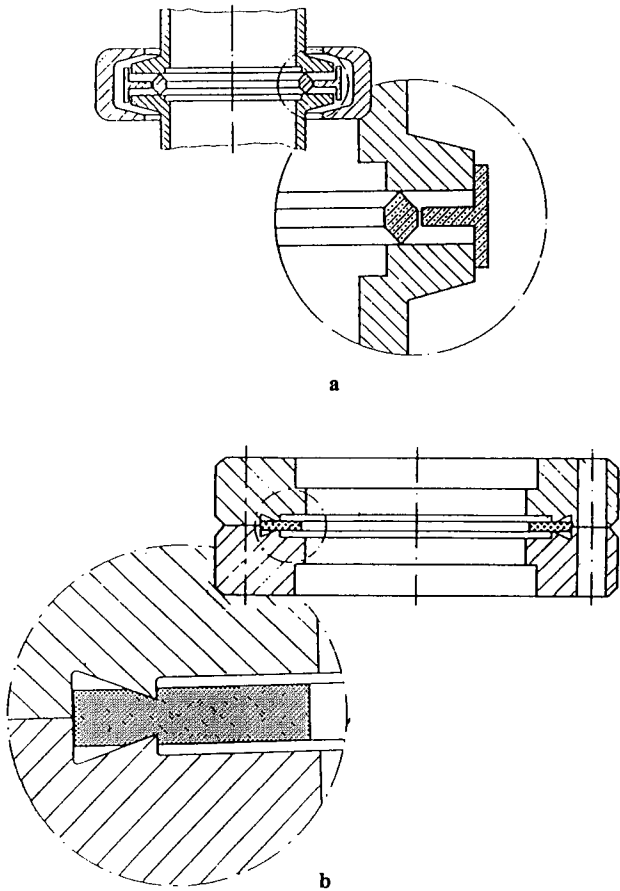
6.4). For demanding applications, stainless steel components are often used. In the high-vacuum range, Viton O-rings (vacuum-baked to 80°C to remove plasticizers) may be used as the sealing element.

For UHV applications, elastomer gaskets are unsuitable because high bakeout temperatures ( $\geq 200^\circ\text{C}$ ) are often required to reduce degassing and extremely low leak rates are demanded. Metal gaskets are usually employed



**Figure 6.4** ISO-K clamp flange connections. (a) With collar flanges on both sides. 1, ISO-K flanges; 2, centring ring and O-ring gasket with outer ring; 3, retaining rings; 4, ISO-F collar flanges; 5, bolt with nut (b) Connection between a clamped and a fixed flange using a collar flange. 1, flange DIN 2501; 2, vacuum sealing disk consisting of centring ring and O-ring gasket with outer ring; 3, ISO-K flange; 4, bolt with nut; 5, collar flange with relating ring DIN 2501

and the materials used may be soft and easily deformed (In, Au, Al) or relatively hard (Ag, Cu). With soft metals, the gaskets may be unconfined between the surfaces to be sealed so that deformation allows them to spread or, as in the Leybold UHV Al gasket (Figure 6.5(a)), the gasket is centred using a support ring which also acts as a compression limiter. In the latter case, the clamp is not of standard design (as, for example, Figure 6.3(a)) but consists of a three-piece clamping collar.



**Figure 6.5** Some ultra-high sealing systems. (a) Leybold system with aluminium sealing ring. (b) ConFlat system

High-purity copper is a widely-used gasket material, and the seals usually rely on a sharp edge biting into the gasket. Weston (1984) has indicated a number of configurations. A sealing mechanism that has been very widely adopted is a Varian design having the trade name ConFlat (Figure 6.5(b)). The ConFlat flange consists of two symmetrical flanges both having circularly-symmetrical knife edges of a particular cross-section.

A flat copper gasket is placed between the flanges and, when they are bolted together, the knife edges bite into the copper causing lateral flow. The outer rim of the channel on the flange faces, however, restricts this and the copper is forced to fill any imperfections on the flange surfaces. Seals thus made are reported to have helium leak rates of below  $10^{-11}$  mbar l s $^{-1}$ ; the

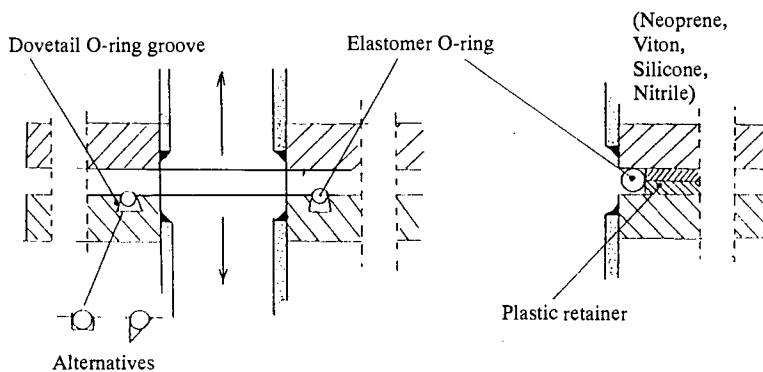
gaskets are not reusable. CF-flanges are very similar to ConFlat flanges and for sizes up to NW 150 CF, the two types mate perfectly well. ConFlat-type seals have been developed (Ishimaru, 1984) with aluminium alloy flanges that incorporate chromium nitride-coated knife edges. The sealing gasket is made of aluminium (Type 1050) with a near mirror-like surface finish and the  $\text{Cr}_2\text{N}$  coating is said to protect against surface scratching and to give 'nearly perfect' protection against sticking between the gasket and the knife edge. The Al-ConFlat flanges are tightened by means of aluminium alloy nuts, bolts and washers. For combinations of Al and stainless steel ConFlat flanges, Heli-coflex seals are preferred. Seals such as these use metal tubular O-rings, either pressurized or filled to atmospheric pressure. For UHV, the seal is coated with a softer metal or with Teflon.

Finally, for certain tasks (for example, door seals), captured O-ring seals are commonly used (Figure 6.6). This system requires little further explanation but it should be pointed out that attention must be paid to the cleanliness of all components and all traces of debris must be removed from sealing surfaces. With O-ring seals, there is often a temptation to apply vacuum grease to the surfaces. This is usually unnecessary but if it is used, *only* the quantity required to make the O-ring surface appear polished must be applied.

## 6.2 Components

### 6.2.1 Valves

Valves are essential for effective use of a vacuum system. They allow isolation of various sections of the equipment during pump-down, maintenance, etc. and also permit the introduction of gases during processing or venting. As with other components, valves used in vacuum engineering must meet



**Figure 6.6** Other sealing systems

requirements that are very different to those encountered in other branches of industry. What is demanded is (Adam and Jokisch, 1987):

1. Low degassing rate from all parts of the valve
2. Low leak rate through the valve-operating mechanism, the valve seat (when the valve is closed) and the valve connections.
3. Insignificant gas entrainment.
4. Ability to withstand pressure differences of 1 bar or more.
5. High conductance in the 'valve open' position.
6. Long life and high reliability.

Other characteristics that are of importance in certain applications have also been given by Adam and Jokisch (1987) and include one or more of the following:

1. Valve activation time.
2. Resistance to temperature, radiation and vibration.
3. Ease of maintenance.
4. Indication of state of valve (open/closed).

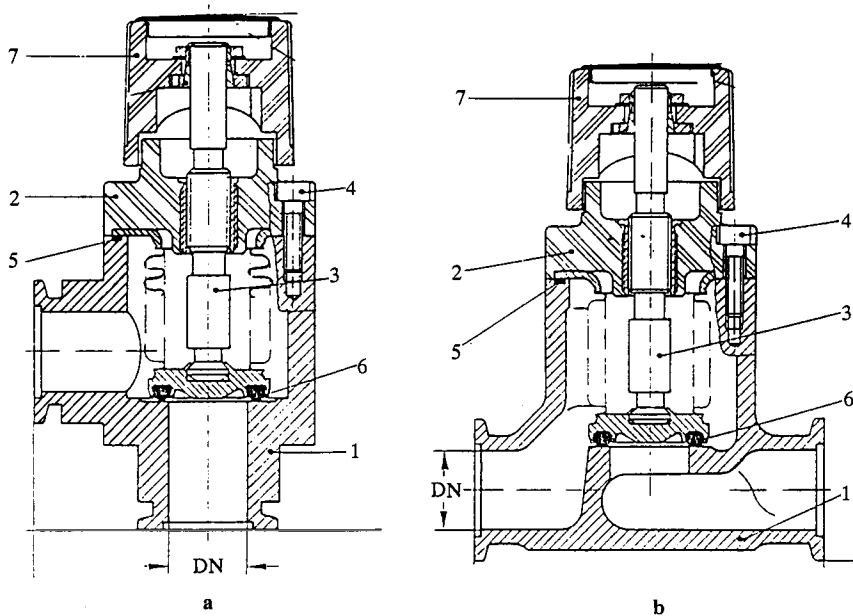
Since the wide variety of valves used in vacuum technology makes classification difficult, possibly the most satisfactory method of dealing with them is according to application, i.e. according to function and pressure range.

#### **6.2.1.1 Standard vacuum valves for rough, medium and high vacuum**

Standard vacuum valves are generally used for the purpose of isolation and gas admission. They do not include valves used for the precise control of gas flow or those that can be baked at high temperatures. The range includes quasi-straight-through valves and right-angle valves, butterfly valves and gate valves.

Small valves (DN10 – DN100) may be operated either manually (for relatively small, conventional systems) or electromagnetically (for automated or remotely controlled facilities). For some applications, motorized valves are available. Very large valves (up to DN630 ISO-F) are generally electropneumatically operated. Aluminium and stainless steel are commonly used in the construction of valves. The latter material is also used internally. For the sealing of the moving parts, the use of metal bellows welded to a collar and to the valve shaft is increasing. A manually operated, bellows-sealed valve is shown in Figure 6.7 where it can be seen that sealing involves the use of an O-ring fixed at the end of the valve plate. Neoprene or Viton are used as sealants; the latter material can be heated to 105°C. Elastomer seals can be used at operating pressures down to approximately  $10^{-6}$  mbar but at lower pressures, outgassing becomes significant and all-metal seals are required. Electropneumatically-operated, bellows-sealed valves are available in sizes from DN10 to DN630. Typical small-sized valves are shown in Figure 6.8. The operation of the valve, which is normally closed by means of a strong closure spring, involves the admission of compressed air (5–9 bar) to the pneumatic cylinder via the servovalve. This drives the piston upwards, compressing the closure spring and opening the valve. When the valve is





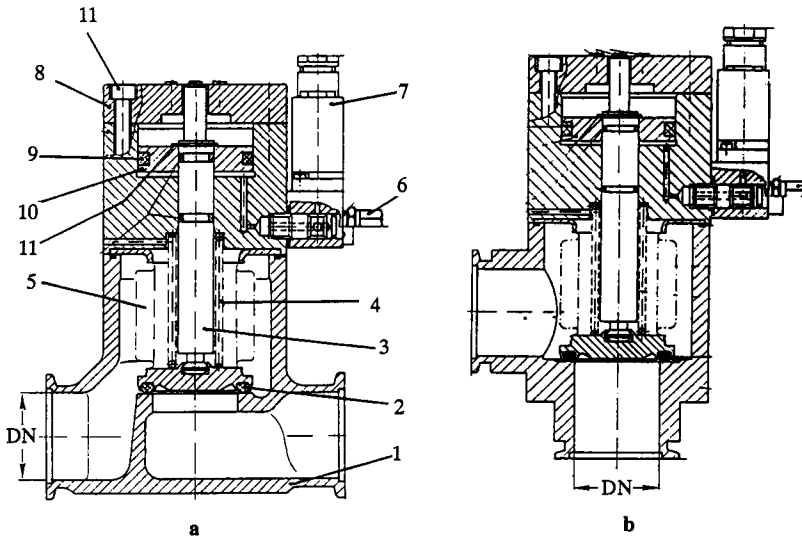
**Figure 6.7** Bellows-sealed standard valves. (a) Right-angle valve.  
 (b) Quasi-straight-through valve. 1, valve body; 2, valve cover; 3, shaft;  
 4, screws; 5, O-ring seal/gasket on valve body; 6, O-ring seal on valve

closed, the servovalve moves, allowing air in the piston to escape. The spring then forces the valve shut.

The opening/closing time of such valves is relatively rapid, ranging from 28 ms for a DN16KF right-angle valve to 125 ms for the similar 40KF version. Versions of this valve also exist that use an elastomer-sealed sliding shaft instead of bellows. This type of valve may also be used for less-demanding applications in the rough- and medium-vacuum range where the requirements for leak rate and gas entrapment are less strict.

Electromagnetically operated valves are available commercially in the size range up to about DN40. They are normally closed, sealing being maintained by a strong spring. During operation, the magnet must be able to overcome both the force of the spring and that due to gas pressure. Control circuits are provided that produce a high current (say, 2–4 A) during valve actuation but switch over to a smaller holding current (about 0.5 A) to maintain the valve in an open position. Because of their relatively small size, electromagnetic valves can open against atmospheric pressure. Valve actuation is rapid, approximately 40 ms or less being required for opening and closing.

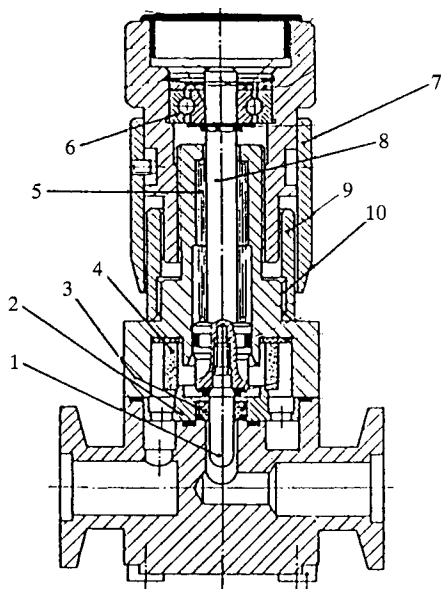
Standard valves may be used for the admission of gas if they are carefully adjusted. More precise valves are available which allow a well-defined gas



**Figure 6.8** *Electropneumatically-operated, bellows-sealed valves (DN 10 KF–DN 50 KF). (a) Quasi-straight-through valve. (b) Right-angle valve. 1, valve body; 2, O-ring seal on valve plate; 3, shaft; 4, closure spring; 5, metal bellows; 6, compressed air connection; 7, 3/2-way servovalve; 8, pneumatic cylinder; 9, O-ring; 10, piston; 11, circlip*

flux to pass and be regulated reproducibly. A variable leak valve is a precision mechanical valve whereby metering is effected by a pathway milled into the valve needle and precise changes in the position of the needle are made with a fine thread. The metering bushing is PTFE whilst the needle, casing and drive devices are made of steel (Figure 6.9). Gas inlet rates are in the range  $2 \times 10^3$  to  $1 \times 10^{-5} \text{ cm}^3 (T_n, P_n) \text{ s}^{-1}$  and, for a valve such as that shown in Figure 6.9, the leak rate across the valve seat is less than  $10^{-9} \text{ mbar l s}^{-1}$  (presumably at ambient temperature). Precision leak valves are often combined in a single unit with a shut-off valve in order to obtain repeatably a set gas inlet value.

The quasi-straight-through valves so far discussed have their connection flanges in line but the fully opened valve does not present an optically unimpeded path to the gas. This can bring about some loss in conductance. For example, for smaller valves (DN10, DN25 and DN40), values for the conductance under molecular flow conditions are, respectively, 1.6/10, 12/7.5 and 32/19  $\text{l s}^{-1}$  for the corresponding right-angle valves and quasi-straight-through valves. High conductance straight-through valves are available, of course, in the form of butterfly valves (Adam and Jokisch, 1987) and gate valves. The latter type is more effective than the former since there are no obstructions to gas flow, within the valve body. For example, in contrast with the above figures for quasi-straight-through valves, the molecular flow conductances of DN25 and 40 gate valves are 29 and 85  $\text{l s}^{-1}$ , respectively.



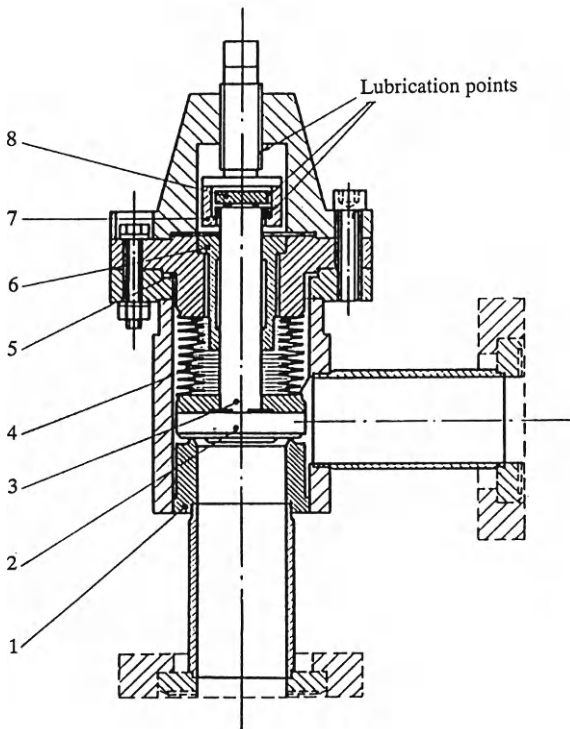
**Figure 6.9** *Cross-section through a precision variable leak valve. 1, valve needle; 2, metering disc; 3, metering bushing; 4, sintered metal filter; 5, spring; 6, ball bearing; 7, adjustable, graduated ring; 8, valve shaft; 9, graduated ring; 10, tolerance ring*

Gate valves are available either as pendulum gates, in which the valve plate is deflected sideways into the required position during operation, or as push-type gates, in which the plate moves linearly, actuated by a rod (see Adam and Jokisch (1987) and Kaiser (1989) for details of system). Both types of valve may be operated manually or pneumatically and, in the latter case, time intervals of less than a second up to a few seconds may be necessary for opening and closing. Depending on the application, sealing of the actuating rod involves either O-rings or bellows. Sealing of the valve itself is usually accomplished using Viton gaskets. Push-type gate valves, characterized by the nominal width of the opening (rather than the connecting flanges) are readily obtained in sizes ranging from DN16KF to DN250 ISO-F and CF-flange sizes from DN35 to 200. High-vacuum gate valves seal against atmospheric pressure in both directions and have a low leak rate (about  $10^{-9}$  mbar l s<sup>-1</sup>) on the valve seat.

#### **6.2.1.2 Ultra-high vacuum (UHV) valves**

UHV valves should have helium leak rates below  $10^{-11}$  mbar l s<sup>-1</sup> and should not contribute to the gas flux within a system. They must also be able to withstand baking at temperatures up to 450°C. These requirements can usually only be met with all-metal valves.

All-metal valves are usually sealed with knife-edge seals (Figure 6.10). Much higher forces are required to achieve the seal than is usual for standard vacuum valves containing elastomers and the drive is usually manual (via a fine screw) or pneumatically actuated. In both cases, it is essential that the mechanism positions the sealing disc precisely so that indentations are aligned with the knife-edge at each closure. Sealing forces have to be maintained at a constant level during baking and should not damage the seal components and thus reduce the lifetime of the valve. It is quite usual, however, for the sealing element to have to be changed after a certain number of operations ( $1000-10^5$  cycles; stated by the manufacturer). For this reason the inner parts of the valve can be dismantled. Further, after a few baking cycles, dry lubrication of the driver mechanism is usually necessary. This can often be achieved, without dismantling, through a special lubrication port. Sealing can be achieved using a gold-plated stainless steel 'nose' or plate. Gold gives a readily deformed, oxide-free surface and should give a valve having long life and requiring a relatively low closing force.



**Figure 6.10** All-metal, right-angle UHV valve (typically DN 16, 25 and 60). 1, valve seat; 2, sealing disc; 3, spindle; 4, bellows; 5, gold wire gasket; 6, guide sleeve; 7, clutch; 8, stellite

### 6.2.2 Other components

In addition to their gas-handling facilities, many vacuum systems must also be capable of transmitting mechanical movement and allowing energy to pass to and from the system.

#### 6.2.2.1 Mechanical movement

The transmission of mechanical movement into a vacuum system may involve linear or rotational movement or a combination. For pressures down to  $10^{-6}$  mbar, relatively small movements at fairly low speeds may be transmitted along rods and shafts sealed with greased elastomers or spring-loaded lipped seals. Mechanical lead-throughs that are required for extreme leak-tightness can be sealed using edge-welded metal bellows. The devices may be relatively simple or they may have great precision, capable of transmitting movement in the X-, Y- and Z-directions to within  $10\ \mu\text{m}$  and rotation about two axes to within  $0.1^\circ$  (Figure 6.11).

For some applications, magnetic coupling may be used. This involves one or more high-field, external drive magnets which transfer their movements to internal magnets coupled to a shaft. Transmissible torque is, however, limited by the strength of the magnets. Alternative systems have been

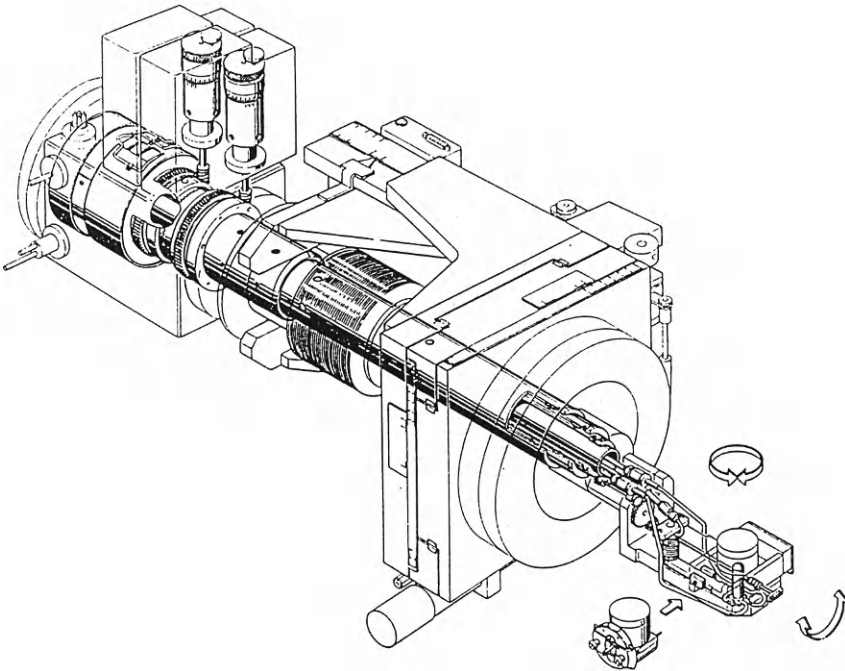


Figure 6.11 A precision UHV d.c.-motor-driven manipulator

described briefly by Weston (1984). One version involves a dynamic PTFE lip seal-type ring held tightly round the shaft by a circular spring. By the use of two seals and evacuation of the intervening space, a low leak-rate can be achieved. A seal which can be used down to  $10^{-8}$  mbar and that allows rotational speeds up to  $5000 \text{ min}^{-1}$  involves the use of a ferrofluid (a colloidal suspension of magnetic particles in a low vapour-pressure carrier). In the absence of a magnetic field, the oil behaves like a normal fluid; in a magnetic field, the liquid is contained and can withstand a high pressure difference.

#### 6.2.2.2 Electrical and other feed-throughs

It is often necessary to connect an item within the vacuum chamber to a voltage source or to a cooling system. Electrical insulators are commonly ceramics, glasses or plastics and the properties of these materials have been discussed earlier in this chapter. For normal cooling, metal tubes are welded or soldered into the chamber wall or to a demountable flange. If cryogenic fluids are used, however, more complex designs may be required. An example of vacuum components requiring both electrical energy and suitable cooling are the water-cooled electron beam evaporators used extensively in the production of thin films (see Section 7.1).

## References

- Adam, A. and Jokisch, G. (1987) *Vacuum*, **37**, 681
- Adam, H. (1989) In *Theory and Practice of Vacuum Technology* (eds M. Wutz, H. Adam and W. Walcher), F. Vieweg and Sohn, Braunschweig/Wiesbaden, p. 492
- Anderson, H.L. and Cohen, E.R. (1989) In *A Physicist's Desk Reference*, 2nd edn, American Institute of Physics, New York, p.36
- Armour, D.G. (1987) *Vacuum*, **37**, 709
- Barrer, R.M. (1951) *Diffusion In and Through Solids*, Cambridge University Press, Cambridge
- Benvenuti, C., Calder, R. and Groebner, O. (1987) *Vacuum*, **37**, 699
- Chen, J.R., Narushima, K. and Ishimaru, H. (1985) *Journal of Vacuum Science and Technology*, **A3**, 2188
- Davies, A.C. (1977) *The Science and Practice of Welding*, 7th edn, Cambridge University Press, Cambridge
- Diels, K. and Jaeckel, R. (1966) *Leybold Vacuum Handbook*, 2nd edn., Pergamon, Oxford, p. 238
- Ding, M.Q. and Williams, E.M. (1989) *Vacuum*, **39**, 463
- Duesing, G. (1987) *Vacuum*, **37**, 309
- Dylla, H.F. (1988) *Journal of Vacuum Science and Technology*, **A6**, 1276
- Elsey, R.J. (1975) *Vacuum*, **25**, 299, 347
- Erikson, E.D., Burger, D.D. and Frazier, B.A. (1985) *Journal of Vacuum Science and Technology*, **A3**, 1711
- Fujita, D. and Homma, T. (1988) *Journal of Vacuum Science and Technology*, **A6**, 230

- Garwin, E.L., Hoyt, E.W., and Nyaiesh, A.R. (1986) *Journal of Vacuum Science and Technology*, **A4**, 2537
- Grunze, M., et al. (1988) *Journal of Vacuum Science and Technology*, **A6**, 1266
- Halliday, B.S. (1987a) *Vacuum*, **37**, 583
- Halliday, B.S. (1987b) *Vacuum*, **37**, 587
- Hseuh, H.C., Chou, T.S. and Christianson, C.A. (1985) *Journal of Vacuum Science and Technology*, **A3**, 518
- Ishikawa, Y. and Odaka, K. (1990) *Vacuum*, **41**, 1995
- Ishimaru, H. (1984) *Journal of Vacuum Science and Technology*, **A2**, 1170
- Ishimaru, H. (1989) *Journal of Vacuum Science and Technology*, **A7**, 2439
- Kaiser, G. (1989) In *Theory and Practice of Vacuum Technology* (eds M. Wutz, H. Adam and W. Walcher), F. Vieweg and Sohn, Braunschweig/Wiesbaden, p. 519
- Kato, S., Oyama, H. and Odagiri, H. (1990) *Journal of Vacuum Science and Technology*, **A1**, 1998
- Kronberger, H. (1958) *Proceedings of the Institute of Mechanical Engineers*, **172**, 113
- Laurenson, L. and Dennis, N.T.M. (1985) *Journal of Vacuum Science and Technology*, **A3**, 1707
- Lindblad, Th., Bagge, L., Bjon, J. and Leven, S. (1987) *Vacuum*, **37**, 293
- Miyamoto, M., Sumi, Y., Komaki, S., Narushima, K. and Ishimaru, H. (1986) *Journal of Vacuum Science and Technology*, **A4**, 2515
- Mohri, M., Maeda, S., Odagiri, H., Hashiba, M., Yamashina, T. and Ishimaru, H. (1984) *Vacuum*, **34**, 643
- Poncet, A.M. (1987) *Vacuum*, **37**, 317
- Tohyama, A., Minami, Y., Yamada, T., Hirohata, Y. and Yamashina, T. (1989) Abstract VSA-WeA5, 11th International Vacuum Congress, Cologne, 25-29 Sept. 1989
- Touloukian, Y.S. (1989) In *A Physicist's Desk Reference*, (Anderson H.L., ed.) American Institute of Physics, New York, p. 336
- Weston, G.F. (1985) *Ultra-High Vacuum Practice*, Butterworths, London
- Weston, G.F. (1984) *Vacuum*, **34**, 619

# 7

## *Applications*

---

The use of vacuum processes in industry and research is enormous and will continue to increase. Applications range from the efficient extraction of highly temperature-sensitive complex molecules in the chemical industry to the efficient use and processing of strategically important elements such as chromium, titanium, nickel, etc. Many 'thin-film' technologies, ranging from the modification of the optical properties of glass surfaces for architectural applications to the deposition of films in the fabrication of integrated circuits, have also been made possible through advances in vacuum engineering. In the present chapter, some important applications will be reviewed.

### **7.1 Deposition of thin films**

As has already been indicated, the deposition of thin films on various substrates is of immense technological significance, areas of particular interest being:

1. Preparation of hard coatings. Tribologically hard coatings include oxides ( $\text{Al}_2\text{O}_3$ ,  $\text{ZrO}_2$ , etc.), nitrides ( $\text{TiN}$ ,  $\text{ZrN}$ ,  $\text{CBN}$ , etc.), borides ( $\text{ZrB}_2$ ,  $\text{TiB}_2$ , etc.) and carbides ( $\text{TiC}$ ,  $\text{ZrC}$ , etc.). Some aspects have been dealt with by Bunshah and Deshpandev (1989) and Sundgren and Henzell (1986).
2. Deposition of metallic coatings of aluminium, zinc, copper, gold and silver on plastic, glass and metals, both for effect and for protection. Applications include the manufacture of decorative and functional packaging, the coating of moulded plastic parts used in the automotive industry and the manufacture of metallized plastic film capacitors for the electrical and electronics industry.
3. Deposition of coatings for precision optics. Coated optical crown glass, sapphire and other substrates are used for the manufacture of broadband anti-reflective coatings, dichroic filters, laser mirrors, interference filters, etc. The range of evaporants is large and includes hard carbon, and a diverse variety of chemical compounds ( $\text{TiO}_2$ ,  $\text{MgF}_2$ ,  $\text{ThF}_4$ ,  $\text{ZnS}$ ,  $\text{ZnSe}$ , etc.). Single or multi-layers can also be laid down.
4. Application of multi-layer films to large areas of glass. Glass with high transparency and low emissivity for the reduction of heat loss is manufactured for architectural use whilst transparent, electrically conducting glass is used for motor vehicles.
5. Layers for passivation, insulation or protection deposited as part of the manufacturing cycle for integrated circuits. Specific examples will be dealt with in Section 7.2.



6. Deposition of single or multiple coatings of metals (Ni, Ti, Cu, steel, etc.), alloys (CoCr, FeNi, indium tin oxide, titania, etc.) on polymer substrates in the preparation of data storage media (magnetic and optic), flexible circuits, transparent heating foils and so on.

Films of precisely defined composition, stoichiometry, stability and even crystal structure are often required and it has been observed that their properties and the extent of adhesion are influenced significantly by the substrate (surface condition and temperature), pressure and the rate and method of deposition. Thin films may be formed by physical or chemical vapour deposition. The latter technique is used extensively in the fabrication of Very Large Scale Integration (VLSI) circuits. The present section will, however, be concerned mainly with aspects of physical vapour deposition.

### **7.1.2 Physical vapour deposition in vacuum**

Conventional vacuum evaporation can produce satisfactory results. In its simplest form, the equipment consists of a chamber that can be evacuated to a low base pressure and can accommodate the substrate(s) and source(s) of coating material. Substrates can range from relatively small items such as lenses for ophthalmic optical use to large areas of plastic film which have to be coated at rates of several square metres per second. Depending on the nature and extent of the substrate and the complexity and precision of the coating required, various types of vacuum system are used. These are shown schematically in Figure 7.1. The material to be deposited is either evaporated thermally in high vacuum or it may be sputtered by exposure to inert gas ions at pressures within the medium-vacuum range.

Solids may be vaporized by resistive heating, by means of electron beams or by inductive heating. For simple systems, the evaporant may be placed on a tungsten support wire or in a boat made of a suitable metal foil (W, Ta, Mo) (see Figure 7.2, for examples). It is essential that there should be no chemical reaction between the evaporant and holder. Metal filament and foil evaporators are resistively heated by the passage of an alternating current (up to a few hundred A). With such systems, the quantity of material vaporized depends on the evaporant and its temperature. The kinetic energy of the vaporized materials also depends on the temperature and is generally in the range 0.1–0.5 eV with a Maxwellian distribution. Further, evaporated particles have a spatial distribution corresponding to the cosine law. For uniformity ( $\pm 5\%$ ) of coating of wide substrates (up to 2 m or more), individual evaporators such as ceramic boats are placed side-by-side and automatically fed with the evaporant in the form of wire from a reel.

Some problems may arise in the use of conventional thermal evaporators. For example, a source of a particular design and material of construction may not be compatible with the range of desired evaporants and, particularly with metal foil boats, their flimsiness means that care must be exercised during setting up otherwise small differences can affect the repeatability of the coating. Electron beam (EB) evaporators may offer considerable advantages,

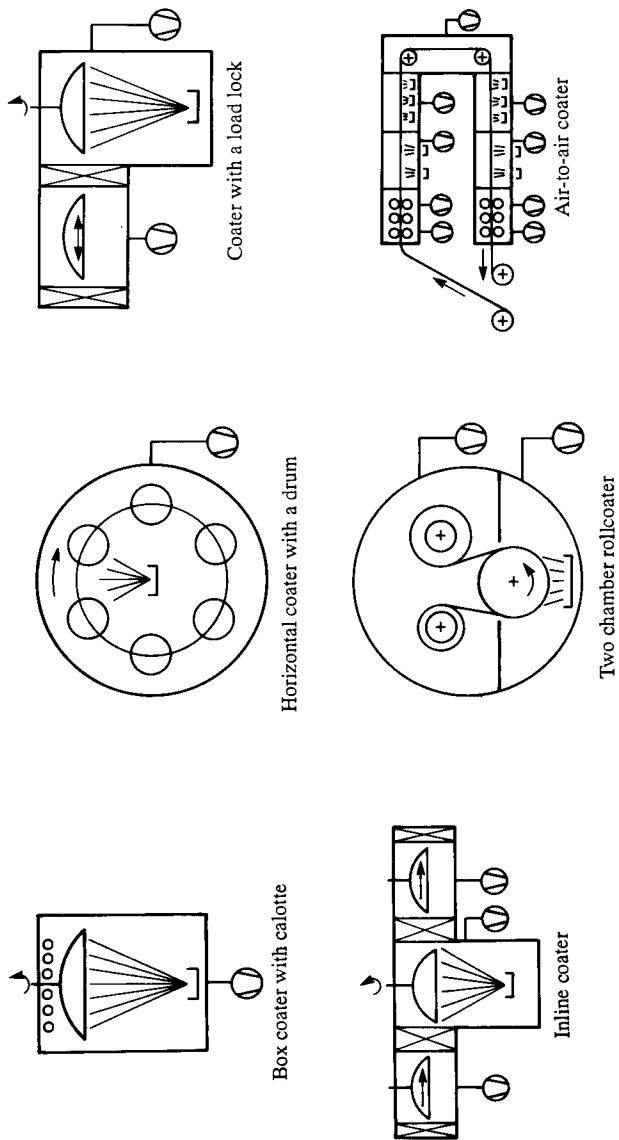


Figure 7.1 Schematic diagram of some PVD coating plants


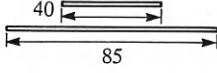
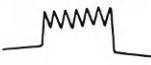
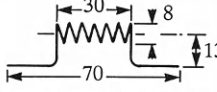
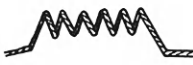
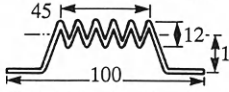

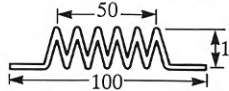

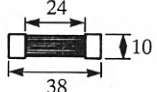

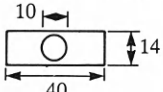

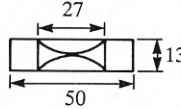

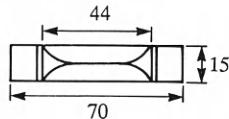
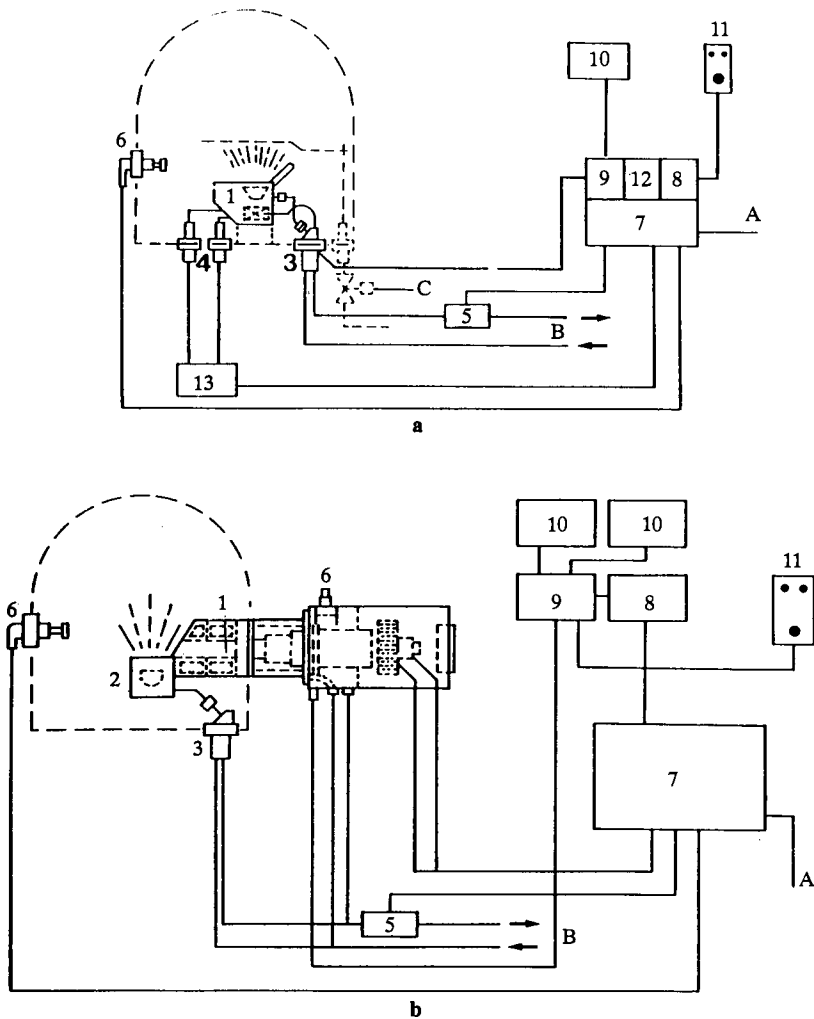
<p>(a)</p> 		<p>0.8 mm Ø 0.7 mm Ø</p>
<p>(b)</p> 		<p>2 × 0.8 mm Ø</p>
<p>(c)</p> 		<p>6 × 0.7 mm Ø</p>
<p>(d)</p> 		<p>18 × 0.7 mm Ø</p>
<p>(e)</p> 		<p>12 wires 0.6 mm Ø</p>
<p>(f)</p> 		<p>Sheet 0.2 mm</p>
<p>(g)</p> 		<p>Sheet 0.3 mm</p>
<p>(h)</p> 		<p>Sheet 0.1 mm</p>

Figure 7.2 Some tungsten evaporation sources used for the PVD of materials such as Al, (a-d), (f-h); Cr, (e-h); MgF<sub>2</sub>, (g) ; NiCr, (e)

particularly for deposition for precision optics and electronics. In an electron beam evaporator, the material to be vaporized is heated by the conversion of the kinetic energy of accelerated electrons. The electron source is usually a directly heated tungsten cathode and the beam generator, crucible and deflection system form a single unit (Figure 7.3). Commercial EB evaporators are available with a range of powers (2–25 kW, for example) and a permanent magnet produces the main deflection of the electron beam to maintain its position within the crucible. To ensure uniform evaporation, it is often



**Figure 7.3** Electron beam (EB) evaporator sources. (a) EB evaporator with  $270^\circ$  electron deflection, free evaporation angle of  $120^\circ$ . 1, E-beam evaporator; 3, combination feedthroughs; 4, high-voltage feedthroughs; 5, water flow monitor; 6, safety switch; 7, high-voltage power supply; 8, emission current controller; 9, X-deflection; 10, programmable beam deflection; 11, remote control; 12, selector switch for max. 3 ESV 4; 13, cathode heating transformer; A, power line; B, water; C, compressed air. (b) Pierce-type EB evaporator with free evaporation angle of  $110^\circ$ . 1, E-beam evaporator; 2, crucible; 3, water feedthrough; 5, water flow monitor; 6, safety switch; 7, high-voltage power supply; 8, emission current or rate control; 9, electron-optical beam control; 10, beam deflection; 11, remote control; A, power line; B, water

possible to oscillate and deflect the beam by means of an additional electromagnetic system for precision. Guns operate at pressures below  $5 \times 10^{-4}$  mbar but high (down to  $10^{-7}$  mbar) and ultra-high vacuum (down to about  $10^{-10}$  mbar) versions are possible. Crucible inserts may be formed from materials such as Mo, Ta and graphite. They can be stationary or rotate and have single or multiple hearths (volumes 1–150 cm<sup>3</sup>). Further, the hearth may be charged with a batch of material or by using wire feeds or rod feeding from beneath the crucible.

Plasma provides an *in situ* source of activated gas and energetic ion species which can be used to enhance various physical and chemical properties. Plasma-assisted processes can be divided into:

1. Plasma-assisted chemical vapour deposition (PACVD (PECVD)) with RF, microwave and other excitation). (See, for example, Musil 1986.)
2. Plasma-assisted physical vapour deposition (PAPVD). This may include d.c., RF, triode and magnetron sputtering, reactive sputtering and activated reactive evaporation.

PECVD processes will be discussed in more detail in the next section but the plasma generally used in thin-film technology is usually a low pressure ( $10^{-5}$ –1 mbar), d.c., RF, or microwave glow discharge. The plasmas are 'cold' and the ions and electrons are not in thermal equilibrium (the electron temperature is in the range 1–10 eV compared with an ion temperature of about 0.1 eV).

Electrons receive energy from the applied field and can activate reactants at near room temperature. Plasm-chemical processes are complicated and are influenced by many factors including RF-power, frequency, method of coupling, gas pressure and flow rate, chamber geometry, etc. Further, bombardment of the substrate by plasma ions can significantly influence film composition, microstructure, and growth rate. By selection of suitable precursors, a variety of materials have been deposited by plasma excitation/dissociation. Some examples are given in Table 7.1

Sputter deposition is an excellent example of PAPVD. The oldest method involves a low pressure plasma generated using an electric field between a positive electrode (anode) and a cathode (Holland, 1978). A parallel electrode arrangement is contained in a chamber which can be evacuated to a base pressure better than  $10^{-5}$  mbar. An inert gas (usually Ar) is admitted to the chamber at a pressure from 1 to  $10^{-2}$  mbar. The discharge is initiated by a

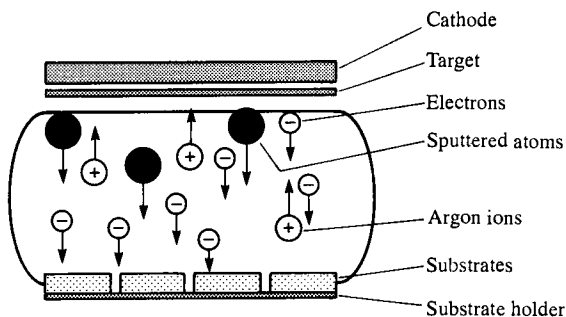
**Table 7.1** *Some compounds generated by plasm-chemical processes*

<i>Deposit</i>	<i>Precursor</i>
Silicides	W–Si from $WF_6 + SiH_4$
Mo	From $H_2/MoF_6$ at $T > 200^\circ C$
Si–Ge alloys	$GeF_4/SiF_4/SiH_4$
Si–C alloys	$SiH_4 (+CH_4, C_2H_4)$

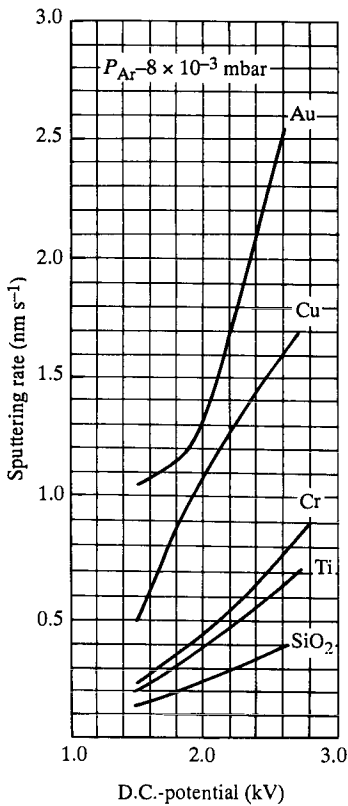
few free electrons that exist and are accelerated by the electric field. A steady state is quickly established and the gas begins to glow and a current flows between the electrodes (Figure 7.4). The electric field between cathode and anode is not uniform and most of the voltage drop occurs close to the cathode in a region known as the 'cathode dark space'. Only ions arriving in this region will take part in sputtering. The remainder are lost in the gas. Beyond the cathode dark space, there is a region of high ionic density (the negative glow) where secondary electrons can ionize gas. Secondary electrons can gain sufficient energy to reach the substrate and are a major source of substrate heating and temperatures between 300°C and 500°C can be established. Increasing both the working pressure and the substrate-cathode distance can reduce their effect, the latter decreases the deposition rate and the former can increase gas incorporation into the layer.

The conditions for d.c. sputtering are relatively wide. The potential difference can be within the range 1–5 kV with cathode current densities of several mA cm<sup>-2</sup>. Data showing sputtering rate as a function of d.c. potential for various targets are shown in Figure 7.5. From this, it can be seen that the rate is relatively low for a metal such as gold and, comparatively, extremely low for insulators such as SiO<sub>2</sub>. This situation can be greatly improved by feeding a high frequency alternating voltage to the cathode (RF sputtering). After the plasma has ignited, the very different mobilities of the two types of charge carrier in the RF field lead to a net accumulation of negative charge on the cathode surface.

A capacitor in series prevents this charge leaking through an external circuit. The negative d.c. potential provides the accelerating voltage gradient for positive gas ions and influences significantly the sputtering rate. Reactive RF sputtering is a technique widely used to grow thin films of compound material. The process involves sputtering either a single elemental target in a reactive atmosphere or a compound target in an inert gas mixed with a small amount of reactive gas for stoichiometry control. Many examples of the use of the technique are to be found in the literature. For example, Kaneko *et al.*



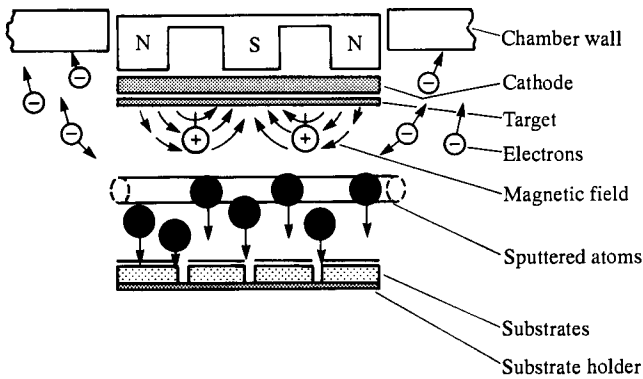
**Figure 7.4** Schematic diagram of d.c. sputtering



**Figure 7.5** Plot of sputtering rate against d.c. potential for various targets

(1988) deposited crystalline  $\text{WO}_3$  films by sputtering a tungsten target in the presence of an  $\text{Ar} + \text{O}_2$  mixture at about  $5 \times 10^{-2}$  mbar.  $\text{Cu}_x\text{S}$  has deposited by RF sputtering from a  $\text{Cu}_2\text{S}$  target in the presence of  $\text{Ar} + \text{H}_2$  (Iborra *et al.*, 1987).  $\text{H}_2$  permitted control of the stoichiometry of the film.

By confinement of the plasma immediately in front of the cathode by means of a magnetic field (Figure 7.6), very high degrees of gas ionization at relatively low pressures are obtained and, consequently, an increase in the sputtering rate by a factor of 5–10 in comparison with conventional methods (Table 7.2). Penning first suggested the use of a magnetic field to increase the probability of ionizing collisions between electrons and neutral gas although the technique of magnetron sputtering was not established until the mid-1970s. In detail, a negative potential is applied to the target and a discharge generated in the region between it and the substrate. Positive ions bombard the target surface, bringing about sputtering and the emission of secondary electrons. These enter the region of crossed electric and magnetic fields (about 0.04 T) and follow cycloidal paths with a net drift that is orthogonal to



**Figure 7.6** Schematic diagram of planar magnetron sputtering system

$\vec{E}$  and  $\vec{B}$ . This traps electrons. In regions of efficient electron trapping, ionization probability is a maximum. This increases the plasma density and gives high deposition rates ( $> 10 \text{ nm s}^{-1} \text{ kW}^{-1}$ ). Although the rate increases with power, other factors have a significant effect. Magnetic field design is particularly important, determining the uniformity of erosion of the target (Almeida, 1989).

Deposition rates decrease with increasing gas pressure. This is because sputtered atoms and molecules passing through the plasma region suffer multiple collisions with sputtering gas atoms and lose initial energy. A related factor is the target–substrate distance (Rizk *et al.*, 1989). During travel, sputtered atoms make multiple collisions and may be lost through deposition on the surroundings (Rizk *et al.*, 1990). Obviously, depending on the mean free path of the molecules, many collisions can occur and the number

**Table 7.2** Typical sputtering rates for a 150 mm magnetron at 3.5 kW ( $20 \text{ W cm}^{-2}$ )

Material	Rate	
	$\text{nm s}^{-1}$	$\mu\text{m min}^{-1}$
Al	11.0	0.66
Au	50.0	3.0
Cr	12.0	0.72
Mo	15.0	0.90
Nb	12.0	0.72
Pd	36.0	2.16
Si	10.0	0.60
W	10.0	0.60
$\text{Al}_2\text{O}_3$	2.0*	0.12
Ni/Cr	12.0	0.72
$\text{SiO}_2$	2.5*	0.15



increases with the target distance. Rizk *et al.* (1989) calculated that, travelling 55 mm, between 20 and 80 collisions would occur with  $2.5 \times 10^{-2}$  and 0.1 mbar Ar, respectively.

Diode/magnetron sputtering is used for:

1. Metallization of semiconductor devices.
2. Deposition of magnetic layers for floppy and rigid disks.
3. Coating architectural glass.
4. Growth of hard coatings.

A range of metals and alloys have been deposited (see, for example, Spencer and Howson, 1986 and Tan, *et al.*, 1991) and, by means of reactive magnetron sputtering, films of oxides such as vanadium oxide (Kusano *et al.*, 1988), indium tin oxide and cadmium tin oxide (Lewin *et al.*, 1986) and nitrides ( $\text{TiN}_x$ , Musil *et al.*, 1988;  $\text{SiN}_x$ , Paule *et al.*, 1987) can be prepared.

Recently, the demand for thin films of very well defined composition, stoichiometry, crystal structure and stability has led to the development of deposition techniques involving the use of ion beams (Armour *et al.*, 1986). Processes that are available include:

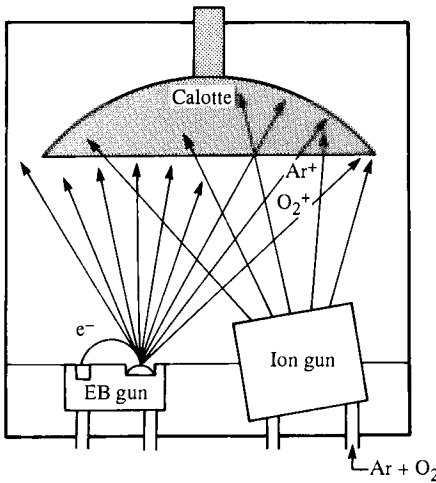
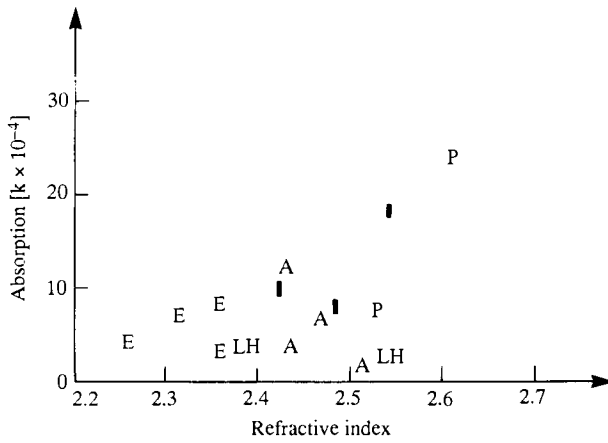
1. Ion beam-assisted deposition.
2. Ion beam sputtering.
3. Reactive ion beam sputtering (ion implantation).

Several reviews of the use of ion beams in non-semiconductor applications are available (see, for example, Colligon, 1986; Dearnaley *et al.*, 1986). Ion implantation is, of course, not a deposition technique but a versatile and highly controllable method for the modification of surfaces by the introduction of buried layers. For example, the resistance of stainless steel to high-temperature oxidation is increased by the implantation of 180 keV  $\text{Al}^+$  while  $\text{N}_2^+$  implantation improves the wear resistance of steels (for knives, moulds, etc.), titanium (for prostheses) and tungsten carbide (for wire-drawing dies). With ion-assisted deposition, the already complex, multi-step process of condensation from the gas phase (see Maissel and Glang, 1983) is influenced by other effects including:

1. Sputtering of weakly-bonded ad-species, including impurities.
2. Bombardment-induced diffusion.
3. Physical mixing at the interface which enhances adhesion.

These in turn are influenced by the substrate temperature and thermal treatment and ion energy.

Ion-assisted coating processes may involve the simultaneous ion bombardment and coating of the substrate (Figure 7.7). The target itself may or may not have been sputtered by bombardment with ions from a separate source. Ion sources which are extensively used have a Kaufmann-type configuration. Ions are generated by electron-impact ionization in a gas such as Ar using thermionic electrons from a filament. A magnetically sustained plasma is thus ignited at low pressures and ions extracted and accelerated towards the



**Figure 7.7** Schematic diagram showing ion-assisted deposition. E, evaporation with EB gun; A, ion-assisted evaporation; I, ion-beam sputtering; P, ion plating; S, sputtering; LH, results of Goetzelmann *et al.* (1989) (Ref. J. M. Bennett, E. Pelletier, G. Albrand, J. P. Borgogno, B. Lazarrides, C. K. Carniglia, R. A. Schmell, T. H. Allen, T. Tuttle-Hart, K. H. Guenther and A. Saxer. From *Applied Optics*, 28, 3303 (1989))

sample by applying an appropriate potential to a grid. The use of a filament may restrict the use of Kaufmann sources to non-reactive gases. Oxygen and other reactive gas ions may, however, be generated using a RF-excited source (Goetzelmann *et al.*, 1989). Ion-assisted processes can yield adherent, high density coatings for a variety of applications including optical thin films (Varasi *et al.*, 1986) and wear-resistant layers. Satisfactory material can,

however, be prepared only under well-controlled conditions. Duckworth *et al.* (1987), for example, investigated the effects of some deposition parameters (pumping speed, gas flow, bias voltage) on the composition, structure and microhardness of titanium aluminium nitride coatings, deposited on stainless steel tools by magnetron sputter ion plating (Muenz *et al.*, 1982) using a 50–50 atomic % Ti–Al target and Ar/N<sub>2</sub> atmospheres. Maximum hardness was obtained with Ti<sub>2</sub>Al<sub>2</sub>N<sub>4</sub> and, in order to form this compound, it was found necessary to ensure not only the correct flux of the constituent elements at the surface but also the provision of sufficient energy to allow stable structures to be obtained.

Goetzelmann *et al.* (1989) studied the deposition of TiO<sub>2</sub> layers starting with a source of Ti<sub>2</sub>O<sub>3</sub> in the presence of a partial pressure of oxygen of  $3 \times 10^{-4}$  mbar. Ions from a Kaufman-type source with ion kinetic energies over 500 eV were used to bombard the substrate (Figure 7.7). Conventional processes yield inhomogeneous coatings, the refractive index of which decreases with thickness. IAD yielded perfectly homogeneous layers with a refractive index of 2.47 at 550 nm.

In order to control and monitor deposition processes, coating rate and thickness control must be carried out. Monitoring may be carried out by a variety of techniques, including the use of quartz crystal resonators, *in situ* photometry, electron impact emission spectroscopy and, to a lesser extent, ellipsometry. Although essential to the successful performance of a particular deposition process, film-thickness monitoring usually has little relevance to the vacuum technology and some of the methods will, therefore, be described only briefly.

In quartz crystal monitors, a plano-convex quartz plate, incorporated into an oscillator circuit, provides and maintains a suitable resonant frequency. In the presence of a deposit on the surface of the plate, the frequency changes according to the mass of the deposit, the exposed area of the crystal and a constant that depends on the distribution of the deposit. After calibration of the monitor in the deposition system it may be used to control both the rate and the thickness. Commercial quartz crystal monitors are relatively compact. The crystal (a thickness of approximately 0.3 mm provides a frequency in the range 6.0–7.0 MHz) is placed between two parallel surface electrodes and mounted in a water-cooled stainless steel housing of approximately 30 × 15 mm. The exposed surface is approximately 8 mm in diameter and may be mounted up to 80 cm from the point of connection with external feed-throughs. In this regard, it is advisable always to wrap the electrical connections on a monitor with aluminium foil to prevent short circuiting due to penetration of conductive material. Quartz crystal monitors are usually compatible with both high and ultra-high vacuum systems, they are capable of thickness measurement from 0.1 to 10<sup>5</sup> nm at rates from 0.01 to 100 nm s<sup>-1</sup> on an almost continuous basis. However, the crystals must be changed at appropriate intervals.

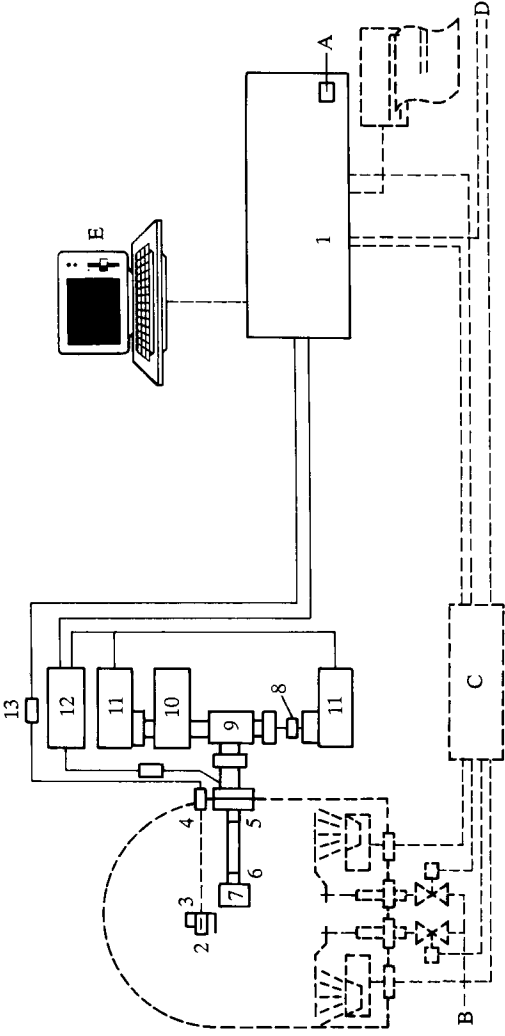
Thickness monitoring during the preparation of precision multilayer optical coatings must be carried out with excellent resolution and stability over long periods of time. For this purpose, double-beam-type photometers have been

developed which measure either the reflectance or transmittance of the substrate or a test glass (Zoeller *et al.*, 1989). In an *in situ* photometer developed by Boos *et al.* (1986), light emitted from a suitable source (halogen lamp, 400–2400 nm; deuterium lamp, 200–400 nm) is split into measurement and reference beams using fibre-optic bundles. The measurement beam passes into the coating chamber via an optical vacuum feedthrough and is focused on the substrates. Both continuous and intermittent measurements may be performed. After reflectance or transmittance at the test point, the measurement beam is combined with the reference beam via two chopper discs rotating on a common axis between the light source and the measuring bundle return and between the source and the reference bundle. Light then passes to the detector with the sample and reference beams displaced in time.

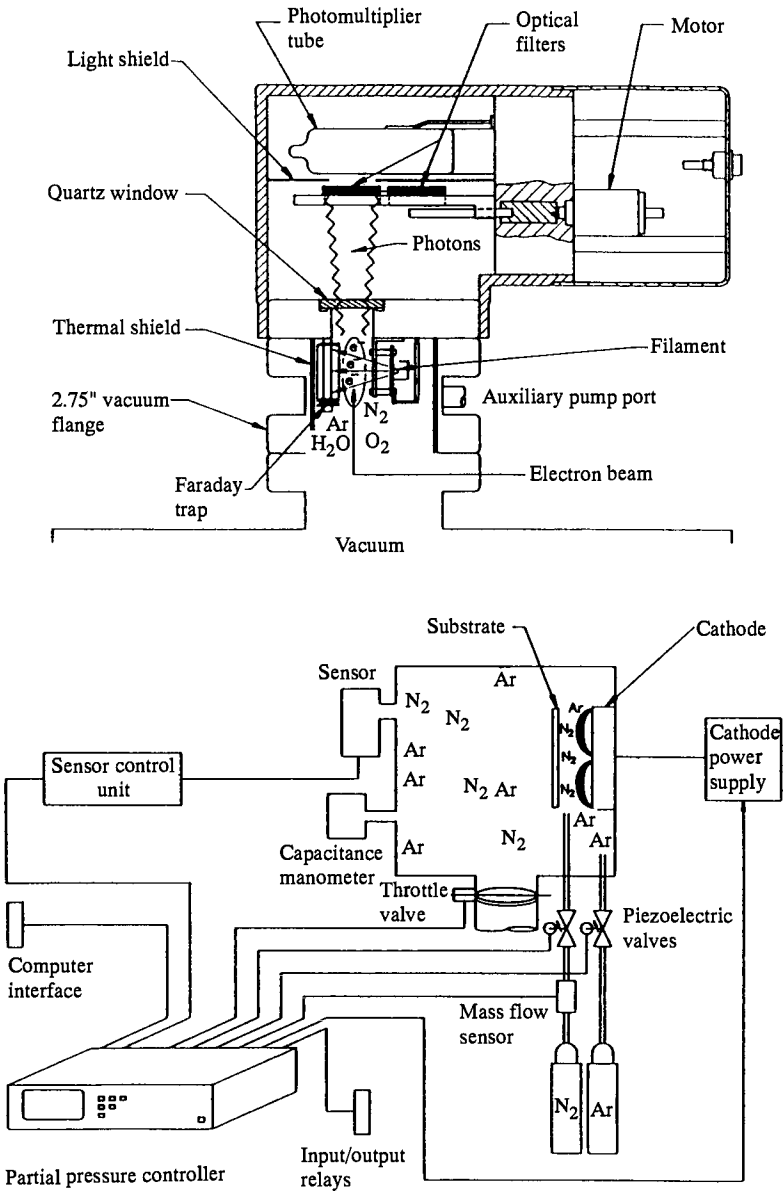
A technique termed EIES (electron impact emission spectroscopy) has been exploited both for the measurement of film thickness, control of deposition rate and also for partial pressure control during, for example, reactive high-rate sputtering and evaporation processes. In EIES, material (either vapour emerging from an evaporation source or gas particles from the chamber) is bombarded by a low-energy electron beam. Excitation may occur in which outer-shell electrons are promoted to higher energy levels, emitting characteristic photons on falling back to the ground state. Photons generated during this process pass through a vacuum-tight window transmitting in the appropriate wavelength range. Outside the vacuum chamber, the appropriate wavelengths are separated by a narrow-band interference filter or a grating monochromator. For example, characteristic lines can be observed for copper at 218.2, 324.7 and 327.4 nm while lines for aluminium are at 309.3 and 396.1 nm and this is directly proportional to the number density of the emitting material in the sensor.

Figure 7.8 shows a coating chamber fitted with both quartz crystal and EIES sensor heads, the outputs of which are fed into a deposition controller. Residual gases in a vacuum system such as O<sub>2</sub>, N<sub>2</sub>, H<sub>2</sub>O, etc. may also be measured by EIES. Figure 7.9(a) shows the sensor in which electrons are emitted from an Ir/ThO<sub>2</sub> filament. Emission of photons from the gas molecules is monitored as before and partial pressure can easily be determined by calibration against, say, a capacitance manometer. N<sub>2</sub> has a characteristic line at 392 nm while H<sub>2</sub>O emits at about 310 nm. The incorporation of an EIES partial pressure monitor into a process chamber is shown in Figure 7.9(b). Information from the sensor is received by a partial pressure controller which regulates gas partial pressure by the adjustment of piezoelectric valves.

Finally, layer thickness measurements have been carried out using ellipsometry. The technique can be used for the determination of the optical properties of surfaces. For use in vacuum systems, the source is attached to the system and polarized laser light (780 nm) passed through stress-free windows to impinge on the substrate with an angle of incidence of about 70°. The reflected beam again passes a stress-free, vacuum-tight window to an analyser before arriving at a silicon diode photodetector. This measures the intensity of the beam at various settings of the analyser prism and the state of



**Figure 7.8** Diagram showing a process chamber fitted with a quartz crystal sensor and EIES sensor for the control of two evaporators and shutters.  
1, deposition controller; 2, quartz crystal sensor; 3, sensor head with shutter; 4, feedthrough for quartz crystal; 5, optical feedthrough for EIES; 6, straight optical coupling; 7, sensor; 8, filter; 9, beam splitter; 10, monochromator; 11, photodetector assembly; 12, sensor head supply; 13, oscillator; A, power line; B, compressed air; C, power supply; D, electrical cabinet; E, computer



**Figure 7.9** Schematic diagram of (a) an EIES sensor used for residual gas measurements on a vacuum system and (b) the sensor incorporated into a partial pressure controller for reactive sputtering

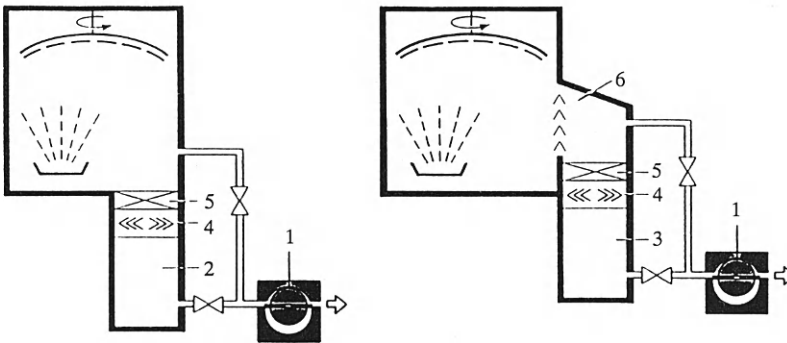
polarization of the reflected light beam can be deduced from this by Fourier analysis. The final step is the calculation of the psi-delta signature from which refractive index, absorption and layer thickness can be determined. Presently, the drawback with ellipsometry is that it is too slow to be used for on-line process control although it is capable of giving precise data on a layer. Nevertheless, *in situ* ellipsometry has given valuable insights into some surface processes (see, for example, Thomas *et al.*, 1989).

### 7.1.3 Deposition systems

#### 7.1.3.1 Batch coaters

High-vacuum coaters which are designed for handling small- to medium-sized batches of substrates are used particularly in the optics industry. In the design of such equipment, attention has to be paid to the presentation of the substrates and their pretreatment (glow-discharge and ion cleaning, heating) and the source of coating material. Additional factors that have to be considered include ease of access and the useable chamber area. Several years ago, batch coaters were usually bell jars which could be raised and lowered onto a base plate which incorporated feed-throughs for evaporation sources, substrate cleaning facilities, etc. Over a period of time box coaters developed in which access to the chamber was via a hinged door. Unfortunately, the pumping port was connected to the base plate and this could take up approximately 30% of the useable area. In recent developments, the preferred position for the pumping port is in the chamber wall thus freeing the base for the accommodation of feedthroughs for sources and monitoring equipment.

Figure 7.10 shows two designs of box coater. The vacuum chamber is usually made of stainless steel with a diameter in the range 500–1100 mm. Access to the chamber is via a door having a width which is approximately



**Figure 7.10** Schematic diagram of the configuration of a modern, high-vacuum coating system. 1, mechanical pump; 2, oil diffusion pump ( $3000 \text{ l s}^{-1}$ ); 3, oil diffusion pump ( $12000 \text{ l s}^{-1}$ ); 4, baffle (water and/or  $\text{LN}_2$  cooled); 5, valve; 6, chevron baffle

30% of circumference. In modern coaters, the interior of the chamber is fitted with a shield that can be heated or cooled. Heating is often required during loading/unloading in order to minimize adsorption of moisture whilst cooling may be an advantage during evaporation since it inhibits desorption from the surfaces. Depending on the degree of cleanliness required and the throughput, box coaters can be evacuated with diffusion, cryo or turbomolecular pumps. If substrates with high outgassing rates (such as PMMA or CR39) are used then additional pumping capacity for water vapour can be incorporated in the form of an LN<sub>2</sub>-cooled baffle or Meissner trap. Pressure measurement with such systems usually involves the use of Pirani and hot- or cold-cathode ionization gauges whilst control of the deposition process is carried out using a quartz crystal monitor, photometer or one of the devices indicated earlier.

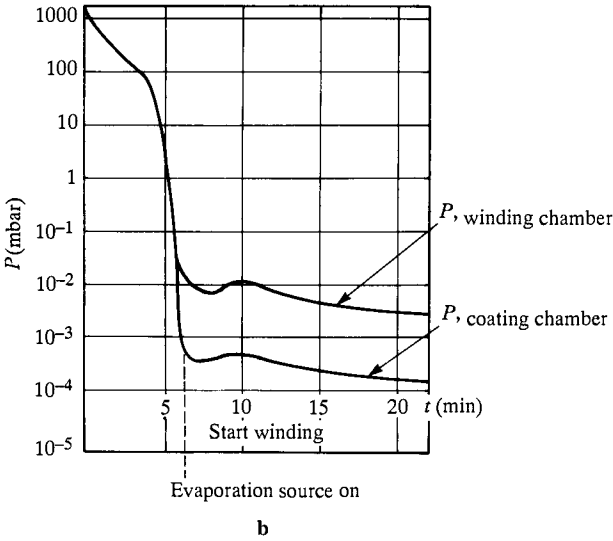
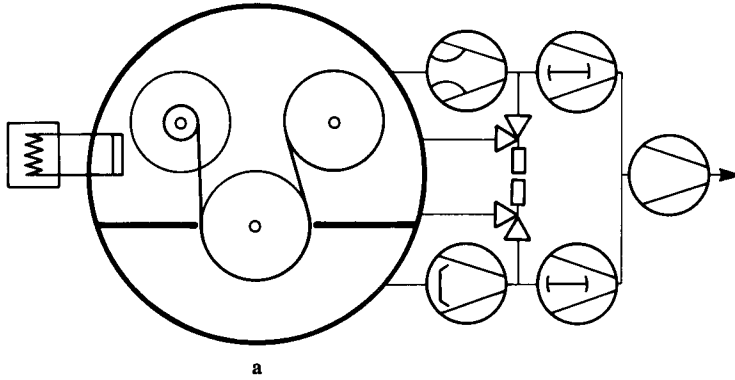
Box coaters are also used extensively in many other areas of thin-film research and development, including investigations into metallization by various techniques, ion-assisted deposition and sputtering and some highly specialized areas of research such as the deposition of high  $T_c$  superconductors. For such applications, a wide range of substrate-conditioning methods, coating sources and process-monitoring equipment must be available. Other facilities may include load-lock connections to external systems for, say, surface analysis by SIMS and Auger electron spectroscopy. Coating systems capable of being evacuated down to  $10^{-9}$  mbar using both turbomolecular and cryopumps are now commercially available.

#### 7.1.3.2 Web coaters

In recent years, the market for vacuum metallized plastic films and papers has increased significantly. For packaging materials, the vacuum deposition of aluminium onto a film is the preferred method of preparation. The use of aluminium is extensive because it is a relatively inexpensive material which has excellent barrier properties against water, light and oxygen (thereby increasing storage life) and produces a coating with an attractive appearance. A layer of aluminium which is only  $0.04\ \mu\text{m}$  thick has the required barrier properties.

Commercially available web coaters can accommodate rolls of paper or plastic with widths from 0.2 to 2 m and with thicknesses from  $1.5\ \mu\text{m}$  to 0.5 mm. They can coat at rates up to  $10\ \text{m s}^{-1}$ . The winding and coating chambers are separately pumped (Figure 7.11(a)). The coating chamber is operated at a pressure of about  $10^{-4}$  mbar maintained by diffusion pumps while the winding chamber is equipped with oil vapour booster pumps that can accommodate large quantities of gas at about  $10^{-2}$  mbar. A pressure–time profile for the two chambers is shown in Figure 7.11(b). Paper may have a residual moisture content up to 5% (w/w) and by the incorporation of cold traps (operating with LN<sub>2</sub> or with a refrigerant at  $-75^\circ\text{C}$ ) within the winding chamber, extremely high pumping speeds for water vapour are obtained. Layers of ice that are formed are usually removed automatically by heating the trap. With web coaters, the evaporant is usually fed continuously as a wire to resistively heated ceramic boats. Up to 24 boats are required for substrate widths of more than 2 m and each is supplied by current from a separate controller thus

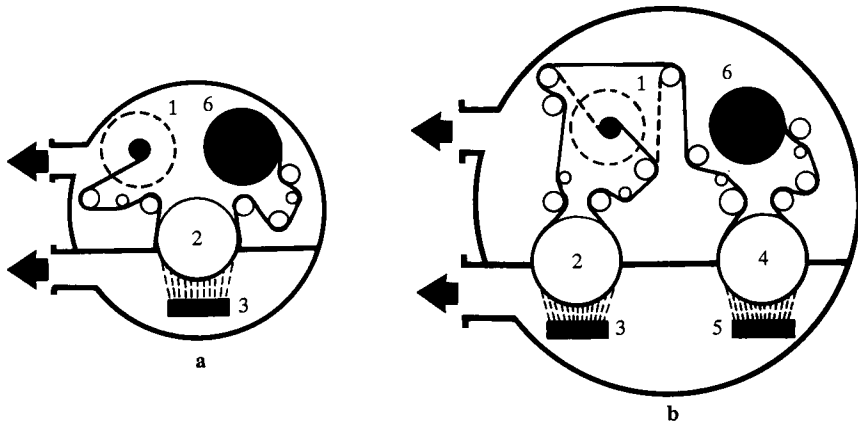




**Figure 7.11** Schematic diagram of a two-chamber vacuum web coater for packaging material. (a) Pumping system. (b) Typical P versus t curve

ensuring a high degree of uniformity in the coating. In some configurations, coating may be carried out on one or both sides of the substrate (Figure 7.12).

A specialized activity in the field of web coating is the preparation of metallized films for use in capacitors. The substrates may be capacitor paper, polyester, polypropylene or polycarbonate ranging in thickness from 1–2  $\mu\text{m}$  (ultra-thin polyester and polycarbonate films) up to 10–20  $\mu\text{m}$  for power capacitors. Depending on the construction of the capacitor, the metal layers may be aluminium, zinc or a combination, applied to one or both sides of the



**Figure 7.12** Schematic diagram of a system for (a) one-side and (b) two-side coating of packing material or capacitors. 1, unwind; 2, coating drum; 3, coating source; 4, second coating drum; 5, second coating source; 6, rewind

substrate. The basic design of aluminium coaters has been discussed earlier. Zinc coaters usually involve one-chamber systems and pre-coating the substrate with silver must be carried out in order to enhance the adhesion of zinc. In certain cases, the coating drum is cooled during the deposition process for efficient heat removal from films that would otherwise be damaged. Data storage media such as floppy disks and magnetic tape are also produced by coating a polymer web with a multi-layer film produced by sputtering or electron beam evaporation. Details of these systems are given in Table 7.3. A web coater may contain several sputtering cathodes, which must be rigorously

**Table 7.3** Characteristics of vacuum web coaters for the manufacture of data storage media

	Floppy disks	Video tape	Substrate	Coating	Storage density (bits/inch)
Coater with Magnetron sputtering	U	NU	PET (70–100 $\mu\text{m}$ )	CoNi	$6 \times 10^4$
			Polyimide (25–50 $\mu\text{m}$ )	CoCr	$9 \times 10^4$
Coater with EB-evaporation	U	U	PET (4–20 $\mu\text{m}$ )	CoNi	$7.5 \times 10^4$
			Polyimide (10–20 $\mu\text{m}$ )	CoCr	$9 \times 10^4$
				NiFe	

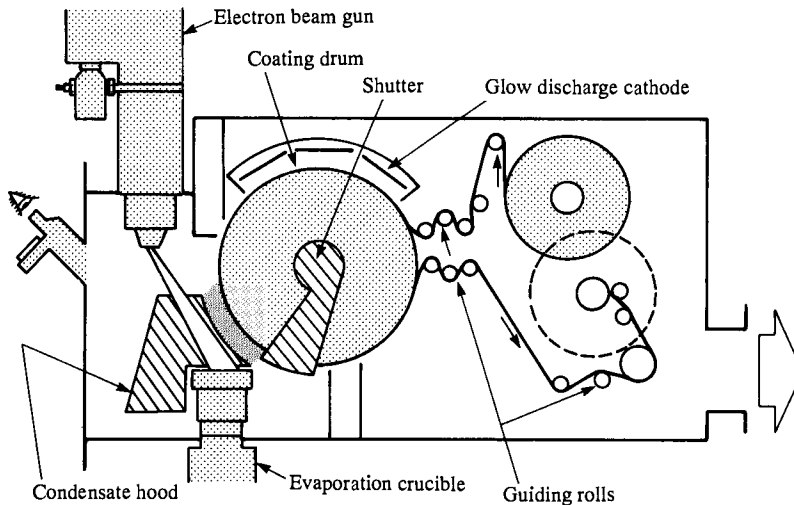
U = used for; NU = not used.

separated, together with other stations in which the web is treated by glow discharge, plasma-enhanced deposition and other processes. A schematic diagram is shown in Figure 7.13.

### 7.1.3.3 *In-line Coaters*

#### (i) *Large-area coating*

Vacuum coating of large substrate areas is used to manufacture low-emissivity and solar control glass for architectural use. The process is also used to produce transparent, electrically conducting and reflective coatings for use in the automotive industry. For such applications, strict control must be exerted on the coating process, and the coatings themselves must have optical properties that are constant to within 0.5%. The largest standard coaters can deal with up to two million m<sup>2</sup> glass/year and usually consist of a series of chambers through which the glass is transported. After a preliminary cleaning at atmospheric pressure, substrates (which may consist of sheets up to 3 × 6 m) are placed into a vacuum-lock entry/glow discharge chamber and the pressure reduced to about 10<sup>-2</sup> mbar. The ignition of a glow discharge in Ar/O<sub>2</sub> may be necessary for further cleaning of the substrate. From this chamber, substrates pass via a transfer chamber which holds a queue of material, and allows a transition from discontinuous to continuous flow, to the coating chamber. Within this chamber, various sputtering modules are arranged in series. Each is separately pumped (usually by turbomolecular pumps) and has its own gas inlet system for reactive or non-reactive sputtering. Low emissivity films consist of a 10 nm thick silver layer and two layers with high reflectance in the infra-red region but high transmittance in



**Figure 7.13** *Vacuum web coater for the production of data storage media*

the visible region of the spectrum. For solar control, a 'hard' metal layer – to control the transmission of light and energy – is deposited in conjunction with two oxide interference films which affect the colour seen in reflection. After coating, material passes again through a transfer chamber to a vacuum-exit lock.

*(ii) Modular systems*

In-line systems are also used for the production of sophisticated data storage media including rigid magnetic, optical and magneto-optical disks. The last type of disk usually consists of two protective layers (AlN or SiO<sub>2</sub>), a metal alloy layer (for example, FeCoTb) and a laser-light reflecting coating (Al). For magnetic disks, recording layers of NiFe, CoCr (perpendicular) or Cr, CoNi(Cr) (longitudinal) and C on aluminium are used. For the production of high-quality disks, loading and unloading is performed in clean rooms. Modular systems allow various deposition procedures to be incorporated into a particular coating process. These include various cleaning (by d.c. glow discharge or RF-sputter etch) and sputtering (RF diode, d.c. diode, RF magnetron, etc.) stages. High-vacuum pumps such as turbomolecular or cryopumps are used to evacuate the load locks and the deposition chamber. In the most sophisticated production facilities where various coating procedures may be used, a process computer is usually used to store the relevant 'recipes'.

For other systems where the deposition process may involve a relatively simple procedure (such as metallization of compact discs and CD-ROMs), annular chambers are used in which individual discs are coated. With circular-path coaters, loading and unloading takes place at the same place and vacuum locks are provided between the coater and this point. Up to 1500 discs per hour can be produced in a relatively small unit and, based on this throughput, approximately 1 s is available for the evacuation of a polycarbonate (for CD manufacture) disc of 120 mm diameter and 1.2 mm thick. The vacuum pumps used on a typical commercial circular coater (annular vacuum chamber volume about 45 litres) are a combination of turbomolecular (1000 l s<sup>-1</sup>), Roots (450 m<sup>3</sup> h<sup>-1</sup>) and rotary vane pumps. Aluminium (55–70 nm thick) is deposited by magnetron sputtering and up to 10<sup>5</sup> coatings can be obtained from a source.

Circular path, single-disk coaters are also available for the deposition of multiple layers (Al<sub>2</sub>O<sub>3</sub>, AlN, SiO<sub>2</sub>, Te-alloys, etc.) during the manufacture of magneto-optical disks. Process stations can be configured for etching, heating and d.c.- or RF-sputtering processes. In a typical configuration, for magneto-optical disks, triple film coatings can be deposited consisting of a dielectric layer, a layer of the active medium and a final dielectric layer. The vacuum system consists of a load lock chamber, evacuated with a Roots-rotary vacuum pump combination, a degassing chamber (turbomolecular pumped), circular transfer line and processing chamber (with multiple turbomolecular pumps) and an unloading chamber. A throughput of up to 180 disks/hour can be obtained with appropriate pumping and sputtering rates, yielding a cycle period of 20 s.

## 7.2 Vacuum technology in the semiconductor industry

Since its invention in 1947 and its incorporation into primary planar integrated circuits in 1959, there have been tremendous developments in the design of integrated circuits and the technology required for their manufacture. Silicon is the starting element for the great majority of these devices although other materials, based on compounds of Groups III and V and II and VI of the periodic table, are of importance (Sze, 1983; Moss and Ledwith, 1988). With present-day devices, the packing density is determined primarily by the lateral dimensions of the patterns, which define the shape of the transistors and electrical interconnections, that can be reliably produced by lithography. As can be seen in Table 7.4, current trends in Very Large Scale Integration (VLSI) technology indicate that, in the 1990s, advanced devices will be based on the ability to produce features that are between 0.5 and 0.25  $\mu\text{m}$  in size. This will make significant demands on the production capabilities for lithography.

The basic steps in the fabrication of circuits are:

1. Growth of thin layers of material on the substrate (e.g. oxidation of Si to  $\text{SiO}_2$ ; deposition of  $\text{Si}_3\text{N}_4$ ).
2. Formation of patterns to define the shape of transistors and electrical interconnections. This may involve photo-, X-ray or EB lithography.
3. Introduction of dopants to create regions within the semiconductor that are responsible for switching. Doping may be accomplished by high-temperature diffusion or, preferably, by ion implantation.

In practice, the fabrication sequence can be very complex, involving many photolithographic steps, layer depositions and ion implantations. An examination of the conditions necessary for these processes indicates that a range of reactants and reaction products must be handled, many of which are toxic, corrosive or flammable. Several steps must be performed under vacuum and highly-sophisticated systems are required (Duval, 1988; O'Hanlon and Fraser, 1988). A summary of some processes, reactants and vacuum condi-

**Table 7.4** *Trend in device manufacture (from Speight, 1987)*

	1980s	1990s
Device dimensions ( $\mu\text{m}$ ):		
Lateral	3 – 1	1 – 0.1
Vertical	1 – 0.05	0.05 – 0.005
Materials	Si, GaAs, InP	Si, InP – AlGaAs, LiNbO <sub>3</sub>
Wafer size (cm)	5–7.5	7.5–10
Complexity (number of transistors)	$10^4$ – $10^5$	$> 10^6$

tions is given in Table 7.5. The types of vacuum pump involved are given in Table 7.6.

The backing pump is the critical component in many of the applications and the use of oil-sealed rotary vane pumps in the semiconductor industry has been reviewed (Bachmann and Berges, 1986; Kuhn and Bachmann, 1987). An adequate supply of oil having the correct properties is essential for their normal operation and, particularly in semiconductor processing, problems can arise because of chemical attack on the fluid by the pumped material and the accumulation of substances (solids, polymers, etc.) which can both alter its properties and block the oil pathways. To some extent, the problem can be overcome by the use of the appropriate pump fluid and sophisticated, continuously operated filters.

Perfluoroalkyl ethers (PFAPE) and perfluoropolyethers (PFPE) are relatively unreactive but they are decomposed by Lewis acids (e.g.  $\text{AlCl}_3$ ,  $\text{BCl}_3$ ). If the latter compounds are to be handled successfully, highly refined mineral oil ('white oil') must be used. Protection is also afforded by the use of filters which can remove particles mechanically (porous or fibrous material) or can eliminate certain substances by adsorption (charcoal, finely divided alumina, Fuller's earth, etc.). Recently, there has been an accelerating trend towards the elimination of fluids and sealants from vacuum pumps; and 'dry' pumps capable of working between  $10^{-1}$  mbar and atmospheric pressure have been developed (Burger *et al.*, 1990).

Processing equipment requiring a high throughput of gas in the medium-vacuum range (O'Hanlon, 1980) usually requires Roots-backing pump combinations. A significant feature of Roots pumps is that the pumping chamber should be free of fluid. Although lubricants are present in both the motor end and gear end of the pump, these areas are separated from the working chamber by piston rings and O-rings. Pumps fitted with canned motors are particularly vacuum tight and leaks of ambient air into the pump are thus minimized (Figure 7.14). Further, by control of the rotational speed of the pump by means of a frequency converter used in conjunction with a pressure gauge and controller, the pressure and pumping speed can be suitably adjusted to match the process. Of the high-vacuum pumps, turbomolecular pumps are used for plasma etching, ion implantation, sputtering and plasma-enhanced chemical-vapour deposition.

The presence of corrosive gases and vapours and abrasive particles makes the use of protected pumps necessary. Protection is usually afforded by the use of suitable fluids in pumps with lubricated bearings and the admission of a purge gas such as dry  $\text{N}_2$  to provide a continuous flow of gas into the forevacuum area. The latter device inhibits the penetration of process material (both in the gas and solid phase) into the motor area of the pump. Oil-diffusion pumps present problems not only because of the reactivity of the pump fluid but also because of backstreaming. The use of liquid nitrogen traps is not recommended since trapping of highly reactive gases and products (including toxic and corrosive material) can occur. Refrigerator-cooled cryopumps are used in similar applications to turbomolecular pumps. They generate low pressures cleanly and have high pumping speed. Because they

**Table 7.5** Some processes carried out in vacuo during the fabrication of integrated circuits

Parameter	Process					
	Epitaxy	CVD*	Plasma deposition	Etching†	Ion implantation	MBE
Base pressure (mbar)	$10^{-3}$	$10^{-4}$	$10^{-4}$	$10^{-5}$	$10^{-8}$	$10^{-11}$
Working pressure (mbar)	50–150	1–0.1 (LP–) $5\text{--}5 \times 10^{-2}$ (PE–) 2–500 (MO–)	$3\text{--}5 \times 10^{-2}$	$5\text{--}5 \times 10^{-3}$	$10^{-1} \text{--} 10^{-4}$	$10^{-3} \text{--} 10^{-8}$
Process gas	$\text{SiH}_4$ , $\text{SiCl}_4$ , $\text{SiH}_2\text{Cl}_2$ , $\text{PH}_3$ , $\text{B}_2\text{H}_6$	$\text{SiH}_4$ $\text{SiH}_2\text{Cl}_2/\text{N}_2\text{O}$ $\text{SiH}_2\text{Cl}_2/\text{NH}_3$	$\text{SiH}_4$ + various ( $\text{O}_2$ , $\text{CO}_2$ , inert, hydrocarbons)	halogenocarbons ( $\text{CF}_3\text{Br}$ , $\text{CCl}_4$ , $\text{C}_2\text{F}_6$ , ( $\text{Cl}_2$ )) $\text{BCl}_3$ , $\text{SiF}_4$ , $\text{SF}_6$	$\text{BF}_3$ $\text{PH}_3$ $\text{AsH}_3$	$\text{AsH}_3$ , $\text{PH}_3$
Reaction products	Various	$\text{SiO}_2$ , $\text{HCl}$ , $\text{NH}_4\text{Cl}$ , $\text{H}_2$	Various	See text	See text	See text
Use	epi-Si	poly-Si $\text{SiO}_2$ $\text{Si}_3\text{N}_4$	a-Si-H Si-C $\text{SiO}_2$	Si, poly Si, Al, GaAs, metals	Si doping	$\text{In}_x\text{Ga}_{1-x}\text{As}$ $\text{Ga}_x\text{In}_{1-x}$ $\text{As}_{1-y}\text{P}_y$

\* Chemical vapour deposition processes

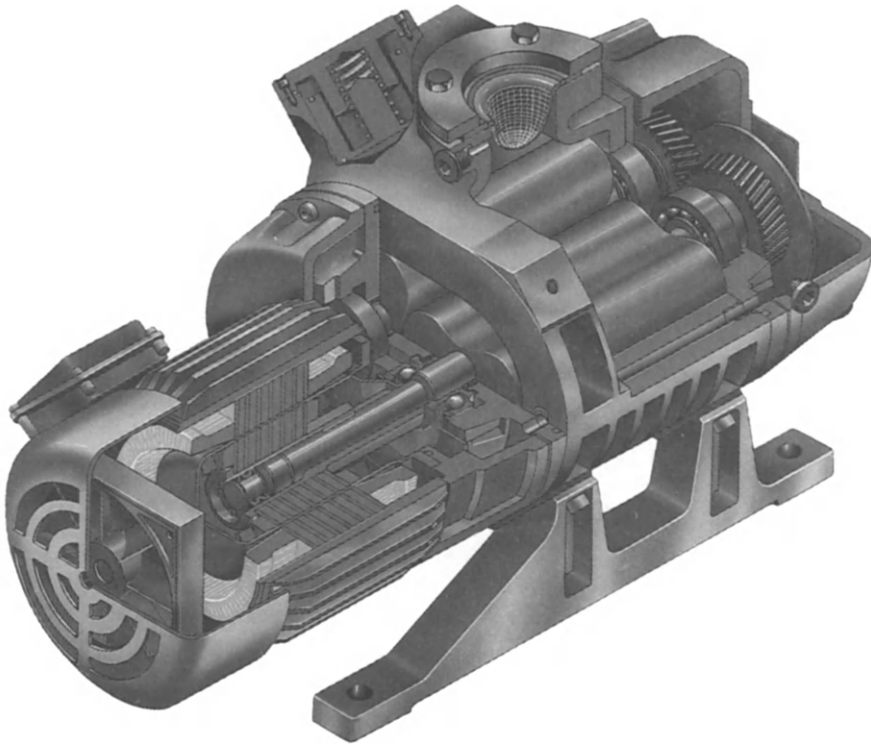
Including PE (plasma enhanced), LP (low pressure), MO (metal-organic) CVD.

† Including plasma etching, reactive ion etching

**Table 7.6** Types of vacuum pump encountered in integrated circuit fabrication process steps

Process	Pump						
	Rotary vane pump	Dry pump	Roots pump	Diffusion pump	Turbomolecular pump	Cryopump	
LPCVD	+	+	+	-	-	-	
PECVD	+	+	+	-	+		
Etching F-based Cl-based metals	+	+	+	(+)	+	+	
MBE	+	+	+	(+)	+	+	
MOVPE	+	+	+	(+)	-	-	
Ion implantation: Source Beam line Target	+	+	-	(+)	+	(+)	
	+	+	-	(+)	+	+	
	+	+	-	(+)	+	+	
Sputtering/evaporation	+	+	-	-	+	+	





**Figure 7.14** *Leybold Roots vacuum pump type WSU 501*

are entrapment pumps, however, care should be taken for their safe regeneration.

To highlight some of the points raised, some important processes in semiconductor production will now be reviewed.

### **7.2.1 Deposition processes**

#### **7.2.1.1 Chemical vapour deposition (CVD)**

The formation of thin films is essential during the fabrication of VLSI circuits. The deposited materials have to fulfil various functions including:

1. Passivation and the provision of insulation and barriers between layers.
2. Protection of a structure during etching and subsequent processing.
3. Provision of conductive links within devices.

The materials used include metals and alloys (Cr, Al, W), semiconductors (Si) and insulators ( $\text{Si}_3\text{N}_4$ ,  $\text{SiO}_2$ ).

CVD is a relatively simple yet versatile technique. It involves the reaction (decomposition, hydrolysis, reduction, ammonolysis, etc.) of an appropriate

gaseous precursor to yield a thin solid film. Depending on the deposition conditions, one can distinguish between:

1. Low-pressure CVD (LPCVD).
2. Plasma-enhanced CVD (PECVD).
3. Laser CVD (LCVD).
4. Photolytic CVD (UVCVD).

A significant disadvantage of CVD is that relatively high temperatures are involved and control of the phase composition is often difficult. To produce a uniform, coherent, defect-free film, careful control must be exerted on the reaction conditions (John and Jones, 1987). For example, the growth of epitaxial silicon in hydrogen from precursors such as  $\text{SiCl}_4$  and  $\text{SiHCl}_3$  at atmospheric pressure is more likely to produce pattern shift and autodoping than its deposition at low pressures. A summary of some CVD processes is given in Table 7.7.

**Table 7.7** Conditions for the deposition by CVD of Si,  $\text{SiO}_2$  and  $\text{Si}_3\text{N}_4$

Product	Reactants	T (°C)	Conditions
Epitaxial Si	$\text{SiCl}_4$	1150–1250	60–100 mbar
	$\text{SiHCl}_3$	1100–1200	Reduced-pressure
	$\text{SiH}_4$	950–1050	CVD (RPCVD)
Polycrystalline Si	$\text{SiH}_4$ (neat or in $\text{N}_2$ )	600–650	0.2–1 mbar LPCVD
Amorphous Si	$\text{SiH}_4$	< 575	Atmospheric-pressure CVD (APCVD LPCVD)
Low-temperature $\text{SiO}_2$	$\text{SiH}_4/\text{O}_2/\text{N}_2$	300–500	–
Intermediate-temperature $\text{SiO}_2$	$(\text{C}_2\text{H}_5\text{O})_4\text{Si}$ ; Tetraethylortho-silicate or tetraethoxysilane (TEOS) in $\text{N}_2$	500–850	20–80 mbar
High-temperature $\text{SiO}_2$	$\text{Si}_2\text{H}_2\text{Cl}_2/\text{N}_2\text{O}$	900	LPCVD
$\text{Si}_3\text{N}_4$	$\text{SiH}_4$ or $\text{SiH}_2\text{Cl}_2/\text{NH}_3$	700–800	LPCVD

In the case of silicon, dopants can also be introduced by the addition of volatile hydrides such as  $B_2H_6$ ,  $PH_3$  and  $AsH_3$  to the reaction.

Metallic layers of high purity and good adhesion can also be deposited by LPCVD. For example, aluminium can be formed using trimethyl aluminium or triisobutyl aluminium. Tungsten has also been deposited by the reduction of  $WF_6$  with hydrogen under LPCVD conditions. Finally, the formation of thin films of transition metal silicides, which is an important step in VLSI technology, by CVD has been amply demonstrated (Rosser and Tomkins, 1985; Aylett and Tannahill, 1985).

By selection of suitable precursors, a wide range of material can be deposited by plasma excitation. Examples are amorphous silicon, carbon, Si-C and Si-Ge alloys,  $Si_3N_4$ , silicides and silicon dioxide (John and Jones, 1987). In PECVD, plasmas are usually produced by the application of a high frequency electric field across a gas in which a discharge is generated between two parallel plate electrodes. The plasmas are 'cold' in that the temperature of the ions is a few hundred K while that of the electrons is considerably greater. Electrons initiate the deposition process by exciting or dissociating the precursors and, thereafter, the active species migrates to the substrate surface where reaction occurs. The physical and chemical properties of deposited films depend in a complex manner on parameters such as chamber geometry, RF power, frequency and method of coupling, temperature, gas pressure and flow rate. It is usual, therefore, to determine with a single-chamber research and development system the optimum parameters for a process. These can then be transferred to multi-chamber production systems having identical chambers and cathodes. A typical, modern, single-chamber system is made of stainless steel and has a vacuum lock with an integrated wafer (size up to 200 mm) transport system. For low-pressure processes, the chamber is evacuated using a turbomolecular pump backed with either an oil-sealed rotary vane pump or, for demanding operations, an oil-free pump. In many systems, however, pumping is achieved with a combination of Roots and backing pumps.

The precursors used in low-pressure thermal and plasma processes are highly reactive and, unless adequate precautions are taken, they can rapidly destroy the gas-handling equipment. Corrosive gases include  $BCl_3$ ,  $HCl$  and dichlorosilane. Highly toxic ( $PH_3$ ,  $AsH_3$ ,  $B_2H_6$ ) or flammable ( $SiH_4$ ,  $H_2$ ) materials may have additional properties which can cause handling problems. Particulates and dusts may also be formed in LPCVD and PECVD. These include silica and oxides of boron and phosphorus which are generated in any system in which silane,  $B_2H_6$  or  $PH_3$  comes into contact with oxygen. Dust is also generated during the deposition of silicon oxynitride and nitride and, in the latter process, ammonium chloride is formed which deposits in cooler parts of the system. Bearing in mind the properties of the compounds described, rigorous precautions have to be taken to protect the equipment. These include the use of relatively unreactive fluids and oil filters where appropriate, the use of inert gases for ballasting and purging the pump body and the use of suitable scrubbers on the exhaust lines from the pumps. The functioning of these components must be overseen by suitable monitoring equipment.

The use of various vacuum pump oils has already been mentioned and, from the point of view of specific production processes, their suitability is shown in Table 7.8 (for completeness, etching has been included. This will be discussed in a later section).

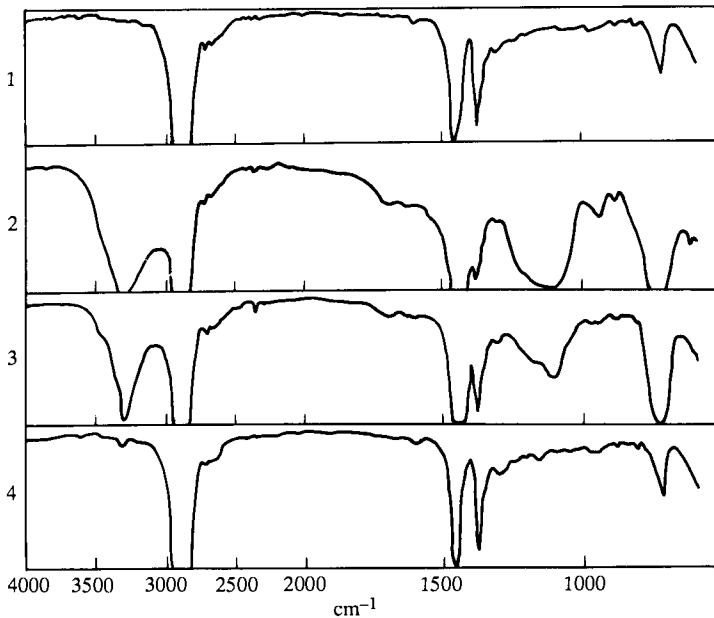
Filtration units are also available commercially to maintain the lubricant in good condition. The necessity for their use became obvious with the widespread use of plasma processing and incorporation into the lubrication system is in the form of full-flow or partial-flow devices (see Figure 2.10, page 40). The effect of oil filtration on a standard hydrocarbon-based vacuum oil is shown in Figure 7.15, from which it can be seen that full-flow filtration maintained the oil in good condition over the duration of the experiment. Considerable care must be taken when handling contaminated fluids and filters and the AVS recommended practices have been described by O'Hanlon and Fraser (1988).

In most semiconductor applications, the use of an inert gas ( $N_2$ ) purge and ballast is invaluable. Ballasting reduces both the condensation of vapours such as TEOS (see Table 7.7) in the pump and can reduce the possibility of explosion with spontaneously flammable material such as silane. Gas flow is usually controlled and adjusted within an appropriate range of flow rates, and a non-return valve is built into the inert gas supply to prevent the influx of air in the case of failure.

Other devices that have improved the performance of vacuum pumps are moisture barrier systems and special traps. Moisture barriers are necessary when moisture-sensitive compounds are handled and back-diffusion of water vapour from the exhaust line into the pump can occur. Although purging the exhaust line with  $N_2$  minimizes the effect, its elimination can only be guaranteed with a barrier. Water-cooled traps have been developed for the LPCVD of silicon nitride. During this process, large amounts of ammonium chloride are generated which forms a gelatinous residue within oil-sealed pumps. Incorporation of a trap cooled to about  $12^\circ\text{C}$  into the vacuum line

**Table 7.8** *Suitability of some oils for some semiconductor processes (Kuhn and Bachmann, 1987)*

<i>Process</i>	<i>Standard hydrocarbon-type oil</i>	<i>White oil</i>	<i>PFPE</i>
Si deposition	(+)	+	-
$Si_3N_4$ deposition	+	+	-
$SiO_2$ deposition (using $O_2$ )	-	-	+
Metal etching	-	-	+
Si, $SiO_2$ and $Si_3N_4$ etching (using F-containing gases)	-	(+)	+



**Figure 7.15** *The effect of oil filtration on vacuum pump oil as shown by infra-red spectroscopy. Curves 1–4 show the spectra of: 1, fresh mineral oil; 2, unfiltered oil after use in a CVD process; 3, as (2) but with a by-pass filter; 4, as (2) but with a full-flow filter*

before the pump improves the situation considerably. Treatment of the effluent from plasma reactors, prior to discharge into the atmosphere, is also necessary. Many compounds can be removed by scrubbing the gases with water or solutions of strong bases and detergents. Other methods of disposal include adsorption and combustion. With scrubbing systems, the exhaust gas and scrubbing liquid counterflow through a reaction column packed with inert spheres. This is an effective method of removing water-soluble substances such as HCl, HF,  $\text{COCl}_2$  and  $\text{NH}_3$  but adsorption on active charcoal may be necessary to remove halogenocarbons. Further, gases such as arsine may be removed with only limited efficiency in scrubbers or may cause difficulties with adsorption beds. Under these circumstances combustion or reaction with ferric chloride may be necessary. Various methods of disposal of effluents have been discussed by Duval (1988).

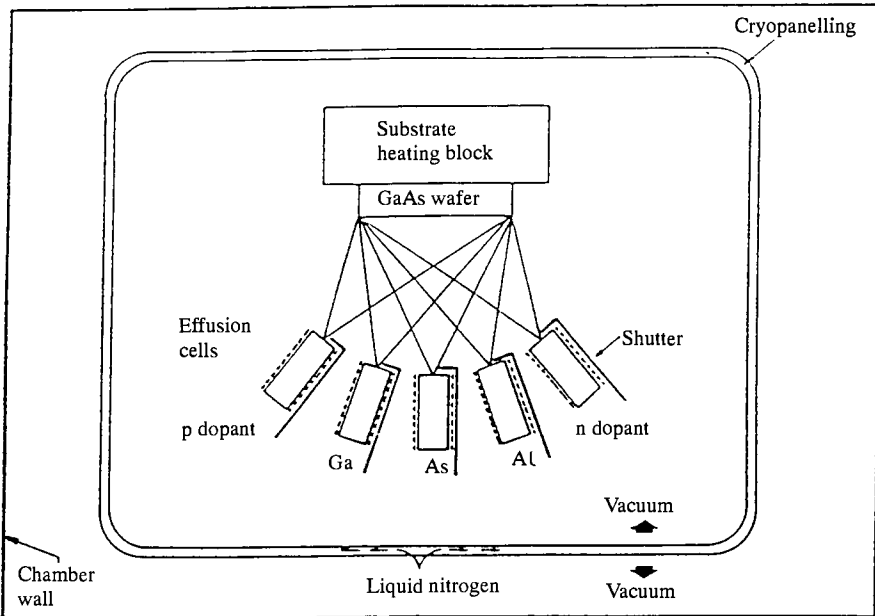
#### **7.2.1.2 Metal organic vapour phase epitaxy (MOVPE)**

MOCVD has been used extensively for the preparation of high purity, polycrystalline and epitaxial layers of a wide range of semiconductor materials (see, for example, Williams, 1989). MOVPE is a closely related technique which yields single crystal deposits. They are processes that are

widely accepted for the production of certain III-V ( $\text{GaAs}$ ,  $\text{InP}$ ,  $\text{Ga}_{1-x}\text{In}_x\text{As}$ ,  $\text{InAs}_{1-y}\text{P}_y$ , etc.) and narrow band-gap II-VI materials. In MOVPE, the vapour of a metal alkyl (trialkylaluminium, -gallium, -indium) is carried in a stream of  $\text{H}_2$  and decomposes on a heated substrate in the presence of a group V hydride. Dopants are introduced as  $\text{H}_2\text{Se}$ ,  $\text{H}_2\text{S}$ ,  $\text{SiH}_4$  (n-type) or diethylzinc, bis-cyclopentadienyl magnesium (p-type). Deposition usually takes place between atmospheric pressure and about 150 mbar. The precursors in both MOCVD and MBE are often pyrophoric and very hazardous chemicals. Because of their toxicity and reactivity, alternatives have been sought for  $\text{AsH}_3$ ,  $\text{PH}_3$  and the metal alkyls. Exhaust materials from the reactor consist mainly of, for example, unreacted group V hydrides and elemental group V species either in the vapour phase or as dust. Some of the ways already indicated may be used to protect the vacuum pumps and clean the discharge.

### 7.2.1.3 Molecular beam epitaxy (MBE)

MBE is an expensive deposition technique which is being used for the preparation of III-V compounds. In this technique, atomic or molecular beams are generated from effusion cells and allowed to impinge on the heated substrate under UHV conditions ( $10^{-10}$  mbar). With correct conditions, a single crystal epitaxial film grows on the substrate which is typically a semiconductor wafer (Figure 7.16). The sources are maintained at room



**Figure 7.16** Schematic diagram of an MBE system for the growth of GaAs/GaAlAs structures (after Davies, 1988; reproduced by kind permission of author and publisher)

temperature for gaseous precursors or heated to produce an adequate vapour pressure for solid-phase material (typically,  $10^{-2} - 10^{-3}$  mbar). A microcomputer is used to control cell and substrate temperatures and the operation of mechanical shutters, allowing the required composition to be achieved. To obtain uniformity over a large area, the substrate is rotated.

Experimental systems for MBE are complex, consisting of stainless steel chambers, pumped into the UHV region with ion pumps or cryopumps. Liquid nitrogen-cooled panels are also included. Substrates are introduced to the growth chamber via a load lock. Surface analytical probes can monitor the chemical and structural properties of the layers before, during and after growth. Some of these facilities may be mounted in a separate chamber.

Some aspects of MBE of III-V compounds have been reviewed by Joyce (1989). Growth of films of ZnTe, ZnSe, ZnS and related compounds by MBE has been discussed by Mason (1987).

### 7.2.2 Etching processes

Plasma etching has replaced wet etching for the fabrication of microcircuits because of its good resolution and adaptability to automation. The purpose of etching is to produce the pattern shape pre-defined by lithography by the removal of some deposited material. Plasma etching techniques may be characterized according to the rate, anisotropy, selectivity and texture (Flamm and Mucha, 1987). With regard to anisotropic/isotropic etching, the former involves preferential etching normal to the surface thus producing a crater which has vertical sidewalls and a flat bottom defined by the original substrate. With isotropic etching, there is no selectivity in the process and, therefore, no preferred direction. A plasma etching system consists essentially of a reactor, which can be maintained at the appropriate pressure ( $1-10^{-2}$  mbar), having opposed, parallel plate electrodes. The reactant gas stream is metered into the reactor and activated by the application of an RF voltage applied between the electrodes. Under these conditions, the substrates to be etched are exposed to reactive neutral and charged species from a plasma. The reaction between etchant and substrate surface should yield a volatile product which leaves the reactor along with unconverted precursors and passes to the vacuum pumps. A number of phenomena may play a role in etching (Flamm and Mucha, 1987) including:

1. Sputtering.
2. Chemical etching (also termed 'isotropic' etching) in which neutral species react with the substrate to yield the volatile product.
3. Ion-enhanced etching in which ion-substrate interactions damage the surface and render it more susceptible to attack by the etchant.
4. Inhibitor-protected sidewall, ion-enhanced etching in which the ions 'clear' inhibitors from certain surfaces.

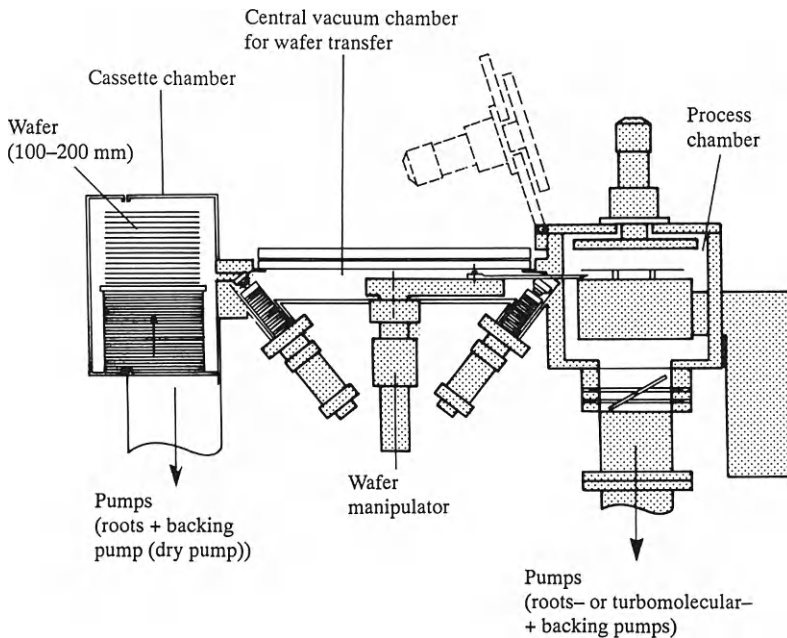
To be effective, the etching process should have a high selectivity at an acceptable rate, a degree of anisotropy and yield a volatile product. Some of the reactants/etchants used in plasma etching are shown in Table 7.9.





single wafer is processed. Currently, the most advanced etchers are based on a central vacuum chamber which accommodates a manipulator which can transfer a wafer from the loading/unloading stations to any one of up to four process chambers. Figure 7.17 shows the main features of this type of system. Depending on the material to be etched, so the configuration may alter. For example, for the reactive ion etching of aluminium and related alloy layers, a three-chamber system may be used – two chambers for etching whilst the third is used for anti-corrosion treatment. A recent advance in configuration of the etching chamber has involved the use of electron cyclotron resonance (ECR). This allows an increase in the density of the plasma by almost an order of magnitude over that generated in a parallel plate reactor.

Plasma etching places great demands on the vacuum system, not only because of the nature of the reactants but because of the reaction products. An excellent illustration is to be found in the reactive ion etching of Al, AlSi and AlSiCu where chlorine-containing reactants (chlorine and  $\text{BCl}_3$ ,  $\text{SiCl}_4$  or carbon tetrachloride) are used. The immediate product of this etching process is solid  $\text{AlCl}_3$  which can be hydrolysed to give hydrogen chloride and aluminium hydroxide. Further, both  $\text{BCl}_3$  and  $\text{Cl}_2$  are highly toxic and reactive and yield HCl on hydrolysis. If carbon tetrachloride is used as the etching gas, then a range of halogenocarbons ( $\text{C}_2\text{Cl}_4$ ,  $\text{C}_2\text{Cl}_6$ ,  $\text{C}_4\text{Cl}_6$ ,  $\text{C}_4\text{Cl}_8$ , etc.) is also generated. Typically, the process chamber will be evacuated by a protected turbomolecular pump backed by an oil-sealed rotary vane pump,



**Figure 7.17** *A single-wafer, cassette-to-cassette plasma etching system*

usually containing a PFPE, equipped with oil filters, an inert gas ballast/purge system and a control and monitoring system.

A great problem encountered with aluminium etching is the large amount of particulate aluminium chloride produced (about 40 g/1000 wafers (4 inch)). This substance tends to collect in the pump oil and has to be removed by filtration. It also brings about considerable decomposition of PFPEs yielding volatile products which leave the pump via the exhaust. Bachmann and Kuhn (1990) have investigated the stability of partially branched (Fomblin Y) and fully branched (Krytox) PFPE oils towards  $\text{AlCl}_3$  generated by etching AlSi wafers and were unable to detect any difference in behaviour. It appeared that about 1 litre of PFPE was lost per 30 000 wafers processed. These authors also observed the appearance of a peak at 1796–1809  $\text{cm}^{-1}$  in the infra-red spectrum of contaminated oils which was ascribed to  $-\text{COCl}$  and a gradual deterioration in the ultimate pressure attainable with a PFPE-sealed rotary vane pump. In the presence of small amounts of moisture, partial hydrolysis of  $\text{AlCl}_3$  will also occur yielding a voluminous, gelatinous precipitate that can block filters. Bachmann and Kuhn (1990) confirmed the advantage of using a moisture barrier system on the exhaust line and also observed that, by the use of a two-stage filter consisting of 10  $\mu\text{m}$  and 3  $\mu\text{m}$  alumina, both the  $\text{AlCl}_3$  and any precipitate formed, could be removed.

Finally, by the use of a claw-type dry pump, it has been shown (Bachmann and Kuhn, 1990) that as long as the partial pressure of  $\text{AlCl}_3$  in the pump is below that of  $\text{AlCl}_3$  at the temperature of the pump exhaust, then no condensation occurs. Further, if an inert gas is admitted to purge the pump stages, the amount of transportable  $\text{AlCl}_3$  increases significantly. Thus at an average pump temperature of 100°C and a gas throughput of 100 standard  $\text{cm}^3 \text{m}^{-1}$ , 2.5  $\text{mg min}^{-1}$  of  $\text{AlCl}_3$  was transported. With 1  $\text{m}^3 \text{h}^{-1}$  of  $\text{N}_2$  purge, under similar conditions, 420  $\text{mg min}^{-1}$  could be removed. Examination of the pump after the simulated etching of  $10^5$  wafers (equivalent to the removal of 4 kg  $\text{AlCl}_3$ ), revealed that it was in perfect condition.

### 7.2.3 Introduction of dopants

The controlled introduction of dopants can be carried out by two methods:

1. High-temperature diffusion.
2. Ion implantation.

With thermal diffusion, the operation is often separated into two process steps:

1. Pre-deposition.
2. 'Drive-in' or dopant redistribution.

#### 7.2.3.1 Diffusion

The pre-deposition process relies on the attainment of a solid-solution of the dopant in the substrate. This is achieved by accumulating an excess of dopant atoms on the surface maintained at a particular temperature for an appropriate time (B, 950–1100°C, 10–40 min; P, 900–1050°C, 10–40 min).

Thereafter, the substrates are removed and treated to remove excess dopant and dopant-rich surface layers. Drive-in is then performed in a high-temperature furnace.

### **7.2.3.2 Ion implantation**

Ion implantation in semiconductors is an established production technique for the precise introduction of dopants. For silicon, the most common implantation species are boron, phosphorus and arsenic and advanced CMOS devices require up to eleven implants (Aitken, 1986). For implantation into III-V compounds, Si and Se are commonly used.

Ion implantation involves the generation of ionized species from a suitable gas or vapour source and their extraction and acceleration towards the target. Prevention of beam neutralization and scattering and the maintenance of cleanliness throughout the system is essential. Although the vacuum levels within the implanter sub-systems (source, extraction/acceleration region, target chamber) may be different, demands on the vacuum system are equally great. Particularly for substrate doping in the semiconductor industry, the pumps must generate and maintain contamination-free conditions and be capable of handling efficiently a range of highly reactive (including toxic and corrosive material) gases and products.

Within the ion source, pressures must be maintained in the range  $10^{-1}$  to  $10^{-3}$  mbar in the presence of gases such as  $\text{BF}_3$ ,  $\text{PH}_3$ ,  $\text{AsH}_3$  (Si implantation) or  $\text{SiF}_4$ ,  $\text{SiH}_4$ ,  $\text{H}_2\text{Se}$  (for III-V compounds). Higher pressures lead to significant ion losses and a reduced dose at the target. Conventional pump sets based on diffusion pumps can contaminate the system, particularly during high-dose implantation. Turbomolecular pumps have obvious advantages but back-streaming from oil-lubricated forepumps must then be considered. In the acceleration region, pressures under  $10^{-7}$  mbar must be achieved to reduce ion neutralization and recombination. Because of their cleanliness and low ultimate pressures, cryopumps are preferred.

Maintenance of high vacuum in the target chamber is essential since beam broadening and charge-exchange with neutrals can lead to dose error. The interaction of the ion beam with the wafer brings about  $\text{H}_2$  evolution from the photoresist. This can cause a rapid pressure increase (from  $10^{-6}$  to  $10^{-3}$  mbar in a few seconds). A clean system with a high throughput for hydrogen is required and again cryopumps or turbomolecular pumps are extensively used.

Recently, there has been an accelerating trend towards the elimination of fluids and sealants from vacuum pumps and significant advances have been made. The current status of clean pumping systems, such as a combination of magnetic-bearing turbomolecular pumps and multi-stage, claw-type dry pumps has been discussed (Hucknall and Kuhn, 1991).

## **7.3 Vacuum technology in metallurgical processes**

In metallurgical applications, the performance of a process at a pressure significantly below atmospheric enables materials that are reactive in the

presence of atmospheric gases to be handled efficiently. This includes increasing the effectiveness of addition of such elements to relatively stable material. It also favours physico-chemical phenomena such as the dissociation of some oxides and nitrides and the removal of dissolved gases and high-vapour pressure material.

The range of elements and alloys that has been processed under vacuum is extensive and includes virtually every transition metal, elements in Groups 2,3,5 and 6 of the Periodic Table, some lanthanoids (Ce, Er, Nd, Sm) and thorium, uranium and plutonium. Alloys include those of aluminium with lithium and titanium as well as complex materials such as special steels and Ni-based and Co-based superalloys. As demand has grown for metals with a very high degree of cleanliness and structural homogeneity, so the use of vacuum processing has increased in the production not only of sophisticated materials but also of low-alloy and carbon steels.

### 7.3.1 Steelmaking

Process developments introduced since the 1950s have completely altered the nature of steelmaking. At the outset processing at sub-atmospheric pressures was carried out merely in order to reduce the hydrogen and nitrogen content of the melt for special forging ingots. The current trend, however, is to use the furnace as the primary melting vessel and perform secondary operations such as refining and the adjustment of chemical composition in, for example, the ladle (Hsiao *et al.*, 1980).

Mass steel is produced for structural use in, for example, general engineering whilst special steels, such as those containing a high proportion of chromium, are found in more demanding applications (chemical and cryoengineering; in the manufacture of gas-turbine engines, etc.). Degassing has a profound influence in steelmaking, improving the quality and reducing production costs, and a very large number of processes are available (Table 7.10 and Figure 7.18).

**Table 7.10** Processes used in vacuum steel degassing

LL	Ladle-to-ladle degassing
RH/CAB	Vacuum circulation process/calcium argon blowing
TD	Tap degassing
VD	Vacuum ladle degassing
VAD	Vacuum arc degassing
VCP	Vacuum circulation process
VID	Vacuum induction degassing
VOD	Vacuum oxygen decarburization in ladles
VODC	Vacuum oxygen decarburization in converters
VT	Vacuum ingot teeming

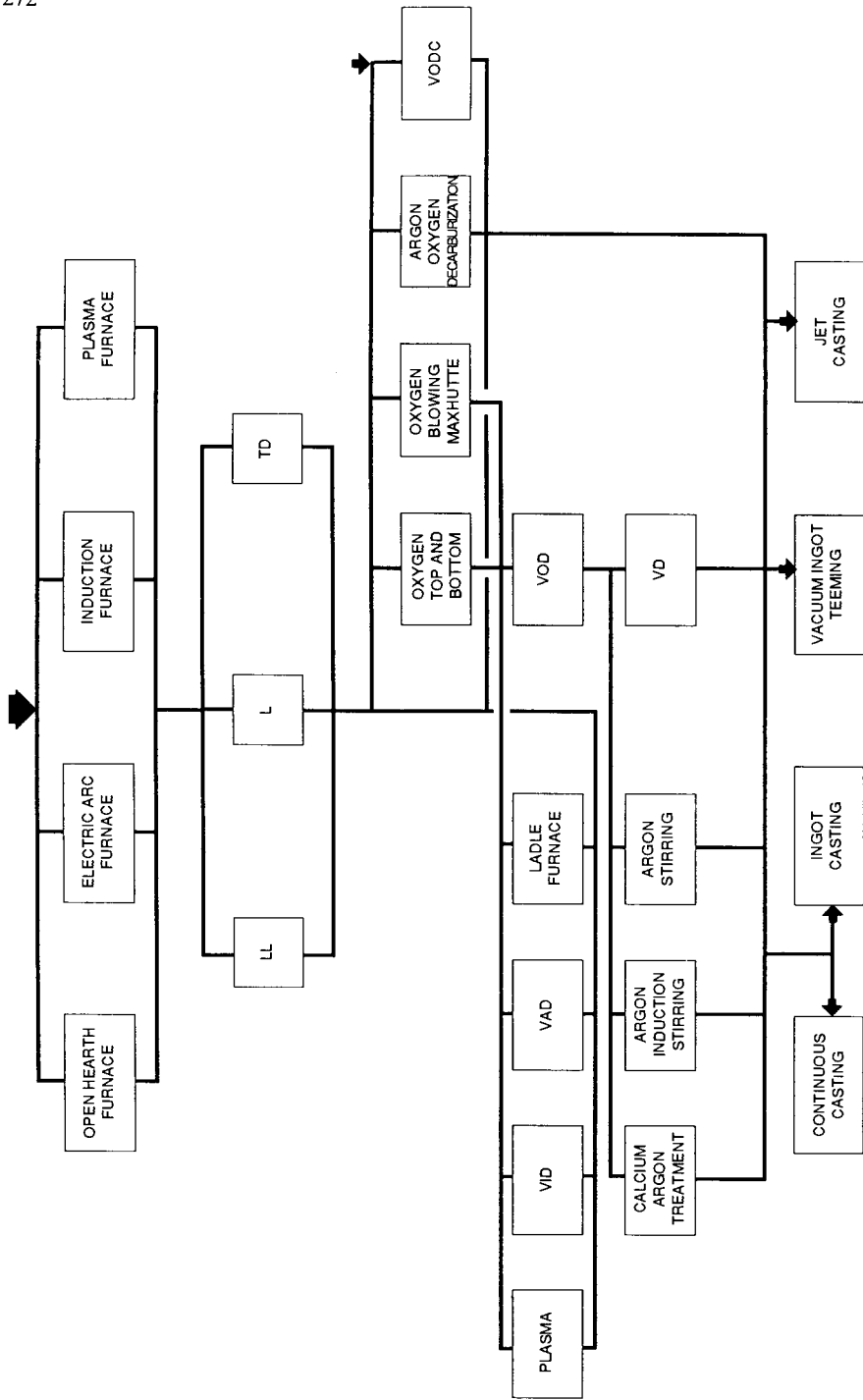


Figure 7.18 Process routes in special steel production

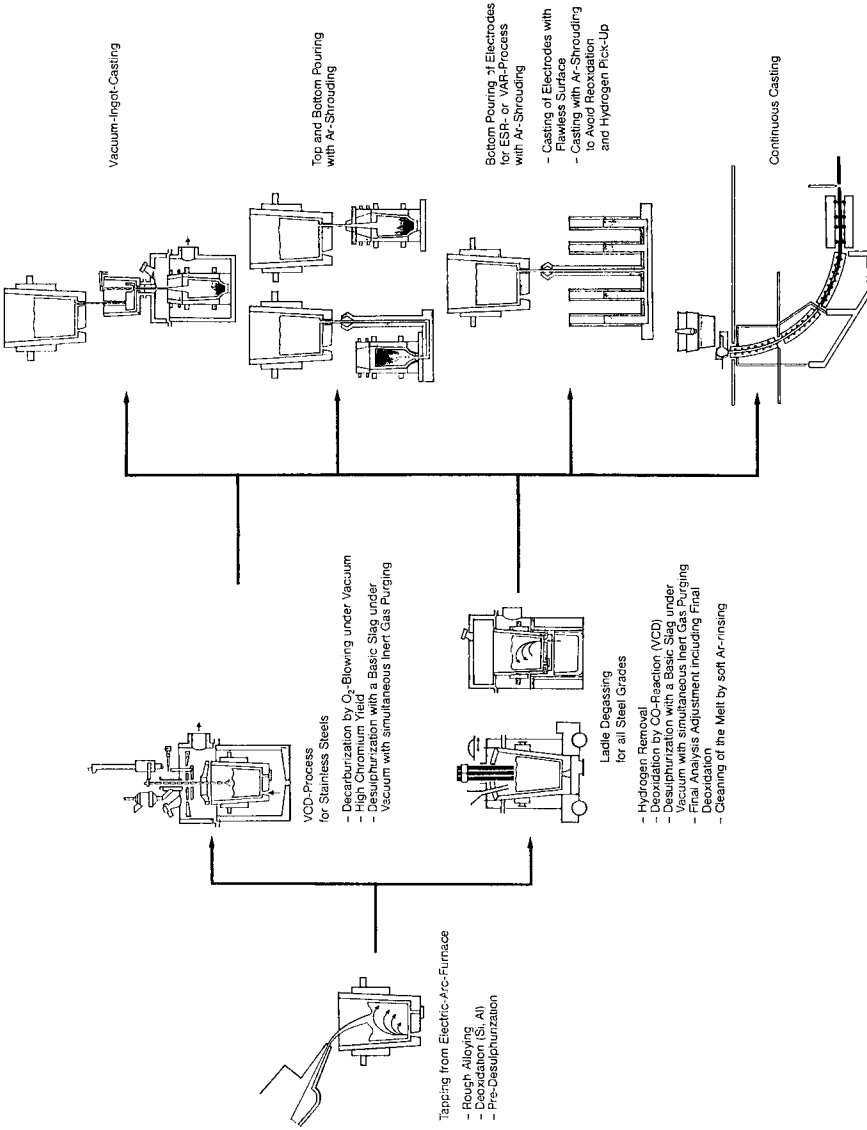
Depending on the nature of the steel and the melt weights under consideration, certain processes are preferred (Figure 7.19). For example, vacuum teeming (involving degassing of the metal stream) will show benefits with special steels, although its use in mass steel production may be limited. Vacuum ladle degassing (VD), on the other hand, is useful for all types of steel in batches from 20 to 300 t. Vacuum oxygen decarburization in ladles (VOD) is also restricted to the production of special steels (high Cr steels and alloys; batch size 10–100 t) whilst VODC can be used both for high-chromium and structural steels. Vacuum induction degassing (VID) is particularly suitable for melt weights below 15 t of liquid metal (Choudhury and Brueckmann, 1987) (Figure 7.19).

For steels other than high-Cr steels, the phosphorus and carbon content of the melt is reduced in the furnace which is then tapped into the ladle. A well-known reaction in vacuum-treated melts is expressed by the Vacher–Hamilton equation:

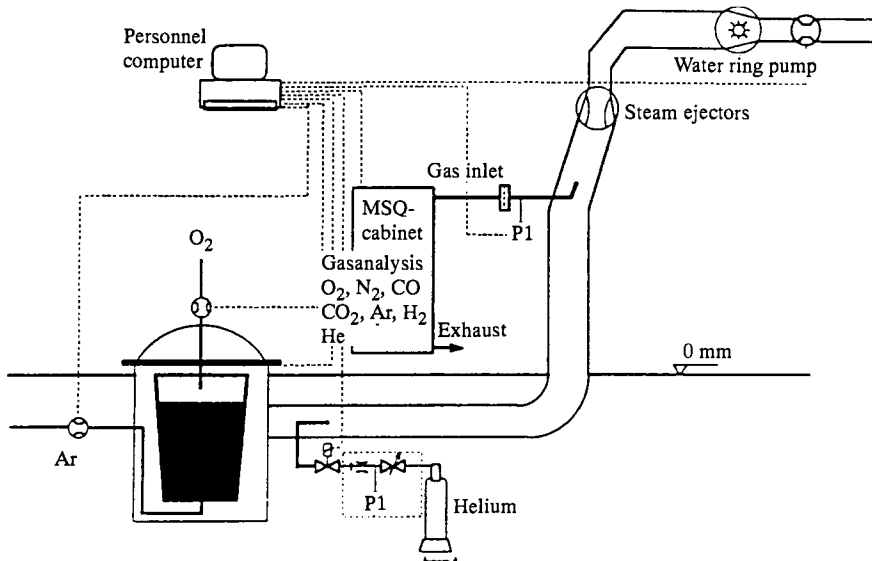
$$[C] \times [O] = 0.0025 p_{CO}$$

which describes the relationship between dissolved oxygen and carbon content. According to Tix *et al.* (1959), the C + O reaction, even at  $10^{-4}$  mbar, reaches an equilibrium value considerably in excess of theory. For this reason, deoxidation by the addition of aluminium and/or silicon (yielding the corresponding oxides) is carried out during tapping. These oxides can be removed by the application of a metallurgically active slag. Further, a basic slag also brings about some sulphur removal during tapping. After heating to the desired temperature, the melt is degassed under vacuum by the introduction (through the ladle bottom) of an inert gas such as argon and, simultaneously, by reaction with the basic slag. During this treatment, the concentration of elements such as hydrogen and sulphur, which are detrimental to physical properties such as toughness, is reduced. For example, starting with a sulphur content of about 200 ppm before tapping, ladle degassing reduces this to about 7 ppm; after 15 minutes at 1 mbar,  $H_2$ -content declines to below 2 ppm. At the end of the actual degassing process, ‘soft rinsing’ with Ar is carried out in order to further remove oxides by flotation and coagulation. Stirring increases the efficiency of the refining process. This is achieved by ensuring excellent mass transfer between metal, slag and inert-gas phase-boundaries. The chemical reactions describing deoxidation/desorption, have been reviewed by Choudhury *et al.* (1987).

The economic production of high-chromium steels and alloys usually involves low-cost materials such as ferrochromium with a high carbon content. Carbon removal by conventional oxygen blowing into the melt leads to a heavy loss of chromium due to oxidation (oxygen blowing, at 1700°C and a pressure of 1 atmosphere, into a melt containing 17% Cr leads to chromium oxidation if the carbon content reaches 0.4% (Kneuppel, 1983)). By the use of vacuum oxygen decarburization in ladles (Figure 7.20) a carbon content of less than 100 ppm can be achieved without intolerable chromium loss. For example, published data (Kneuppel, 1983) show that, at 20 mbar, chromium oxidation at 1700°C is not significant at a carbon-content of 0.015%.



**Figure 7.19** Possible treatment steps in ladle metallurgy



**Figure 7.20** Schematic diagram of VOD system with control (Leybold AG)

Decarburization during the VOD phase can be divided into three stages (Choudhury and co-workers, 1988):

1. Start of pressure-dependent reactions during pump-down after argon purging.
2. Relatively constant decarburization, depending on oxygen flow rate to a limiting C content. During oxygen blowing, the pressure is maintained between 20 and 50 mbar.
3. After interruption of the oxygen supply, the pressure falls to below 10 mbar and there is simultaneous decarburization involving the C–O reaction and chromium oxidation.

By mass spectrometric analysis of the gases leaving the process vessel and simultaneous measurement of flow rate, the residual carbon content of the melt can be calculated. This minimizes the risk of heavy chromium loss through overblowing. Experimental data obtained with 30 t melts (Choudhury *et al.*, 1988) have indicated that the maximum rate of decarburization was  $0.12 \text{ kg s}^{-1}$  ( $0.024\% \text{ C min}^{-1}$ ) for initial carbon contents between 0.25 and 0.45%.

### 7.3.2 Manufacture of high-purity metals and complex alloys

Vacuum induction melting (VIM) is the preferred technique for the manufacture of material that has significant reactivity towards atmospheric gases. Such materials include complex Ni-, Fe- and Co-based alloys (collectively

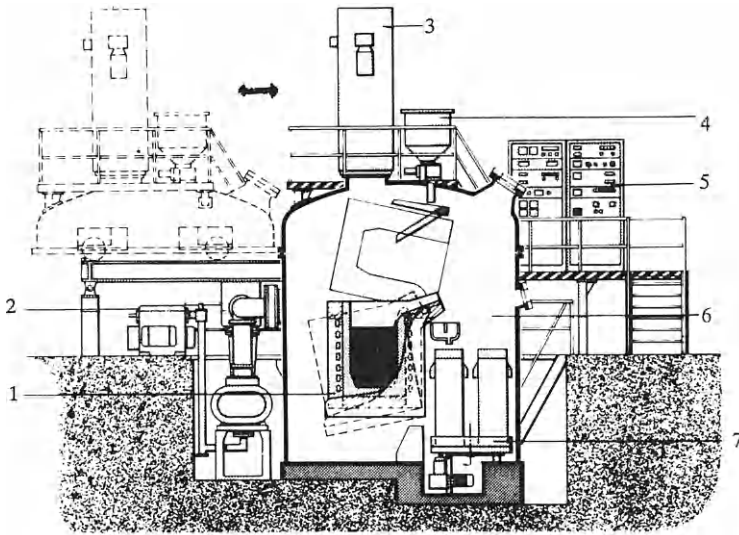


known as the superalloys), high purity metals (such as oxygen-free copper) and a range of aluminium alloys containing, for example, Li, Zr, Ti, Be, Ce, etc. VIM not only reduces significantly the absorption of gas into reactive melts but it also permits the addition of elements such as Hf, Al and Ti to other materials without significant loss due to nitride or oxide formation.

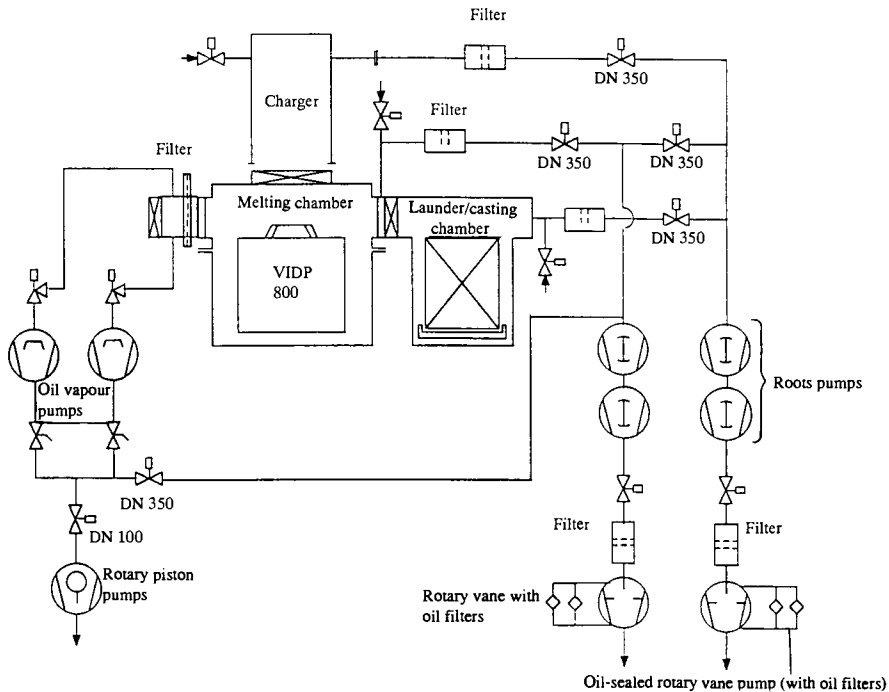
Metallurgy based on VIM tends to be limited to pressure-dependent reactions such as the removal of C, O, N and H and the evaporation of elements such as Pb, Bi, Te, Sb, Sn, etc. that have a high vapour pressure and can alter significantly the physical properties of some material (Kent, 1974). Problems can arise with VIM, however, in the case of additions of desirable alloying elements such as manganese and magnesium.

Vacuum induction melting furnaces are generally not operated with an active slag and any present tends to precipitate on the crucible wall thereby limiting the scope of refining operations. Because of this, unless suitable filtration and pouring techniques are used, melts may not be as clean as those produced by other vacuum metallurgical processes.

VIM furnaces vary in size from units handling a few kg to those which can accommodate tonnes of material. Production systems currently in use can deal with charge weights in the range 1–30 t. Most industrial-scale VIM furnaces consist of a melt chamber (housing the induction furnace assembly) and, often, a second vacuum chamber incorporating the moulds (Figures 7.21 and 7.22). With conventional units, pumping systems of large capacity are



**Figure 7.21** *Typical VIM furnace. 1, vacuum induction furnace insert; 2, vacuum pumping system; 3, bulk charger; 4, fine charger; 5, control cabinets; 6, melting and mould chamber; 7, mould turntable*



**Figure 7.22** Schematic diagram of the vacuum system for a VIDP furnace

required to maintain the pressure in the range  $10^{-1}$  to  $10^{-3}$  mbar. A diagram of the pumping system for a 5 t VIM furnace is shown in Figure 7.23. The pumping train consists of oil vapour booster pumps with diffusion/ejector stages, backed by three-stage Roots/rotary piston pump sets. Some characteristics for various types of vacuum induction furnace are given in Table 7.11.

The quality of material produced by VIM depends to a certain extent on the maintenance of a low pressure during melting and various potential gas sources have been identified in conventional furnaces.

These include:

1. *Process gas from the melt* – The extent of this contribution depends on the material being processed. It also depends on the melting period, the charge material and the frequency of charging.
2. *Outgassing from the crucible* – A newly bricked crucible will obviously evolve more gas than one which has been exposed to several melts.
3. *Desorption from the chamber walls* – It is extremely difficult to quantify this contribution. During melting material is evolved which settles on surfaces in the form of finely divided deposits which can absorb significant amounts of gas during exposure to atmospheric gases.
4. *Leaking cooling water/hydraulic lines.*
5. *Air leaks through seals and welds.*



**Table 7.11** Characteristics of vacuum induction furnaces (typical data for 5 t furnaces). Processes used in vacuum steel degassing

Characteristic	Conventional VIM (1-chamber)	VID	VIP
Chamber volume (m <sup>3</sup> )	80	6	8–11
Inner surface area (m <sup>2</sup> )	160	16	22
Operating pressure (mbar)	10 <sup>-1</sup> to 10 <sup>-3</sup>	1 to 10 <sup>-2</sup>	10 <sup>-1</sup> to 10 <sup>-3</sup>
Pumping speed (m <sup>3</sup> h <sup>-1</sup> × 10 <sup>3</sup> )	15 (at 10 <sup>-2</sup> mbar)	5 (at 10 <sup>-1</sup> mbar)	10 (at 10 <sup>-2</sup> mbar)
Pouring	Under vacuum or inert gas	Air	Under vacuum or inert gas
Applications	Superalloys; melt, treat, pour	Melting and secondary metallurgy for tool-, forging- and special steels; non-ferrous metals	Superalloys, high-purity non-ferrous metals and alloys

VID = Vacuum induction degassing; technique incorporates feature of a simple vacuum induction furnace with those of metallurgy in ladles.

VIP = Vacuum induction degassing and pouring.

Over a period of time, the design of VIM equipment has developed, usually in order to increase productivity. In some designs, the mould chamber can be prepared without disturbing the melting operation and vice versa. Significant advances, however, have been brought about by paying particular attention to the gas sources within the system and the trend is to use vacuum chambers of smaller volume which have significantly lower desorption and outgassing rates. Other improvements can be achieved in the following ways:

1. Elimination of cooling water/hydraulic lines within the vacuum chamber.
2. Use of material with an appropriately low degassing rate within the system.
3. Selection of suitable seals and feed-throughs to minimize leak rates.
4. Process control involving, among other things, monitoring of the gas composition within the furnace.

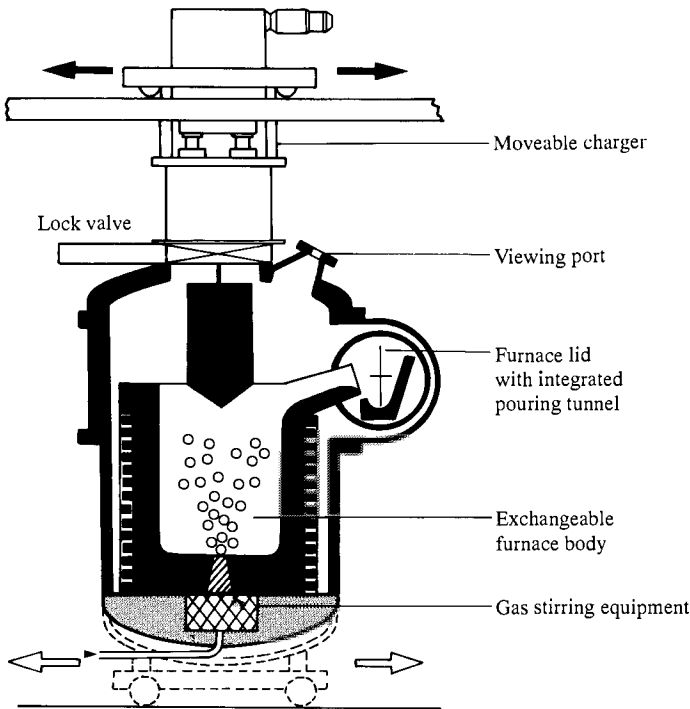
A larger melt surface area exposed to vacuum results in faster outgassing and distillation. Stirring either by inert gas bubbling or electromagnetically

increases outgassing and improves homogenization of the melt (see Winkler and Bakish (1971) for a suitable model for the outgassing kinetics). Further, by increasing the crucible diameter/height ratio to a value greater than 1 in comparison with values of 0.75 typical of air induction furnaces, a larger surface area is obtained.

According to Table 7.11, design improvements can be seen with the VIDP furnace which has a volume significantly less than that of a conventional 5 t-VIM furnace and, subsequently, a lower pumping capacity (Figure 7.24).

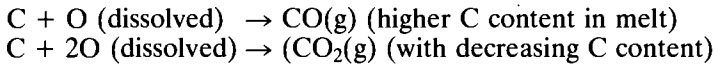
From a metallurgical point of view, advances have involved selection of the appropriate refractories and closer control of temperature in order to reduce reactions with the melt. Further, by the use of suitable filtration and pouring techniques, cleaner products can be obtained (Sutton and Morris, 1984; Apelian and Mutharasan, 1980).

Analysis of the furnaces gases also contributes significantly to the optimization of the melting process in that information regarding degassing and the chemical reactions taking place in the melt can be obtained (Johnson and Sutton, 1977). Attempts have been made to develop a mass spectrometer system for the VIM process and the concentrations of O<sub>2</sub>, CO<sub>2</sub>, H<sub>2</sub>, CO, N<sub>2</sub> and Ar in furnace atmospheres have been obtained (Betz *et al.*, 1988) (Figure



**Figure 7.24** *Vacuum induction degassing and pouring (VIDP) furnace*

7.25). Figure 7. 25 shows that the large initial evolution of carbon monoxide gradually decreases and attains a constant level. The CO<sub>2</sub>-profile suggests that it is a product of CO oxidation although the formation of both may involve:



The increase in N<sub>2</sub> (due partly to leaks and partly to degassing) can also be seen. More information will emerge when analyses are possible for water vapour and hydrocarbons.

### 7.3.3 Remelting processes

Increasing demands for cleanliness and structural homogeneity in, for example, superalloys cannot be met by traditional melting and casting procedures. To satisfy these requirements, processes combining remelting (vacuum arc remelting (VAR) and electroslag remelting (ESR)) with controlled solidification have been developed (Figure 7.26).

#### 7.3.3.1 Vacuum arc remelting (VAR)

VAR is a well-established technique for the melting of a variety of materials including special steels, superalloys, titanium, zirconium and refractory metals. The process was established in the late 1950s for the production of materials for the aircraft industry. VAR involves the continuous melting of a consumable electrode (usually from a VIM furnace) by means of a d.c. arc at pressures in the range  $10^{-2}$  to  $10^{-3}$  mbar (Figures 7.27 and 7.28). In exceptional cases, melting can also be carried out under inert gas ( $P = 100$  mbar) in order to minimize the loss of desirable but volatile alloying elements. Molten metal solidifies in a water-cooled copper mould although He cooling can be used to improve heat transfer between the shrinking ingot and crucible. Ingots with diameters up to 1500 mm (maximum weight 30 t) can be handled. The basic design of the VAR furnace has remained largely unchanged although significant advances have been made in the field of process control and regulation with the object of achieving a fully automated melting procedure.

The benefits of vacuum-melting a consumable electrode involve, of course, the removal of dissolved gases such as H<sub>2</sub> and N<sub>2</sub> and distillation of relatively volatile elements. The process also achieves directional dendritic solidification along the ingot thus avoiding macrosegregation and minimizing microsegregation. Oxide and nitride inclusions are also removed, partly by dissociation and partly by flotation. Defects can occur in VAR ingots, leading to their rejection. These are termed 'tree-ring patterns', 'freckles' and 'white spots' because of their morphology in micro- and macro-etched sections. Tree ring patterns are usually produced by melt-rate variations along the solidus-liquidus interface. Freckles are discontinuities in structure, usually caused by high pool depths and/or movement and segregation in the pool; white spot has been ascribed to either relics of unmelted dendrites from the

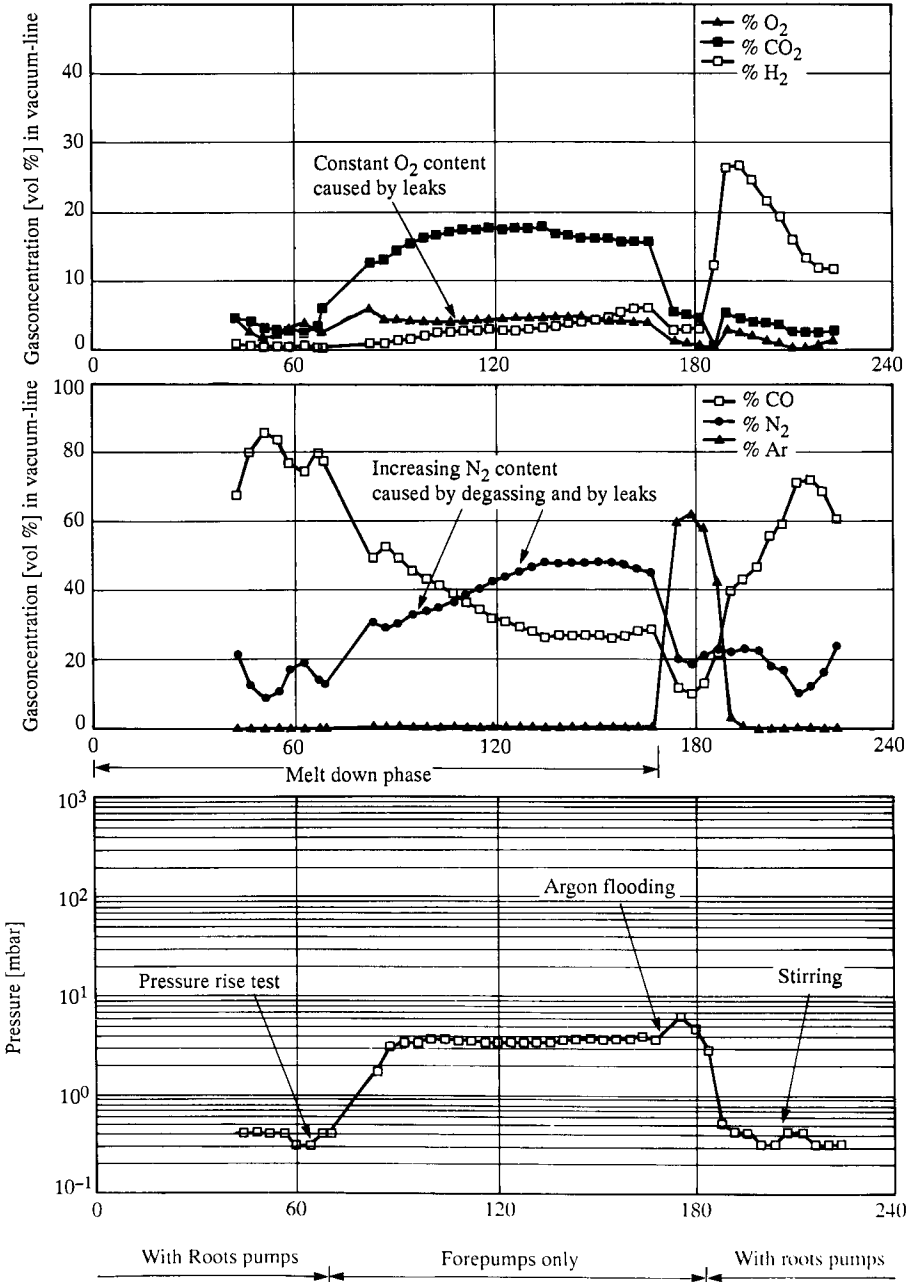
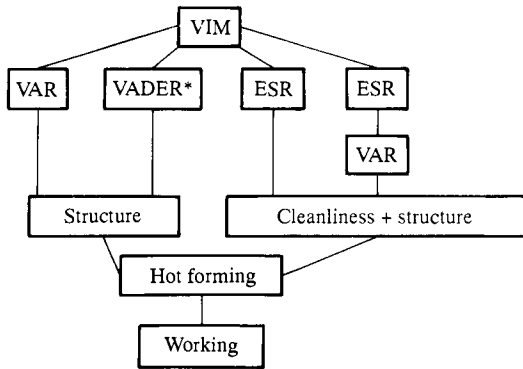
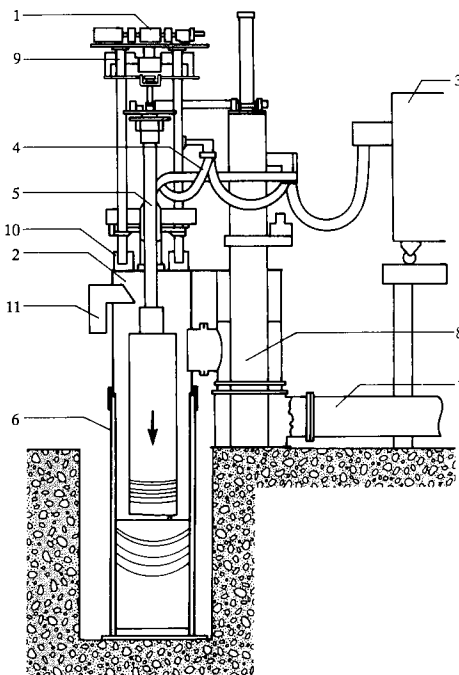


Figure 7.25 Analysis of VIM furnace gases (3.6 t furnace, melt = NiFe)

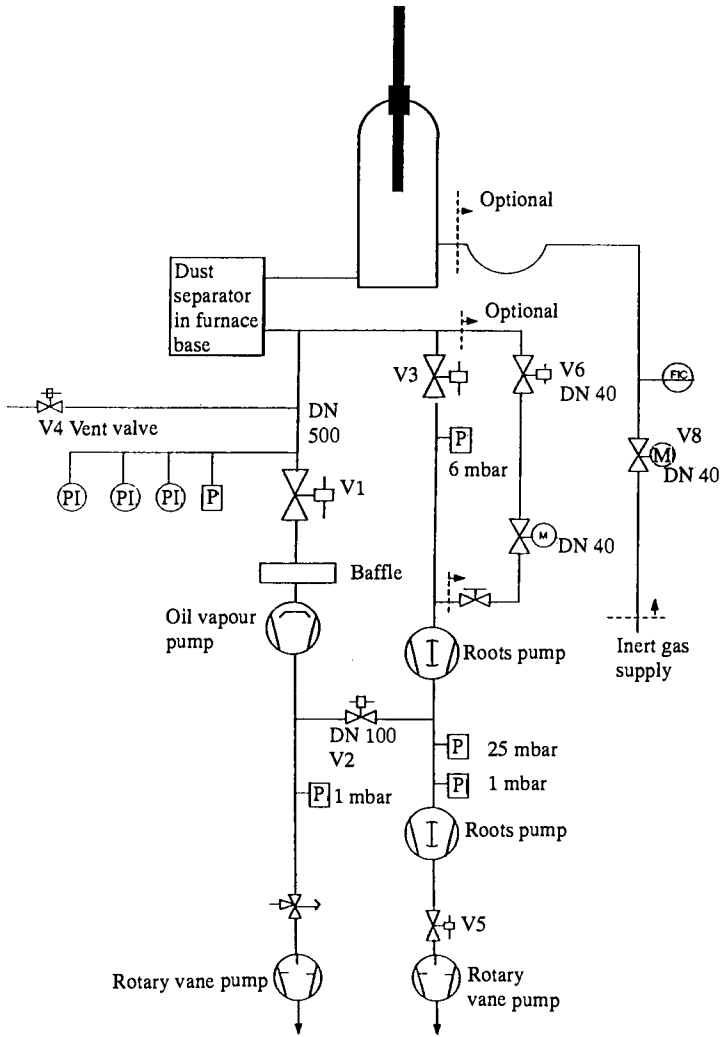


**Figure 7.26** Some procedures necessary to obtain a high degree of cleanliness and structural uniformity from VIM materials. VADER = Vacuum arc double electrode remelting



**Figure 7.27** Schematic diagram of a VAR furnace. 1, electrode feed drive; 2, furnace chamber; 3, aircooled melting power supply; 4, bus bars/cables; 5, electrode ram; 6, waterjacket with crucible; 7, vacuum suction port; 8, movable furnace support frame; 9, X-Y adjustment; 10, load cell system; 11, TV-camera system





**Figure 7.28** Pumping system for the remelting of ingots (about 1000 mm diameter) by VAR

consumable electrode or to pieces of crown falling into the melt pool but remaining unincorporated. Only close control of the melting parameters can avoid these problems.

A recent development of VAR has the acronym VADER (vacuum arc double electrode remelting) in which an arc is struck between two horizontal electrodes that are to be remelted. The process is discussed by Pridgeon *et al.* (1981).

### 7.3.3.2 *Electroslag remelting (ESR)*

In contrast to VAR, remelting in the standard ESR process does not involve striking an arc under vacuum. It involves melting a consumable electrode in a resistively-heated slag based on materials such as  $\text{CaF}_2$ ,  $\text{CaO}$ ,  $\text{Al}_2\text{O}_3$ ,  $\text{MgO}$ ,  $\text{TiO}_2$ , etc. The metal 'drips' through superheated liquid slag and reactions between the metal and slag result in a significant reduction in sulphur and non-metallic inclusions (Choudhury *et al.*, 1987). A further feature of the process is the directional solidification of the ingot from bottom to top and its excellent homogeneity. With ESR under normal air, oxidation is unavoidable. However, with proper slag composition and remelting techniques, oxygen contents less than 20 ppm in alloyed steel are possible.

Experimental ESR under vacuum has been performed (Choudhury, 1986). Inconel 718 was successfully remelted in a calcium fluoride-free slag.

### 7.3.3.3 *Vacuum precision casting*

The use of vacuum casting was encouraged mainly by the demands of manufacturers of aero-engines. A typical production unit for vacuum melting/superheating and precision casting consists of a melting chamber with a mould lock located underneath. The chambers are welded together and can be separated by a water-cooled swivel valve. Within the melting chamber, there is an induction coil and crucible. Pouring may involve tilting the coil or opening the crucible at the bottom. The mould lock is charged and discharged through a door. It is usual to pump the melt chamber to a pressure in the high vacuum region (using a diffusion pump appropriately backed). Based on a 'clean, dry, empty' basis, this is usually  $10^{-5}$  mbar. The mould chamber is separately pumped to approximately  $10^{-2}$  mbar by means of, say, a Roots vacuum pump and a single-stage oil-sealed rotary pump). The actual pressures attained depend, of course, on the gas throughput into the system and this depends on outgassing from the charge, degassing from the mould, general cleanliness of the system, the presence of leaks, etc. These factors were discussed earlier.

Advances in aero-engine technology have been brought about partly by improvements in materials that have allowed the turbines to be operated at much higher temperatures. The improvements include increasing resistance to creep and fatigue. As most failures occur at grain boundaries, attempts have been made to cast material with directionally solidified (DS) or single-crystal (SC) structures. For the production of DS- or SC-castings, it is necessary to encourage solidification at the bottom of the mould through a large temperature gradient and a high axial heat flow at the liquid–solid interface. To achieve this, the mould is attached to a water-cooled copper plate (the chill plate). A precision system allows the mould to be removed from a separately heated section in the chamber in a well-controlled and stable manner.

## 7.4 Vacuum technology in the chemical industry

The aim of the chemical industry is the production of high-value derivatives by the efficient conversion of an appropriate lower-value feedstock. Since adequate rates have to be achieved, it is uncommon to perform chemical reactions under reduced pressure. Chemical processing is not, however, just limited to chemical conversion, it also involves a significant amount of treatment and purification of reactants and products. For example, material from a reactor may, in addition to the required compound, also contain unconverted starting material, catalyst, products of side-reactions, etc. that have to be removed. This can involve thermal processing such as distillation and drying or mechanical treatment such as filtration. These stages may be carried out under vacuum. Because of the nature of the processes performed and the compounds handled, the chemical industry presents a great challenge to vacuum technology. For example, large quantities of air and vapours of water and volatile compounds, must be dealt with and, in some cases, highly aggressive chemicals such as inorganic acids and halogens.

### 7.4.1 Separation processes in the chemical industry

The background to some of the vacuum processes used in the chemical industry can be introduced simply by consideration of some physical transformations in pure materials or unreactive binary mixtures.

Transformations such as boiling and freezing involve a change of phase (liquid  $\rightarrow$  gas; liquid  $\rightarrow$  solid). The guiding principle behind, say, the evaporation of a liquid or its tendency to freeze can be found in any good text on physical chemistry. Based on this, it is a fairly simple exercise to show under what conditions of pressure and temperature each phase of a pure substance is stable. The boundaries between the regions of stability lie at the values of  $p$  and  $T$  where two phases coexist and can be found by finding the dependence of  $p$  on  $T$ . For a liquid/vapour boundary, this is the dependence of vapour pressure on temperature. For any phase change of a pure material, the slope of the  $p$ - $T$  boundary is given by the Clapeyron equation:

$$dp/dT = \Delta S_m / \Delta V_m$$

where  $\Delta S_m$  = change in molar entropy of the two phases

and  $\Delta V_m$  = change in molar volume of the two phases

#### 7.4.1.1 Gas-liquid systems

With the liquid-vapour boundary, the Clapeyron equation becomes:

$$dp/dT = \Delta H_{\text{vap},m} / T \Delta V_m$$

where  $\Delta H_{\text{vap},m}$  = enthalpy of vaporization

If it is remembered that the volume of a vapour ( $V_{m(g)}$ ) is considerably larger than that of the equivalent amount of liquid, then  $\Delta V_m$  can be represented by  $V_{m(g)}$ . Further, if we assume that the vapour behaves perfectly (see Chapter

1), then  $V_{m(g)}$  can be replaced by  $RT/p$  and we obtain the Clausius–Clapeyron equation:

$$d(\ln p)/dT = \Delta H_{\text{vap},m}/RT^2$$

Assuming  $\Delta H_{\text{vap},m}$  doesn't depend on temperature, then:

$$\ln p = \text{const} - \Delta H_{\text{vap},m}/RT$$

or, if the  $p$  versus  $T$  curve is required:

$$p = p^* \exp \left\{ \frac{-\Delta H_{\text{vap},m}}{R} \left( \frac{1}{T} - \frac{1}{T^*} \right) \right\}$$

where  $p^*$  is the vapour pressure at some temperature  $T^*$ . This formula gives the  $p$  versus  $T$  curve representing states of the system where liquid and vapour coexist. It can also be regarded as a plot of boiling point against applied pressure, the normal boiling point being the temperature where the vapour pressure is 1 atmosphere. Obviously, if the total pressure in a system is reduced to a value equal to the vapour pressure at the temperature of the system, the substance evaporates completely at a temperature below the normal boiling point. This means:

1. Distillation/evaporation becomes possible at lower temperatures (thus reducing decomposition/other reactions).
2. Lower-cost energy sources (low pressure steam, hot water) are possible for the process.

Under conditions where a liquid contains several components, then the partial vapour pressure of a particular component (say component A) can be related to the vapour pressure of pure A ( $P_A^*$ ) at the same temperature by Raoult's law.

$$p_A = x_A p_A^*$$

where  $x_A$  is the mole fraction of A in the liquid mixture. Some solutions obey this law very well and, for a mixture of two components, A and B, obeying this rule, then:

$$P = p_A + p_B = x_A p_A^* + x_B p_B^*$$

where  $P$  is the total vapour pressure,

$$= p_B^* + (p_A^* - p_B^*) x_A$$

This shows that the total vapour pressure changes linearly with composition of the liquid.

When vapour and liquid are in equilibrium it seems very likely that the vapour should be richer in the more volatile component. This can be confirmed as follows. Dalton's law gives the composition of the gas phase:

$$y_A = p_A/p \quad y_B = p_B/p$$

where  $y_A$  and  $y_B$  are, respectively, the mole fractions of A and B in the gas phase. Combining this with Raoult's law, we get:

$$y_A = \frac{x_A p_A^*}{p_A^* + (p_A^* - p_B^*)x_A} \quad y_B = 1 - y_A$$

The dependence of the total pressure of the vapour on the composition of the vapour can be shown to be:

$$P = \frac{p_A^* p_B^*}{p_A^* + (p_B^* - p_A^*)y_A}$$

It can be demonstrated that, as the total pressure is reduced, the proportion of the more volatile component in the vapour increases.

Raoult's law may be satisfactory for components that are chemically very similar but strong deviations are observed with very dissimilar materials. If we have to consider real solutions of dissimilar materials, however, it is convenient to assume that, if there is a component present in small amounts in a solvent, its partial pressure will depend linearly on the amount in the solvent:

$$p_B = x_B K_B$$

This is Henry's law in which  $x_B$  is the mole fraction of the 'solute' and  $K_B$  is some constant (with  $[K_B] = [\text{pressure}]$ ) characteristic of the 'solute' and 'solvent'. Henry's law can be applied to estimates of gas solubility. For example, if a gas (G) were dissolved in a liquid (L), then the solubility can be calculated from:

$$p_G = x_G K_{G \text{ in L}}$$

where 
$$x_G = \frac{n(G)}{n(G) + n(L)} \approx \frac{n(G)}{n(L)}$$

thus 
$$n(G) \approx x(G)n(L)$$

$$\approx \frac{p_G n(L)}{K_{G \text{ in L}}}$$

Vacuum degassing is based on Henry's law since, if  $p_G$  decreases with total pressure,  $n(G)$  also falls.

#### 7.4.1.2 Gas–solid systems

The Clausius–Clapeyron equation can be applied but with the replacement of the enthalpy of vaporization by the enthalpy of sublimation:

$$d(\ln P)/dT = \Delta H_{\text{sub,m}}/RT^2$$

$$\text{or } p = p^* \exp \left\{ - \frac{\Delta H_{\text{sub,m}}}{R} \left( \frac{1}{T} - \frac{1}{T^*} \right) \right\}$$

#### 7.4.2 Vacuum pumps

In the chemical industry, most vacuum processes are carried out in the rough–medium range and the pumps normally used are:

1. Liquid ring pumps, usually with water as the service fluid.
2. Oil-sealed pumps such as rotary-vane and rotary plunger pumps.
3. Roots vacuum pumps.
4. Ejector/diffusion pumps.

These pumps are most frequently used in combination and also, because of the nature of the processes, with condensers which are used to reduce the vapour throughput. Details of the pumps used in the industry have been given in Chapter 2 and typical combinations will be discussed in Section 7.4.5.

In the chemical industry, in addition to residual air, a very large number of compounds must be dealt with, ranging from highly reactive, aggressive inorganic compounds to easily polymerized organic molecules such as butadiene, styrene and methacrylic acid. Usually, liquid ring pumps and steam/air ejectors show few problems as long as appropriate materials are used in their construction (see, for example, Mangnall 1989). With oil-sealed pumps, bearing in mind the essential role played by the vacuum fluid, compatibility of the pumped material with the sealant has to be considered carefully. The use of 'inert' fluids in vacuum technology has already been discussed but for specific chemical applications, particularly specialized oils are used (Table 7.12).

When large quantities of condensable vapours have to be dealt with, the use of the gas ballast valve is invaluable (see Section 2.2.2.2). Attention has to be paid, however, to the vapour tolerance of the pump and if this is likely

**Table 7.12** *Properties of some fluids used for vacuum sealing in the chemical industry*

Type	Alkylsulphonic acid ester	Diocetyl phthalate	Glygoyle 500*	Anderol 11†
Viscosity (40°C)(mPa s)	39	28	86	90
Density (20°C)(g cm <sup>-3</sup> )	1.03	0.99	1.01	0.95
Ultimate pressure	+	0	0	++
Temperature resistance	+	+	++	++
Resistance to strong oxidants	--	--	--	--
Polymer solubility	++	++	--	0/+
Solubility of strongly polar organics	++	++	+	+

\* Glygoyle = Synthetic, polyglycol-based oil made by Mobil; it is hygroscopic.

† Anderol = Synthetic, diester-based oil made by Chemie Mineralien AG.

++, good; +, satisfactory; 0, moderate; -, poor, low; --, unsuitable.

to be exceeded then condensers must be incorporated into the system before the pump. To maintain the condition of the lubricant/sealant, it must be drained and replaced at intervals. The purpose of this is to remove particles generated either in the process or by oil-ageing. Delayed oil changes increase mechanical wear but the intervals between changes can be extended by the use of filters (see Chapter 2).

**7.4.3 Condensers**

A condenser is an extremely convenient device for the removal of large amounts of vapour. Vacuum condensers, however, must be used in combination with correctly sized pumps to remove non-condensable gases such as air which have entered the system through leaks or are evolved in the process chamber. Surface condensers are extensively used. In these devices, the condensation surface is usually in the form of a tube through which the coolant flows. Coil condensers can have heat exchange areas up to a few m<sup>2</sup> and have a good leak tightness. To increase the effective heat transfer area/unit volume, commercial condensers provide for more than one pass of coolant through the tubes and the fluid to be cooled, which is in the shell, is routed back and forth by means of baffles (Mangnall, 1989). The usual coolant is water, either fresh or recirculated. In exceptional cases, precooled water or brine can be used but, if the condensate has a high melting point or if only partial condensation is required, coolants with raised temperatures must be used. In batch processes or in situations where small amounts are formed, the condensate is collected and discharged subsequently. The receiver is fitted with three valves – for isolation, air admission and discharge – and normally has a float switch to warn of a high liquid level. For continuous processes, a suitable pump is used for discharge.

Contact condensers are commonly used as intermediate condensers, particularly with steam ejectors where their function is to remove the motive fluid so that subsequent stages have only to deal with ‘permanent’ gases. Cooling water is injected directly into the condenser and reaches the vapour by means of cascade distribution. In the case of ejectors, liquid condensate can be removed either through barometric drain systems with a leg of suitable height ( $h = p_{\text{ambient}} - p_{\text{ultimate, pump}} / \text{density} \times \text{acceleration due to gravity}$ ) or by means of a circulating pump.

**7.4.3.1 Condenser performance**

Condensers are heat exchangers that transfer the heat of condensation of the vapour to the coolant. The rate of heat flow ( $\dot{Q}$  W) is proportional to the exchanger area ( $A$  m<sup>2</sup>), the mean temperature difference ( $\Delta T_m$  in K) and the overall coefficient of heat transfer ( $k$  in W m<sup>-2</sup> K<sup>-1</sup>);

$$\dot{Q} = A \cdot \Delta T_m \cdot k \text{ W}$$

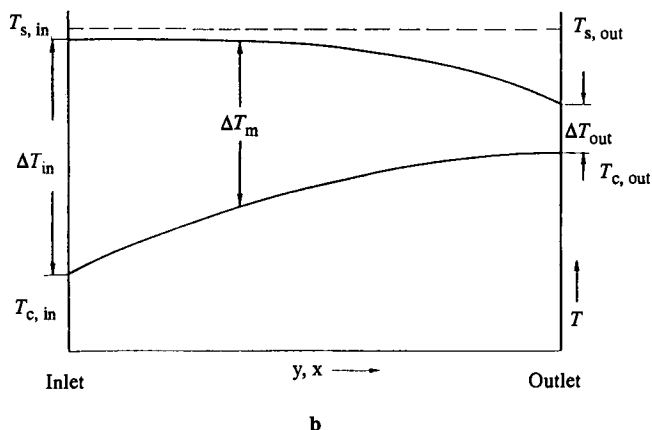
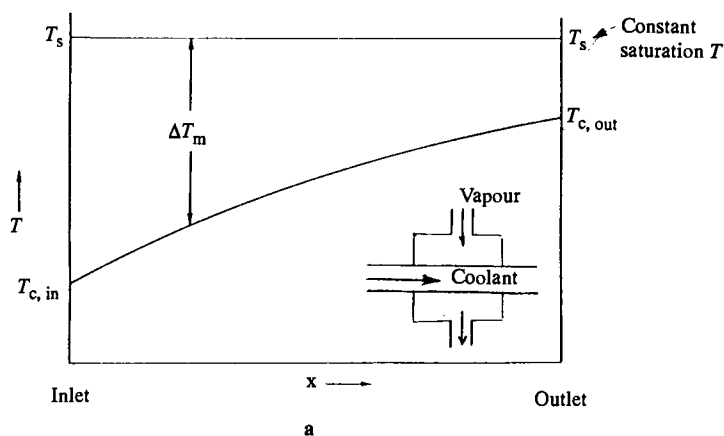
The mass flow rate of the condensate ( $\dot{q}_c$ ) is given by:

$$\dot{q}_c = \frac{\dot{Q}}{r} \text{ kg s}^{-1}$$

where  $r$  = specific heat of condensation ( $\text{J kg}^{-1}$ ).

In an ideal condenser (Figure 7.29(a)) containing only vapour at a constant pressure ( $p_{\text{vap}}$ ) throughout, the temperature of the coolant increases from its inlet ( $T_{\text{c,in}}$ ) to the outlet temperature ( $T_{\text{c,out}}$ ) because of the absorbed heat flux ( $\dot{Q}$ ). The actual temperature rise is determined by the mass flow rate of the coolant ( $\dot{m}_c$ ) and the relationship is given by:

$$T_{\text{c,out}} - T_{\text{c,in}} = \frac{\dot{Q}}{c_p \times \dot{m}_c}$$



**Figure 7.29** Variation of vapour and coolant temperature for a coil-type condenser ( $T_c$  = coolant temperature,  $T_s$  = vapour temperature). (a) Ideal condenser. (b) Real condenser



where  $c_p$  is the specific heat capacity of the coolant ( $\text{J kg}^{-1} \text{K}^{-1}$ ;  $C_p$  for water =  $4200 \text{ J kg}^{-1} \text{K}^{-1}$ ). In practice, condenser temperatures are as shown in Figure 7.29(b) and in the equation for the rate of heat flow, the log mean temperature difference should be used for  $\Delta T_m$ ;

$$\Delta T_m = \frac{\Delta T_{\text{in}} - \Delta T_{\text{out}}}{\ln (\Delta T_{\text{in}}/\Delta T_{\text{out}})}$$

For  $\Delta T_{\text{in}}/\Delta T_{\text{out}} < 3$ , an error of less than 10% is introduced if the simple algebraic mean is taken ( $\Delta T_m = (\Delta T_{\text{in}} + \Delta T_{\text{out}})/2$ ).

The heat flow from a warm gas to a coolant flowing behind a metal wall can be regarded as being analogous to the flow of current in a simple d.c. circuit ( $Q = \Delta T/R$  where  $\Delta T$  is the temperature potential and  $R$  is the thermal resistance;  $i = \Delta E/R_e$  where  $\Delta E$  is the electrical potential and  $R_e$  is the electrical resistance). The reciprocal of the overall heat transfer coefficient ( $h$ ) is equivalent to the thermal resistance.

$$\frac{1}{h} = \frac{1}{\alpha_c} + \frac{d}{\lambda} + \frac{1}{\alpha_{\text{cool}}} \quad \left( Q = \frac{\Delta T}{R} \right)$$

where  $\frac{1}{\alpha_c}$  = thermal resistance at the gas side;  
 $[\alpha] = \text{W m}^{-2} \text{K}^{-1}$

$\frac{d}{\lambda}$  = thermal resistance of the condenser wall;  
 $[\lambda] = \text{W m}^{-1} \text{K}^{-1}$

$\frac{1}{\alpha_{\text{cool}}}$  = thermal resistance to heat transfer on the coolant side.

$1/\alpha_{\text{cool}}$  is favourable if turbulent flow is maintained and if 'fouling' is avoided. Some empirical values for  $k$  relevant to the condensation of water vapour in water-cooled vacuum condensers are given in Table 7.13. Table 7.13 shows that  $h$  is adversely affected by the presence of large amounts of permanent gas which tend to accumulate near the condensation surface, thereby impeding the passage of vapour. The heat transfer coefficient depends on the properties of the fluid and its velocity ( $h \propto k/\delta$  where  $k$  is the thermal conductivity of the fluid and  $\delta$  is the thickness of the stagnant film at the surface). With organic liquids,  $k$  is lower and  $\delta$  can be larger (due to higher viscosity) than the values for water. For example, for pure light hydrocarbons and pure organic solvents,  $h$  is about  $90 \text{ W m}^{-2} \text{K}^{-1}$ ).

#### 7.4.3.2 Pressure distribution in a condenser

A common situation encountered in the chemical industry is the condensation of a vapour from a mixture containing permanent gas (often due to an air leak). Thus the inlet total pressure is equal to the sum of the partial pressures of the vapour and permanent gas:

$$P_{\text{IN}} = p_{\text{vap.in}} + p_{\text{perm.in}}$$

**Table 7.13** Values for the overall heat transfer coefficient of various types of condenser\*

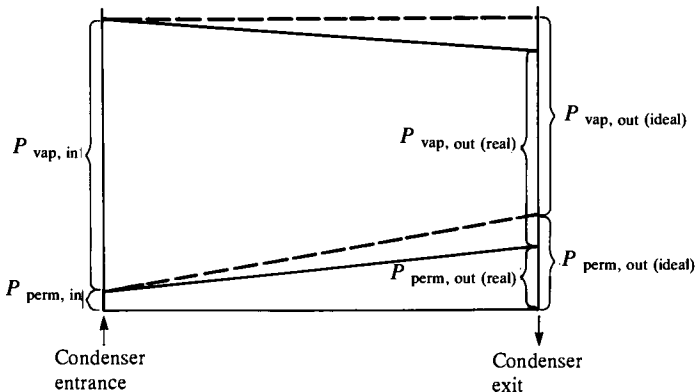
Condenser type	$h$ ( $\text{W m}^{-2} \text{K}^{-1}$ )	Reference
Turbine; pure vapour	3500	†
Small, coiled tubes; pure vapour	1200	†
Coiled tube:	800	†
Vapour + permanent gas (about 5% at exit)		
Vapour + permanent gas (about 30% at exit)	400	†
Shell-and-tube condenser (single):		
Pure vapour	560	‡
Vapour + 10% permanent gas	220	‡

\* Coefficients are usually based on *average* conditions of  $T$ ,  $P$ , fluid properties, etc. Appreciable variations can occur.

† Shell or tube side; based on  $\frac{3}{4}$  in diameter tubes (Mangnall, 1989).

‡ Fauser, 1989.

During flow through the condenser, a small pressure drop will occur because of the flow resistance. This means that  $P_{\text{out}}$  will be less than  $P_{\text{in}}$  (by 30%, realistically). The pressure distribution is shown in Figure 7.30, from which it can be seen that the partial pressure of vapour at the exit is reduced while that of the permanent gas increases. The partial pressure changes can be calcu-



**Figure 7.30** Pressure distribution in a condenser.  
 - - - - , ideal situation ( $P_{\text{in}} = P_{\text{out}}$ );  
 ———— , real situation ( $P_{\text{in}} > P_{\text{out}}$ )

lated. For example, if a volume ( $V$ ) of the mixture enters the condenser over a period of time ( $t$ ), then:

$$q_{PV,vap} = p_{vap} \times \dot{V} = \dot{m}_{vap}/M_{vap} \cdot (RT)$$

$$q_{PV,perm} = p_{perm} \times \dot{V} = \dot{m}_{perm}/M_{perm} \cdot (RT)$$

and  $P_{IN} = p_{vap,in} + p_{perm,in}$

$$\begin{aligned} \frac{p_{vap}}{P} &= \frac{p_{vap}}{p_{vap} + p_{perm}} = \frac{q_{PV,vap}}{q_{PV,vap} + q_{PV,perm}} = \frac{q_{PV,vap}}{q_{PV,tot}} \\ &= \frac{\dot{m}_{vap}/M_{vap}}{\dot{m}_{vap}/M_{vap} + \dot{m}_{perm}/M_{perm}} \end{aligned}$$

$$\begin{aligned} \text{and } \frac{p_{perm}}{P} &= \frac{q_{PV,perm}}{q_{PV,tot}} \quad \text{and} \quad \frac{p_{vap}}{p_{perm}} = \frac{q_{PV,vap}}{q_{PV,perm}} \\ &= \frac{\dot{m}_{vap}/M_{vap}}{\dot{m}_{perm}/M_{perm}} \end{aligned}$$

If a mixture, consisting of 95% water vapour + 5% air, for example, flows into the condenser and 90% of the vapour is condensed, then the following relationship can be established:

$$\begin{aligned} \dot{m}_{TOT,IN} &= \dot{m}_{vap,IN} + \dot{m}_{perm,IN} \\ \dot{m}_{vap,IN} &= 0.95 \dot{m}_{TOT,IN} \\ \dot{m}_{perm,IN} &= 0.05 \dot{m}_{TOT,IN} \end{aligned}$$

$$\left( \frac{p_{vap}}{p_{perm}} \right)_{IN} = \frac{0.95 \dot{m}_{TOT,IN}}{0.05 \dot{m}_{TOT,IN}} \times \frac{29}{18} = 30.6 \quad (\bar{M}_{air} = 29 \text{ g mol}^{-1})$$

$$\left( \frac{p_{perm}}{p_{TOT}} \right)_{IN} = \frac{0.05 \dot{m}_{TOT,IN}/29}{0.95 \dot{m}_{TOT,IN}/18 + 0.05 \dot{m}_{TOT,IN}/29} = 0.03$$

$$\left( \frac{p_{vap}}{p_{TOT}} \right)_{IN} = 0.97$$

With 90% condensation of vapour, the respective mass flow rates of vapour and air leaving the condenser are  $0.1 \times 0.95 \dot{m}_{TOT,IN}$  and  $0.05 \dot{m}_{TOT,IN}$ :

$$\begin{aligned} \left( \frac{p_{vap}}{p_{TOT}} \right)_{OUT} &= \frac{0.095 \dot{m}_{TOT,IN}/18}{0.095 \dot{m}_{TOT,IN}/18 + 0.05 \dot{m}_{TOT,IN}/29} \\ &= 0.754 \end{aligned}$$

Thus, even with 90% condensation,  $p_{\text{vap}}$  is 75% of the total pressure of gases leaving the condenser. The total mass flow which has to be dealt with by the vacuum pump can be also calculated:

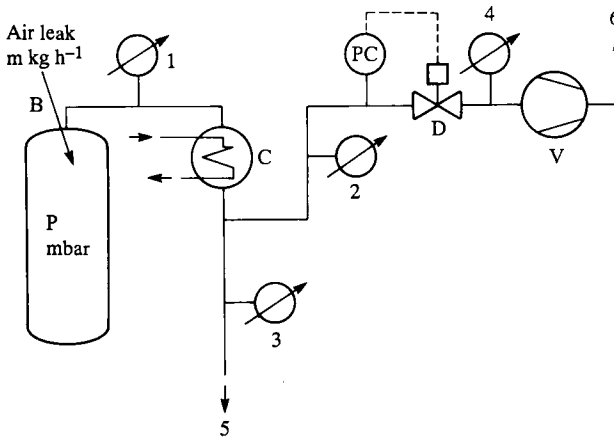
$$\frac{\dot{m}_{\text{TOT,out}}}{\dot{m}_{\text{TOT,IN}}} = \frac{\dot{m}_{\text{TOT,IN}} (0.095 + 0.05)}{\dot{m}_{\text{TOT,IN}}} = 0.145$$

This represents 14.5% of the incoming flux.

#### 7.4.3.3 Condenser–vacuum pump combinations

In the chemical industry, it is quite usual for large amounts of vapour to be incorporated in the gas leaving a vacuum vessel and the problem can be dealt with using condensers. To select the size of a vacuum pumping system fitted with an inlet condenser, various factors must be taken into consideration, including the required working pressure, the total leak rate of the plant and the gas temperature at the condenser outlet. This can be seen if we consider a system, as indicated in Figure 7.31. Here a pressure of  $P$  is maintained in the vacuum vessel and at the condenser inlet in the presence of an in-leak of air. With an ideal condenser, the total pressure at the condenser outlet would also be  $P$  but, in practice, it would be approximately  $P - 30\%$ . According to the formulae developed in Section 7.4.3.2, at the condenser outlet

$$\dot{m}_{\text{vap,OUT}} = \dot{m}_{\text{air}} \frac{M_{\text{vap}}}{M_{\text{air}}} \times \frac{p_{\text{vap}}}{p_{\text{air}}} \text{ kg h}^{-1}$$



**Figure 7.31** Schematic diagram of a typical vacuum system with condenser on the inlet valve of the pumps. B, vacuum vessel; C, condenser (coolant temperature,  $T_c$ ); D, throttle valve; V, pump(s); PC, pressure controller; 1–4, pressure gauge points; 5, condensate discharge; 6, pump discharge

In this relationship,  $p_{\text{vap}}$  is the vapour pressure of the condensable at the condenser outlet temperature and  $p_{\text{air}} = (P - 30\%) - p_{\text{vap}}$ . From the ideal gas relationship:

$$PV = \frac{m}{M} RT$$

the PV-throughput for the vapour may be found:

$$Q_{\text{PV,vap}} = \frac{\dot{m}_{\text{vap,OUT}}}{M_{\text{vap}}} \times R \times T_{\text{condenser}} \text{ mbar l s}^{-1}$$

where  $[Q_{\text{PV}}] = \text{mbar l s}^{-1}$  if  $[\dot{m}_{\text{vap}}] = \text{g s}^{-1}$ ,  $[T] = \text{K}$ ,  $[M_{\text{vap}}] = \text{g mol}^{-1}$  and  $R = 83.14 \text{ mbar l mol}^{-1} \text{ K}^{-1}$ .

Similarly, the PV-throughput for the in-leaked air can also be found:

$$Q_{\text{PV,air}} = \frac{\dot{m}_{\text{air}}}{M_{\text{air}}} \times R \times T_{\text{condenser}} \text{ mbar l s}^{-1}$$

with the units as described above.

The total PV-throughput at the temperature of the condenser is, therefore,

$$Q_{\text{PV,tot}} = Q_{\text{PV,vap}} + Q_{\text{PV,air}}$$

and  $Q_{\text{PV,tot}} = (P - 30\%) \times S_{\text{eff,pump}}$

and  $S_{\text{eff,pump}} = \frac{Q_{\text{PV,tot}}}{(P - 30\%)} \text{ l s}^{-1}$

Multiplication by  $3.6 \text{ s h}^{-1} \text{ l}^{-1} \text{ m}^3$  gives  $S_{\text{eff,pump}}$  in units of  $\text{m}^3 \text{ h}^{-1}$ .

Calculations such as these show that the required effective pumping speed is:

1. Directly proportional to the in-leakage rate.
2. Proportional to the vapour pressure of the condensable at the outlet.

They also show that leakage in vacuum plants also cause emissions from the plant ( $\dot{m}_{\text{vap,OUT}}$ ). The use of a further pump outlet condenser may be required.

It is necessary, in vacuum systems with inlet condensers, to maintain the effectiveness of the condenser in support of the pump. This can be achieved in a number of ways using the appropriate control systems:

1. A sensor is used to monitor the temperature in, say, a vessel in which volatiles are being evolved. A pressure increase will raise the boiling temperature and this deviation from set conditions causes an actuator to change the volume rate of flow through the pump. This can be achieved either by increasing the rotational speed of the pump motor (for Roots pumps) or by increasing the gas inlet area of a regulating valve. The fall in pressure then restores the original conditions.
2. A pressure regulator compares the condenser inlet pressure with a pre-set valve. Increases in pressure cause a throttle valve (mounted in front of the pump) to open, thereby increasing the pumping speed.

3. Pressure variations within the vessel can result from variations in the energy supplied to an evaporation process via heating fluid. This can be controlled using a variable valve in its circulation system. This is actuated via either a pressure sensor/comparator located near the condenser inlet or a temperature sensor/comparator on the vessel itself.
4. The gas temperature between the condenser and pump can be monitored if it is necessary to maintain the pressure of vapour at the condenser outlet at a level that will not exceed the vapour tolerance of the vacuum pump. This can be used to actuate a control valve in the heating fluid circulation system.

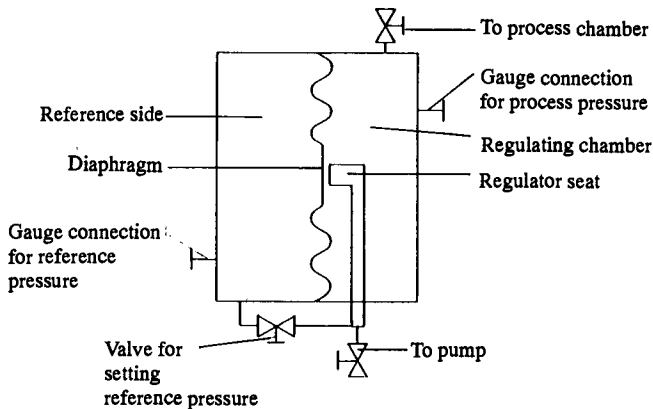
#### 7.4.4 Pressure measurement and control

It is unusual in the chemical industry to run processes at pressures below  $10^{-3}$  mbar. For this reason, pressure measurement usually involves direct-reading devices such as diaphragm gauges and capacitance manometers. Of the indirect-reading type, only the Pirani gauge works well in the pressure range. The chemical industry may also present particular problems and the nature of the pumped material must be carefully assessed for corrosion and/or explosion hazard and the appropriate gauge selected and correctly installed.

Bourdon tube gauges are sturdy and corrosion-resistant if the tube is made of, say, austenitic stainless steel but are of limited accuracy. The more precise capsule gauge is not usually recommended for chemical applications since the lever system would be in direct contact with process gases. For accurate pressure measurement below 50 mbar, gauges such as the precision diaphragm gauge and capacitance manometer are suitable as long as corrosion-resistant materials are selected for the diaphragm. In some gauges the mechanical deformation of a diaphragm is converted into an electrical signal and response to pressure change is rapid (a few tens of milliseconds). Compression gauges (e.g. McLeod and Kammerer gauges) are probably not suitable for pressure measurement. Firstly, they are not continuously operating devices and, secondly, condensation will take place in the gauge during compression if the medium to be measured contains a significant proportion of vapour. The latter fact means that the measurement represents the partial pressures of non-condensables and an unknown amount of residual vapour.

The indication of indirect-reading gauges, such as the Pirani gauge, depends on the type of gas in the system. For example, if fluids of high molecular mass are predominant, the indicated pressure, particularly around  $10^{-2}$  mbar can be considerably in error. If a Pirani gauge operates on the constant resistance principle, response time is short and it may be used for process control as well as pressure monitoring.

The maintenance of a constant working pressure is of importance in vacuum processes such as degassing, drying, distillation, etc. Accumulation of gas by a change in the leak rate or in vapour pressure can perturb the process greatly. Devices are available that adapt the volume rate of flow through the vacuum pump in response to a varying gas load. For example, the diaphragm pressure regulator consists of a reference and measuring side separated by an elastomer diaphragm (Figure 7.32). When the pressure on both sides is equal,



**Figure 7.32** *Schematic diagram of a diaphragm pressure regulator*

the regulator seat is covered by the diaphragm. If the pressure in the process chamber increases, the seat is uncovered and connection to the pump is made. As the reference pressure is reached again, the diaphragm re-seats and further pressure decrease is prevented. Commercial diaphragm pressure regulators are available with limited maximum rates of gas flow (e.g. 16 and  $50 \text{ m}^3 \text{ h}^{-1}$ ). Their control range is  $10\text{--}10^3$  mbar and the accuracy is  $\pm 2\%$  of the set value. The response time is a few milliseconds. Regulators of this type are particularly suitable for use in hazardous locations and with aggressive gases.

## 7.4.5 Applications

### 7.4.5.1 Distillation

In conventional distillation at atmospheric pressure, heat is applied to the distilland in a boiler, and rapid evaporation occurs at the boiling point. The more volatile components pass into the vapour phase and are subsequently condensed. Although atmospheric stills are useful for materials with a low boiling point, they are far less successful in handling compounds with molecular weights much above 250 owing to decomposition before boiling.

One approach to the problem involves the reduction of the pressure in the still, but there is a practical limit to what can be achieved merely by the evacuation of conventional distillation apparatus (Ridgway Watt, 1963). Under conditions of intermediate or molecular flow, the rate at which gas travels down a conductance depends on the random diffusion of molecules rather than the size or efficiency of the pumping system. For example, with significant lengths of relatively narrow pipework, it is unlikely that the pressure at the distilling surface will be less than a few mbar even if the pressure in the receiver is in the medium vacuum range.

To operate efficiently at pressures below 1 mbar, equipment must be designed to overcome the problems associated with low-pressure gas flow. In so-called molecular stills, the condenser faces the evaporator across a relatively short distance within the vacuum chamber which is pumped via a wide manifold. Under these conditions, there is no well-defined boiling range and feed molecules leave the evaporator surface at any temperature, the evaporation rate being given by the Knudsen relationship. The first type of practical molecular still was the falling-film still. In such units the distilland flows downwards under gravity as a thin film over the surface of a heated evaporator. The film thickness and evenness depends on the feed flow-rate and viscosity and conditions on the surface. Generally, films of thickness 0.1–2 mm are formed and the exposure time of the distilland to elevated temperatures can vary between tens and hundreds of seconds. With falling-film units, the product is condensed externally and undistilled residue is cooled and passed to another still. The limitations of the plant are the development of 'hot spots' (leading to decomposition of the distilled material) and limits on achievable vacuum due to flow restrictions in the vapour handling line. An excellent monograph on molecular stills was prepared by Ridgway Watt (1963).

The 'thermal damage' to a sensitive distilland caused by exposure to elevated temperatures can be assessed by calculation of the decomposition hazard ( $D$ ):

$$D = P \times t$$

where  $P$  is the pressure and  $t$  is the heating time. Some results are shown in Table 7.14.

Some of the disadvantages noted with falling-film evaporators can be overcome by the use of a wiped-film evaporator in which a mechanical device is used to spread the distilland over the evaporator. By this means, hot spots

**Table 7.14** Comparison of different distillation processes according to decomposition hazard

<i>Still type</i>	<i>Heating time (s)</i>	<i>P (m Torr)*</i>	<i>D</i>
Laboratory pot still	3600	$760 \times 10^3$	$2.7 \times 10^9$
Laboratory pot still	3600	1	$3.6 \times 10^3$
Laboratory falling-film still	200	1	200
Wiped film evaporator + column	25	1	25
Improved wiped film evaporator	10	1	10

\* 1 Torr = 1.33 mbar,  $\therefore 1\text{mTorr} = 1.33 \times 10^{-3}$  mbar.



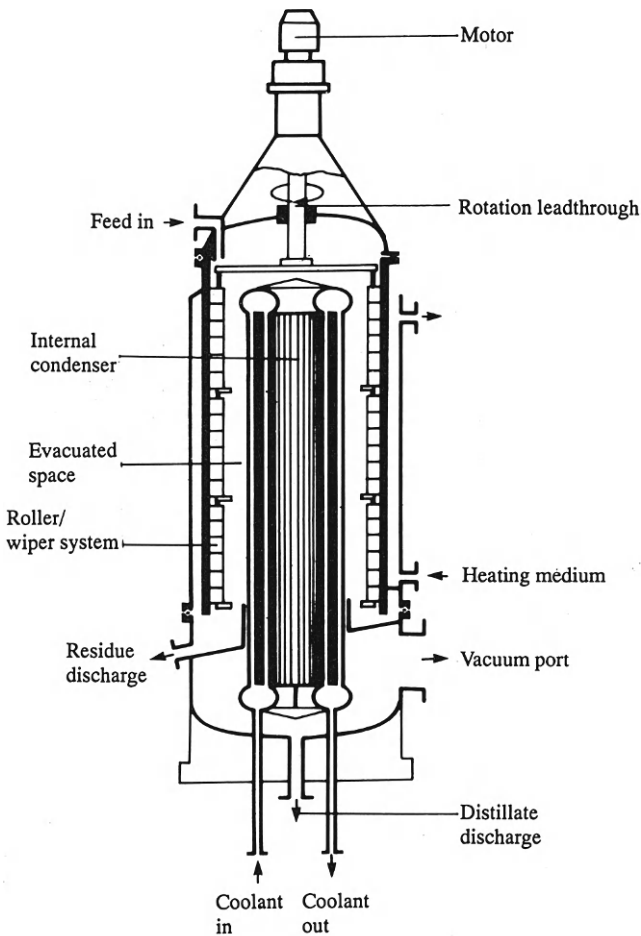
are avoided and heat and mass transfer are improved. With conventional units, vapour again leaves the evaporator for an external condenser. Design improvements have led to the development of stills in which the evaporator consists of a vertical cylinder with the evaporator. The thermal exposure time of mechanically agitated films depends on the properties of the material being handled and the form of the wiper but residence times in the evaporator of 5–15 s are found.

Strictly speaking, the term molecular distillation should be applied to a process in which the distance between the evaporator and condenser is less than the mean free path of molecules at the working pressure. In practice, such conditions can only be arranged in small units with an extremely low distillation rate. These are not economically viable for production purposes. Developments in wiped-film evaporator practice have led to short-path evaporators which work at pressures between 1 and  $10^{-2}$  mbar with evaporation surface areas between 0.1 and 36 m<sup>2</sup>. Feed rates of 20–200 kg m<sup>-2</sup> h<sup>-1</sup> are also possible (Figure 7.33). For many products, there are no precise calculations that describe the influence of parameters such as temperature, feed rate, peripheral load, etc. in a short-path evaporator but empirically obtained data can be transferred from laboratory scale to much larger units.

#### 7.4.5.2 *Drying*

Vacuum drying is an important process in, for example, the pharmaceutical industry. Apart from residual moisture, materials that have to be removed include solvents such as propan-2-one, ethanol, methanol, propan-2-ol and cyclohexanane. Based on known data for the product (maximum tolerable temperature, mass of batch, initial and final solvent loading, etc.) and the available process time, it is often possible to devise a vacuum system that will give a satisfactory product.

As an illustration of the procedure, reference should be made to Figure 7.34. This shows the variation of pressure with time in a system which preliminary experiments have shown to require a pressure  $P$  and a maximum temperature  $T_a$  in order for the drying process to be achieved within the available time. Figure 7.34 shows that after an initial pump-down, the pressure stabilizes at  $p_A$  and  $p_B$  for temperatures  $T_a$  and  $T_b$ , respectively. These correspond closely to the saturation vapour pressures of the evaporating substance at these temperatures ( $T_b$  is obviously lower than  $T_a$ ). If the drying process involves the evaporation of water, the duration of the isobaric phases at  $p_a$  and  $p_b$  corresponds to the time required for the removal of 'free' water. As soon as this is removed, more tightly bound water (adsorbed in the porous structure of the material) is driven off and the required pressure ( $p_{req}$ ) eventually attained. If evacuation is continued, then further reduction in pressure will be observed until either the ultimate pressure of the pump is achieved or gas in-leakage dictates the lower limit. The duration of drying process depends on the mass flow rate of the vapour, and this is determined by the temperature of the drying product. A rule-of-thumb relationship that has proved useful is:



**Figure 7.33** Schematic diagram showing a commercial short-path evaporator/condenser unit (vacuum system not shown)

$$\dot{m}_{\max} = \frac{\frac{2}{3} m_{\text{TOT}}}{\frac{1}{3} t_{\text{avail}}} = 2 \frac{m_{\text{TOT}}}{t_{\text{avail}}}$$

where  $m_{\text{TOT}}$  is the total amount of material to be removed and  $t_{\text{avail}}$  is the time available for drying. If after calculation of the pump size, the observed plateau pressure falls below the predicted level then the heat supplied to the drier is insufficient.

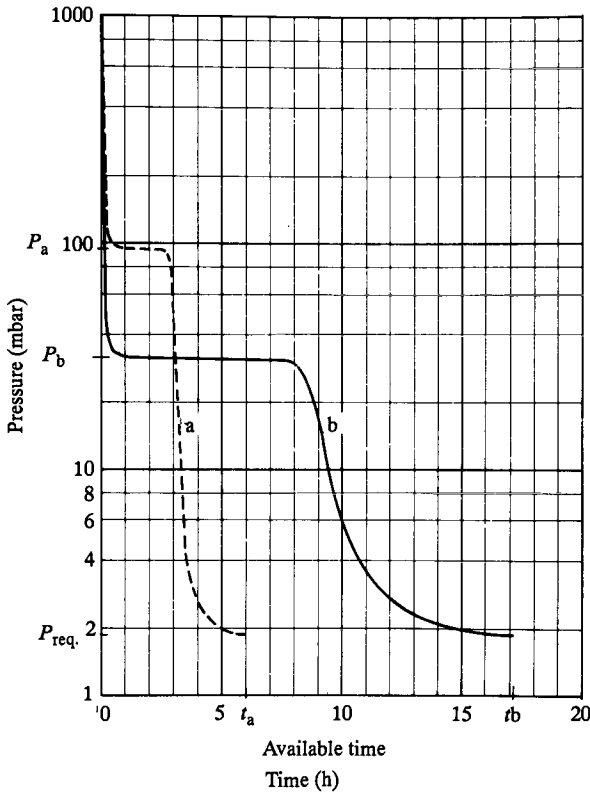


Figure 7.34 Pressure against time behaviour for a drying process: ---,  $T_a$ ; —,  $T_b$  (in both cases, the effective pumping speed of the vacuum system is the same)

7.4.5.3 Others

With air- and moisture-sensitive materials, it is essential to introduce inert gas to the system to reduce the partial pressures of water vapour and air. This can be achieved by evacuation to about 100 mbar, after initially pressurizing the system with inert gas.

References

Section 7.1

Almeida, J.B. (1989) *Vacuum*, **39**, 717  
 Armour, D.G., Bailey, P. and Sharples, G. (1986) *Vacuum*, **36**, 769  
 Boos, M., Klug, W. and Zoeller, A. (1986) *Patentanmeldung*, P36 27 232.9

- Bunshah, R.F. and Deshpandev, C. V. (1989) *Vacuum*, **39**, 955
- Colligon, J.S. (1986) *Vacuum*, **36**, 413
- Dearnaley, G., Goode, P.D., Minter, F.J., Peacock, A.T., Hughes, W. and Proctor, G.W. (1986) *Vacuum*, **36**, 807
- Duckworth, R.G., Maydell, E. and Muenz, W.D. (1987) Presented at the *International Symposium on Trends and New Applications in Thin Films, Strasbourg*, 16–20 March
- Goetzelmann, R., Hermann, R. and Zoeller, A. (1989) Presented at the *Symposium on Optical Coatings, Shanghai*, 23–25 May
- Holland, L. (1978) *Vacuum*, **28**, 437
- Iborra, E., Santamaria, J., Martil, I., Gonzalez-Diaz, G., and Sanchez-Quesoda, F. (1987) *Vacuum*, **37**, 437
- Kaneko, H., Nago, S. and Miyake, K. (1988) *Journal of Applied-Physics*, **63**, 510
- Kusano, E. *et al.* (1988) *Journal of Vacuum Science and Technology*, **A6**, 1663
- Lewin, R., Howson, R.P., Bishop, C.A. and Ridge, M.I. (1986) *Vacuum*, **36**, 95
- Maissel, L.I. and Glang, R. (1983) *Handbook of Thin-Film Technology*, McGraw-Hill, New York
- Muenz, W.D., Hofmann, D. and Hartig, K. (1982) *Thin Solid Films*, **96**, 79
- Musil, J. (1986) *Vacuum*, **36**, 161
- Musil, J., Poulek, V., Vyskocil, J. and Kadlec, S. (1988) *Vacuum*, **38**, 459
- Paule, E., Elizalde, E., Martinez-Duart, J.M. and Albella, J.M. (1987) *Vacuum*, **37**, 396
- Rizk, A., Youssef, S.B., Rizk, N.Z. and Habib, S.K. (1989) *Vacuum*, **39**, 471
- Rizk, N.S., Rizk, A. and Habib, S.K. (1990) *Vacuum*, **40**, 245
- Spencer, A.G. and Howson, R.P. (1986) *Vacuum*, **36**, 103
- Tan, G., Spencer, A.G. and Howson, R.P. (1991) *IEEE Transactions on Magnetics*, **27**, 664
- Sundgren, J.-E. and Henzell, H.T.G. (1986) *Journal of Vacuum Science and Technology*, **A4**, 2259
- Thomas, D.J., Southworth, P., Flowers, M.C. and Greef, R. (1989) *Journal of Vacuum Science and Technology*, **37**, 1325
- Varasi, M., Misiano, C., Mancini, C. and Sartori, P. (1986) *Vacuum*, **36**, 143
- Zoeller, A., Boos, M., Herrmann, R., Klug, W. and Lehnert, W. (1989) *Proceedings of SPIE*, (Society of Photo-optical Instrument Engineers), *Thin-Film Technologies III*, **109**, pp. 106–13

## Section 7.2

- Aitken, D. (1985) *Vacuum*, **36**, 953
- Aylett, B.J. and Tannahill, A.A. (1985) *Vacuum*, **35**, 435
- Bachmann, P. and Berges, H.P. (1986) *Solid State Technology*, **29**, 83
- Bachmann, P. and Kuhn, M. (1990) *Vacuum*, **41**, 1825
- Bürger, H.-D., Rossmannith, E., Crinquette, J.-M. and Taberlet, M. (1990) *Vacuum*, **41**, 1822
- Davies, G. (1988) *Physics Bulletin*, 22

- Duval, P. (1988) *High Vacuum Production in the Microelectronics Industry*, Alcatel/Elsevier Science Publishers B V, Amsterdam
- Flamm, D.L. and Mucha, J.A. (1987) In *The Chemistry of the Semiconductor Industry* (eds S.J. Moss and A. Ledwith), Blackie and Son, Glasgow, p. 343
- Hucknall, D.J. and Kuhn, M. (1991) *Nuclear Instruments and Methods in Physics Research*, **B55**, 439
- John, P. (1980) In *The Chemistry of the Semiconductor Industry* (eds S.J. Moss and A. Ledwith), Blackie and Son, Glasgow, p.98
- John, P. and Jones, B.L. (1987) In *The Chemistry of the Semiconductor Industry* (eds S.J. Moss and A. Ledwith), Blackie and Son, Glasgow, p. 126
- Joyce, B.A. (1989) *Advanced Materials*, (8-0), 270
- Kuhn, M. and Bachmann, P. (1987) *Journal of Vacuum Science and Technology*, **A5**, 2534
- Mason, N.J. (1987) In *The Chemistry of the Semiconductor Industry* (eds S.J. Moss and A. Ledwith), Blackie and Son, Glasgow, p. 139
- O'Hanlon, J.F. (1980) *A User's Guide to Vacuum Technology*, Wiley-Interscience, New York
- O'Hanlon, J.F. and Fraser, D.B. (1988) *Journal of Vacuum Science and Technology*, **A6**, 1226
- Rosser, P. and Tomkins, G. (1985) *Vacuum*, **35**, 419
- Speight, J. (1987) In *The Chemistry of the Semiconductor Industry* (eds S.J. Moss and A. Ledwith), Blackie and Son, Glasgow, p. 1
- Sze, S.M. (ed.) (1983) *VLSI Technology*, McGraw-Hill, Singapore
- Williams, J.O. (1989) *Advanced Materials* (8-9), 282

### Section 7.3

- Apelian, D. and Mutharasan, R. (1980) *Journal of Metals*, **32**, 14
- Betz, U., Kemmer, H., Schlebusch, D. and Schwarz, W. (1988) Paper presented at the Ninth International Vacuum Metallurgy Conference on Special Melting, San Diego, April
- Choudhury, A. (1986) Vacuum electroslag remelting. Paper presented at the *International Vacuum Metallurgy Conference, Pittsburgh*
- Choudhury, A. and Brueckmann, G. (1987) *Presented at the UN Seminar on the Economic Aspects of Secondary Steelmaking, Dresden, 15-19 June*
- Choudhury, A., Brueckmann, G., Wagner, H., Knell, F. and Mueller, F. (1987) 'ESR-The Status of the Remelting Process under Slag', Leybold publication 36-811.02
- Choudhury, A., Brueckmann, G., Scholz, H., Schmitt, Ch. and Rogge, B. (1988) *Metallurgical and Plant Technology*, Vol. 5, Verlag Stahleisen, Dusseldorf, p.44
- Hsiao, T., Lehner, T. and Kjellberg, B. (1980) *Scanning metals*, **9**
- Johnson, W.E. and Sutton, W.H. (1977) Residual Gas Analysis applied to VIM. In *Proceedings of the 35th Electric Furnace Conference, AIME*, p. 207
- Kent, W.B. (1974) *Journal of Vacuum Science and Technology*, **11**, 1038

- Knueppel, H. (1983) *Desoxidation und Vakuumbehandlung von Stahlschmelzen*, Vol. 2, Verlag Stahleisen, Duesseldorf, p. 299
- Pridgeon, J.W., Darmara, F.N., Huntington, J.S. and Sutton, W.H. (1981) *Metallurgical Treatises 1981*, The Metallurgical Society of AIME, London, p. 201
- Sutton, W.H. and Morris, J.R. (1984) Paper presented at the *31st Meeting of the Investment Casting Institute*
- Tix, A. *et al.* (1959) *Stahl und Eisen*, **79**, 472
- Winkler, O. and Bakish, R. (1971) Papers in *Vacuum Metallurgy*, Elsevier Scientific Publishing, Amsterdam

#### Section 7.4

- Fausser, F. (1989) In *Theory and Practice of Vacuum Technology* (eds M. Wutz, H. Adam and W. Walcher), Vieweg and Son, Braunschweig/Wiesbaden, p. 291
- Mangnall, K. (1971) *A Technical Guide to Vacuum and Pressure Producing Equipment*, Hick Hargreave, Bolton
- Ridgway Watt, P. (1963) *Molecular Stills*, Chapman and Hall, London.

# 8

## *Appendix: units, conversion factors and other data*

---

### 8.1 Units of pressure

Other permissible units of pressure are bar and millibar (mbar). 1 bar corresponds to 100 000 ( $10^5$ ) Pa. 1 mbar equals  $10^{-3}$  bar. A reference condition known as a 'standard atmosphere' (atm) is defined as 101.325 kPa. This should not be used as a unit of pressure.

Units that have been used in the past are based on the use of mercury in barometers. A column of mercury 760 mm high exerts a pressure of 1 atm. The Torr (named after Toricelli, the inventor of the barometer) is (to within one part in 7 million) equal to 1 mm mercury (mm Hg). 1 Torr equals 133.3224 Pa (about 1.33 mbar). One unacceptable unit of pressure is the micron ( $\mu$ ):

$$1 \mu = 10^{-3} \text{ Torr}$$

Table 8.1 gives conversion factors between some pressure units.

### 8.2 Amount of substance

One mole (1 mol) of a substance is defined as that amount that contains as many elementary entities (these can be atoms, molecules or other specified species where appropriate) as there are atoms in 12 g of the carbon isotope,  $^{12}\text{C}$ . This number is given by the Avogadro constant ( $N_A$ ) =  $6.022136 \times 10^{23} \text{ mol}^{-1}$ .

The number of specified elementary entities is  $nN_A$  where  $n$  denotes the amount of the substance being considered.

**Table 8.1** *Conversion factors*

	<i>Pa</i>	<i>bar</i>	<i>mbar</i>	<i>atm</i>	<i>Torr</i>
1 Pa ( $1 \text{ N m}^{-2}$ )	1	$10^{-5}$	$10^{-2}$	$9.8692 \times 10^{-6}$	$7.5006 \times 10^{-3}$
1 bar	$10^5$	1	$10^3$	0.98692	750.06
1 mbar	100	$10^{-3}$	1	$9.8692 \times 10^{-4}$	0.75006
1 atm	101325	1.01325	1013.25	1	760
1 Torr	133.322	0.001333	1.333	$1.31579 \times 10^{-3}$	1

The amount of substance is given by:

$$n = m/M_r$$

where  $m$  = mass of substance and  $M_r$  = the relative molar mass (the 'molecular weight'; [ $M_r$ ] = g mol<sup>-1</sup>; kg kmol<sup>-1</sup>).

1 mol of particles (atoms, molecules) of a gas behaving perfectly occupies 22.414 l at 1013 mbar and 273K. The volume occupied at 298K is 24.466 l.

Some fundamental physical constants are given in Table 8.2.

**Table 8.2** Fundamental physical constants

Quantity	Symbol	Value	Units
Avogadro constant	$N_A$	6.022136	10 <sup>23</sup> mol <sup>-1</sup>
Molar gas constant	R	8.314510 (83.145)	J mol <sup>-1</sup> K <sup>-1</sup> (mbar l mol <sup>-1</sup> K <sup>-1</sup> )
Boltzmann constant, (R/ $N_A$ )	K	1.380658 (13.80658)	10 <sup>-23</sup> J K <sup>-1</sup> (10 <sup>-23</sup> mbar l K <sup>-1</sup> )
Stefan-Boltzmann constant	$\sigma$	5.67051	10 <sup>-8</sup> W m <sup>-2</sup> K <sup>-4</sup>
atomic mass unit, $m_u = 1/12 m(^{12}\text{C})$	$u$	1.660540	10 <sup>-27</sup> kg

**Table 8.3** Composition of dry atmospheric air at sea level

Component	Mass (%)	Volume (%)	Partial pressure (mbar)
N <sub>2</sub>	75.51	78.1	792
O <sub>2</sub>	23.01	20.93	212
Ar	1.29	0.93	9.47
CO <sub>2</sub>	0.04	0.83	0.31
Ne	1.2 × 10 <sup>-3</sup>	1.8 × 10 <sup>-3</sup>	1.9 × 10 <sup>-2</sup>
He	7 × 10 <sup>-5</sup>	7 × 10 <sup>-5</sup>	5.3 × 10 <sup>-3</sup>
CH <sub>4</sub>	2 × 10 <sup>-4</sup>	2 × 10 <sup>-3</sup>	2 × 10 <sup>-3</sup>
Kr	3 × 10 <sup>-4</sup>	1.1 × 10 <sup>-4</sup>	1.1 × 10 <sup>-3</sup>
N <sub>2</sub> O	6 × 10 <sup>-5</sup>	5 × 10 <sup>-5</sup>	5 × 10 <sup>-4</sup>
H <sub>2</sub>	5 × 10 <sup>-6</sup>	5 × 10 <sup>-5</sup>	5 × 10 <sup>-4</sup>
Xe	4 × 10 <sup>-5</sup>	8.7 × 10 <sup>-6</sup>	9 × 10 <sup>-5</sup>
O <sub>3</sub>	9 × 10 <sup>-6</sup>	7 × 10 <sup>-6</sup>	7 × 10 <sup>-5</sup>
	Σ 100%	Σ 100%	Σ 1013
50% RH at 20°C	1.6	1.15	11.7



**Table 8.4** *Physical properties of some gases*

<i>Gas</i>	<i>Density (kg m<sup>-3</sup>)</i>	$\sigma$ (nm <sup>2</sup> )	$\bar{c}$ (m s <sup>-1</sup> )*	$\bar{l}_p$ (m mbar)
H <sub>2</sub>	0.082	0.27	1770	$11.5 \times 10^{-5}$
He	0.164	0.21	1256	$17.5 \times 10^{-5}$
CH <sub>4</sub>	0.0657	0.46	627	–
O <sub>2</sub>	1.310	0.40	444	$6.5 \times 10^{-5}$
N <sub>2</sub>	1.146	0.43	474	$5.9 \times 10^{-5}$
Air	1.184	–	467	$6.65 \times 10^{-5}$
Ar	1.634	0.36	398	$6.4 \times 10^{-5}$

\* At 25°C and 1.013 bar.

† At 298.16K.

### 8.3 PNEUROP specifications for the characterization of vacuum pumps

Standard procedures have been established for the measurement of the relevant characteristics for different types of vacuum pumps. The following have been published (Table 8.5).

Recommended procedures for pump characterization are given and, depending on the type of pump, include:

1. Volume rate of flow (pumping speed).
2. Ultimate pressure.
3. Water vapour tolerance.
4. Critical backing pressure, etc.

**Table 8.5** *PNEUROP recommendations*

<i>No.</i>	<i>Title</i>	<i>Year</i>
6602	Part 1 Oil-sealed rotary pumps and Roots pumps	1979
5607	Part 2 Vapour pumps	1972
5608	Part 3 Turbomolecular pumps	1973
5615	Part 4 Sputter-ion pumps	1976
66120	Acceptance specification for liquid ring vacuum pumps	1984

Some characteristics are only of importance with certain types of pump and reference must be made to the appropriate chapter. Test equipment is usually common to all procedures and is described below.

### 8.3.1 Apparatus

#### 8.3.1.1 Test dome

Test domes used in the determination of pump characteristics are shown in Figure 8.1. The volume of the dome should be at least five times that of the chamber of the pump under test (the latter calculated by dividing the nominal speed of the pump by its rotational speed). Ideally, the test dome should have the same diameter as the pump inlet. However, the diameter of the dome should not be less than 100 mm and, in certain cases, a transition piece, as indicated in Figure 8.1(a), must be used.

#### 8.3.1.2 Pressure measurement

The PNEUROP specifications recommend the type of pressure measuring device to be used for tests. These are summarized in Table 8.6.

#### 8.3.1.3 Flow measurement

Measurement of the volume of gas admitted to the test dome is carried out at atmospheric pressure. The method adopted depends on the required flow rate and accuracy but it is recommended that, for flow rates greater than 10 mbar l s<sup>-1</sup>, an accuracy of  $\pm 3\%$  should be achieved. For flow rates between 10 and  $1 \times 10^{-3}$  mbar l s<sup>-1</sup> should be determined to within 5%. For lower flow rates,  $\pm 10\%$  is suggested. Methods for fluid flow measurement are summarized in Table 8.7.

### 8.3.2 Procedure

For practical purposes, the volume rate of flow of a given gas is given as  $Q_{pv}$  divided by the equilibrium pressure  $P$  established at a specified position in a test dome under certain operating conditions ( $S^* = Q_{pv}/P$ ). Pumping speed is determined by maintaining a constant pressure at the pump inlet during measurement. This is brought about by keeping the pressure, measured at a point on the dome, constant during the test.

The apparatus is assembled as shown in Figures 8.2 and 8.3, for example. Prior to measurement, the pump(s) are filled with the prescribed quantity and grade of oil. If primary pumps are necessary (as with diffusion and turbomolecular pumps), the manufacturer's recommendations should have been followed.

The dome is evacuated, with the leak valve closed until the pump has reached its operating temperature and a constant pressure is achieved. Test gas (usually ambient air) is then introduced to achieve the required pressure. Once this pressure has been achieved, it should remain steady ( $\pm 2.5\%$ ) for 30 minutes before a reading is taken. The pumping speed is measured point-by-point, starting at the lowest pressure, for different pump-inlet



**Table 8.6** Pressure gauges recommended by PNEUROP

Range (mbar)	Gauge	Accuracy
> 20	U-tube	± 1 mbar
	Diaphragm	± 5% } indicated
	Capacitance manometer*	± 2% } value
20 to $1 \times 10^{-2}$	Capacitance manometer*	± 2%
	McLeod gauge†	± 5%
	Pirani	± 10%
1 to $1 \times 10^{-3}$	Capacitance manometer*	± 2%
$10^{-2} - 10^{-6}$	Hot cathode ionization gauge	± 10%

\* Calibrated.

† With trap at  $-80 < T < -10^\circ\text{C}$ ;  $T_{\text{Hg}} > 25^\circ\text{C}$ .**Table 8.7** Flow measuring equipment recommended by PNEUROP

Flow rate (mbar l s <sup>-1</sup> )	Method	Accuracy
> 1	Float-type devices (rotameters)	± 5%
	Orifice devices	
10 to $10^{-3}$	Displacement (burette)	± 5%
3 to about $10^{-2}$	Calibrated capillary	± 5%
$> 5 \times 10^{-4}$	Thermal flowmeters	± 10%
$< 10^{-3}$	Conductance	± 10%

pressures. For each point, the following data are obtained:  $P_{\text{atm}}$ ,  $P_{\text{inlet}}$  and volume of gas ( $V$ ) at  $P_{\text{atm}}$  pumped during the measurement period ( $t$ ).

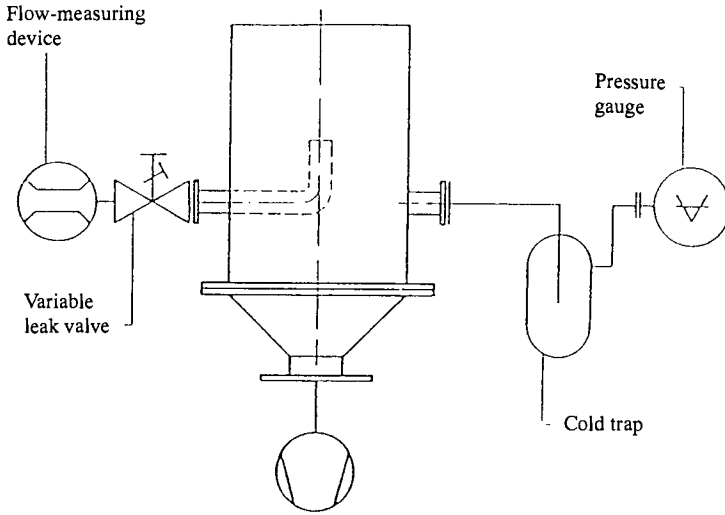
Then,

$$S^* = \frac{Q_{\text{pv}}}{(P - P_0)}; \quad [S^*] = \text{m}^3 \text{h}^{-1} \text{ or } \text{l s}^{-1}$$

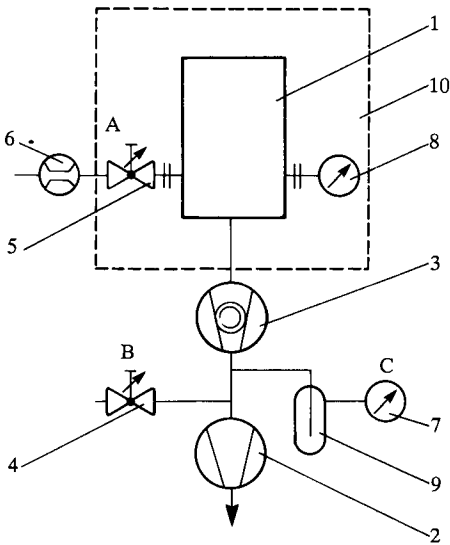
where  $Q_{\text{pv}}$  is the gas throughput measured at atmospheric pressure,  $P$  is the pressure maintained and measured in the dome and  $P_0$  is the equilibrium pressure in the dome prior to the start of measurements:

$$= \frac{VP_{\text{atm}}}{t(P - P_0)} \Rightarrow \frac{VP_{\text{atm}}}{tP}$$

Values of  $S^*$  are plotted against  $P$ .



**Figure 8.2** Arrangement for the measurement of the pumping speed of an oil-sealed rotary pump. (Reproduced by kind permission of the British Compressed Air Society)



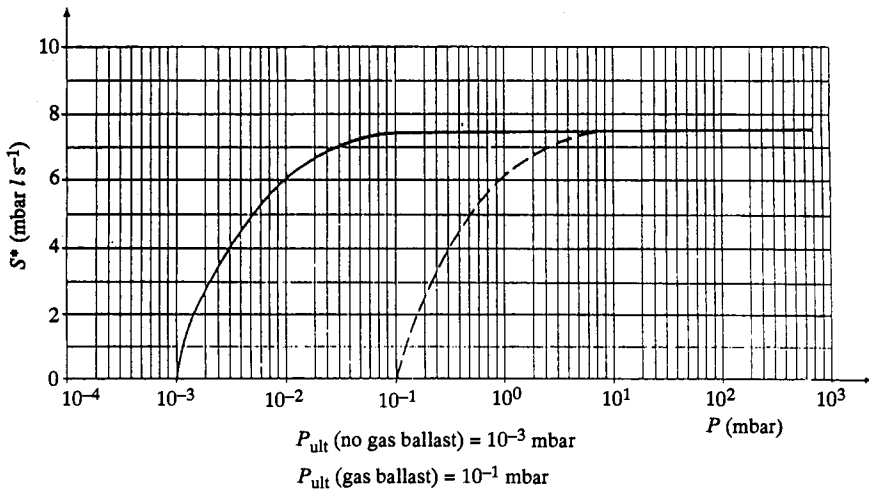
**Figure 8.3** Arrangement for the measurement of the pumping speed of a turbomolecular pump. 1, test dome; 2, backing pump; 3, turbomolecular pump; 4, gas inlet valve; 5, gas inlet valve; 6, flowmeter; 7, 8 pressure gauge; 9, cold trap; 10, heating jacket. (Reproduced by kind permission of the British Compressed Air Society)

A typical plot of the variation of  $S^*$  with  $P$  for an oil-sealed rotary vacuum pump is shown in Figure 8.4. Variations of  $S^*$  with  $P$  for other types of vacuum pumps will be discussed in the relevant section.

### 8.3.3 Measurement of ultimate pressure

The ultimate pressure of a vacuum pump is the lowest pressure that the pump reaches asymptotically at its intake. It is measured using a test dome with the gas inlet valve closed. For oil-sealed rotary pumps, the importance of distinguishing between ultimate total pressure and ultimate total pressure due to permanent gases is emphasized. Thus a cold trap must *not* be inserted between the dome and the gauge and the blanked-off total pressure measurement must be made using a diaphragm-type vacuum gauge. The required pressure is reached when three consecutive measurements show a constant value. The ultimate pressure for mechanical pumps reflects the 'tightness' of the pump (presence of leaks, function of gas exhaust, etc.).

Some comments must be made regarding high vacuum pumps. In the PNEUROP Acceptance Specifications for vapour pumps it is recommended that values for the ultimate pressure are not specified. For turbomolecular and sputter-ion pumps, however, a procedure is laid down for the measurement of the 'ultimate operational pressure'. The pressure, measured using a hot cathode ionization gauge degassed according to the manufacturer's instructions, 48 h after bake-out, is then regarded as the ultimate operational pressure.



**Figure 8.4** Variation of pumping speed with pressure for a two-stage, oil-sealed rotary vane pump —,  $P_{\text{ult}}$  (no gas ballast) =  $10^{-3}$  mbar; ---,  $P_{\text{ult}}$  (gas ballast) =  $10^{-1}$  mbar

# Index

---

- Adsorption (sorption) pump, 96–9
- Aflas, 219 (table)
- Air ejector, 76, 77 (fig)
- Alloy, 207–8
  - aluminium, *see* Aluminium/aluminium alloy
  - copper, 216
  - degassing, 208–11
  - nickle-containing, 214, 214 (table)
  - permeation, 211–16
  - vapour pressure, 208
- Aluminium/aluminium alloy, 214, 215 (table), 216
  - degassing for alloys, 215 (table)
  - etching, 269
  - physical vapour deposition evaporation sources, 238 (fig)
- Area-related outgassing (pump-down time), 23 (fig)
  
- Back-streaming, 82–4
- Baffle, 82–3, 84 (fig)
- Ballast, 263
- Batch coater, 250–1
- Bayard-Alpert gauge, 141–22, 143, 144–6
- Bounce-back, 105
- Bourdon tube gauge, 130
- Box coater, 250–51
- Bubble test, 174
- Bulk getter (NEG) pump, 101
- By-pass line, 61–2
  
- Capacitance manometer, 133
- Capsule vacuum gauge, 130–31
- Ceramics, 218–20
- Chemical industry, 286–302
  - condenser, *see* Condenser distillation, 298–300
  - drying, 300–2
  - gas–liquid separation, 287
  - gas–solid separation, 288
  - pressure control, 297–8
  - pressure measurement, 287–8
  - vacuum pumps, 288–90
  - vacuum sealing fluids, 289 (table)
- Clapeyron equation, 287
- Clausius–Clapeyron equation, 287
- Claw type pump, 64–7
- Coating system, *see* Deposition system
- Cold trap, spherical, 84 (fig)
- Compression gauge, 297
- Compression vacuum gauge, 128–30
- Condensation, effect on pump performance, 41–5
- Condenser, 72–4, 290–7
  - coil-type, 291 (fig)
  - combined with vacuum pump, 295–7
  - performance, 290–2
  - pressure distribution, 292–5
- Conductance formulae, 15 (example)
- ConFlat flange, 225
- Copper/copper alloy, 216
- Cryocondensation, 107, 109 (fig)
- Cryocooler, 114–18
- Cryogen, 113
  - cooling potential, 113 (table)
  - use in cryopump, 113, 114 (table)
- Cryopump, 107–24
  - bath, 113–14
  - capacity, 112–13
  - evaporator, 113–14
  - pumping speed, 111–12
  - refrigerator-cooled, 114–24
  - starting pressure, 110
  - stay-down time, 112
  - ultimate pressure, 110–11
  - use in:
    - nuclear fusion technology, 121–2
    - semiconductor processing, 124
    - space simulation, 123
- Cryosorption, 107–8, 109 (fig)
- Cryotrapping, 108, 109 (fig)
  
- Dalton's law, 4–5, 287
  - combined with Raoult's law, 288

- Degassing, 24, 208–11  
 area-related, 23 (fig)
- Dempster-type mass spectrometer, 152
- deposition/deposition process:  
 chemical vapour deposition (CVD),  
 260–4  
 ion-assisted, 244–6  
 metal organic vapour phase epitaxy  
 (MOVPE), 264–5  
 molecular beam epitaxy (MBE),  
 265–6  
 physical vapour deposition (PVD),  
 236–50  
 coating plant, 237  
 sputter, 240–4  
 thin film, 235–55
- Deposition system:  
 batch coater, 250–1  
 in-line coater, 254–5  
 webb coater, 251–4, 255 (fig)
- Desorption, 208–10
- Diaphragm pressure regulator, 297–8
- Diaphragm switch, 130–31
- Diaphragm vacuum gauge, 131–2
- Diffusion:  
 dopant introduction by, 269–70  
 leak, 202–3
- Diffusion pump, 79–85  
 back-streaming, 82–4  
 critical backing pressure, 85  
 fluids, 81–2
- Diode-type pump, 104 (fig), 105
- Discharge-gas cooler, 62
- Distillation, 298–300
- Dopant, 269–70
- Dry vacuum pump, 64–9  
 claw-type, 64–7  
 molecular drag, 67–9  
 piston, 67  
 Roots-type, 64–7  
 scroll, 69
- Drying, vacuum, 300–302
- Ejector pump, 70 (fig), 70–1  
 air, 76–7  
 oil, 74–6  
 steam, 71–4
- Elastomer, 216–17
- Electron impact emission spectroscopy  
 (EIES), 247  
 sensor, 249 (fig)
- Electron impact ionization, 153–4
- Electroslag remelting (ESR), 285
- Ellipsometry, 247
- Entrapment pump, 96–124  
 adsorption, 96–9  
 cryopump, *see* Cryopump  
 getter, 99–103  
 sputter-ion, 103–6  
 diode-type, 104 (fig)
- etching process, 266–9
- Falling-film still, 299
- Film deposition, *see* Deposition/  
 deposition process
- Fluid entrainment pump, 69–76
- Gaede molecular drag pump, 67
- Gaede–Ishii effect, 149
- Gas:  
 imperfections, 7  
 in vacuum induction melting furnace,  
 282 (fig)  
 kinetic theory, *see* Kinetic theory  
 mixtures, 4–5  
 perfect (ideal), 3–4  
 properties, 171 (table)  
 pure mass spectra, 164 (fig)  
 rational speed/compression ratio of  
 turbomolecular pump, 193 (fig)  
 sources within vacuum systems, 3 (fig)
- Gas flow, 7–10  
 flow rate, *see below* throughput (flux  
 rate)  
 resistance/conductance, 9–10  
 effective pumping speed, 10  
 throughput (flow rate), 8–9  
 mass throughput (mass flow rate), 8  
 molar throughput (molar flow  
 rate), 8  
 volume throughput (volume flow  
 rate), 8–9
- Gas flow calculation, 10–17  
 pressures  $10^3$ –1 mbar, 10–13  
 nozzles, apertures, orifices, 10–11  
 viscous flow in tubes, 11–13  
 pressures  $1$ – $10^{-3}$  mbar, 16–17  
 under conditions of high/ultra-high  
 vacua, 13–16  
 conductance of short tube, 14–15  
 curved/bent tube, 15–16



- Gas flow calculation (*cont'd*)  
 flow through long tube, 14  
 flow through orifice, 14
- Gas transfer pump, 2 (fig), 79–95  
 diffusion, 79–85  
 turbomolecular, *see* Turbomolecular pump
- Gay-Lussac, 4
- Getter pump, 99–103
- Gifford–McMahon:  
 cold head, 117 (fig), 118 (fig), 119 (fig)  
 refrigeration cycle, 116 (fig)  
 refrigerator, 114–15
- Glass, 219
- Henry's law, 288
- Helium-specific mass spectrometer leak detector, 190–201  
 counterflow, 192 (fig), 198 (fig), 200 (fig)  
 double-focussing, 196 (fig)  
 lay-out, 193–9  
 main flow, 191 (fig), 194 (fig)  
 operation, 199–201
- Hot spots, 299, 299–300
- In-line coater, 254–5
- Ion implantation, 270
- Ionization gauge, 139–46  
 Bayard–Alpert, 141–2, 143, 144–6  
 cold cathode, 139–41  
 high pressure, 143–4  
 hot cathode, 141–3
- Instability for noble gases, 105
- Kammerer compression gauge, 129
- Kinney rotary pump, 47 (fig)
- Kinetic theory, 5–6  
 collisions, 6  
 mean free path, 7  
 velocity distribution, 6
- Kinetic vacuum pump, 69
- Knudsen conductance formulae, 14
- Knudsen number, 7–8
- Kruger–Shapiro assumption, 86
- Leak:  
 calibrated, 201–3  
 capillary, 201–2  
 diffusion, 202–3  
 rates, 171 (table)
- Leak detection, 168–206  
 bubble tests, 174  
 definition, 169–73  
 formulae, 169–73  
 gas-phase tracer test, 174  
 halogen-containing compound use, 179  
 Helium use, 174–9  
 Helium, 168, 177 (fig), 179 (fig)  
 sample probe, 178 (fig)  
 pressure drop method, 173  
 pressure rise method, 180–1  
 search gas use, 181–7  
 sniffer use, 174–9  
 units, 169–73  
 vacuum plant, 203–6
- Leak detector, 187  
 contamination, 205  
 plant, 205–6  
 halogen, 187–90  
 drawbacks, 190  
 relative sensitivity to halogenocarbons, 188 (fig)  
 heated anode detector, 187–90  
 helium-specific mass spectrometer leak detector, 190–201  
 counterflow, 192 (fig), 198 (fig), 200 (fig)  
 lay-out, 193–9  
 main flow, 191 (fig), 194 (fig)  
 operation, 199–201  
 Tesla coil detector, 187
- Leybold Roots vacuum pump, 260 (fig)
- Leybold rotary piston pump, 46 (fig)
- Leybold UHV A1 gasket, 224
- Liquid ring pump, 27–30  
 pumping speed/pressure curves, 31 (fig)  
 service-fluid temperature effect on performance, 31 (fig)
- McLeod gauge, 126 128–9
- Mass spectrometer leak detector, helium specific *see* Helium-specific mass spectrometer leak detector
- Maxwell–Boltzmann distribution, 6
- Metal(s):  
 high purity, manufacture, 275–81

- pure, 207–16
- Metal bellows pump, 67, 68 (fig)
- Metal organic vapour phase epitaxy (MOVPE), 264–5
- Metallurgical processing, 270–85
  - complex alloy manufacture, 275–81
  - high purity metal manufacture, 275–81
  - remelting, 281–5
  - steelmaking, 271–5
- Mineral oil, *see under* Oil
- Molecular beam epitaxy (MBE), 265–6
- Molecular drag pump, 67–9
- Molecular still, 299
- Motive fluid, 69
  
- NEG bulk getter pump, 101
- Neoprene, 219 (table)
- Nickel, 214
- Nickel-containing alloy, 214
  - composition, 214 (table)
- Northey-type claw pump, 54–5
  
- Ohm's law, 9
- Oil:
  - filtration, 263, 264 (fig)
  - mineral, 37, 38–41 *passim*
  - quality assessment, 39 (table)
  - use in semiconductor process, 263 (table)
- Oil-booster pump, 75, 76 (fig)
- Oil-ejector pump, 75
- Oil-sealed vacuum pump function, 36–41
- Oil vapour ejector, 74–6
- O-ring, 222–3, 226
- Outgassing, 210–11
  - area-related (pump-down time), 23 (fig)
  
- Paul, W., 152
- Penning cell, 103
- Penning experiments, 139
- Penning gauge/Pirani gauge combined, 141
- Perbunan, 219 (table)
- Perfluoroalkyl ether (PFAPE), 257
- Perfluoropolyether (PFPE), 257
- Permeation, 211
  
- Photometer, double-beam type, 246–7
- Pirani gauge, 135–8 *passim*, 297
  - Penning gauge combined, 141
- Piston pump, 67
- Plasma etching, 266–9
- Plasma-chemical process, 240
- Plastic, thermosetting, 216
- PNEUROP, 9
  - specifications for vacuum pump, 308–13
- Polyethylene, 216, 219 (table)
- Polymer, 216–17
  - characteristics, 219 (table)
- Polypropylene, 216
- Pressure leak testing, 173–9
- Pressure measurement, 126–66
  - compression vacuum gauge, 128–30
  - ionization gauge, 139–46
    - Bayard–Alpert, 144–46
    - cold cathode, 139–41
    - high pressure, 143–4
    - hot cathode, 141–3
  - liquid level manometer, 127
  - mechanical vacuum gauge, 130–33
    - Bourdon tube gauge, 130
    - capacitance manometer, 133
    - capsule vacuum gauge, 131–2
    - diaphragm vacuum gauge, 131–2
  - residual gas analyser (RGA), 153–66
  - spinning rotor gauge, 146–8
  - thermal conductivity vacuum gauge, 134–8
  - vacuum gauge calibration, 148–51, 152 (fig)
    - dynamic method, 150 (fig)
  - vacuum gauge connection, 151–2
- Pressure relief valve, 61–2
- PTFE, 216, 219 (table)
- Pressure-sensitive switch, 59–60, 130
- Pump-down time (area-related outgassing), 23 (fig)
- pump performance:
  - condensation effect on, 41–5
  - service-fluid temperature effect on, 31 (table)
- PVC, 219 (table)
  
- Quadrupole mass spectrometer:
  - applications, 165–6
  - qualitative analysis, 162–3
  - quantitative measurement, 163–5

- Quartz crystal monitor, 246, 248 (fig)  
 Quick-test sniffer, 175
- Raoult's law, 288  
 Refrigerator, 114  
 Refrigerator-cooled cryopump, 114  
 (table), 114–24  
 Residual gas analyser, 153–66  
 characteristics, 160–2  
 ion detection, 158–60  
 ion sources, 154–5  
 mass filter, 156–8, 159 (fig)  
 quadrupole mass spectrometer, 165–6  
 qualitative analysis with quadrupoles,  
 162–3  
 quantitative measurements with qua-  
 drupoles, 163–5  
 Reynolds number, 8, 12  
 Roots-type pump, 64–7  
 Roots vacuum pump, 50–9  
 diffusion pump, 79–85  
 Edwards, 81 (fig)  
 dry vacuum pump, 64–9  
 Edwards, 65 (fig)  
 Leybold, 260 (fig)  
 longitudinal section, 50–1  
 operation, 51  
 pressure-sensitive switch, 59–60  
 pumping chamber clearances, 51 (fig)  
 rotary vane pump, 30–6  
 Leybold, 36 (fig)  
 speed control, 63–4  
 turbomolecular pump, 85–95  
 Balzers, 88 (fig)  
 Leybold, 90 (fig)  
 use of:  
 by-pass line, 60–2  
 discharge-gas cooler, 62  
 pressure-relief valve, 60–2  
 Rotary piston pump (rotary plunger  
 pump), 45–9  
 oil-sealed/function of sealant, 36–41  
 pumping speed/pressure curves, 46  
 (fig), 47 (fig)  
 working cycle, 48 (fig), 49 (fig)  
 Rotary pump, 27–49  
 condensation effect on, 41–5  
 liquid ring, 27–30  
 oil-sealed, function, 36–41  
 piston, 45–9  
 rotary vane, *see* Rotary vane pump
- Rotary vane pump, 30–36  
 oil-sealed/function of sealant, 37–43  
 pumping speed/pressure curves, 37  
 (fig)  
 single-, two-stage, ultimate pressures,  
 34 (table)  
 vapour effect on performance, 41–3  
 vapour tolerance, 43–5  
 water vapour tolerance, 43, 44 (table)  
 Rubber, 216  
 RUTA pump system, pumping speed  
 curves, 22 (fig)
- Satellite propulsion system, 177 (fig)  
 Scroll pump, 69  
 Sealant, 37, 38–9  
 Semiconductor industry, 256–70  
 circuit fabrication, 258–9 (figs)  
 deposition process, 260–6  
 dopants, 269–70  
 etching process, 266–9  
 Short path evaporator/condenser, 301  
 (fig)  
 Sniffer, 174–9, 189  
 Quick-Test, 175  
 Solvay refrigerator, 114  
 Sorption (adsorption) pump, 96–9  
 Sputter-ion pump, 103–6  
 diode-type, 104 (fig)  
 Sputtering, 241–4  
 Steam ejector, 71–4, 75 (fig)  
 Steel:  
 degassing, 271 (table), 279 (table)  
 mild (carbon steel), 213  
 stainless, 213–14  
 Steelmaking, 271–5  
 Still, 299  
 Stirling refrigerator, 114  
 Suction fluid, 69  
 Synthetic fluid, 37, 38–41 *passim*
- Tesla coil detector, 187  
 Thermoplastic, 216  
 Thermosetting plastic, 216  
 Titanium sublimation pump, 100, 102  
 (fig)  
 Triode pump, 105, 106 (fig)  
 Turbomolecular pump, 85–95  
 compression ratio/rotational speed for  
 gases, 193 (fig)

- design, 88–90
  - hydrocarbon contamination during deceleration, 91 (fig)
  - operation, 90–3
  - pumping speed variation, 92 (fig)
  - theory, 86–8
  - twin-inlet, 199 (fig)
  - use in:
    - electrical industry, 95
    - electronics, 95
    - nuclear technology, 94–5
    - with magnetic bearings, 90 (fig)
- Vacuum:**
- high, 2 (table)
    - standard valves, 227–30
  - medium, 2 (table)
    - standard valves, 227–30
  - rough, 2 (table)
    - standard valves, 227–30
  - ultra-high, 2 (table)
    - valves (UHV), 230–1
- Vacuum arc remelting (VAR), 281–4**
- furnace, 283 (fig)
  - pumping system, 284 (fig)
- Vacuum drying, 300–302**
- Vacuum firing, 211**
- Vacuum gauge:**
- calibration, 148–51, 152 (fig)
    - dynamic method, 150 (fig)
  - connection, 151–2
  - mechanical, 130–3
    - Bourdon tube gauge, 130
    - capacitance manometer, 133
    - capsule vacuum gauge, 130–31
    - diaphragm vacuum gauge, 131–2
- Vacuum induction degassing (VID), 273**
- Vacuum induction degassing and pouring (VIDP) furnace, 280 (fig)**
- Vacuum induction melting (VIM), 275–81**
- analysis of furnace gases, 282 (fig)
  - furnace characteristics, 279 (table)
  - pumping system for two-chamber furnace, 287 (fig)
- Vacuum ladle degassing (VD), 273, 274 (fig)**
- Vacuum leak detection, 179–87**
- large plant, 184 (fig)
  - localization, 183 (fig)
- Vacuum oxygen decarburization (VOD), 273, 275**
- Vacuum precision casting, 285**
- Vacuum system, 1, 2 (fig)**
- characteristics, 17–18
  - cleaning, 220–1
  - components:
    - electrical energy supply, 226–33
    - feed throughs, 233
    - mechanical movement, 232–3
    - valves, 232–3
  - fabrication, 207, 221–6
  - gas sources within, 3 (fig)
  - materials, 207–20
    - alloys, 207–16
    - ceramics, 218–20
    - glass, 218–20
    - polymers, 216–18
    - pure metals, 207–16
    - pure oxides, 218–20
  - pump-down time, 18–26
- VADER (vacuum arc double electrode remelting), 284**
- Valve, 226–33**
- Van Atta, 16**
- Vapour pressure, 208**
- Very Large Scale Integration (VLSI) circuit, 236**
- current trends, 236, 236 (table)
- Viton, 219 (table)**
- Vuilliez's scroll pump, 64**
- Water-cooled guard ring, 83**
- Web coater, 251–4, 255 (fig)**